NTIS #PB97- 141600

SSC-396

OPTIMIZED DESIGN PARAMETERS FOR WELDED TMCP STEELS

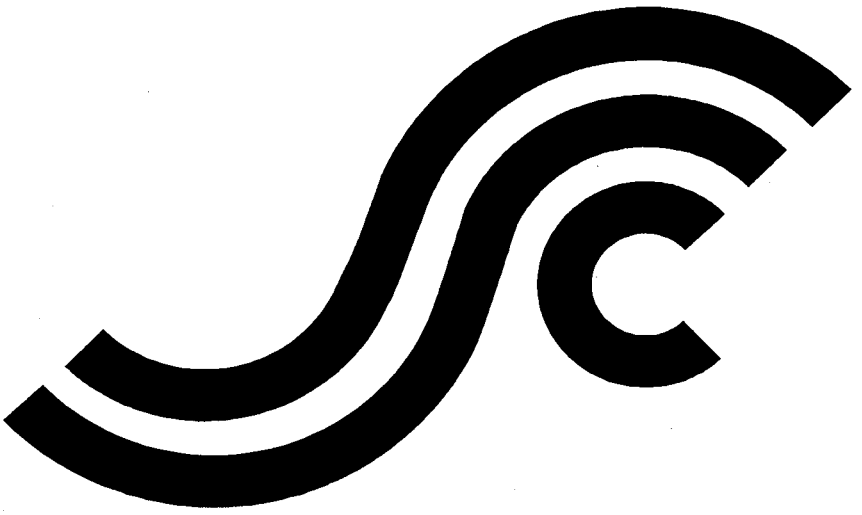

SHIP STRUCTURE COMMITTEE

1997

SHIP STRUCTURE COMMITTEE

The SHIP STRUCTURE COMMITTEE is constituted to prosecute a research program to improve the hull structures of ships and other marine structures by an extension of knowledge pertaining to design, materials, and methods of construction.

RADM J. C. Card, USCG (Chairman)
Chief, Office of Marine Safety, Security
and Environmental Protection
U. S. Coast Guard

Mr. John Grinstead
Director, Policy and Legislation
Marine Regulatory Directorate
Transport Canada

Mr. Edwin B. Schimler
Associate Administrator for Ship-
building and Technology Development
Maritime Administration

Dr. Donald Liu
Senior Vice President
American Bureau of Shipping

Mr. Robert McCarthy
Director, Survivability and Structural
Integrity Group (SEA O3P)
Naval Sea Systems Command

Mr. Thomas Connors
Acting Director of Engineering (N7)
Military Sealift Command

Dr. Ross Grahm
Head, Hydronautics Section
Defence Research Establishment-Atlantic

EXECUTIVE DIRECTOR

CDR Stephen E. Sharpe, USCG
U. S. Coast Guard

CONTRACTING OFFICER TECHNICAL REPRESENTATIVE

Mr. William J. Siekierka
Naval Sea Systems Command

SHIP STRUCTURE SUBCOMMITTEE

The SHIP STRUCTURE SUBCOMMITTEE acts for the Ship Structure Committee on technical matters by providing technical coordination for determinating the goals and objectives of the program and by evaluating and interpreting the results in terms of structural design, construction, and operation.

MILITARY SEALIFT COMMAND

Mr. Robert E. Van Jones (Chairman)
Mr. Rickard A. Anderson
Mr. Michael W. Touma
Mr. Jeffrey E. Beach

MARITIME ADMINISTRATION

Mr. Frederick Seibold
Mr. Richard P. Voelker
Mr. Chao H. Lin
Dr. Walter M. Maclean

U. S. COAST GUARD

CAPT George Wright
Mr. Walter Lincoln
Mr. Rubin Sheinberg

AMERICAN BUREAU OF SHIPPING

Mr. Glenn Ashe
Mr. John F. Conlon
Mr. Phillip G. Rynn
Mr. William Hanzalek

NAVAL SEA SYSTEMS COMMAND

Mr. W. Thomas Packard
Mr. Charles L. Null
Mr. Edward Kadala
Mr. Allen H. Engle

TRANSPORT CANADA

Mr. Peter Timonin
Mr. Felix Connolly
Mr. Francois Lamanque

DEFENCE RESEARCH ESTABLISHMENT ATLANTIC

Dr. Neil Pegg
LCDR Stephen Gibson
Dr. Roger Hollingshead
Mr. John Porter

SHIP STRUCTURE SUBCOMMITTEE LIAISON MEMBERS

SOCIETY OF NAVAL ARCHITECTS AND MARINE ENGINEERS
Dr. William Sandberg

CANADA CENTRE FOR MINERALS AND ENERGY TECHNOLOGIES
Dr. William R. Tyson

U. S. NAVAL ACADEMY
Dr. Ramswar Bhattacharyya

U. S. MERCHANT MARINE ACADEMY
Dr. C. B. Kim

U. S. COAST GUARD ACADEMY
CDR Bruce R. Mustain

U. S. TECHNICAL ADIVSORY GROUP TO THE INTERNATIONAL STANDARDS ORGANIZATION
CAPT Charles Piersall

AMERICAN WELDING SOCIETY
Mr. Richard French

NATIONAL ACADEMY OF SCIENCES - MARINE BOARD
Dr. Robert Sielski

NATIONAL ACADEMY OF SCIENCES - COMMITTEE ON MARINE STRUCTURES
Dr. John Landes

WELDING RESEARCH COUNCIL
Dr. Martin Prager

AMERICAN IRON AND STEEL INSTITUTE
Mr. Alexander D. Wilson

OFFICE OF NAVAL RESEARCH
Dr. Yapa D. S. Rajapaske

MASSACHUSETTS INSTITUTE OF TECHNOLOGY
CAPT Alan J. Brown

STUDENT MEMBER
Mr. Jason Miller
Massachusetts Institute of Technology

Member Agencies:

American Bureau of Shipping
Defence Research Establishment Atlantic
Maritime Administration
Military Sealift Command
Naval Sea Systems Command
Transport Canada
United States Coast Guard

Ship Structure Committee

An Interagency Advisory Committee

Address Correspondence to:

Executive Director
Ship Structure Committee
U.S. Coast Guard (G-MSE/SSC)
2100 Second Street, S.W.
Washington, D.C. 20593-0001
Ph: (202) 267-0003
Fax: (202) 267-4816

SSC-396
SR-1358

February 27, 1997

OPTIMIZED DESIGN PARAMETERS FOR WELDED TMCP STEELS

Thermo-mechanical control processed (TMCP) steel has been increasingly used by the marine industry since the early 1980's. TMCP steel is known to have some distinct advantages in properties not found with conventionally processed (normalized) steel, yet is subject to the same design approach and criteria as applied to conventionally processed steel.

This investigation has studied whether in fact an optimized design approach that is more beneficial to the industry could be developed for welded TMCP steel. Weldability and mechanical performance characteristics were evaluated. Properties such as strength, ductility, strain hardening, fracture toughness, fatigue initiation and propagation, corrosion fatigue initiation and propagation, hydrogen cracking, Heat Affected Zone (HAZ) toughness, and HAZ softening were included in the study.

No substantial advantages in mechanical properties that could support a design approach with optimized parameters were discovered. On the contrary, a widely applied correlation of fracture toughness testing methods was found to be non-conservative for TMCP steel. The investigation confirmed several key advantages related to weldability and also identified several areas where additional work is needed to better characterize the properties of TMCP steel.

J. C. CARD
Rear Admiral, U. S. Coast Guard
Chairman, Ship Structure Committee

1, 2x

Technical Report Documentation Page

1. Report No.	2. Government Accession No.	3. Recipient's Catalog No.
SSC-396	PB97-141600	

4. Title and Subtitle	5. Report Date
Optimized Design Parameters for Welded TMCP Steels	January 1997
	6. Performing Organization Code
	8. Performing Organization Report No.
7. Author(s)	SR-1358
L. Malik, R. Yee, B. Graville, and A. Dinovitzer	
9. Performing Agency Name and Address	10. Work Unit No. (TRAIS)
Fleet Technology Limited 311 Legget Drive Kanata, Ontario K2K 1Z8 Canada	11. Contract or Grant No. DTCG23-94-C-E01047
	13. Type of Report and Period Covered
12. Sponsoring Agency Name and Address	Final Report
Ship Structure Committee c/o U.S. Coast Guard (G-MSE-SSC) 2100 Second Street, S.W. Washington, D.C. 20593-0001	14. Sponsoring Agency Code G-M

15. Supplementary Notes

Sponsored by the Ship Structure Committee. Jointly funded by its member agencies.

16. Abstract

In this report, data on the static strength, toughness, and fatigue properties of accelerated cooled TMCP steels and their weldments have been compiled from various sources. Potential for advantageous application in ship structure design has been examined. Fabrication characteristics of the TMCP steels, mainly weldability and line heating, are also briefly reviewed. Tensile test data indicates that the yield to tensile ratio of the accelerated cooled TMCP steels tends to be slightly higher than steels produced by other steelmaking routes. Accelerated cooled TMCP steels possess excellent toughness and should easily meet toughness requirements to prevent brittle fracture in ships at a design temperature of 0C. In addition, TMCP steels have better weldability and HAZ toughness. As a result, accelerated cooled TMCP steels allow for more economic fabrication and greater weld joint integrity as they are more likely to have an economic edge for yield strengths up to 500 MPa and plate thicknesses up to 50 mm. Classification Societies have recently introduced explicit fatigue design criteria for welded joints in ships. These criteria are however largely based on S-N data for basic welded joints fabricated from non-TMCP steels. Available S-N data for as-welded joints fabricated from accelerated cooled TMCP steels indicates that these joints share similar characteristics, and that there is no significant difference between high cycle fatigue strengths of as-welded joints fabricated from non-TMCP steels and accelerated TMCP steels, even if soft HAZs are present in the TMCP steel joints. Fatigue strength of such joints can be improved to increase with increasing tensile strength by using weld improvement techniques. Improvements have also been observed in limited tests of TMCP steel welded joints.

17. Key Words	18. Distribution Statement
TMCP, Weldability, Ductility, Strain, Hardening, Fatigue, Fracture, Propagation, HAZ	Distribution Unlimited, Available From: National Technical Information Service U.S. Department of Commerce Springfield, VA 22151 Ph. (703) 487-4650

19. Security Classif. (of this report)	20. SECURITY CLASSIF. (of this page)	21. No. of Pages	22. Price
Unclassified	Unclassified	277	$49.00

Form DOT F 1700.7 (8/72) Reproduction of form and completed page is authorized.

NIST
United States Department of Commerce
Technology Administration
National Institute of Standards and Technology
Metric Program, Gaithersburg, MD 20899

METRIC CONVERSION CARD

Approximate Conversions to Metric Measures

Symbol	*When You Know*	*Multiply by*	*To Find*	*Symbol*
	LENGTH			
in	inches	2.5	centimeters	cm
ft	feet	30	centimeters	cm
yd	yards	0.9	meters	m
mi	miles	1.6	kilometers	km
	AREA			
in^2	square inches	6.5	square centimeters	cm^2
ft^2	square feet	0.09	square meters	m^2
yd^2	square yards	0.8	square meters	m^2
mi^2	square miles	2.6	square kilometers	km^2
	acres	0.4	hectares	ha
	MASS (weight)			
oz	ounces	28	grams	g
lb	pounds	0.45	kilograms	kg
	short tons (2000 lb)	0.9	metric ton	t
	VOLUME			
tsp	teaspoons	5	milliliters	mL
Tbsp	tablespoons	15	milliliters	mL
in^3	cubic inches	16	milliliters	mL
fl oz	fluid ounces	30	milliliters	mL
c	cups	0.24	liters	L
pt	pints	0.47	liters	L
qt	quarts	0.95	liters	L
gal	gallons	3.8	liters	L
ft^3	cubic feet	0.03	cubic meters	m^3
yd^3	cubic yards	0.76	cubic meters	m^3
	TEMPERATURE (exact)			
°F	degrees Fahrenheit	subtract 32, multiply by 5/9	degrees Celsius	°C

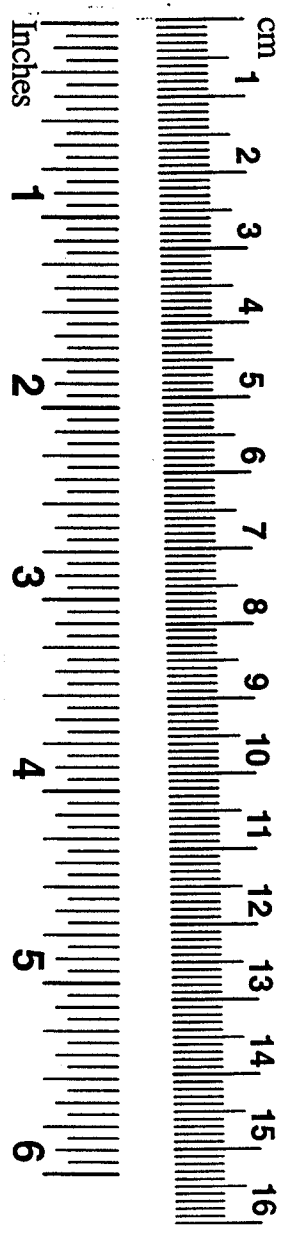

Approximate Conversions from Metric Measures

Symbol	*When You Know*	*Multiply by*	*To Find*	*Symbol*
	LENGTH			
mm	millimeters	0.04	inches	in
cm	centimeters	0.4	inches	in
m	meters	3.3	feet	ft
m	meters	1.1	yards	yd.
km	kilometers	0.6	miles	mi
	AREA			
cm^2	square centimeters	0.16	square inches	in^2
m^2	square meters	1.2	square yards	yd^2
km^2	square kilometers	0.4	square miles	mi^2
ha	hectares (10,000 m^2)	2.5	acres	
	MASS (weight)			
g	grams	0.035	ounces	oz
kg	kilograms	2.2	pounds	lb
t	metric ton (1,000 kg)	1.1	short tons	
	VOLUME			
mL	milliliters	0.03	fluid ounces	fl oz
mL	milliliters	0.06	cubic inches	in^3
L	liters	2.1	pints	pt
L	liters	1.06	quarts	qt
L	liters	0.26	gallons	gal
m^3	cubic meters	35	cubic feet	ft^3
m^3	cubic meters	1.3	cubic yards	yd^3
	TEMPERATURE (exact)			
°C	degrees Celsius	multiply by 9/5, add 32	degrees Fahrenheit	°F

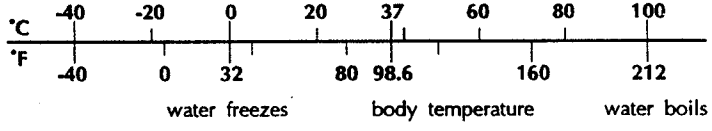

TABLE OF CONTENTS

Page

1.0 INTRODUCTION 1
1.1 Background and Objectives 1
1.2 High Performance, Accelerated Cooled TMCP Steels 3
2.0 APPROACH 10
3.0 DATA BASE 11
4.0 DATA ANALYSIS 13
4.1 Base Metal Tensile Properties 13
4.2 Base Metal Toughness Properties 17
4.3 HAZ Toughness Properties 23
4.4 Weld Metal Toughness 26
5.0 DESIGN IMPLICATIONS (STATIC STRENGTH AND FRACTURE) 63
5.1 Static Strength 63
5.1.1 Allowable Yield Strength 63
5.1.2 Actual Tensile Properties of TMCP Steels 65
5.2 Fracture Prevention (Base Metal) 67
5.3 Fracture Prevention (Heat affected zone) 73
6.0 FATIGUE PROPERTIES OF TMCP STEELS 80
6.1 Fatigue Cracking in Ship Structures 80
6.2 Fatigue Crack Growth in Air 82
6.2.1 Region I Crack Growth in Steels 84
6.2.2 Region II Crack Growth in Steels 84
6.2.3 Region III Crack Growth In Steels 86
6.2.4 Short Crack Growth in Steels 87
6.3 Crack Initiation In Steels in Air 89
6.3.1 S-N Data 89
6.3.2 $\Delta\varepsilon$ vs N Data 91
6.3.4 $\Delta K_{eq} / \sqrt{\rho}$ vs N Data 92
6.4 Corrosion Fatigue of Steels in Sea Water 93
6.4.1 Growth of Long Fatigue Cracks 93
6.4.2 Growth of Short Fatigue Cracks 96
6.4.3 Crack Initiation in Steels 97
6.5 The Effect of Sour Crude Oil 99
6.6 S-N Data for Welded Joints 100

TABLE OF CONTENTS (continued)

Page

7.0 FABRICATION CONSIDERATIONS IN USE OF TMCP STEELS..... 146
7.1 Weldability.....146
7.2 Fabrication Concerns.....146
7.3 Other Applications of TMCP Steels.....151
8.0 SUMMARY AND RECOMMENDATIONS FOR FURTHER WORK..... 161
9.0 REFERENCES..... 169

APPENDICES

APPENDIX A LIST OF PERSONS/ORGANIZATIONS THAT RESPONDED TO REQUEST FOR TECHNICAL INFORMATION AND DATA

APPENDIX B SOURCE DOCUMENTS FOR DATA COMPILED IN THE DATA BASE (APPENDIX C)

APPENDIX C THE ASSEMBLED DATA BASE
SHEET 1 STEEL DESCRIPTIONS
SHEET 2 BASE METAL TENSILE DATA
SHEET 3 BASE METAL TOUGHNESS DATA
SHEET 4 WELD DESCRIPTIONS
SHEET 5 CROSS-WELD STRENGTH DATA
SHEET 6 HAZ TOUGHNESS DATA
SHEET 7 WELD METAL TOUGHNESS DATA

APPENDIX D APPROACH USED TO ARRIVE AT CURRENT SHIP STEEL CVN REQUIREMENTS IN CLASSIFICATION SOCIETY RULES: NKK APPROACH (1979)

LIST OF FIGURES

Page

Figure 1.1: Vector diagram showing the influence of various strengthening mechanisms on strength and toughness Ref. [1.1] 5
Figure 1.2: Toughness and strength relation for various types of steel Ref. [1.2] 6
Figure 1.3: Definition of TMCP Steels Ref. [1.4] 7
Figure 1.4: Carbon equivalent ranges for steel types Ref. [1.4] 7
Figure 1.5: Comparison of alloying elements in terms of their effect on HAZ CTOD toughness Ref. [1.12] 8
Figure 1.6: Effect of carbon equivalent value CEV = C + Mn/6 + (Cr + Mo + V)/5 + (Ni + Cu)/15 on yield strength of various grades of steel produced by different processing routes Ref. [1.14] 9
Figure 4.1: Yield strength in the transverse direction versus that in the longitudinal direction for TMCP steel plates 28
Figure 4.2: Ratio of the yield strength in the transverse direction to that in the longitudinal direction versus the TMCP steel plate thickness 29
Figure 4.3: Yield strength of the TMCP steel plates measured at half thickness location versus that measured at the quarter thickness location 30
Figure 4.4: Ratio of yield strengths measured at half thickness and quarter thickness locations versus the TMCP steel plate thickness 31
Figure 4.5: Yield to tensile strength ratio for TMCP steel plates versus the yield strength 32
Figure 4.6(a): Regression line for TMCP steel plates from Figure 4.5 superimposed on yield/tensile strength ratio data given in Ref. [4.1] 33
Figure 4.6(b): Regression line for TMCP steel plates from Figure 4.5 superimposed on yield-tensile strength ratio date given in Ref. [4.2] 34
Figure 4.6(c): Regression line for TMCP steel plates from Figure 4.5 superimposed on yield-tensile strength ratio date given in Ref. [4.3] 34
Figure 4.7: Strain hardening exponent calculated from the yield/tensile strength ratio, using two different models 35
Figure 4.8: Uniform elongation measured in tensile tests. Ref. [4.9] 35
Figure 4.9: Histogram of the (actual-specified minimum) yield strength for TMCP steel plates 36
Figure 4.10: Comparative distribution of (actual-specified minimum) yield strength for marine steels [Ref. 4.10] and TMCP steel plates 36
Figure 4.11: 50% CVN fracture appearance transition temperature for TMCP steel plates of various yield strengths 37
Figure 4.12: 50% CVN fracture appearnce transition temperature for TMCP steel plates of various thicknesses 37
Figure 4.13: Difference in 50% FATT between half-thickness (t/2) and quarter thickness (t/4) locations of TMCP steel plates 38
Figure 4.14: Difference in the 50% FATT between transverse (T) and longitudinal (L) orientations of TMCP steel plates 38
Figure 4.15: Distribution of the Pellini nil-ductility transition temperature (ASTM E 208) of TMCP steel plates 39

LIST OF FIGURES (continued)

Page

Figure 4.16: Relationship between 50% FATT and NDTT in TMCP steels 39
Figure 4.17: Relationship between NDTT and $_{V}T_{E}$ Ref. [4.12] 40
Figure 4.18: CVN energy at NDTT versus %(10S + C) Ref. [4.13] 40
Figure 4.19: 40J CVN transition temperature minus NDTT versus %(10S + C) Ref. [4.13] 41
Figure 4.20: Relation between 40J CVN transition temperature and NDTT for steels with %(10S + C) >0.25 Ref. [4.13] 41
Figure 4.21(a):CTOD toughness as a function of temperature for a 50 mm thick, EH 36 mod (TMCP) steel in the longitudinal orientation 42
Figure 4.21(b):CTOD toughness as a function of temperature for a 20 mm thick, 440 MPa yield (NVF 440) TMCP steel 43
Figure 4.22(a):CTOD fracture toughness of steels C (25 mm thick, normalized) and F (20 mm thick, TMCP) as a function of temperature, referenced to the nil-ductility transition temperature 44
Figure 4.22(b):CTOD fracture toughness of steels D (50 mm thick, normalized) and E (50 mm thick, TMCP) as a function of temperature, referenced to the nil-ductility transition temperature 45
Figure 4.23: Relation between and 0.2 mm CTOD transition temperature and NDTT 46
Figure 4.24: Wide plate specimens (deep center notch) tested in Japan for initiation toughness of TMCP steels 46
Figure 4.25: Results of wide plate tests on a TMCP steel plate Ref. [4.17] 47
Figure 4.26: Double tension test for measuring crack arrest toughness 47
Figure 4.27: Compact crack arrest test 48
Figure 4.28: Crack arrest toughness values relative to the CVN transition temperature (all data) 48
Figure 4.29: K_{ca} results for DT and Esso tests only 49
Figure 4.30: K_{ca} results in DT and Esso tests for TMCP (accelerated cooled) steels 49
Figure 4.31: K_{ca} results in DT and Esso tests for non-TMCP steels 50
Figure 4.32: Summary of K_{ca} values from Ref. [4.19] 320-355 MPa yield strength ship steels 50
Figure 4.33: Summary of K_{ca} values from Ref. [4.20] 392 MPa yield strength ship steels 51
Figure 4.34: Effect of splitting index on crack arrest toughness Ref. [4.21] 51
Figure 4.35: Relation between the temperature for K_{ca} = 124 MPa$\sqrt{m}$ and CVN FATT 52
Figure 4.36: Relation between the temperature for K_{ca} = 186 MPa$\sqrt{m}$ and CVN FATT 52
Figure 4.37: Relation of crack arrest properties (T124) to NDTT 53
Figure 4.38: Relation of crack arrest properties (T186) to NDTT 53
Figure 4.39: Average heat affected zone toughness determined from CVN specimens notched at the fusion line in welds made at 3.0 kJ/mm heat input or lower 54
Figure 4.40: Average heat affected zone toughness determined from CVN specimens notched at the fusion line in welds made at heat inputs ranging from 3 to 7 kJ/mm 54

LIST OF FIGURES (continued)

Page

Figure 4.41: Average heat affected zone toughness determined from CVN specimens notched at the fusion line in welds made at heat inputs greater than 10 kJ/mm.....55
Figure 4.42: Minimum reported heat affected zone CVN toughness at fusion line @ -60°C in welds made at various heat inputs 55
Figure 4.43: Comparison of the average CVN toughness at the subcritical heat affected zone (or fusion line + 5 mm) location with base metal toughness, at the quarter thickness location.....56
Figure 4.44: Comparison of the minimum CVN toughness reported at the subcritical heat affected zone (or fusion line + 5 mm) location with base metal toughness, at the quarter thickness location 56
Figure 4.45: Minimum HAZ fusion line CTOD toughness in a set tested at -10°C to -15°C as a function of weld heat input.....57
Figure 4.46: Achievable (0) and Target (X) TMCP steel HAZ properties (42J CVN and 0.1 mm CTOD) at various design and test temperatures for 470 MPa or lower yield strength steels 57
Figure 4.47: Heat affected zone fusion line CTOD toughness values reported for TMCP steels for welds made at a heat input of 3 kJ/mm or less.....58
Figure 4.48: Heat affected zone fusion line CTOD toughness values reported for TMCP steels for welds made at heat inputs in the range of 3 to 7 kJ/mm 58
Figure 4.49: Heat affected zone fusion line CTOD toughness values reported for TMCP steels for welds made at heat inputs greater than 10 kJ/mm.....59
Figure 4.50: Data for machined notched centre cracked wide plate tests for fusion line (HAZ). CTOD temperature determined from lower bound of reported data (limited tests), T (155) found from regression ln K_c against 1/T°K.....59
Figure 4.51: Statistical representation of CTOD data for various types of loading Ref. [4.24] 60
Figure 4.52: Average CVN toughness of weld metals depositing using the submerged arc and gas metal arc welding processes (data for submerged arc welds shown at a temperature 2°C higher than the actual test temperature).....60
Figure 4.53: Average CVN toughness of weld metals deposited using the shielded metal arc and flux cored arc welding processes (data for shielded metal arc welds shown at a temperature 2°C higher than the actual test temperature).....61
Figure 4.54: Average CTOD of weld metals deposited using the gas metal arc and submerged arc welding processes (data for submerged arc welds shown at a temperature 2°C higher than the actual test temperature).....61
Figure 4.55: Average CTOD toughness of weld metals deposited using the shielded metal arc and flux cored arc welding processes (data for shielded metal arc welds shown at a temperature 2°C higher than the actual test temperature).....62
Figure 5.1: Calculation of high tensile steel factor as explained in Ref. [5.1].....75
Figure 5.2: Actual tensile strength of the TMCP steel plates plotted against their specified minimum yield strength.....75

LIST OF FIGURES (continued)

Page

Figure 5.3: Actual tensile strength of the TMCP steel plates plotted against their actual yield strength 76
Figure 5.4: Absolute design tensile margin of safety (actual tensile strength - 0.7 x specified minimum yield strength) as a function of the specified minimum yield strength 76
Figure 5.5: Plot of the design tensile margin of safety normalized with respect to the specified minimum yield strength, versus the specified minimum yield strength 77
Figure 5.6: Relation between K_c (base metal) and temperature for 390 MPa yield steels 78
Figure 5.7: Relation between K_{ca} (base metal, L-direction) and temperature for 390 MPa yield steels 78
Figure 5.8: Fracture analysis diagram as developed by Pellini Note relation of initiation curve for small surface cracks to arrest curve for through-thickness cracks (TTCs) 79
Figure 6.1: Basic shape of da/dN vs ΔK curve 105
Figure 6.2: Plot of Δk_{th} vs R-ratio for different steels from [6.16] 105
Figure 6.3 106
Figure 6.4 107
Figure 6.5 108
Figure 6.6: da/dN vs ΔK data for various steels, weld metals and heat affected zone metal from [6.22]. Letters indicate growth by striation mechanism 109
Figure 6.7 110
Figure 6.8a 111
Figure 6.8b 112
Figure 6.9a 113
Figure 6.9b 114
Figure 6.10 115
Figure 6.11: Schematic representation of short crack behaviour from [6.32] 116
Figure 6.12a 117
Figure 6.12b 118
Figure 6.13: Fatigue limit vs ultimate tensile strength data for: (a) smooth steel rotating beam specimens [6.38]; and (b) smooth steel pulsating tension specimens [6.39] 119
Figure 6.14a 120
Figure 6.14b 121
Figure 6.15 122
Figure 6.16: Hysteresis stress-strain loop for strain-controlled specimen [6.32] 123
Figure 6.17a 124
Figure 6.17b 125
Figure 6.18a: Typical da/dN vs ΔK data for steels in sea water without cathodic protection [6.47] 126
Figure 6.18b: Typical da/dN vs ΔK data for steels in sea water with cathodic protection [6.47] 127

LIST OF FIGURES (continued)

Page

Figure 6.19a: Free corrosion data....128
Figure 6.19b: Data for cathodically protected specimens....129
Figure 6.20 130
Figure 6.21 131
Figure 6.22 132
Figure 6.23 133
Figure 6.24: Cruciform joints: (a) with constant ratio of attachment plate thickness to plate thickness; (b) constant attachment plate thickness 134
Figure 6.25 135
Figure 6.26 136
Figure 6.27 137
Figure 6.28a 138
Figure 6.28b 139
Figure 6.29 140
Figure 6.30 141
Figure 6.31 142
Figure 6.32 143
Figure 6.33 144
Figure 6.34 145
Figure 7.1: CE (IIW) and P_{cm} for TMCP steels plotted against the specified minimum yield strength 152
Figure 7.2: CE (IIW) and P_{cm} for TMCP steels plotted against their actual yield strength 152
Figure 7.3: Ratio of tensile strengths determined in cross-weld and base metal tensile tests plotted against the weld heat input 153
Figure 7.4: Effect of specimen width on tensile strength of welded joint Ref. [7.6]....154
Figure 7.5: Relationship between HAZ tensile strength and carbon equivalent (Ceq) Ref. [7.6]....155
Figure 7.6: Relationship between Ho/t and Ceq Ref. [7.6]) 156
Figure 7.7: Mechanical properties of plates after line-heating (transverse direction) Ref. [7.9]....157
Figure 7.8: CVN toughness of a 40 mm thick TMCP steel as a function of peak temperature during flame straightening Ref. [7.10]....158
Figure 7.9: Tensile properties of line heated 15 mm thick panels 159
Figure 7.10: Tensile properties of line heated 50 mm thick panels 159
Figure 7.11: Improved weldability of accelerated cooled TMCP steels....160

LIST OF TABLES

Page

Table 5.1: Effect of the high tensile steel factor (HTSF) on allowable yield stress (AYS) and safety margin with respect to the specified minimum ultimate tensile strength (SMUTS-AYS) 64
Table 5.2: Calculated HTSF values for higher strength steels to maintain a constant safety margin (SMUTS-AYS) of 167 MPa 64
Table 5.3: Actual and predicted HTSF, and predicted safety margin based on Kitada's formulation 64
Table 5.4: Effect of higher SMYS on failure probability under various assumed distributions for the service stresses 67
Table 5.5: ABS Material Class Requirements for Various Ship Structural Members (Design Temp; 0°C) 69
Table 5.6: Material Classes as defined in ABS Rules for Building and Classing Steel Vessels .70
Table 5.7: Calculated required fracture toughness for high strength steels to meet material classes IV and V requirements 70
Table 5.8: CTOD data (three point bend specimens) for some higher strength steels 71
Table 5.9: Crack arrest toughness values for two high strength steels 72
Table 5.10: Required fracture toughness for heat affected zone (fusion line) 73
Table 7.1: Change in CVN transition temperature due to line heating thermal cycles 149
Table 7.2: Mechanical properties of 385 MPa yield strength TMCP Steel. Ref. [7.11] after simulated heat treatment (thermal conditions, 60S heating, 60S holding at T_{max}, cooling according to $t_{8/5}$ 20S) for 15 mm test plate material 149
Table 7.3: Influence of different line heating conditions on the impact transition temperatures of 15 mm and 50 mm thick plates 150

LIST OF SYMBOLS

AYS	Allowable yield strength for steels in Classification Society Rules taking into account High Tensile Steel Factor
b	Fatigue strength exponent
β	Fraction of the steel's yield strength that is deemed to represent the weld residual stress magnitude
C	Carbon
c	Fatigue ductility exponent
C, m	Constants in the Paris Law describing the fatigue crack growth in Region II of da/dN vs ΔK plots
C.E.	IIW carbon equivalent to assess the weldability of steels
Ca	Calcium
CR	Control Rolled
CTOD	Crack tip opening displacement, a measure of fracture toughness (or crack driving force)
CVN	Charpy Vee Notch (toughness test used to measure notch toughness of steel as a function of temperature)
da/dN	Fatigue crack growth rate
ΔK_{eq}	Sharp crack equivalent stress intensity factor range for a notch
ΔK_{th}	Threshhold stress intensity factor range below which the crack growth rate is negligibly small
E	Young's Modulus
ε_f	Fatigue ductility coefficient
ε_p	Plastic strain
ε_u	True strain corresponding to uniform elongation/maximum stress in a uniaxial tensile test
FATT	Fracture Appearance Transition Temperature in CVN test, i.e., temperature at which broken CVN specimens display 50% shear
FL5	Notch location of "fusion line + 5 mm"
HAZ	Heat Affected Zone
HTSF	High tensile steel factor which reduces the yield strength of high strength steels that can be used for design purposes in Classification Society Rules
ICHAZ	Intercritical HAZ
K	Crack driving force
K	Strength coefficient in Ludwik model of the true stress-true strain curve
K_{Ia}	Plain strain crack arrest toughness
K_{Ic}	Plain strain fracture toughness
K_c	Apparent fracture toughness measured using linear elastic fracture mechanics
K_{ca}	Crack arrest toughness estimated using static analysis
K_{max}	Maximum stress intensity factor during cyclic loading
K_{min}	Miminum stress intensity factor during cyclic loading
K_T	Value of K_{max} corresponding to Region II-Region III transition in da/dN vs ΔK plots

LIST OF SYMBOLS (continued)

Mo	Molybdenum
N	Nitrogen
N	Number of stress reversals during cyclic loading
n	Strain hardening exponent in Ludwik model of true stress-true strain curve
Nb	Niobium
NDTT	Nil-ductility Transition Temperature as determined by Pellini's drop weight test
P	Phosphorous
P_{cm}	Weldability index developed in Japan for lower carbon (<0.15%) steels
ppm	Parts per million
R	Algebraic ratio of minimum to maximum load during cyclic loading
ρ	Root diameter of notch
σ	Stress
S	Sulphur
S	Thickness corrected design stresses range
$\sigma_{1.0}$	True stress for a true strain = 1.0
σ'_f	Fatigue strength coefficient
SCHAZ	Subcritical HAZ
σ_D	Design stress = coefficient of yield strength utilization (α) x allowable yield strength
S_f	Fatigue limit
σ_f	Flow stress = average of steel yield and ultimate tensile strengths
SMUTS	Specified Minimum Ultimate Tensile Strength
SMYS	Specified Minimum Yield Strength
S_r	Design stress range allowed by relevant S-N design curve
σ_R	Residual stress
t	Plate thickness
T_{124}	Transition temperature for K_{ca} = 124 MPa$\sqrt{m}$
T_{186}	Transition temperature for K_{ca} = 186 MPa$\sqrt{m}$
$t_{8/5}$	Time for weld to cool from 800°C to 500°C.
Ti	Titanium
T_r	Actual plate thickness
TT, Te	Transition temperature corresponding to certain absorbed energy in the CVN test or certain % shear on the fracture surface of CVN specimens
V	Vanadium
YR	Yield Ratio = yield strength/ultimate tensile strength

1.0 INTRODUCTION

1.1 Background and Objectives

The past three decades have seen a revolution in steelmaking practices driven by a demand for steels with better weldability and toughness and to reduce reliance on costly alloying elements. Concurrently, there has been a trend towards the use of increasingly higher strength steels in order to reduce structural weight and fabrication costs. Steel makers have been meeting these challenges by developing a range of new techniques for controlling steel properties. These methods are based on fundamental research carried out during the 60's [1.1] that sought to understand the role of various strengthening mechanisms in steels (**Figure 1.1**). Recognition of the importance of a fine grain structure for improving both the strength and toughness resulted in controlled rolling (CR) processes and ultimately in sophisticated thermomechanical control processes (TMCP). Such steels, compared to conventional grades, can combine higher strength and excellent low temperature toughness (**Figure 1.2** [1.2]).

The term TMCP has been used loosely in the literature to describe a wide range of processing routes. For marine structural steels, the Classification Societies [1.3] and Japanese authors [1.4] have categorized these processes as follows:

(i) controlled rolling is a procedure in which the final rolling temperature is controlled within the range used for normalizing treatments so that austenite completely recrystallizes.

(ii) thermomechanical controlled processing involves the strict control of steel temperature and rolling reduction, and under this category three types are defined. As seen in **Figure 1.3**, steel Types I and II do not involve any accelerated cooling and differ in one main respect, viz., the temperature range over which mechanical deformation (thickness reduction) by rolling is performed. Thus, in Type I steels, rolling is performed at relatively low temperatures corresponding to the dual phase austenite-ferrite region of the continuous cooling transformation diagram. In comparison, Type III steels incorporate accelerated cooling after rolling, over a limited temperature range (interrupted accelerated cooling) depending on the target properties and other mill to mill variables.

Compared to control rolled and Type I and II TMCP steels, the accelerated cooling in Type III TMCP steels allows for achievement of greater degree of through thickness uniformity of grain size and mechanical properties, especially in thicker plates (say, more than 25 mm thick) while maintaining a leaner steel chemical composition (**Figure 1.4**). Leaner, optimized chemical compositions, especially low carbon levels, limit the degradation in the heat affected zone (HAZ) toughness properties in relation to that of the base material, thus making it easier to meet stringent HAZ fracture toughness requirements such as those in API Recommended Practice 2Z [1.5]. The steels' weldability, as defined in terms of the resistance of the heat affected zone to

hydrogen cracking during welding, is also enhanced. The risk of forming a crack sensitive HAZ is a function of the hardenability of the steel which can be related to steel composition through the IIW carbon equivalent or weldability index Pcm. In accelerated cooled TMCP steels, these indices can be sufficiently low so that such steels may often be welded without any preheat.

The procurement cost of accelerated cooled steels is also expected to be lower than that for conventional normalized or quenched and tempered steels because of the savings resulting from the need for one less reheating cycle.

It is due to these advantages that virtually all the TMCP steel applied in offshore structures has been the accelerated cooled type, some of the examples being Norske Hydro's Osberg jacket (355 and 380 MPa yield strength), Brage and Troll Olje platforms (420 MPa yield strength); TLP tendons for Conoco's Jolliet project (420 MPa yield); Shell's MARS TLP deck (355 and 420 MPa yield strength), etc.

In the area of ship structures, the thicknesses involved are relatively smaller and HAZ toughness requirements are not as demanding as those for offshore structural steels. However, the accelerated cooled steels can still offer the advantage of achieving the relatively modest HAZ toughness levels but at very high welding heat inputs, typical of high productivity welding processes used mostly in Japan. One of the earliest applications of the accelerated cooled, TMCP steels (350 MPa yield) has been the VLCCs built in Japan during the early 80s. Higher strength accelerated cooled TMCP steels up to 400 MPa yield strength have been used for fabricating ship strength decks and side shells [1.6-1.8]. More recently, 500 MPa yield strength, accelerated cooled steel has been used in the fabrication of the Finnish icebreaker Feneca.

It has also been learned [1.6, 1.7, 1.9] that some of the shipyards in Japan and Europe try to maximize the use of accelerated cooled TMCP steels as much as possible for ship structure fabrication. However, this is primarily due to the advantages of lower fabrication costs resulting from excellent weldability and acceptable HAZ toughness at high heat inputs. No attempt seems to have been made so far to take advantage of the higher strength and excellent base metal toughness of these steels in the design of ship structures.

It is in light of this background that the Ship Structure Committee initiated the present project that had the **objectives** of:

(a) compiling a data base of static strength, fracture and fatigue properties of accelerated cooled TMCP plate steels and their weldments;

(b) developing recommendations for appropriate changes in ship structural material qualification and design criteria.

However, before delving into the work performed and conclusions arrived at in the project, it would be useful to elaborate on the elements that characterize today's state-of- the- art high performance, accelerated cooled TMCP steels.

1.2 High Performance, Accelerated Cooled TMCP Steels

It should be appreciated that accelerated cooling on its own does not lead to the excellent combination of properties that have been reported for these steels. Accelerated cooling offers incremental advantages only, and to obtain the best performance, other components of steel making technology must be optimized as well [1.10]. These are summarized below:

(i) **Clean Steel** - Minimizing the amounts of sulfur (S), phosphorous (P) and free nitrogen (N) in the steel is beneficial from the point of view of enhancing base metal as well as heat affected zone toughness. Low S contents also improve through thickness ductility and resistance to lamellar tearing, and low P and N are particularly important for HAZ toughness. Achievable levels for these elements in commercial practice are approximately 10, 40 and 30 PPM respectively for S, P and total nitrogen contents.

(ii) **Inclusion Shape Control** - Even when S content is as little as 10 PPM, there is a tendency to form flattened manganese sulphide inclusions at the plate mid-thickness location which can affect through thickness ductility and resistance to hydrogen induced cracking. Using Ca or rare earth metals, the inclusions are turned to a less harmful globular shape.

(iii) **Decrease Centerline Segregation** - Most of the world steel production today is continuously cast into slabs which tend to have a band at mid-thickness location that is enriched with impurities (C, S, P, Nb and Mn). This centerline segregation is undesirable from the point of view of through thickness ductility and hydrogen induced cracking susceptibility. Magnetic stirring of the molten metal in the caster and thickness reduction when the steel is still solidifying are examples of techniques that have been developed to minimize centerline segregation.

(iv) **Optimized Composition and Rolling Schedule** - While at first glance, most TMCP steel compositions look similar, there are subtle differences in the amount of microalloying elements (Nb, Ti) present. There are complex interactions between these elements and C and N that depend on their absolute amounts present as well as on control rolling variables. By optimizing the composition in conjunction with the controlled rolling schedules, the steel producers are able to achieve the necessary grain size and microstructure control, and thus the targeted properties.

The steel cleanliness and composition also influence the HAZ toughness properties. Fundamental studies [1.11, 1.12] have shown that elements such C, Mo, Nb, V, N and B are deleterious from the point of view of achieving superior HAZ fracture toughness (see **Figure 1.5**). At the same time, thermally stable titanium nitride precipitates and rare earth oxysulfides help limit grain growth in the HAZ and also produce more favorable intragranular microstructure [1.10]. Some of the other innovative approaches [1.13] that steel makers have used to help improve HAZ toughness are to have controlled amounts of finely dispersed Al_2O_3 or TiO_2 particles in the steel which help restrict grain growth in the HAZ, even in rather high heat input welds.

Most TMCP steel producers have performed developmental work to optimize steel composition, liquid metal treatment and subsequent rolling and cooling schedules appropriate to their own equipment and facilities, and given proprietary names to the processes such as OLAC (On Line Accelerated Cooling), MACS (Multipurpose Accelerated Cooling System), etc.

Finally, it is useful to note that advantages of steel cleanliness, inclusion shape control and control of centerline desegregation can also be obtained in control rolled, non-accelerated cooled TMCP, and conventional normalized and quenched and tempered steels as well. However, as pointed out earlier, accelerated cooling leads to incremental benefits over the former set of practices involving control rolling. Similarly, the additional heating cycle required for normalizing, and quenching and tempering heat treatments implies that the grain size achieved cannot be as fine with these heat treatments as is potentially possible in accelerated cooled steels. This factor, along with the effect this additional heating cycle has on carbonitride precipitates, means that HAZ microstructure control is more feasible in accelerated cooled steels than in conventionally heat treated steels.

Conversely, beyond a target yield strength level of 500 MPa, it becomes difficult to retain lean chemistry and through thickness uniformity of microstructure and with present day technologies, it becomes more economical to follow the quench and temper route for thick (>50 mm) plate steels with yield strength levels of 550 MPa or greater (see **Figure 1.6**). Consistent with this observation, the current Classification Society rules allow the TMCP steels to be furnished to a maximum thickness and yield strength of 50 mm and 500 MPa, respectively.

(Accelerated cooled TMCP line pipe steels with minimum specified yield strength of 550 MPa have been commercially produced but the thickness is typically 25 mm or less.)

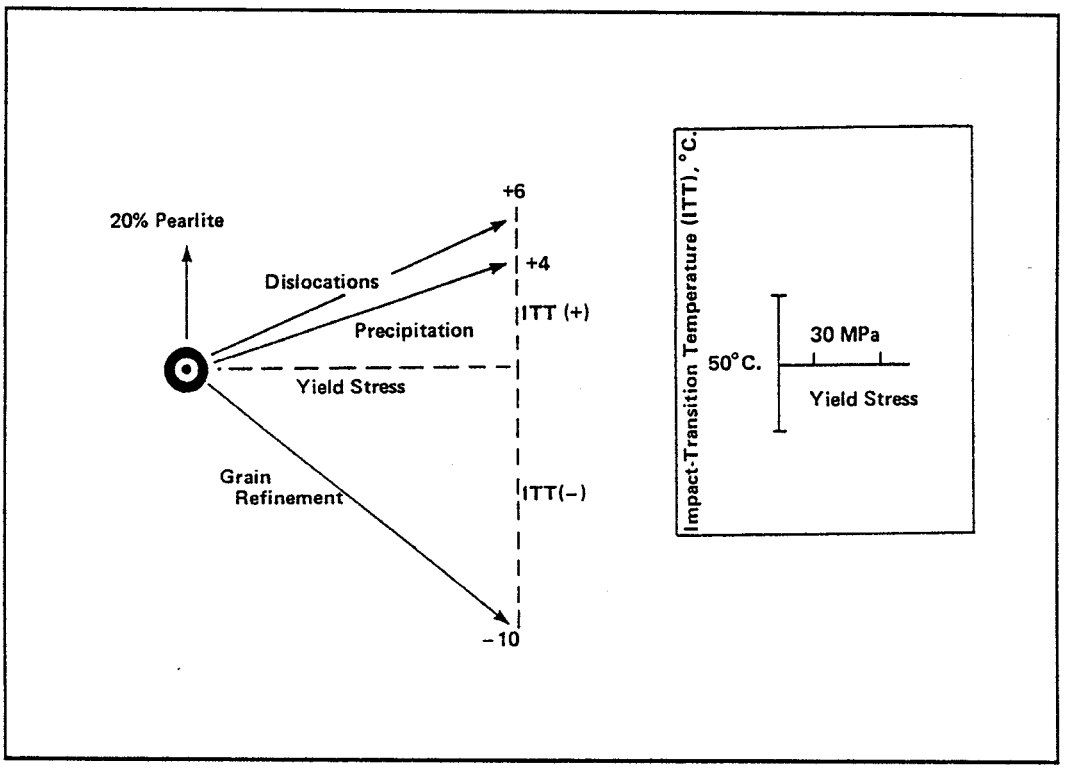

Figure 1.1: Vector diagram showing the influence of various strengthening mechanisms on strength and toughness Ref. [1.1]

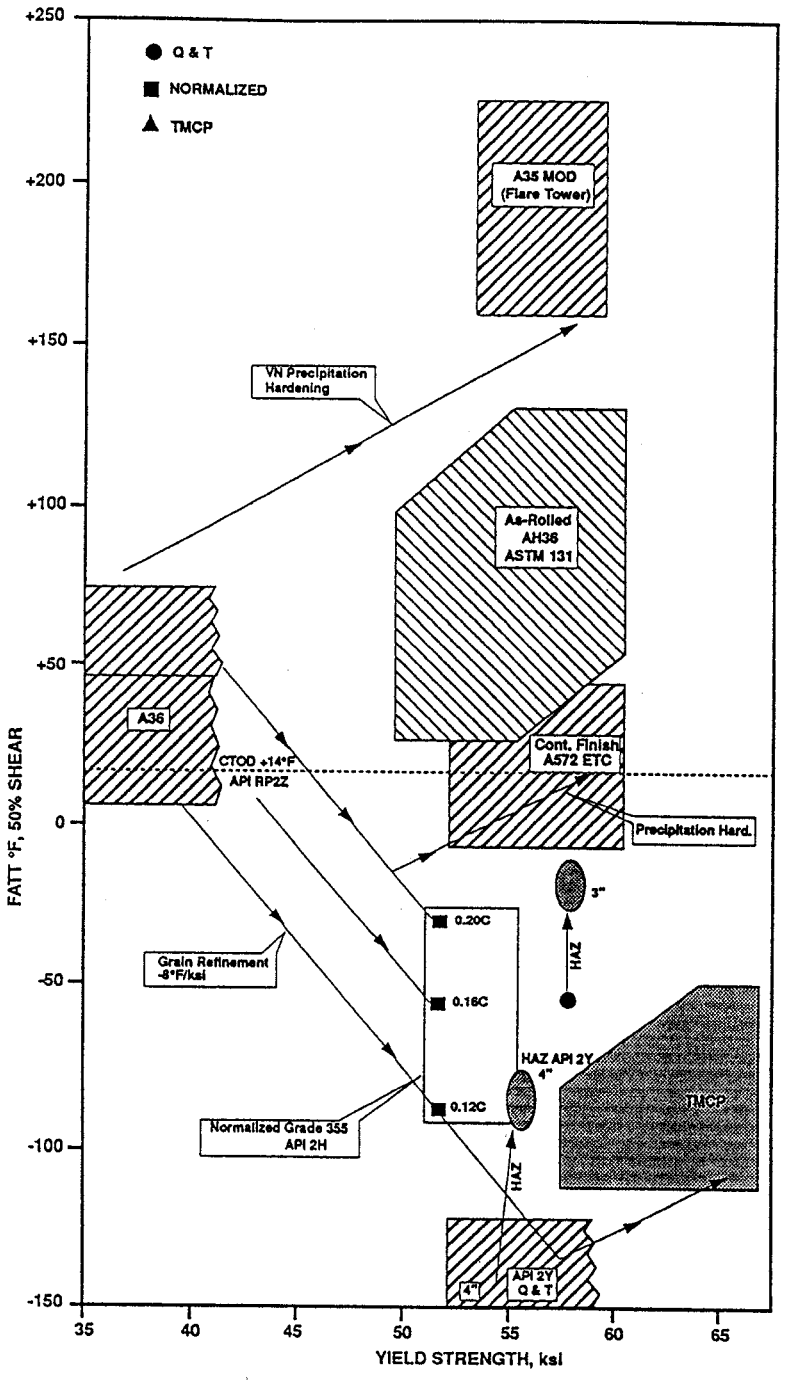

Figure 1.2: Toughness and strength relation for various types of steel Ref. [1.2]

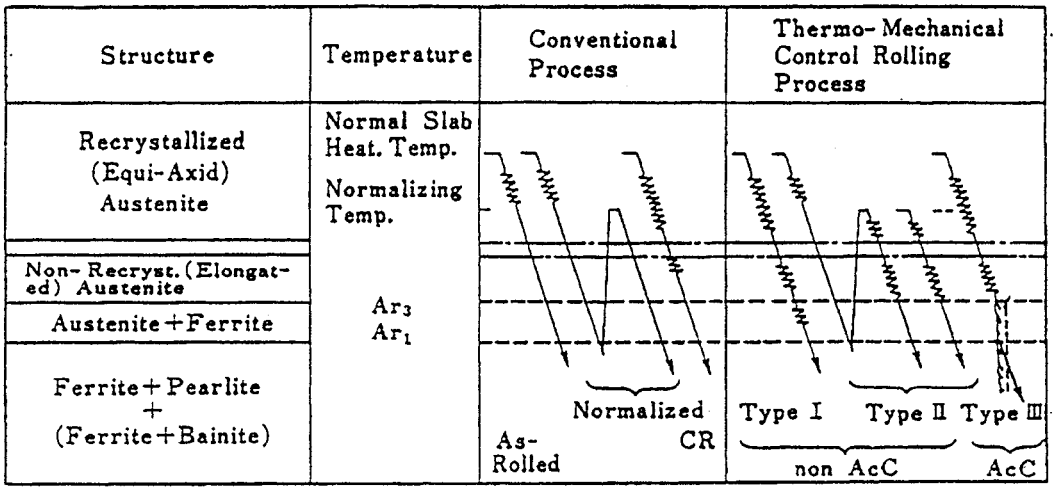

Figure 1.3: Definition of TMCP Steels Ref. [1.4]

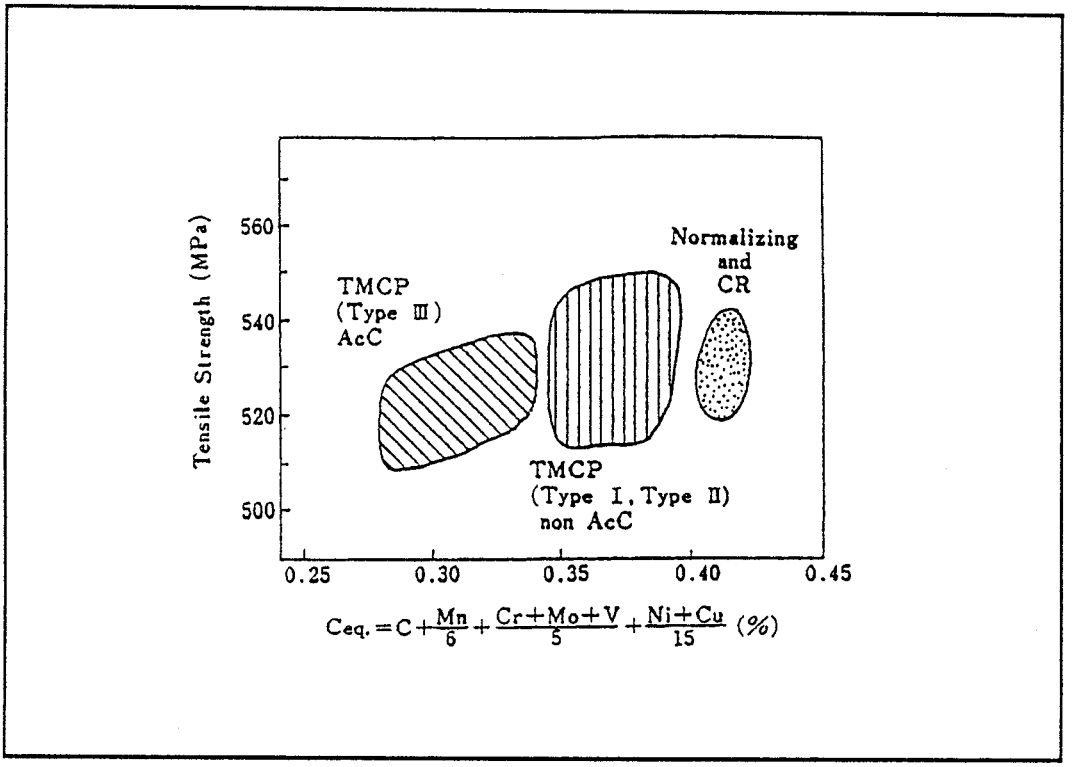

Figure 1.4: Carbon equivalent ranges for steel types Ref. [1.4]

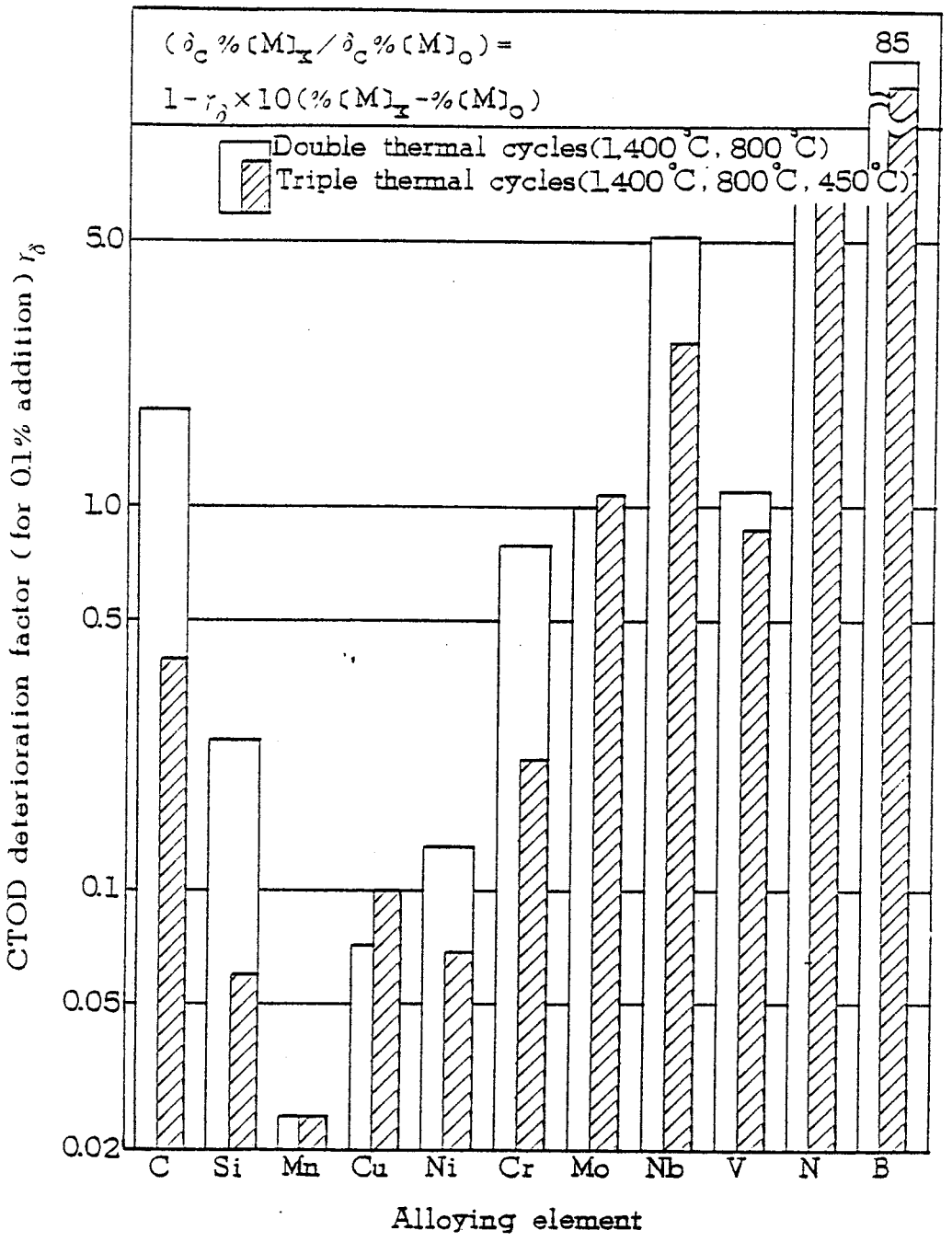

Figure 1.5: Comparison of alloying elements in terms of their effect on HAZ CTOD toughness Ref. [1.12]

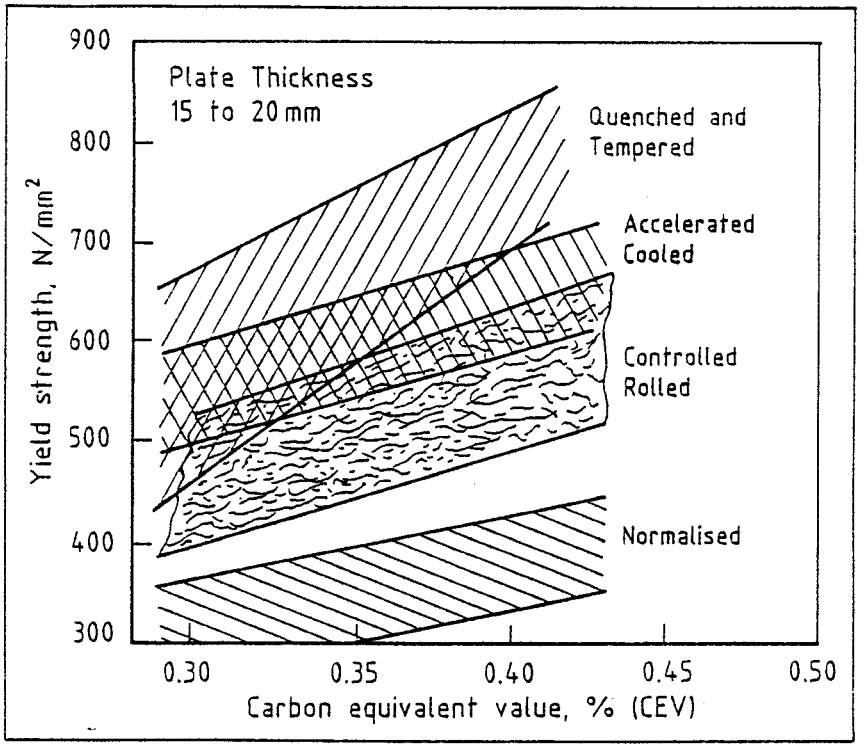

Figure 1.6: **Effect of carbon equivalent value CEV = C + Mn/6 + (Cr + Mo + V)/5 + (Ni + Cu)/15 on yield strength of various grades of steel produced by different processing routes Ref. [1.14]**

2.0 APPROACH

In the first stage of the project, the main focus was collection of as much material property data as possible for both, the base materials and their weldments. The data was obtained mostly from publications in the open technical literature, however, steel makers and users were also approached as were some of the research organizations investigating TMCP steels. Only accelerated cooled steels have been considered in the project and attempt has been made to exclude data obtained from laboratory size melts, i.e., data compiled usually pertains to prototype type or full scale heats made using production facilities. Also, since there has been a continuing development effort in optimizing steel compositions and rolling practices, most of the data collected has been that published in the last eight years or so. Direct quenched steels where the accelerated cooling is at a higher rate and continuous to the ambient temperature rather than being interrupted are also accelerated cooled TMCP steels; however, no significant relevant data on such steels could be found.

Classification Societies were also approached, mainly to obtain an understanding of the "high tensile steel factor (HTSF)" which does not permit the design allowable stress to increase in the same proportion as the steel's minimum specified yield strength above 235 MPa..

A list of persons/organizations who responded to requests for data and technical information is given in **Appendix A**.

The strength and toughness data were compiled in a data base and then analyzed to determine how TMCP steels might influence material specification/qualification and design criteria. In making the recommendations, the approach taken has been to conform to the existing overall philosophy and suggest changes or modifications due to the particular unique characteristic(s) of the TMCP steels.

The material property data represent the resistance side of the resistance - demand design equations, and data analysis can indicate the level of material performance that could be reliably achieved in practice. The data collection and analysis for strength and fracture properties are discussed in Sections 3 and 4, respectively. Potential for taking advantage of these unique properties of the TMCP steels in design (demand side) is discussed in Section 5.

The volume of data relating to fatigue characteristics of TMCP steels and weldments was relatively much smaller and the number of test variables sufficiently large so that no meaningful data base amenable to analysis would have been possible. In Section 6, therefore, the fatigue data from various studies on TMCP steels are discussed individually in comparison with "similar" test data from conventional steels.

Some of the other pertinent issues in the use of TMCP steels are covered in Section 7, and then the salient conclusions and recommendations are summarized in Section 8.

3.0 DATA BASE

As mentioned earlier, the data base focused on the tensile properties of the base material and toughness of the base metal and the heat affected zone. Information regarding steel composition and weld metal toughness achievable with currently available commercial welding consumables were also compiled. The source documents for the data are listed in **Appendix B**. It should be added at this point that a vast majority of the assembled data pertains to steels produced by seven steel producers, viz., Kawasaki, Nippon Steel, NKK, Sumitomo and Kobe in Japan, Rautarukki in Finland and Dillinger Hutte GTS, a subsidiary of Usinor Sacilor Group in France. There are some documents originating from Italy and Germany but the data are very limited.

In all, the base metal and heat affected zone property data has been collected from 58 documents containing information (some detailed and some limited) on 121 steels of different composition and/or thickness. All the data collected from the documents has been summarized in seven Excel spread sheets. Steels of different chemical composition or thickness in the same source document are assigned a different record number which is then the common reference number for that steel in each of the first six spread sheets which summarize base metal characteristics in sheets 1 to 3, and information pertaining to HAZ toughness in sheets 4 to 6. The seventh spread sheet contains the weld metal toughness data.

The information presented in each of the spreadsheets, when available, is as follows:

Sheet 1: source document reference from Appendix B, steel record number, minimum specified yield strength, thickness and chemical composition;

Sheet 2: steel record number, thickness, minimum specified yield and ultimate tensile strengths, actual yield and ultimate strength and corresponding information regarding specimen location with respect to thickness (full thickness, quarter thickness and half thickness) and specimen orientation (longitudinal or transverse) with respect to the dominant rolling direction.

Sheet 3: steel record number, average impact energy absorbed in the Charpy Vee Notch (CVN) test at selected sub-zero temperatures (-40°C, -60°C or -80°C) as a function of specimen orientation (longitudinal or transverse) and location with respect to thickness, Pellini's drop weight nil-ductility transition temperature (NDTT), and base metal crack tip opening displacement (CTOD) toughness and the corresponding test temperatures.

The data on crack arrest toughness properties was rather limited and, therefore, the data collected in a previous project has been combined into that collected here for the purposes of analysis.

Sheet 4: steel record number, thickness and groove shape employed in making the welds.

Sheet 5: steel record number, weld heat input, cross weld tensile strength and the location of the specimen failure (base metal, HAZ or weld metal);

Sheet 6: steel record number, weld heat input and process, CVN test data (specimen location with respect to thickness, notch location with respect to fusion boundary, test temperature, and average and minimum absorbed energies), CTOD test data (all reported values for specimens notched to sample the grain coarsened HAZ, test validity in terms of amount of grain coarsened HAZ sampled if such data was available, specimen size and the test temperature).

The HAZ toughness values have been compiled only when the heat affected zone sampled was along a groove surface perpendicular to the plate surface except when the heat inputs were high enough (usually >10 kJ/mm) to weld the plate in one to four passes, depending on thickness.

Sheet 7: source document number, welding process, welding consumable trade name and designation, welding position, heat input, plate thickness and groove shape , CVN and CTOD test data (specimen location with respect to thickness for CVN specimens, test temperature, average and minimum values for both the toughness parameters).

A hard copy of the assembled data is included in **Appendix C**.

4.0 DATA ANALYSIS

4.1 Base Metal Tensile Properties

Orientation Effect

Tensile properties of steel plates can be dependent on the specimen orientation with respect to the rolling direction. The relationship between the yield strengths measured in the longitudinal and transverse directions was therefore examined first. As seen in **Figure 4.1,** the yield strength in the transverse direction tends to be higher than that in the longitudinal direction, by about 10 MPa. In order to assess the dependence of this difference on plate thickness, the ratio of yield strengths in the transverse and longitudinal directions is plotted against the plate thickness in **Figure 4.2**. The trend line suggests that the difference is more pronounced at smaller thicknesses. (Note: Linear regression lines for the data collected are shown in several figures. However, this has been done solely to assess the trends, and the actual regression equations should be used with caution.)

In conventional (hot rolled, normalized or quenched and tempered) and not so clean steels as those considered here, the yield strength in the longitudinal direction tends to be somewhat higher and that is why standard specifications require tensile tests to be conducted in the transverse direction. The reason for this anomaly is not readily apparent. One potential explanation may lie in texture that can develop in steels involving rolling at relatively low temperatures. Irrespective of the exact reason, it requires consideration of specifying tensile tests in the longitudinal direction rather than the transverse.

Thickness Location Effect

When plate steels cool after rolling (either naturally or due to accelerated cooling), the cooling rate is lowest at the center (mid-thickness) location and progressively higher towards the plate surface. Also, since the TMCP route involves thickness reductions at relatively low temperatures, there is usually a deformation gradient through the thickness during the rolling process. These effects can lead to differences in microstructure development with thickness, often resulting in a larger grain size at the center and consequently, locally inferior mechanical properties.

For yield strength, this is explored in **Figure 4.3** which suggests that yield strength at the mid-thickness locations is indeed lower than that at the quarter thickness position. This difference it seems, can be as large as 50 MPa though more commonly, the difference is less than 20 MPa and seems to be some what smaller at higher yield strengths than at lower. The effect of plate thickness on this difference is examined in **Figure 4.4**. Although there is considerable scatter, the data suggest that the yield strength differential increases with plate thickness, and thus points to the need for full thickness, or mid-thickness tensile tests in addition to those from the quarter thickness location for thick plates.

Yield to Ultimate Tensile Strength Ratio

Also referred to as the yield ratio, it was calculated from all the compiled tensile test results and then plotted against the yield strength as shown in **Figure 4.5**. As expected, this ratio increases with increase in yield strength. In order to compare this data with that in the literature, linear regression line for the data in Figure 4.5 is superimposed on literature data [4.1 to 4.3] in **Figures 4.6(a), (b) and (c)**. The data from literature covers a much wider range of yield strengths, and all types of steels (cast, normalized, quenched and tempered and presumably, TMCP as well) and a visual examination of the location of the trend line from Figure 4.5 in relation to literature data suggests that the TMCP steels tend to have a higher yield ratio for a given yield strength level.

Some steel companies have developed chemistries and processing routes to obtain dual phase ferrite-bainite TMCP steels that have low yield ratio (<0.75) while achieving yield strengths as high as 500 MPa [4.4, 4.5]. However, the chemistries involve higher carbon levels (about 0.15 wt%) that are not conducive to high HAZ toughness.

Several of the structural design codes specify an upper limit for the yield ratio. For example, steels intended for use in gas carriers where the stress relief is performed by proof loading, must have a yield ratio ≤ 0.8. Similarly, design codes for buildings requiring plastic hinge formation, limit the ratio to 0.8 for the steels employed, whereas offshore structural steel and line pipe steels requirements allow the ratio to be 0.85. An average value of 0.85 for the yield ratio would, at present, limit the use of TMCP steels to a yield strength value less than 500 MPa.

At present, specifications for ship structural steels have no upper limit for yield ratio. Nonetheless, it is an important characteristic of the ship structural steels as it influences the absolute safety margin with respect to the design stress (See Section 5.1.2).

The yield ratio is, also indicative of steel's strain hardening behavior which in turn influences the fracture behaviour (R-curve and failure assessment diagram). Unfortunately, in the literature there is no systematic data on the work hardening behavior of TMCP steels and an attempt was therefore made to infer it from the yield ratio. There are various models in the literature to relate the yield ratio to the strain hardening behavior. One of these is based on the Ludwik model of the true stress-true plastic strain behavior of specimens tested under uniaxial tension. According to this model,

$$\sigma = K\left(\varepsilon_p\right)^n \tag{4.1}$$

where σ is the true stress, ε_p is the true plastic strain, K is the strength coefficient and n is the strain hardening exponent. Based on this model, it can be shown that

$$n = \varepsilon_u \tag{4.2}$$

and $$YR = (.00544/n)^n \quad (4.3)$$

where ε_u is the true plastic strain corresponding to the uniform elongation and YR is the yield ratio.

Another empirical model that has been proposed by Reemsnyder [4.6] to relate the strain hardening exponent to the yield ratio is as follows:

$$n = 1.72424 - 6.09797 \times YR + 8.32582 \times (YR)^2 - 3.96535 \times (YR)^3 \quad (4.4)$$

The predicted values of n from the calculated yield ratios, based on the Ludwik and Reemsnyder models are shown plotted against the steel yield strength in **Figure 4.7**, and it is clear that the two approaches predict significantly different values of n for a steel of a given yield strength. However, Reemsnyder's correlation is considered more reliable as it is based on a large data set of strain hardening exponent values that were experimentally determined according to ASTM Standard E646. There were only two documents [4.7, 4.8] in the collected literature that provide values for n for comparison, and these along with the predicted values from the models are as follows:

Yield Strength, MPa	Yield Ratio	Measured n	n from Ludwik Model	n from Reemsnyder Model
430	0.86	0.24	0.06	0.12
446	0.82	0.06	0.075	0.14

The measured "n" values are, however, outside the range of both the correlations mentioned above. The authors of these papers did not report how the "n" values were computed. Also, for the steel with a yield ratio of 0.82, the stress-strain curve showed a uniform elongation of about 15% which makes the reported "n" value suspect. It is clear, therefore, that no reliable data about the strain hardening behaviour of TMCP steels is available at this time. Furthermore, in one of the documents published by NKK Corporation [4.9], the uniform elongations measured have been from about 24 to 50% for TMCP EH36 steels, depending on the specimen dimensions. As seen in **Figure 4.8**, for a standard 12.7 mm diameter specimen with a 50 mm gauge length, the expected uniform elongation for the steels tested would be about 35% which in turn, based on the Ludwik model, would imply n values of about 0.3. Such high n values for ferritic steels are rare, and clearly there is a need for further assessment of strain hardening and uniform elongation properties of TMCP steels. Conceivably, the uniform elongation depends more strongly on the steel cleanliness and work hardening rate on the relative magnitudes of the yield and tensile strengths, and the Ludwik model may not describe the true stress-true strain behavior of modern clean steels such as the TMCP steels.

Actual vs Specified Minimum Yield Strength

Statistical variation in the actual strength properties of the steel is an important input for reliability based design and probabilistic structural analysis. Also, one of the concerns expressed in structural applications of high strength TMCP steels has been their potentially higher yield strength in relation to the specified minimum which, with the use of the same welding consumables as in pre-established practice, can now increase the probability of unintentionally undermatched weld metals.

Therefore, in order to assess the yield strength variation of TMCP steels, the difference between the actual and specified minimum yield strengths (SMYS) was plotted in the form of a histogram for steels with SMYS in the ranges 330 to 360, 380 to 420, and 440 to 500 MPa. As seen in **Figure 4.9**, the mean yield strength seems to be higher than the SMYS by about 60 to 70 MPa for steels with less than 420 MPa SMYS, and by about 50 MPa for 440 to 500 MPa SMYS steels.

Huther et al [4.10] have also examined the statistical characteristics of the yield strength distribution of marine structural steels with SMYS in the range 315 to 420 MPa. Based on the statistical information provided by the authors, the relative frequency of yield strength differential (i.e., actual yield strength - the specified minimum) for steels with SMYS of 345 and 400 MPa are plotted in **Figure 4.10** and compared with that for TMCP steels.

The marine structural steels with SMYS of 345 and 400 MPa correspond to the mid points of the 330 to 360, and 380 to 420 MPa yield strength ranges of the TMCP steels. The higher strength marine steel (400 MPa) appears to provide a smaller yield strength differential than the corresponding range (380 to 420 MPa) of TMCP steels. Both the 345 and 400 MPa marine steels appear to present a higher level of variability in yield strength as illustrated in **Figure 4.10** and in the table below which compares their respective coefficients of variability.

	Coefficient of Variation (COV)	
	330 to 360 MPa	380 to 420 MPa
TMCP	7.5 %	5.2 %
Marine Steels (Huther et. al.)	8.0 %	8.0 %

Through Thickness Ductility

Lamellar tearing can be a concern in restrained T and cruciform welded joints. To avoid such possibilities, the material specifications invariably ask for a minimum of 25% (Classification Rules) to 35% (offshore structures) reduction in area for tensile specimens extracted in the through thickness orientation. Several of the collected documents report these values which, due to the clean steel technology employed, are typically much higher. Thus, the lowest % reduction in area value seen in one of the documents was 55%; however, a vast majority of the reported values were greater than 70%, indicating that lamellar tearing should not be a concern with TMCP steels.

Nonetheless, due to texture development and resulting anisotropy in mechanical properties, splits parallel to the original plate surface can still be occasionally seen in tensile or toughness tests in the upper shelf region. However, based on through thickness tensile tests with continuous notch/thread along the specimen gauge length to evaluate their significance, Zettlemoyer concluded [4.11] that splitting was not structurally significant.

4.2 Base Metal Toughness Properties

A majority of steel specifications require Charpy V-notch (CVN) impact tests to be carried out on the steel to provide a measure of its notch toughness. Usually a minimum absorbed energy, whose value depends on steel yield strength and specimen orientation, must be met at a specified test temperature. In addition, the CVN tests provide a useful indication of the variation in properties within and between plates, i.e., they serve a purpose as a quality control tool separate from their function as a measure of toughness.

Data on TMCP steels shows that CVN results are usually well in excess of the minimum specified. In many cases the CVN results show upper shelf behavior with energy values of 200-300 J at the specified temperature. In **Figure 4.11**, the CVN 50% fracture appearance transition temperature (50% FATT) in the transverse direction at the quarter thickness position is shown plotted against yield strength for a range of TMCP steels from the present data base. **Figure 4.12** shows the 50% FATT plotted against thickness.

There are a few data points in these figures representing transition temperatures higher than -60°C, however, these are all for samples extracted after strain aging the steel. The data compiled in the data base indicates that after 5% strain followed by strain aging at 250°C raises the transition temperature by up to 35°C, the average value being 24°C. Otherwise in the as received condition, all the steels in the data base had transition temperatures below -60°C, and some steel manufacturers can achieve transition temperatures lower than -100°C, even in the higher strength grades and larger thicknesses.

Effect of Charpy Specimen Position

Most specifications require the Charpy impact specimen to be taken from a position midway between the plate surface and the center, i.e., the t/4 position. Allowing for the usual 0.5 mm between the surface of the plate and the top machined surface of the specimen, the true t/4 position would only be sampled in plates greater than 22 mm thickness. Some standards, such as CSA S473, call for impact tests at the t/2 position which was a deliberate requirement to check for centerline segregation and adequate properties throughout the thickness. Also, as mentioned before, the cooling rate variation with respect to thickness can lead to lower toughness at the mid-thickness location.

To examine the effect of specimen position in TMCP steels, the difference in the 50% FATT between the t/2 and the t/4 positions has been determined for the TCMP steels where both positions were tested in the same plate. The results are plotted in **Figure 4.13** as a function of the plate thickness. The data includes specimens in both the longitudinal and transverse orientations. The figure shows that in most cases the t/2 position has a higher transition temperature than the t/4 position by an amount ranging up to 35°C. Interestingly, the effect of thickness is quite variable and presumably depends on the processing parameters selected by individual steelmakers.

Effect of Charpy Specimen Orientation

Charpy impact specimens with their length parallel to the rolling direction (longitudinal specimens, L) generally show a higher absorbed energy than those taken transverse (T) to the rolling direction. Traditionally, longitudinal specimens have been specified with transverse specimens only being required for those applications where the plate was stressed in the transverse direction. For example, in a pressure vessel the shell plates formed with the rolling direction in the hoop direction only require longitudinal tests whereas the 'petal' plates of a fabricated head, stressed in all directions, require longitudinal and transverse tests. To account for the differences in toughness due to orientation, Classification Societies call for an impact energy in transverse specimens that is 2/3 that in longitudinal specimens.

With the very low sulfur levels of modern clean steels, the difference between properties in the longitudinal and transverse directions diminishes and this has led to some standards (e.g., CSA S473) specifying only transverse specimens. The effect of specimen orientation in the present study has been examined by determining the difference in the 50% FATT between the L and T directions.

The results are plotted in **Figure 4.14** as a function of plate thickness. Notwithstanding the scatter in the data, its linear regression indicated a general trend of decreasing difference with increasing plate thickness. In thinner plate, with extensive final reduction during rolling, the longitudinal properties are significantly better than those transverse. However, in thicker material where a cross-rolled plate may receive only a small final reduction in rolling, the transverse CVN properties may actually be better than those in the longitudinal direction.

NDTT and Relation with CVN Properties

Classification Societies usually retain the option to call upon additional toughness tests beyond the CVN impact testing. The Pellini's drop weight test to determine the Nil-Ductility Transition Temperature (NDTT) is one such test and it is, in fact, specified in a number of standards such as API 2W and CSA S473 for the qualification of the steel. The drop weight test essentially measures crack arrest properties i.e., the ability of the steel to arrest a small running crack initiated in a brittle region at the dynamic yield stress. The NDTT, as determined by the drop weight test therefore, has real physical significance as a measure of fracture behavior. A histogram of all the NDTT values compiled in the data base is therefore presented in **Figure 4.15,** and it shows that most steels have an NDTT of -60°C or lower, and that an average value for all the steels is about -80°C. (The bar at -55°C represents data points satisfying -50°C≥NDTT >-55°C. It should also be added that some of the data is for specimens extracted from quarter and half thickness locations).

As an alternate material toughness specification approach, it is of interest to examine the relation between NDTT and CVN properties. In **Figure 4.16**, the NDTT values from the data base are plotted against the corresponding 50% FATT determined from the CVN tests. The data show that the NDTT is consistently higher than the 50% FATT and that the difference seems to increase as the 50% FATT decreases. A similar trend has been earlier observed in a study by the ISIJ (Iron and Steel Institute of Japan) as quoted by Kurihara et al. (4.12) and shown in **Figure 4.17**. Here, the NDTT is plotted against the Charpy Vee Notch energy transition temperature (vTe; the energy value is not specified) for a wide range of steel types, and although the scatter is large, there is a correlation represented by the equation.

$$\text{NDTT } (^{\circ}\text{C}) = 0.65\ \text{vTe} - 11.5 \quad \text{(correlation coef: 0.81)} \tag{4.5}$$

The authors conclude from this that there is an increasing shift between NDTT and vTe as the temperature decreases which they summarize as:

$$\begin{aligned} &\text{NDTT} > -33\ ^{\circ}\text{C} \quad &&: \text{NDTT} < \text{vTe} \\ &\text{NDTT} = -33\ ^{\circ}\text{C} \quad &&: \text{NDTT} = \text{vTe} \\ &\text{NDTT} < -33\ ^{\circ}\text{C} \quad &&: \text{NDTT} > \text{vTe} \end{aligned} \tag{4.6}$$

An alternative explanation to this behavior has been proposed by Graville & Tyson [4.13] following a study during the development of the Canadian standard for offshore structures. They noted that a close correlation existed between NDTT and vT40 (40 J transition temperature) for older steels that were characterized by their carbon and sulfur content (wt % (10S + C) > 0.25)). The newer, clean steels with very low carbon and sulfur showed increasing differences between the NDTT and the 40 J transition temperature. **Figure 4.18** is taken from the earlier study and shows the CVN energy at the NDTT as a function of wt % (10S + C). In **Figure 4.19**, the difference between the NDTT and the 40 J transition temperature is shown. Although there is substantial scatter these results show that any correlation between CVN and NDTT is dependent on the steel type as expressed by the wt % (10S + C) level.

In **Figure 4.20**, NDTT is plotted against vT40 only for those steels with wt % (10S+C) >0.25 and a good correlation is observed. In comparison, all the steels in Figure 4.16 have compositions such that wt% (10S+C) <0.15 and consequently, the 50% FATT is generally well below the NDTT and the 40J transition temperature would be a bit further below.

It thus appears that the slope of the line determined from the ISIJ data may not be an effect of temperature directly but rather the result of the older steels having a higher transition temperature and NDTT. In order to achieve the low transition temperature in modern steels, very low carbon and sulfur levels have been used which increases the shift between NDTT and Charpy transition. The effect does not appear to be related to the use of TMCP per se but clearly its use permits a lower carbon.

These observations are of special significance when introducing TMCP steels into applications for which standards and specifications only require CVN testing. Many of the CVN requirements are based on correlation established with older steels that usually had wt % (10S+C) >0.25. These include API RP2A requirements for offshore structures which are based on the original Pellini fracture analysis diagram and the AASHTO bridge steel requirements based on correlation between CVN and K_{1c} tests at dynamic and intermediate strain rates.

The minimum CVN requirement of these specifications, if applied to a modern, clean, TMCP steel, would not necessarily provide the same implied fracture behavior. This is not to say these steels are not suitable for these applications. CVN requirements are usually comfortably exceeded and other fracture tests may demonstrate adequate properties. Rather, the minimum CVN requirements, in themselves do not assure the same fracture behavior with modern clean steels as they did with the older steels. For this reason, where some assurance of crack arrest behavior is required, some recent standards have specified the Pellini's drop weight test in addition to Charpy tests.

The NDTT is determined following the ASM Standard E208 [4.14] which states that the result is insensitive to the specimen orientation with respect to the rolling direction. It is only in one document [4.15] obtained in this study that the effect of specimen orientation on the NDTT was examined, and for the accelerated cooled, Cu bearing age hardenable steel investigated, the NDTTs differed by 15°C for the two orientations , -70°C for the longitudinal and -85°C for the transverse orientations. Unfortunately, this document does not report if the CVN properties were also superior in the transverse direction since the main trend of the data in Figure 4.14 is the opposite, i.e., CVN toughness is superior in the longitudinal orientation. The orientation dependence of the NDTT for TMCP therefore needs further study.

Initiation Fracture Toughness and Relation with NDTT

The initiation fracture toughness of TMCP steels has been evaluated using either the small scale CTOD tests or the larger wide plate tests, the latter conducted almost entirely in Japan. However, the volume of fracture toughness data available is quite limited.

For fracture toughness data based on small scale tests, only 14 of the 121 steels documented in the data base have their CTOD fracture toughness reported at limited number of test temperatures (-10° to -100°C), all at a quasistatic loading rate. All the reported average values, except one (0.7 mm), at test temperatures of -60°C or higher, are greater than 1 mm.

The fracture toughness data for TMCP steels at elevated loading rates is even more sparse. A recent study [4.16] at Fleet Technology Limited, however, did examine this aspect for several steels including two TMCP steels and the results obtained for the latter are shown in **Figures 4.21 (a)** and **(b)**. The intermediate and impact loading rates in these tests corresponded to strain rates of 5×10^{-2} and 5 s^{-1}, respectively (stress intensity factor rates of 6.54×10^{3} and 6.54×10^{5} MPa$\sqrt{m}$ s^{-1}). Between the quasi-static and impact loading rates, the shift in transition temperature corresponding to 0.2 mm CTOD toughness is about 45°C for the 20 mm, nominally 440 MPa yield steel. Similarly, for the 50 mm thick EH36 modified steel, the increase in 0.2 mm CTOD toughness transition temperature from a quasi-static to an intermediate loading rate is about 50°C. However, even at the elevated loading rates examined, the 0.2 mm CTOD transition temperature is -45°C or lower for the steels tested.

The above referenced study [4.16] examined the elevated loading rate CTOD toughness values for other conventional steels (hot rolled, normalized) as well, and attempted to relate it to CVN properties and the NDTT. Though no correlation could be found with CVN properties, one could be established with respect to the NDTT. Thus, **Figure 4.22 (a)** shows the CTOD toughness transition curve referenced to the NDTT for the 20 mm TMCP, nominally 440 MPa yield steel (NDTT = -85°C) and a 25 mm thick, normalized steel (NDTT = -40°C). **Figure 4.22 (b)** shows similar data for the 50 mm thick EH36 modified TMCP and a normalized steel with NDTTs of -55° and -35°C, respectively. It is clear that on an absolute temperature scale, the transition curves for TMCP and normalized steels would be quite apart; however, referencing the temperature with respect to the steel's NDTT leads to similar transition curves for the two types of steels. Based on such results, the authors go on to suggest a relationship between the 0.2 mm CTOD transition temperature and the NDTT (**Figure 4.23**) according to which one should be able to achieve 0.2 mm CTOD at intermediate and impact loading rates at test temperatures corresponding to (NDTT + 5°C) and (NDTT + 20°C), respectively.

As mentioned above, wide plate tests [4.17] have also been employed to assess the initiation fracture toughness of TMCP steels. The specimen size is typically 500 mm x 400 mm and contains a 160 to 240 mm long center notch with ends sharpened with a 0.1 mm saw (**Figure 4.24**). The tests are conducted at a quasistatic loading rate, and the results are plotted as K_c (a pseudo linear elastic fracture toughness parameter estimated from the peak load attained in the test and the initial notch size) versus the reciprocal of the test temperature in Kelvin (**Figure 4.25**). Invariably, maximum load behavior is observed for test temperatures higher than -100°C.

Crack Arrest Properties and Relation with Other Properties

A number of different tests have been used to assess crack arrest properties of steels. These include wide plate tests, such as the Esso and double tension tests (**Figure 4.26**), and small scale tests such as the compact crack arrest test (**Figure 4.27**). Results from all types of test for a variety of steels assembled in a previous study [4.18] are shown in **Figure 4.28** plotted against the difference between the test temperature and the CVN transition temperature (50% FATT). Although there is a general trend of increasing crack arrest toughness as the temperature increases above the CVN transition temperature, the scatter is very large and the CVN test would not appear to give a reliable indication of crack arrest toughness.

The data in this figure, however, are from many types of tests and these do not necessarily measure the same quantity. The temperature gradient double tension test and the Esso test have been widely used in Japan to measure the crack arrest parameter K_{ca}. This quantity is determined from the stress and arrested crack length by static analysis but is not necessarily the same as the plane strain crack arrest toughness K_{1a} determined from a compact crack arrest test. In the double tension test crack arrest occurs under essentially plane stress conditions resulting from a large plastic zone size. K_{ca} values, therefore, usually show a steep transition, rising more rapidly with temperature than K_{1a} values.

Data for double tension and Esso tests are shown in **Figure 4.29** where again large scatter is observed when K_{ca} is plotted relative to the CVN transition temperature. **Figures 4.30** and **4.31** show the data separated on the basis of whether the steel was TMCP (accelerate cooled) or not. Because of the large scatter it is not possible to draw any firm conclusions from these graphs but there is the suggestion that the curve for TMCP steels is shifted to higher temperatures indicating a lower CVN transition temperature would be required to provide the same K_{ca} value.

Crack arrest toughness K_{ca} values for 320-355 MPa yield strength ship steels have been summarized in Reference 4.19 and are shown in **Figure 4.32**. The results show a substantial improvement in K_{ca} for TMCP steels, except for some accelerated cooled steels, over conventional normalized steels. The two dotted lines at 400 and 600 Kgf.$\sqrt{}$mm/mm2 (124 and 186 MPa$\sqrt{}$m) are two specific crack arrest toughness criteria based on analysis of ship fractures. Results for 392 MPa yield strength ship steels [4.20] are shown in **Figure 4.33**.

The superior crack arrest performance of some TMCP steels has been related to the phenomenon of splitting. As the crack propagates, the steel splits along a plane parallel to the plate surface at the mid-thickness. Splitting reduces the through-thickness constraint and enhances crack arrest. Splitting is more common in the non-accelerated cooled steels that receive significant rolling reduction in the two phase temperature range. The tendency to splitting has been characterized by a splitting index, SI, and the effect of SI on the K_{ca}=186 MPa$\sqrt{}$m transition temperature is shown in **Figure 4.34** [4.21].

K_{ca} data for a wide range of steels including recent TMCP steels has been analyzed by regression analysis to determine the T124 and T186 transition temperatures for K_{ca}=124 and 186 MPa$\sqrt{m}$ respectively. Since wide plate tests to determine K_{ca} are expensive and are not normally specified, it is of interest to examine the relation between K_{ca} and other conventional toughness tests. This gives some indication of the crack arrest capability provided by existing specifications using conventional tests. In **Figures 4.35** and **4.36**, the T124 and T186 values calculated from regression analysis have been plotted against the 50% CVN FATT. A general correlation is observed with T124 about 50°C above the FATT, but scatter is significant.

When T124 and T186 are plotted (**Figures 4.37** and **4.38**) against the NDTT, the scatter is reduced and a good correlation is observed with T124 about 20°C above the NDTT and T186 about 40°C above the NDTT. It is of interest to compare these results with the original Pellini fracture analysis diagram which shows the FTE (fracture transition elastic) about 35°C above the NDTT.

Summary Base Metal Toughness

The relationships between the various measures of toughness discussed above suggest that an NDTT requirement (Drop Weight Test) is better than a CVN requirement for base metal toughness specification since the former gives an indication of the initiation and arrest fracture toughness of the material. Thus, at NDTT + 20°C, the dynamic initiation (CTOD) toughness and crack arrest toughness of the steel are expected to be about 0.2 mm and 124 MPa$\sqrt{m}$, respectively; at NDTT + 40°C, the crack arrest toughness, K_{ca}, is expected to be 186 MPa$\sqrt{m}$, a value suggested by NKK to be sufficient to arrest cracks based on analysis of ship fractures. (For example, for EH grades of steels, an NDTT temperature of -40°C (same temperature as that specified for conducting CVN tests) would ensure K_{ca}=186 MPa $\sqrt{m}$ at 0°C, the design temperature for ships.

Adoption of a crack arrest criterion for material toughness may have important implications for damage tolerance since the limit to fatigue crack growth is then likely to be structural or plastic instability or leakage, etc., rather than brittle fracture.

4.3 HAZ Toughness Properties

CVN Toughness

The heat affected zone represents a region of great microstructural heterogeneity and the toughness measured depends on the steel composition, the thermal cycle (plate thickness, heat input), the test technique as well as the notch location with respect to the fusion boundary. Usually, the lowest toughness is recorded for the grain coarsened heat affected zone, adjacent to the fusion boundary and the data analysis here therefore focuses on results obtained from specimens notched at this location. For ease of presentation, the data has been plotted as the average absorbed energy in a set of three specimens versus the test temperature for three ranges of weld heat input (3.0 kJ/mm or less, greater than 3.0 kJ/mm and up to 7 kJ/mm, and finally,

equal to or greater than 10 kJ/mm). Any effects that might result due to differences in the thickness of the steel welded or due to the location of the CVN specimen with respect to the plate thickness (subsurface, quarter thickness, mid-thickness or root) have been ignored.

As seen in **Figures 4.39** and **4.40**, at heat inputs up to 7 kJ/mm, a vast majority of the average values are significantly greater than 50J at test temperatures as low as -60°C. When the heat input is 10 kJ/mm or greater, the data base is smaller (**Figure 4.41**) and at -60°C, there is a cluster of data points at about 50 J absorbed energy. To assess the lower bound CVN absorbed energy, the minimum value at -60°C in any data set is plotted against the weld heat input in **Figure 4.42**. It confirms that a large proportion of the steels that form the data base are likely to easily meet typical fusion line CVN absorbed energy specifications (27 to 50 J) down to temperatures of -60°C as long as the heat input is maintained below 7 kJ/mm.

Recently, Barnes et al [4.22] observed some instances of low CVN absorbed energies at the "Fusion Line + 5 mm" (FL5) location of the HAZ which for the heat inputs employed in offshore structure fabrication would correspond to the subcritical HAZ. The authors suggest the underlying reason to be analogous to increase in CVN transition temperature due to strain aging. They further suggest that TMCP steels may be more prone to this type of embrittlement than the quenched and tempered steels, as the increase in 36 J transition temperature due to strain aging for the two TMCP steels examined by them were 40°C and 72°C compared to 38°C for the quenched and tempered steel. The respective increases in the transition temperature at the FL5 location were 29°C, 60°C and 11°C. (In the data base compiled for the project, the largest increase in transition temperature due to strain aging was reported to be 35°C.)

In order to see if the HAZ data collected in this project supports this scenario, the average CVN energy for specimens extracted from the FL5 or subcritical HAZ (SCHAZ) locations were plotted against the test temperature and compared with similar data for the respective base metals. As seen in **Figure 4. 43**, there is trend towards decrease in absorbed energy/increase in transition temperature though the changes can not be reliably quantified. A similar plot using the minimum absorbed energy at the FL5/SCHAZ location is shown in **Figure 4.44** and since the variation in base metal CVN energy at any temperature is usually small, it shows the potential for degradation in the CVN toughness in this region of the HAZ. The limited data thus supports the need for continuous HAZ CVN testing at the FL5 location.

CTOD Toughness

Much of the recent development work on TMCP steels has focused on achieving good CTOD properties in the HAZ. The CTOD test has been widely applied for offshore structures as a means of assuring resistance to fracture initiation from welds. The test is characterized, however, by large scatter and when applied to the heat affected zone with its heterogeneous structure, very low CTOD values are often recorded. The frequent occurrence of low CTOD values makes it difficult to meet specified values, and considerable effort has been expended to understand the cause.

The low values are generally associated with "local brittle zones" i.e., small regions of low toughness, which result in low CTOD's when they occupy 15% or more of the specimen crack front. Specifications, such as API RP2Z, have strict specimen examination requirements to ensure the sample detects local brittle zones. The identification of the causes of local brittle zones and the effects of steel chemistry and processing have resulted in steels with much improved HAZ CTOD toughness.

Considerable quantities of steels have been supplied with HAZ fusion line CTOD requirements (typically 0.2 or 0.25 mm) at -10°C (and -15°C for Hibernia). Consequently, there is a fair amount of data in the literature at this test temperature. The CTOD properties of the heat affected zone depend on the heat input of the welding process and this may place a limit on the type of process that can be used. In ship building operations, high heat input, one-sided welds are used. For many offshore structures, however, the heat input in fabrication does not exceed 5 kJ/mm. Results from analysis of the present data base are shown in **Figure 4.45.** The CTOD plotted is the minimum value reported in each data set for tests at -10°C. The data base includes various types of steel but the results illustrate the difficulty of achieving high CTOD values with very high heat input welds.

There is not extensive experience of commercial steel supply with HAZ CTOD toughness requirements at much lower temperatures. Still, based on CTOD tests carried out at lower temperatures, the steel companies in Japan claim that steel (up to 420 MPa yield strength, and 60 mm thickness) can be supplied to meet coarse grain HAZ CTOD requirement of 0.1 mm as long as the heat input is kept below 5 kJ/mm (see **Figure 4.46**). This level of CTOD toughness at the design temperature is suggested by Yajima et al [4.23] to be adequate for ship structures with structural redundancy and arctic marine structures which are usually statically loaded.

The HAZ fusion line CTOD data at lower test temperatures compiled in the project are summarized in **Figures 4.47 to 4.49**, for the three heat input ranges selected. The data suggest that sourcing steels to meet 0.1 mm CTOD at fusion line should be quite feasible, especially if heat input is 7kJ/mm or lower. At -50°C, however, it may be difficult to reliably achieve the target 0.1 mm value.

Significance of HAZ CTOD Toughness vis-à-vis Structural Integrity

There has been considerable effort to study the relation between CTOD toughness values in the conventional three point bend tests with large scale fracture performance. There is a strong body of opinion that current CTOD requirements are overly conservative and too restrictive. One approach has focused on crack arrest properties of the steel, arguing that initiation from a small local brittle zone is inconsequential if the surrounding material is capable of arresting the crack. Other work has concentrated on comparing CTOD results with behavior in slowly loaded wide plate tests. During the 1980's, the preferred test was a plate 400 mm wide plate with a center crack of 2a=240mm loaded in tension. The results of the test are expressed as K_c, the apparent fracture toughness as calculated from the crack size and fracture stress using linear elastic fracture mechanics and then assuming that its dependence on temperature can be described reasonably well by the relation

$$K_c = K_o \exp -1/T(K) \qquad (4.7)$$

Some results of K_c from the deep notch wide plate test have been analyzed to determine the transition temperature for K_c=155 MPa$\sqrt{m}$ and the results are shown in **Figure 4.50** plotted against the estimated transition temperature for a CTOD of 0.1 mm. The data base is rather small and although a clear trend exists, the scatter is large.

Toyoda [4.24] has used statistical analysis to show the relation between small scale CTOD tests and large scale behavior and his results are summarized in **Figure 4.51**. An important aspect is the relation between bending CTOD and tension CTOD coupled with the effect of crack depth. Both experiments and finite element analysis of crack tip stresses show that critical CTOD's in a typical, tensile loaded application would be higher than those in the small scale three point bend test.

In recent years, surface notched wide plate tests have been done to demonstrate large scale fracture behavior and these often show general yielding behavior before fracture despite low CTOD's in the three point bend test. However, the limitations of these wide plate tests in revealing large scale behavior, have recently been discussed by Spurrier [4.25].

4.4 Weld Metal Toughness

The weld metal toughness data available in the literature (from consumable manufacturers, weld procedure qualification records, and other independent investigations) have been generated mostly in the context of offshore structures which means that heat inputs are limited to about 5 kJ/mm. The average CVN absorbed energies and CTOD toughness values in a set of specimens tested from weld metals deposited using the shielded metal arc (SMA) gas metal arc (GMA), flux cored arc (FCA) and single and multiwire submerged arc (SA) (heat input < 5 kJ/mm) welding processes are summarized in **Figures 4.52 to 4.55**. (The data points are intentionally plotted at 2°C higher than the actual test temperature for SMA and SA processes for the sake of clarity.) These figures indicate that better toughness is achievable with the GMA and SA welding processes than with SMA or FCA welding processes.

Nonetheless, consumables seem available for all of the above-mentioned welding processes that could meet the requirements of 40 J CVN absorbed energy at -60°C and 0.2 mm average CTOD toughness to at least -15°C, if not lower.

In the context of ship structures, toughness data from Japanese steel producers is available for weld metals deposited using high heat input multiwire submerged arc and electrogas welding processes. The welding consumables for these processes are made by Kawasaki Steel, Kobe Steel and Nippon Steel and the data indicate that for weld heat inputs in the range 10 to 20 kJ/mm, 40 J CVN toughness could be comfortably met at -40°C, and occasionally at -60°C as well. Weld metal CTOD toughness have also been determined in joint investigations by Kawasaki Steel and Mitsubishi Heavy Industries and average CTOD values as high as 1.5 mm (minimum 1.2 mm) at -50°C have been recorded [4.23, 4.26] for a weld heat input of 19.3 kJ/mm though a more typical value may be 0.39 mm average (0.135 mm minimum) for a weld heat input of 20.2 kJ/mm [4.27]. The toughness values seem to be inferior at a heat input of 14.2 kJ/mm (4.23) and it is probably related to the weld metal solidification pattern and macrostructural aspects.

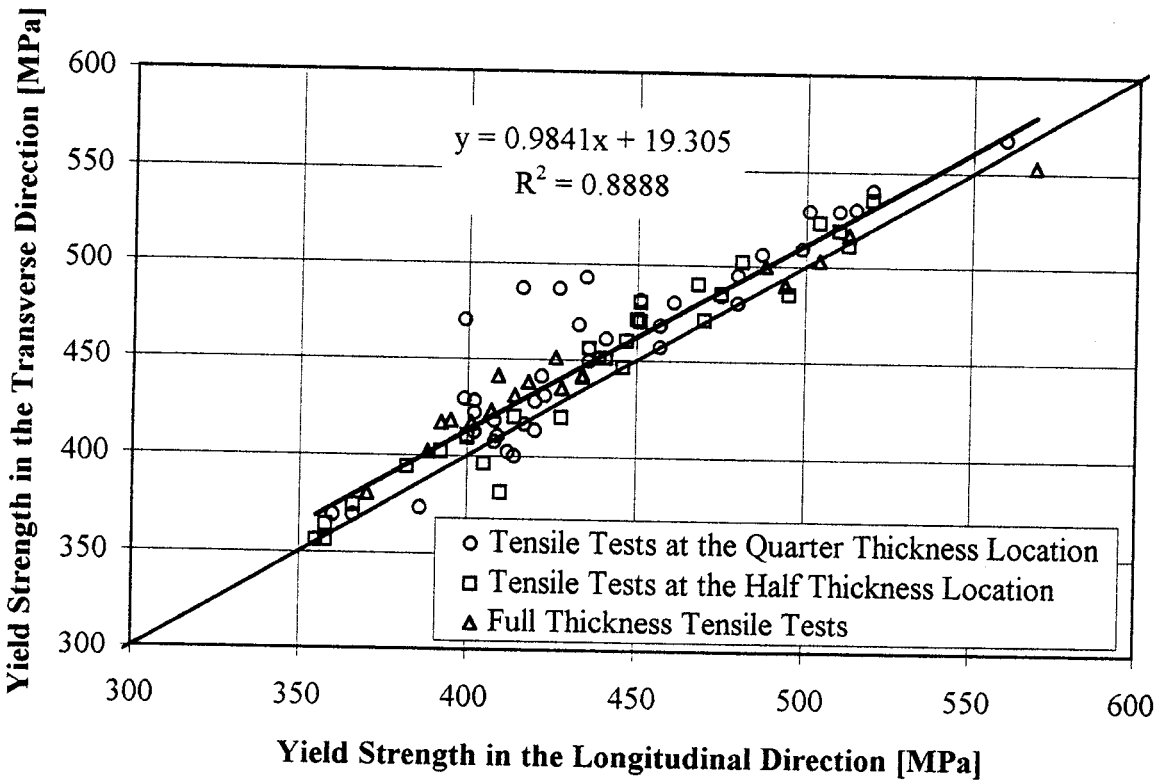

Figure 4.1: Yield strength in the transverse direction versus that in the longitudinal direction for TMCP steel plates

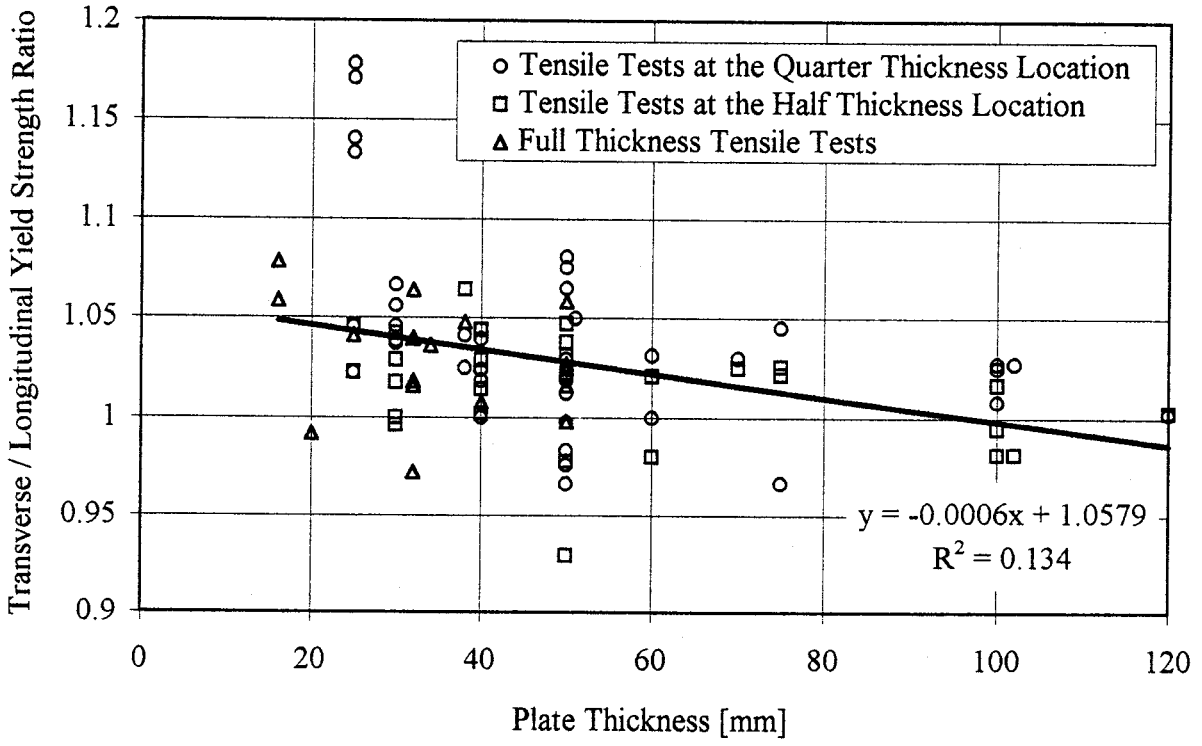

Figure 4.2: Ratio of the yield strength in the transverse direction to that in the longitudinal direction versus the TMCP steel plate thickness

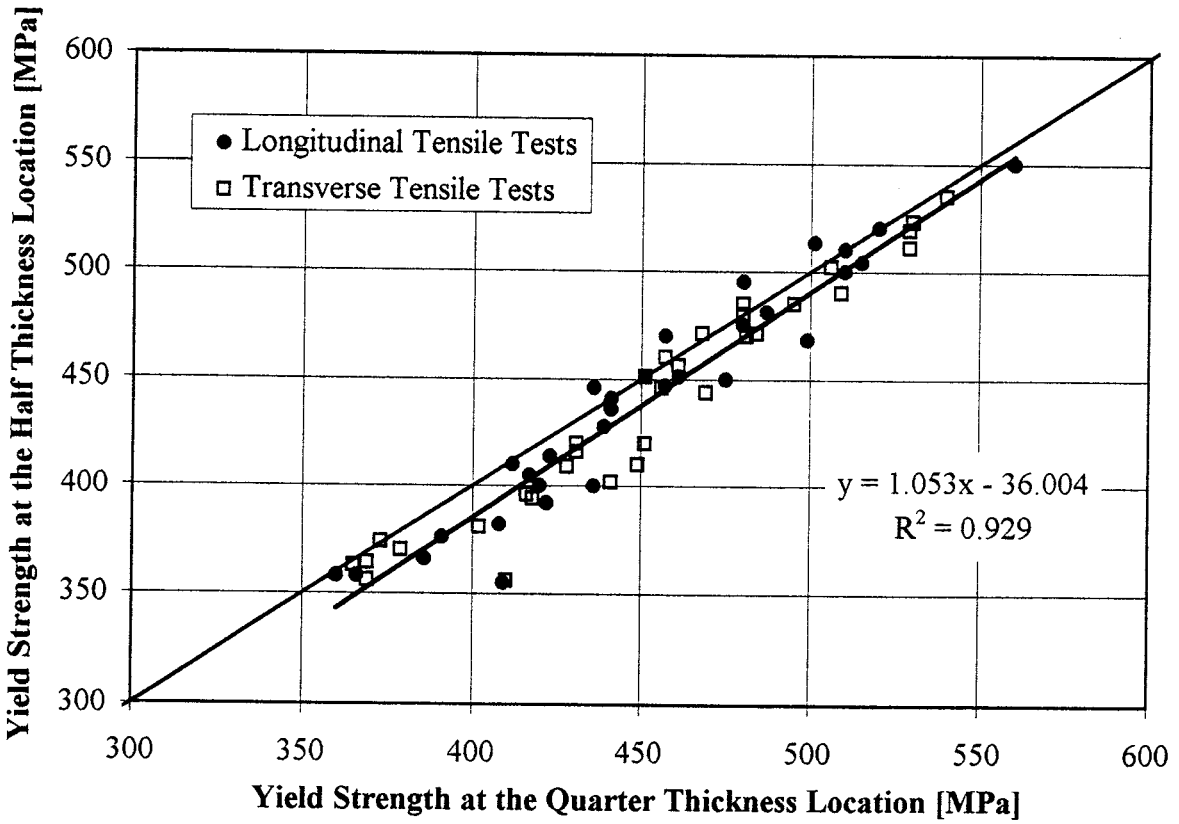

Figure 4.3: Yield strength of the TMCP steel plates measured at half thickness location versus that measured at the quarter thickness location

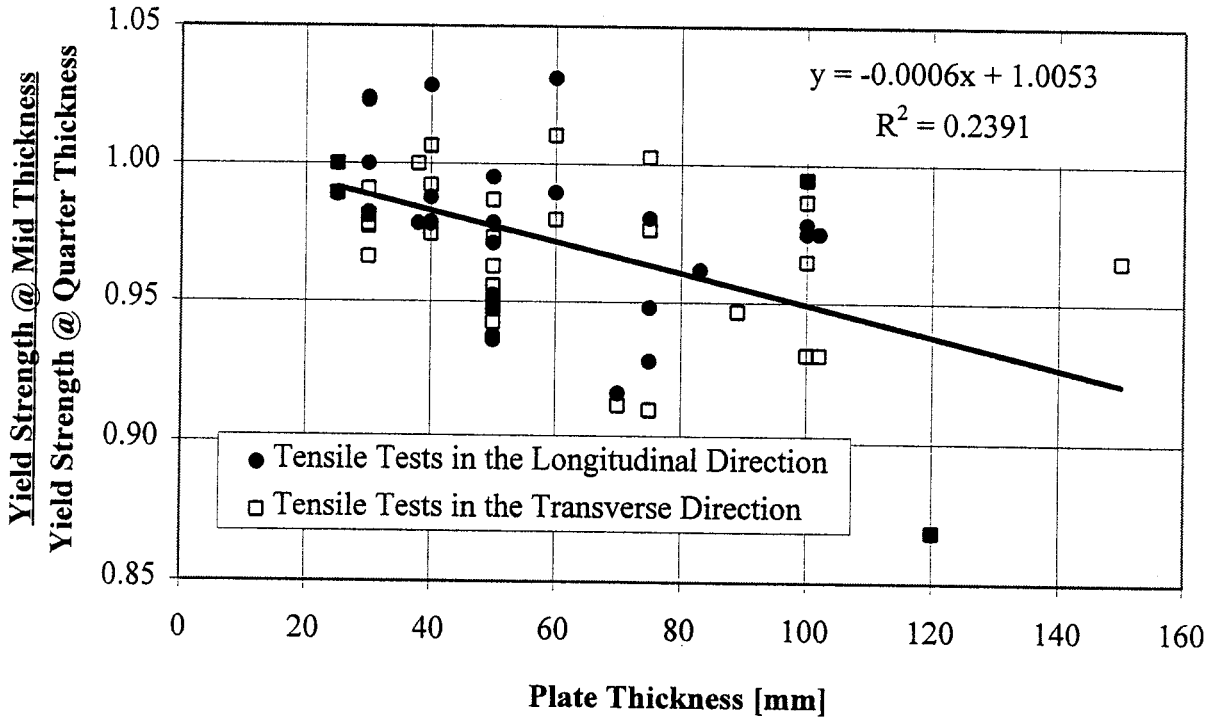

Figure 4.4: Ratio of yield strengths measured at half thickness and quarter thickness locations versus the TMCP steel plate thickness

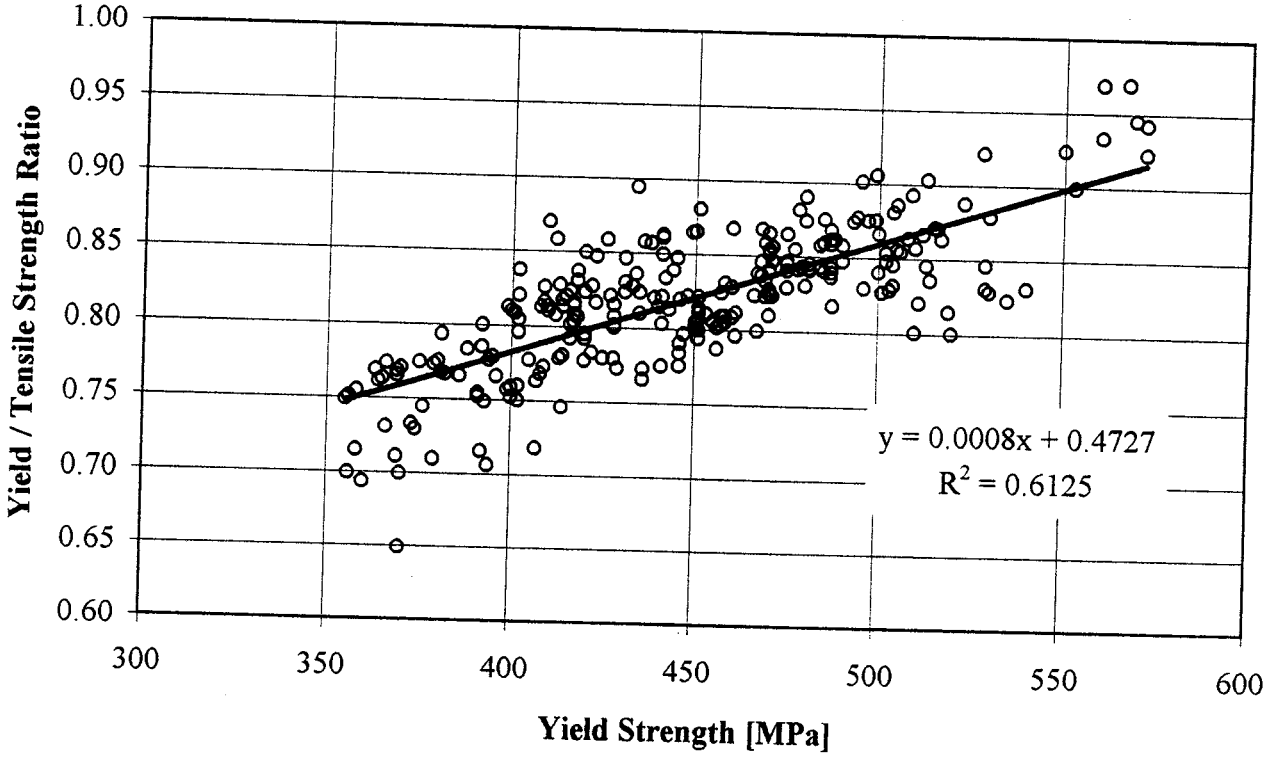

Figure 4.5: Yield to tensile strength ratio for TMCP steel plates versus the yield strength

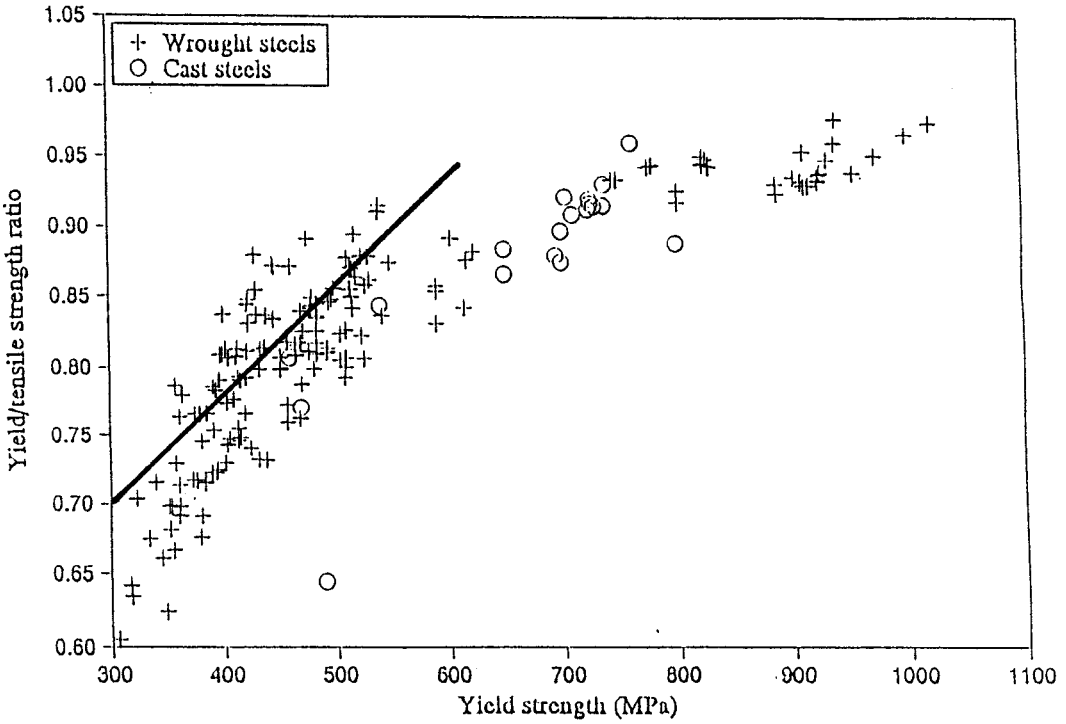

Figure 4.6(a): Regression line for TMCP steel plates from Figure 4.5 superimposed on yield/tensile strength ratio data given in Ref. [4.1]

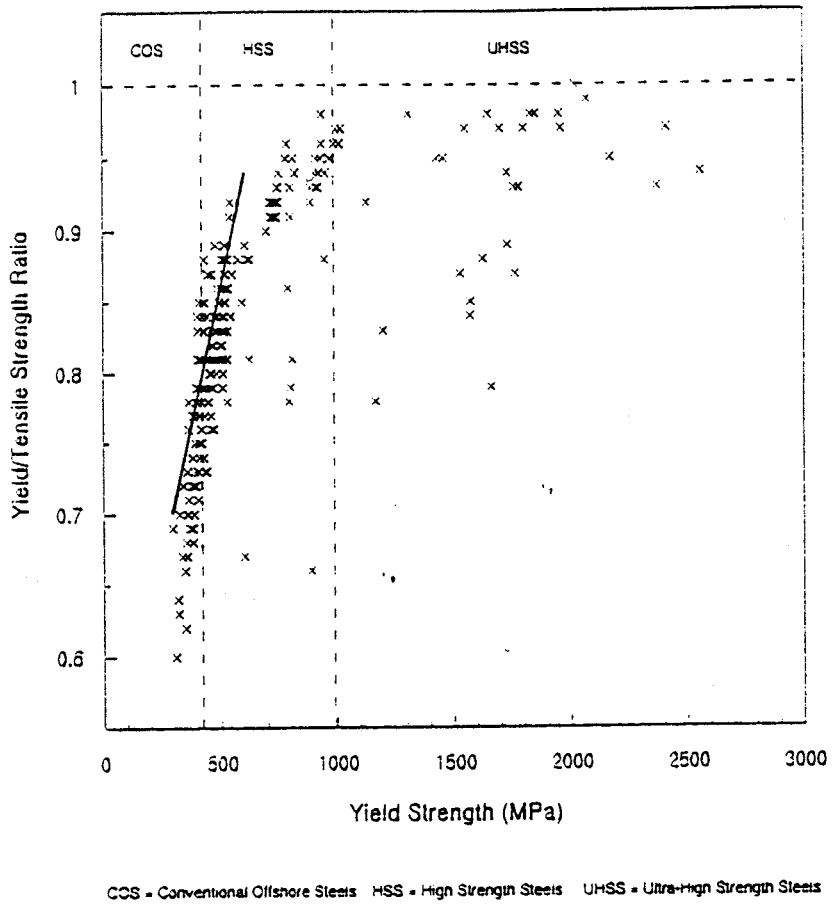

Figure 4.6(b): Regression line for TMCP steel plates from Figure 4.5 superimposed on yield-tensile strength ratio date given in Ref. [4.2]

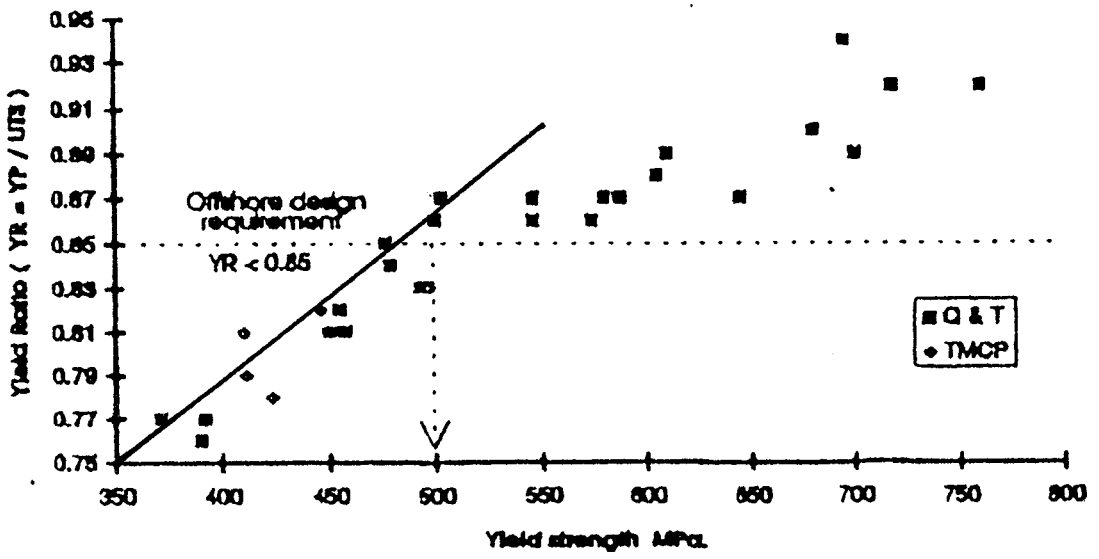

Figure 4.6(c): Regression line for TMCP steel plates from Figure 4.5 superimposed on yield-tensile strength ratio date given in Ref. [4.3]

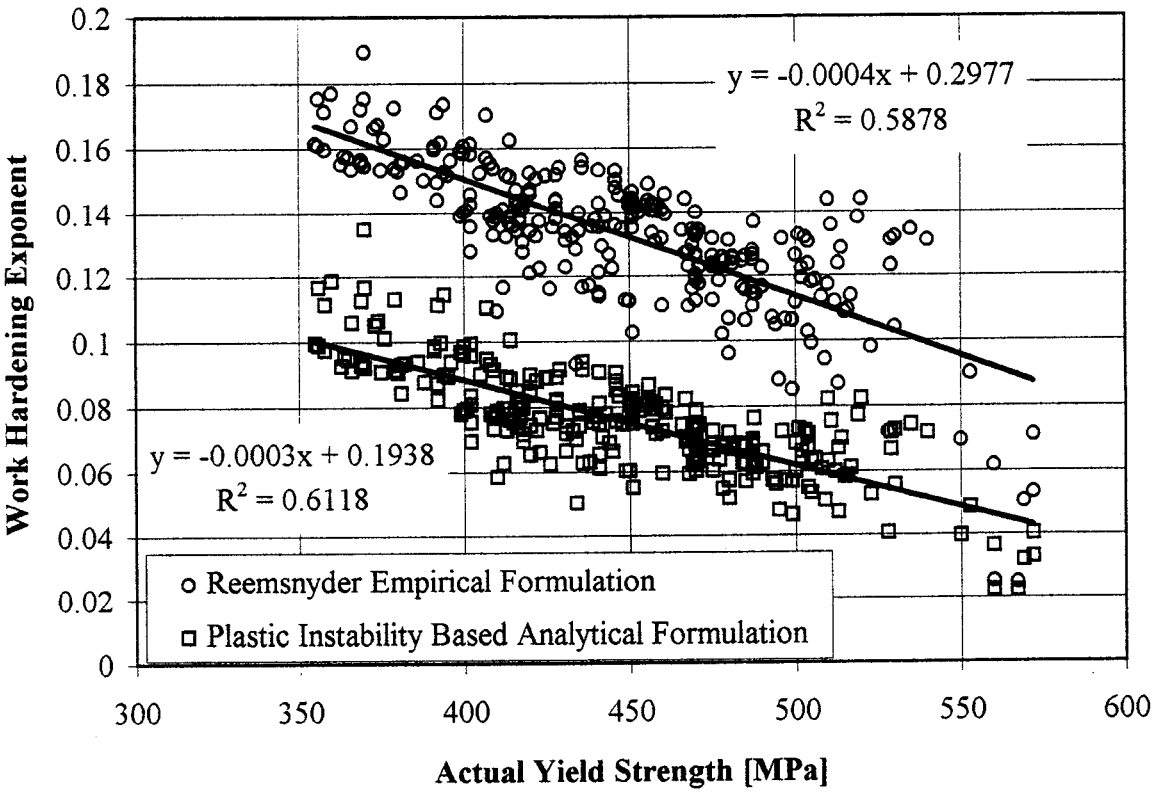

Figure 4.7: Strain hardening exponent calculated from the yield /tensile strength ratio, using two different models

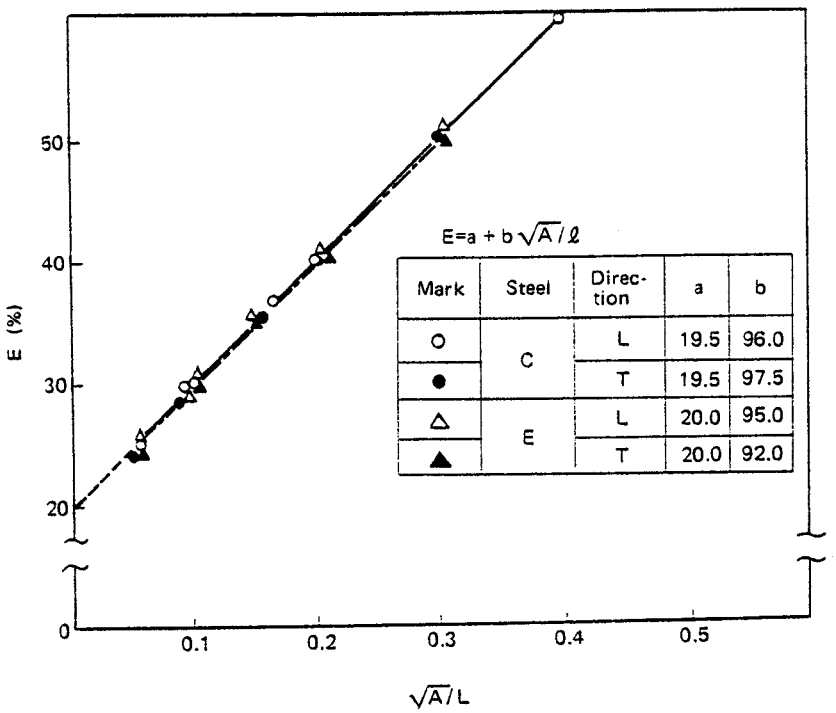

Figure 4.8: Uniform elongation measured in tensile tests Ref. [4.9]

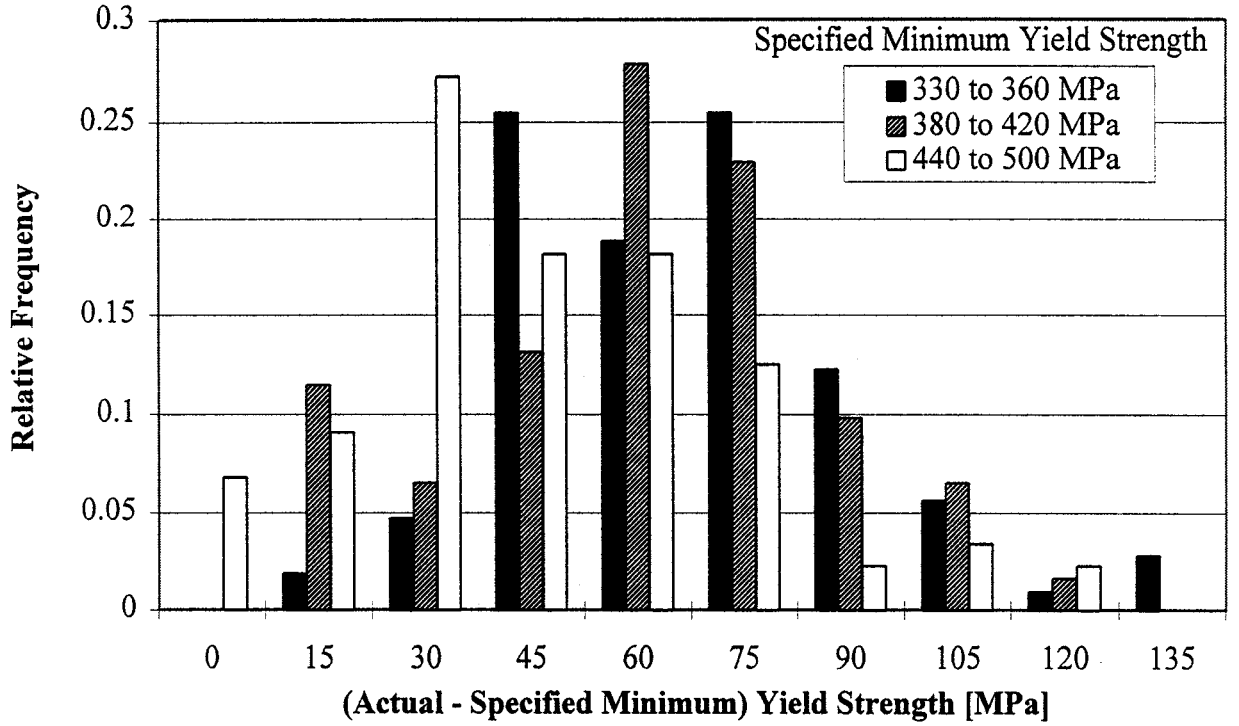

Figure 4.9: Histogram of the (actual-specified minimum) yield strength for TMCP steel plates

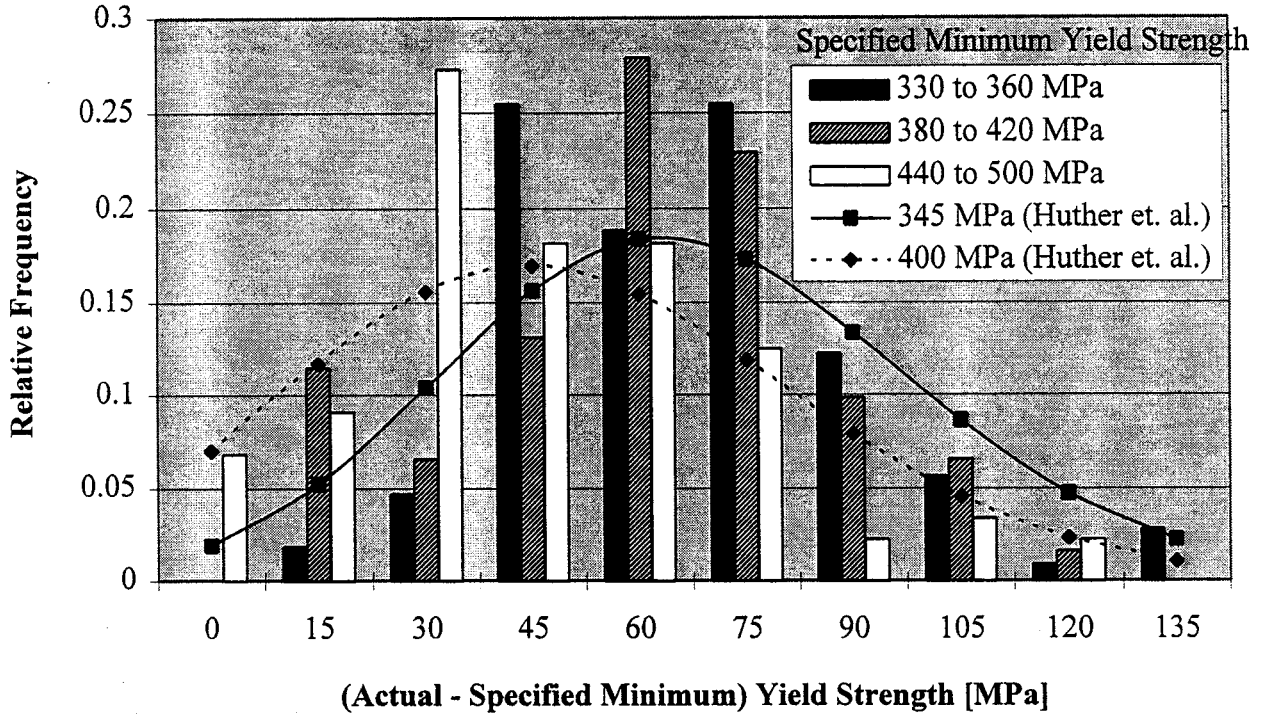

Figure 4.10: Comparative distribution of (actual-specified minimum) yield strength for marine steels [Ref. 4.10] and TMCP steel plates

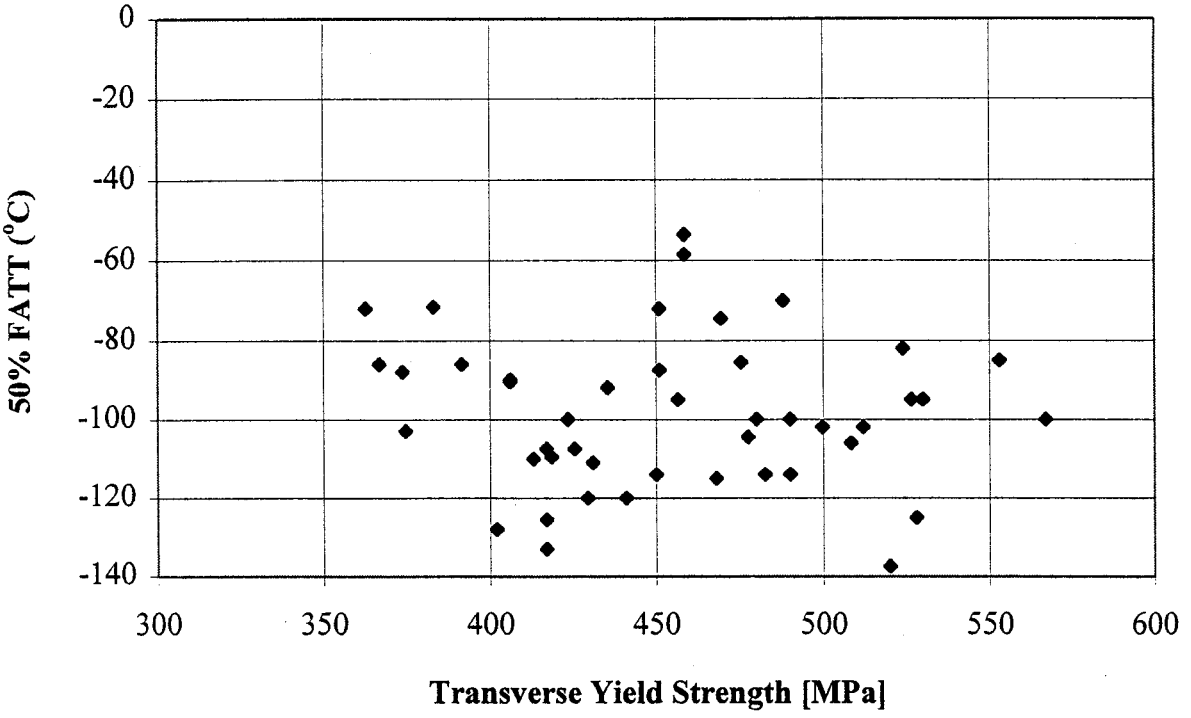

Figure 4.11: 50% CVN fracture appearance transition temperature for TMCP steel plates of various yield strengths

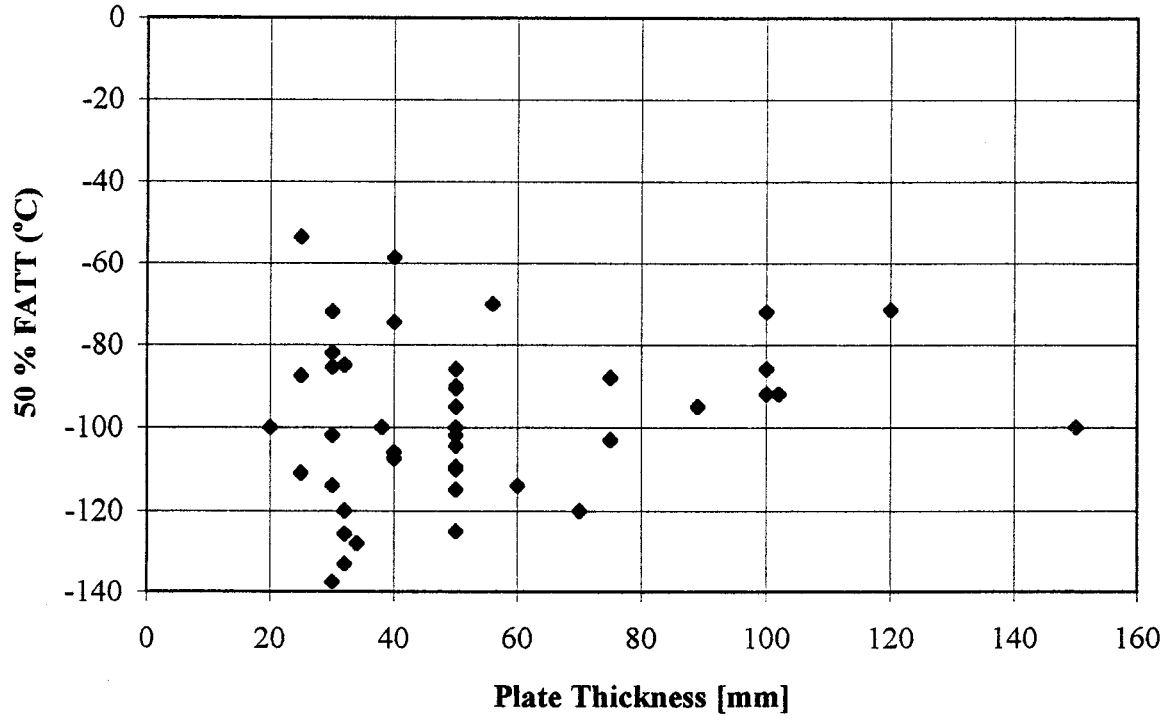

Figure 4.12: 50% CVN fracture appearnce transition temperature for TMCP steel plates of various thicknesses

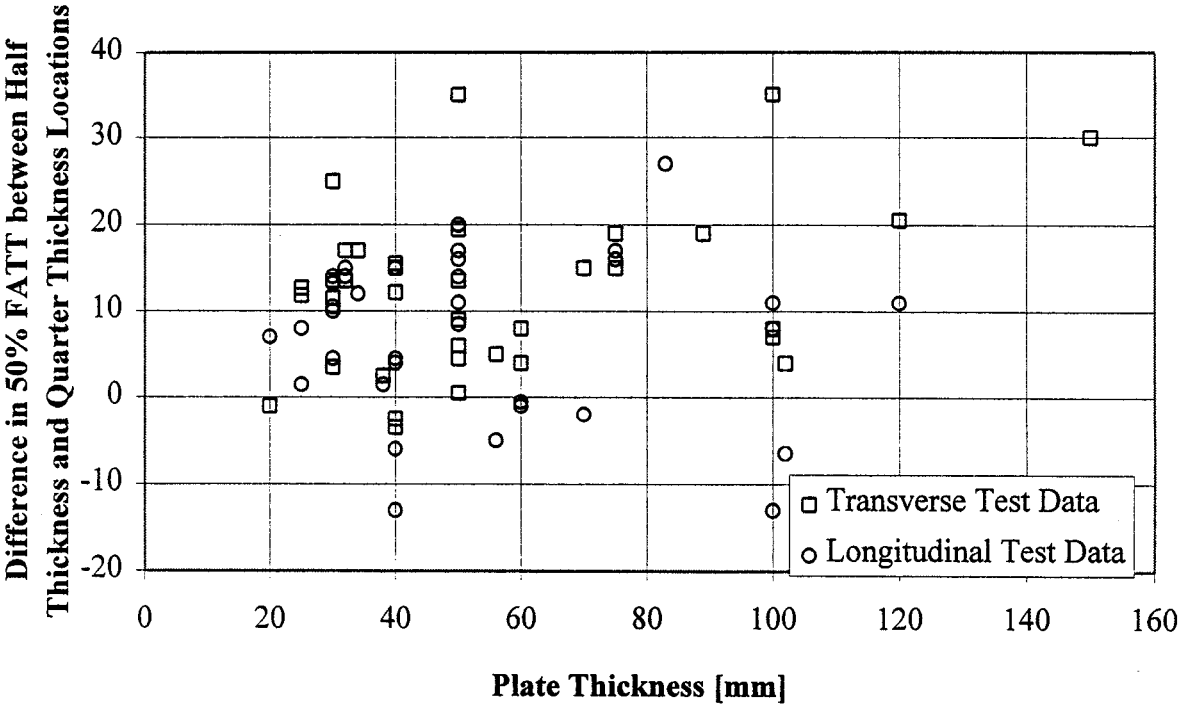

Figure 4.13: Difference in 50% FATT between half-thickness and quarter thickness locations of TMCP steel plates

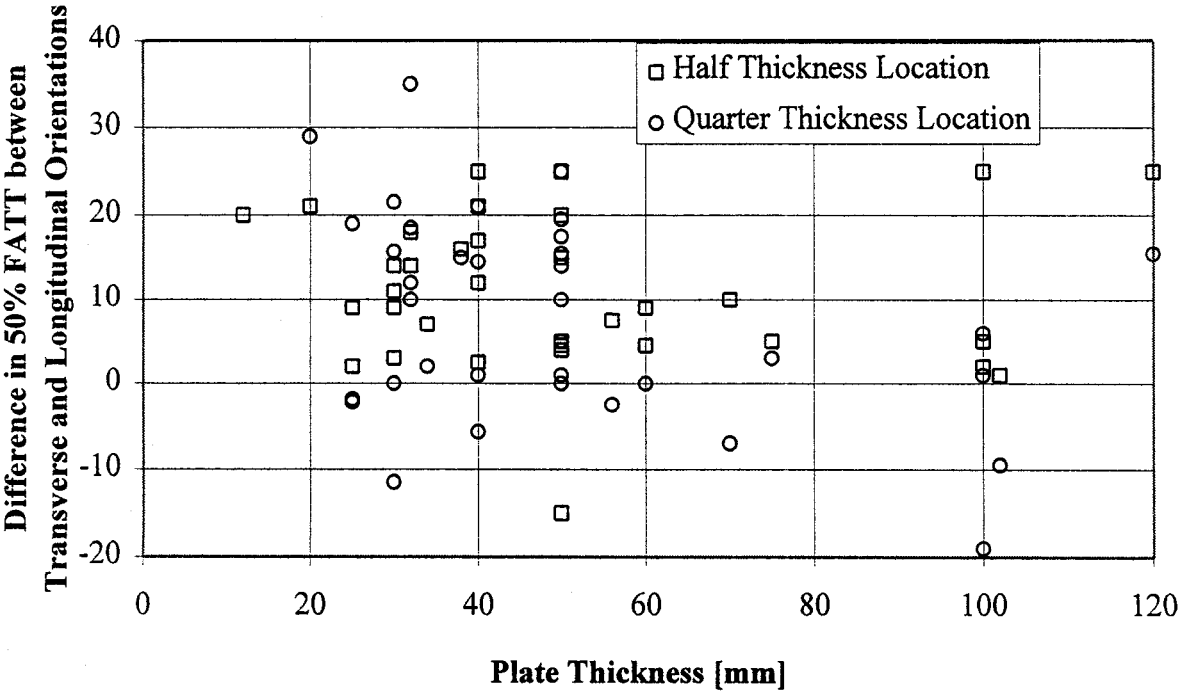

Figure 4.14: Difference in the 50% FATT between transverse and longitudinal orientations of TMCP steel plates

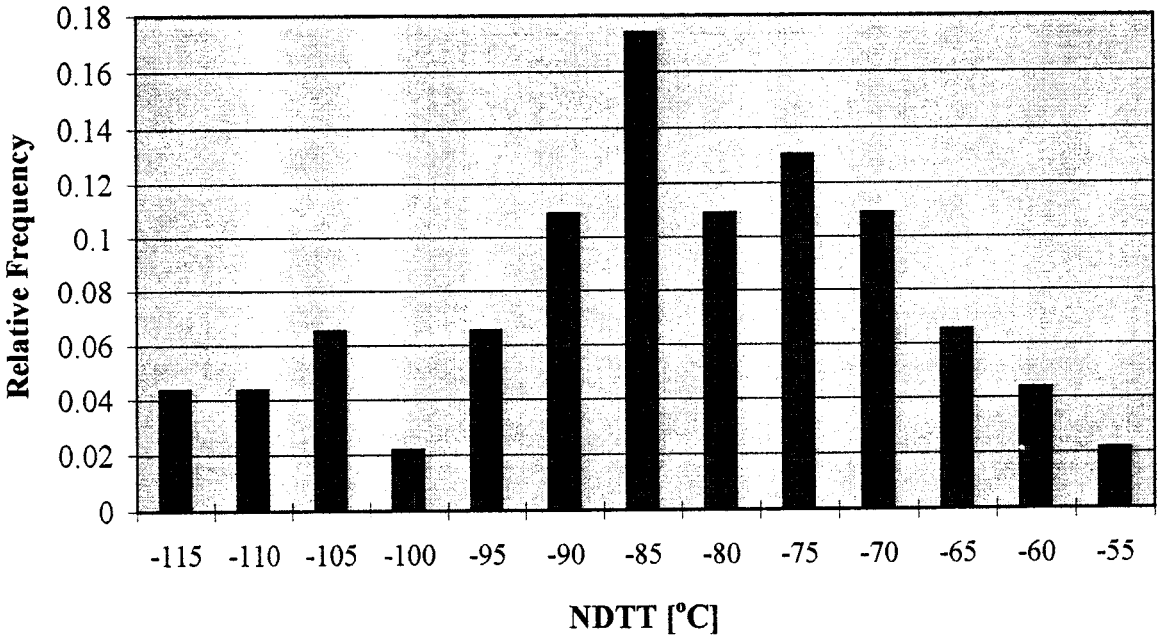

Figure 4.15: Distribution of the Pellini nil-ductility transition temperature (ASTM E 208) of TMCP steel plates

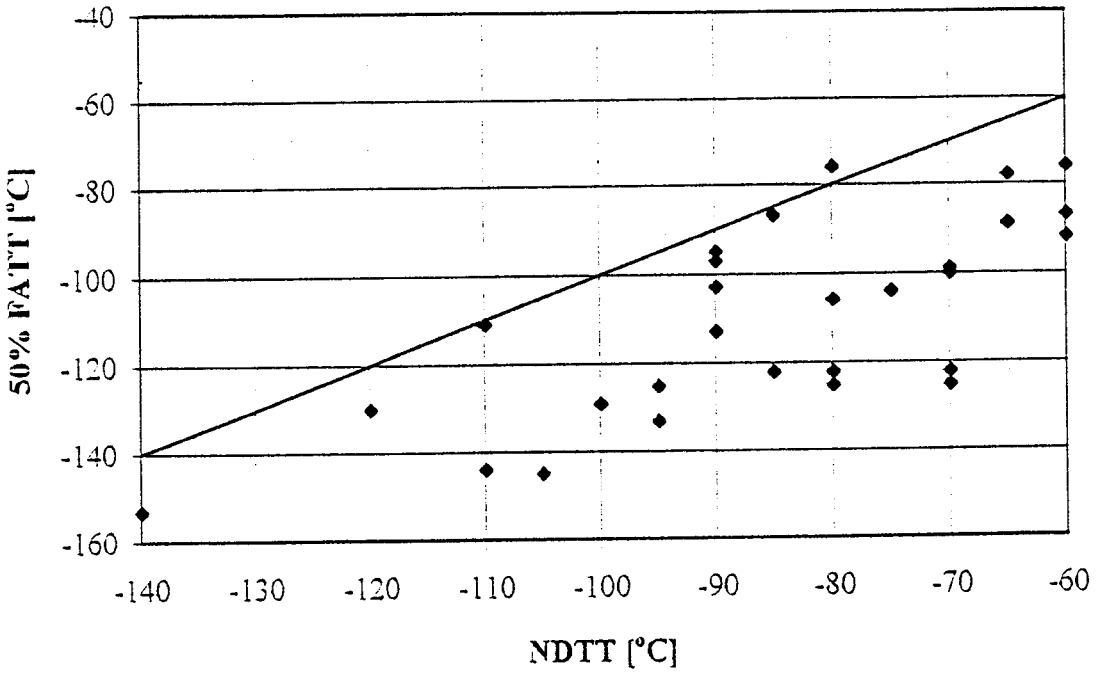

Figure 4.16: Relationship between 50% FATT and NDTT in TMCP steels

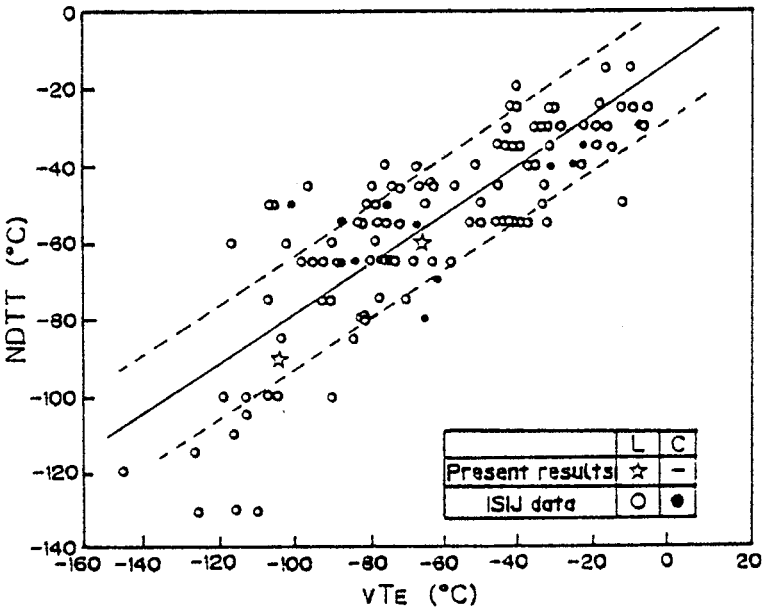

Figure 4.17: Relationship between NDTT and $_VT_E$ Ref. [4.12]

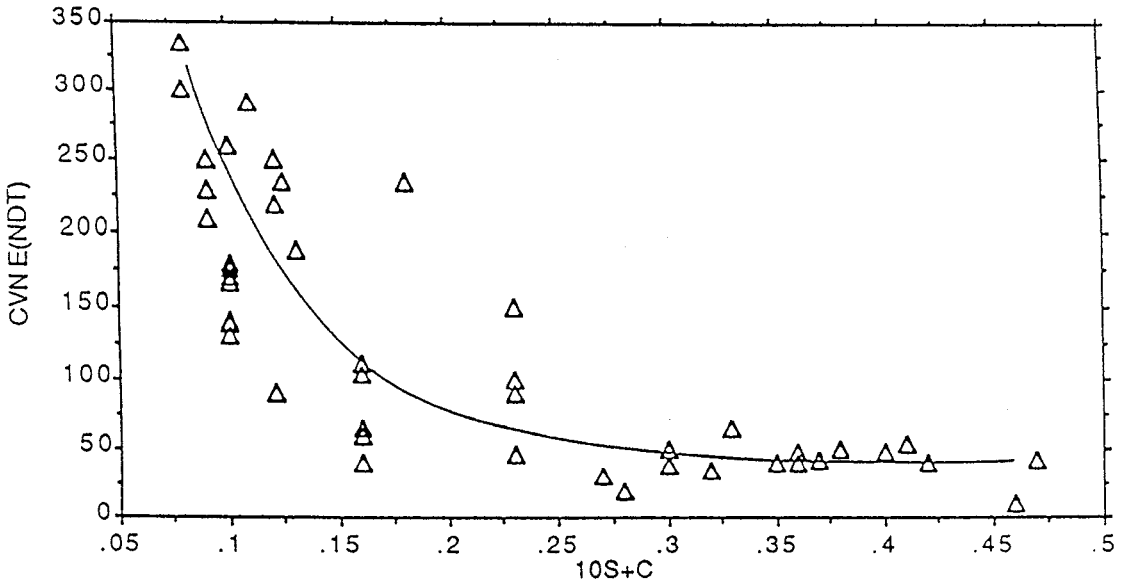

Figure 4.18: CVN energy at NDTT versus % (10S + C) Ref. [4.13]

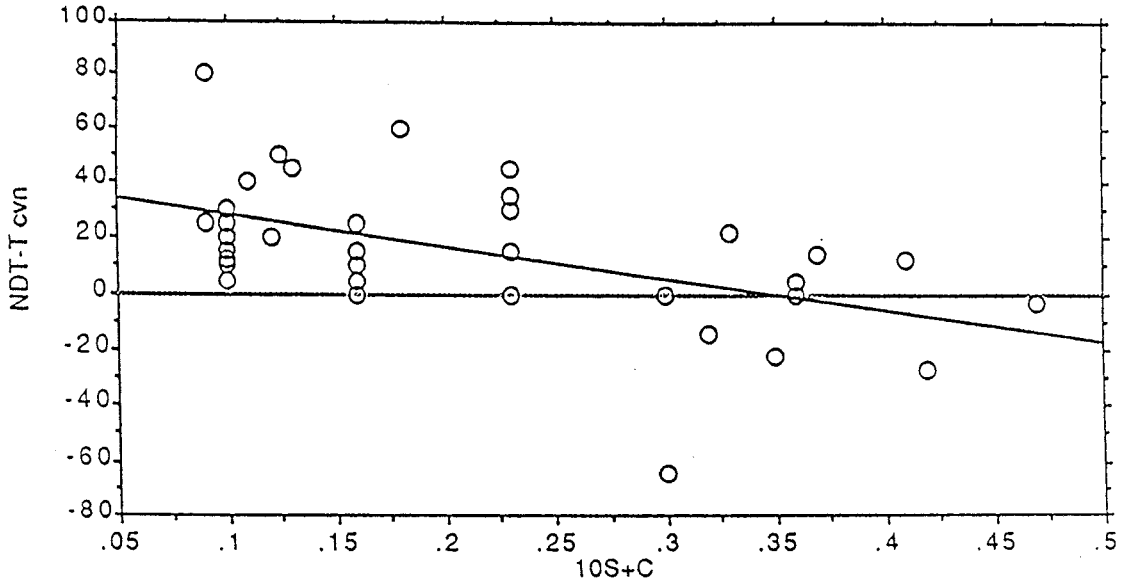

Figure 4.19: NDTT - 40J CVN transition temperature versus % (10S + C) Ref. [4.13]

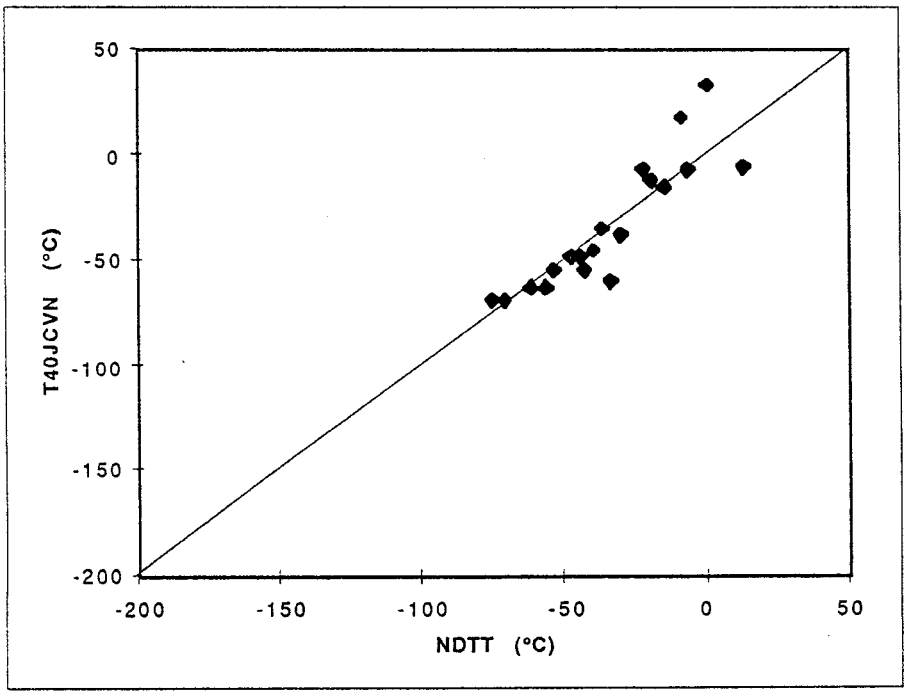

Figure 4.20: Relation between 40J CVN transition temperature and NDTT for steels with % (10S + C) >0.25 Ref. [4.13]

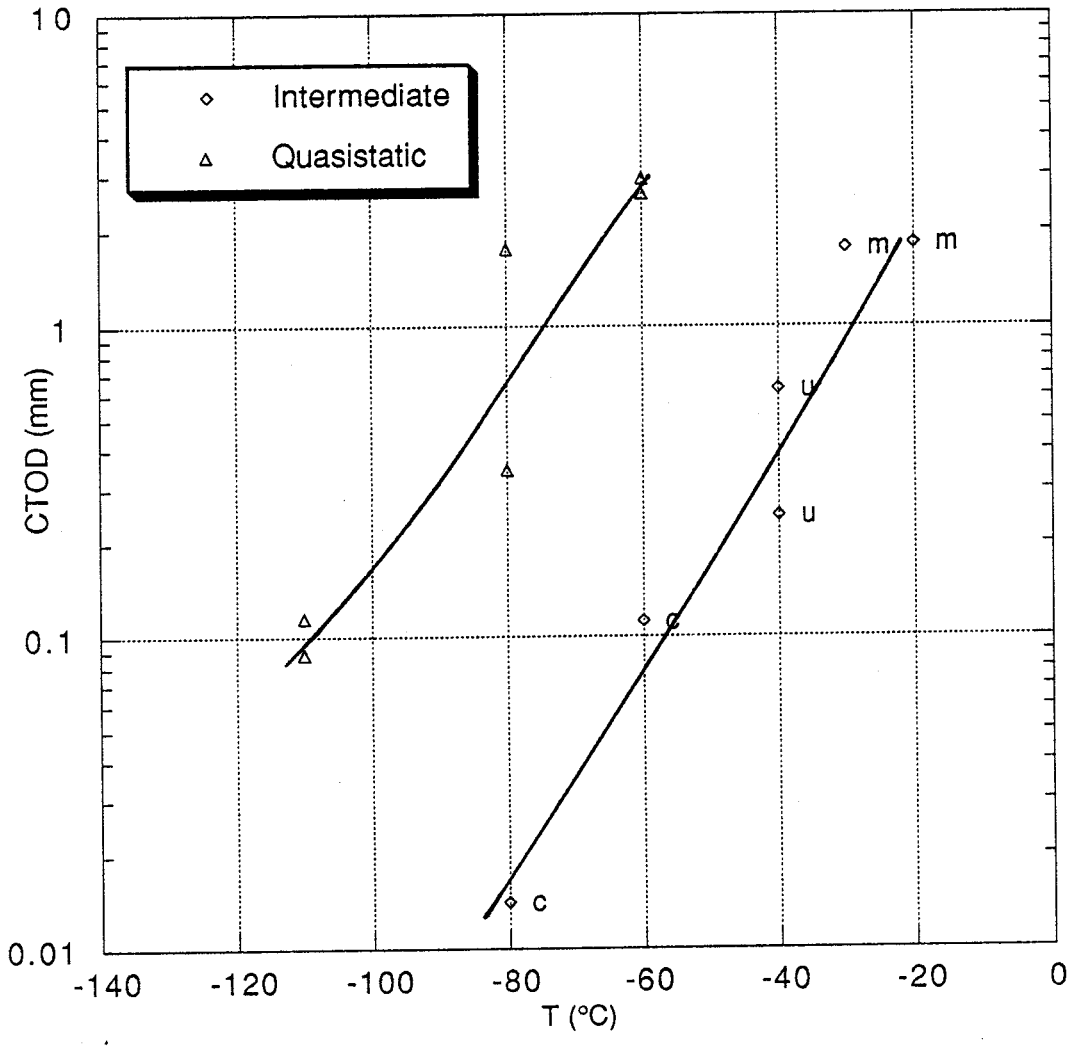

Figure 4.21(a): CTOD toughness as a function of temperature for a 50 mm thick, EH 36 mod (TMCP) steel in the longitudinal orientation

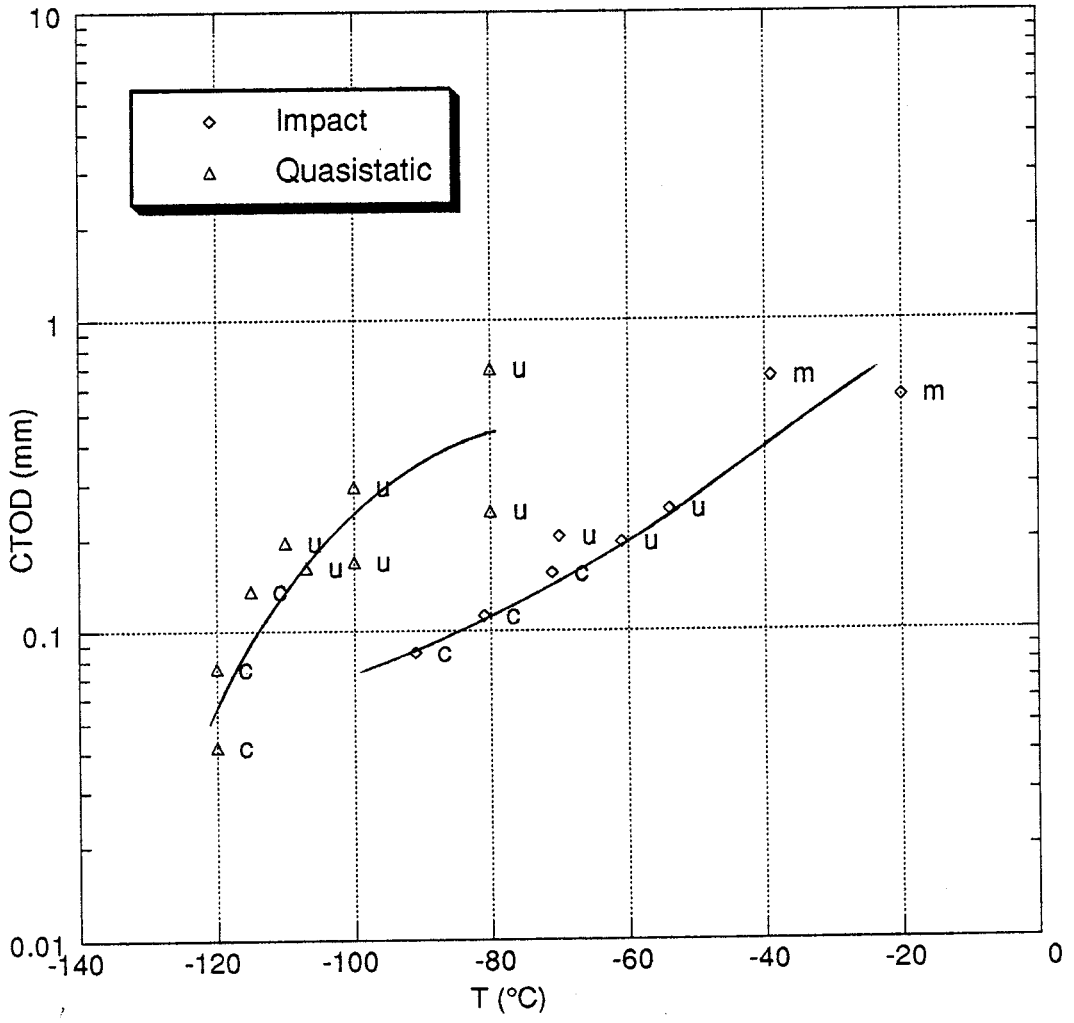

Figure 4.21(b):CTOD toughness as a function of temperature for a 20 mm thick, 440 MPa yield (NVF 440) TMCP steel

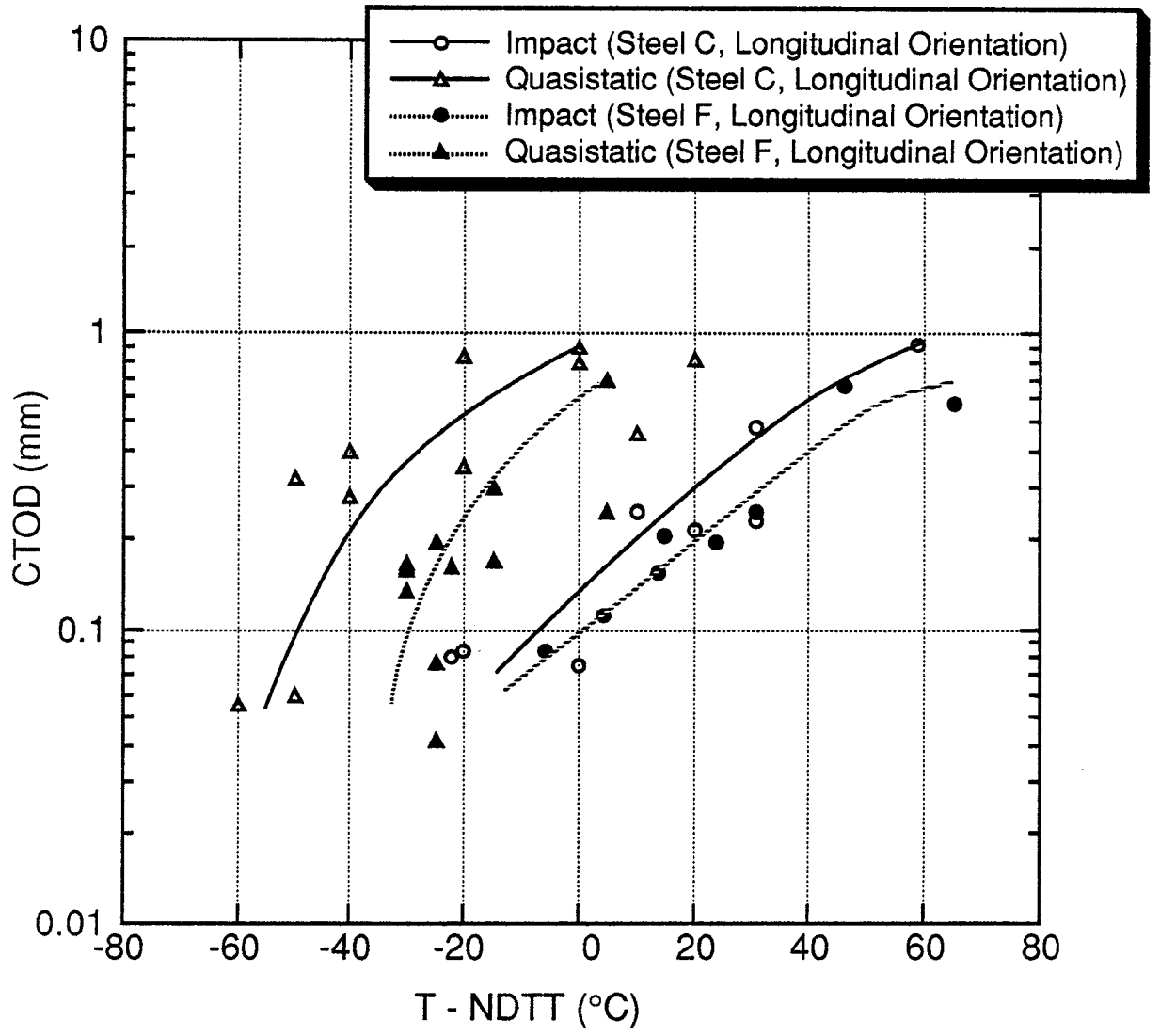

Figure 4.22(a):CTOD fracture toughness of steels C (25 mm thick, normalized) and F (20 mm thick, TMCP) as a function of temperature, referenced to the nil-ductility transition temperature

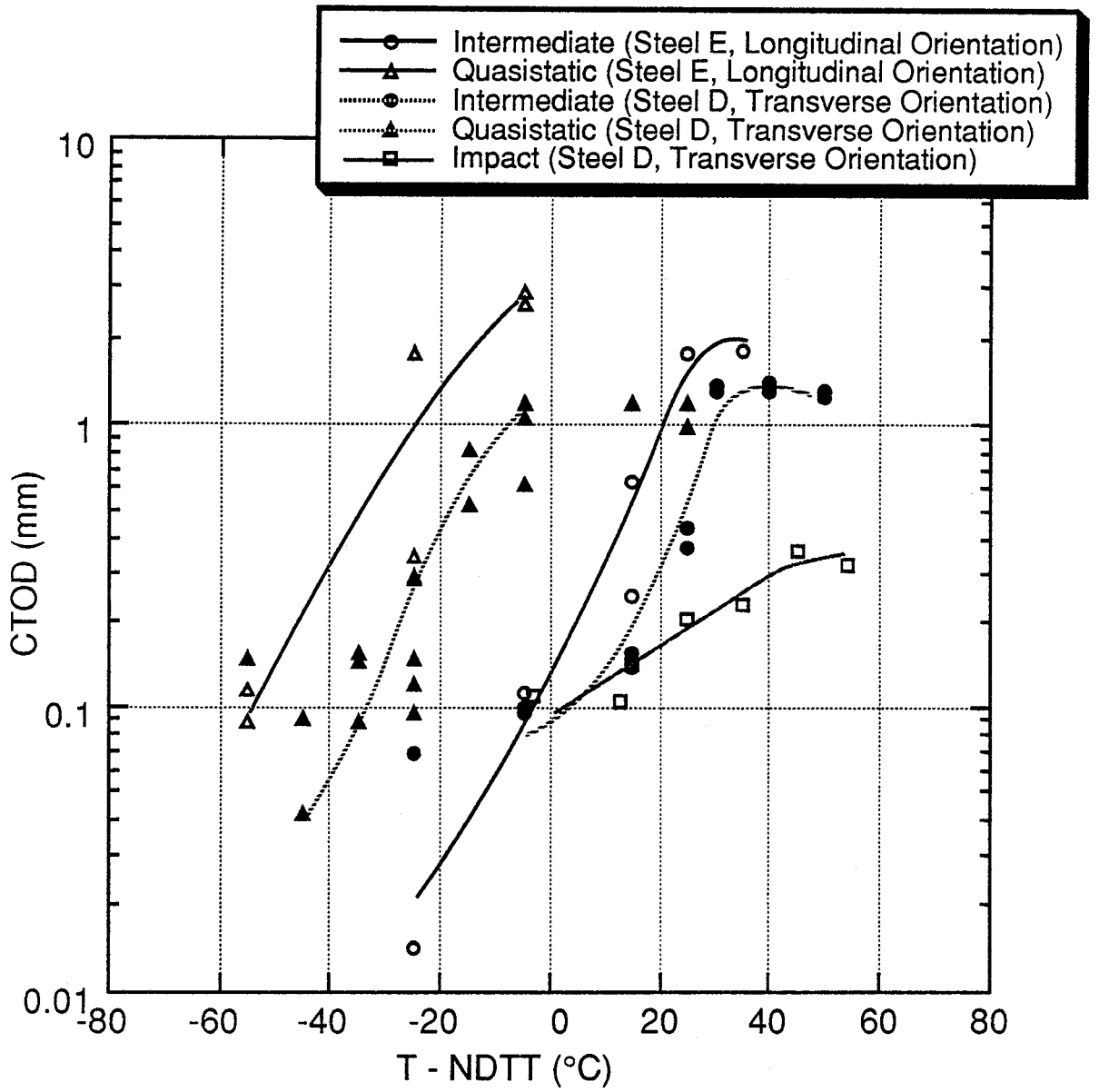

Figure 4.22(b):CTOD fracture toughness of steels D (50 mm thick, normalized) and E (50 mm thick, TMCP) as a function of temperature, referenced to the nil-ductility transition temperature

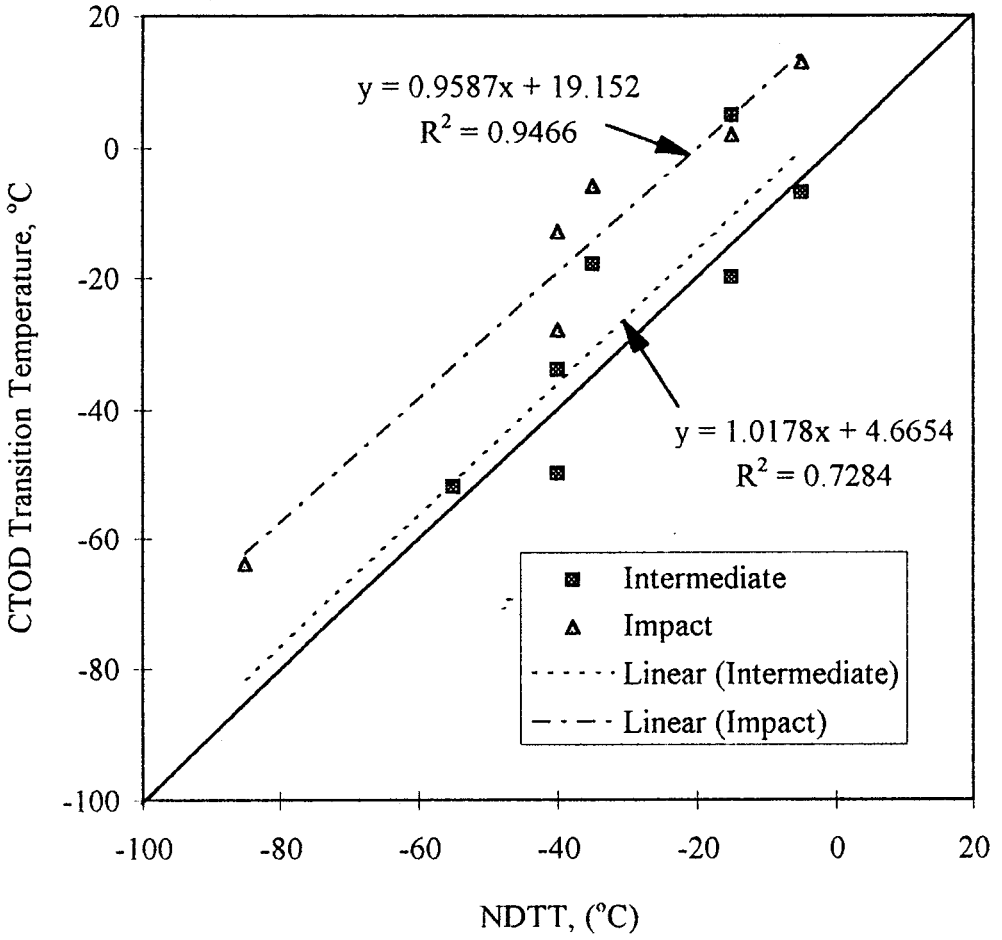

Figure 4.23: Relation between 0.2 mm CTOD transition temperature and NDTT

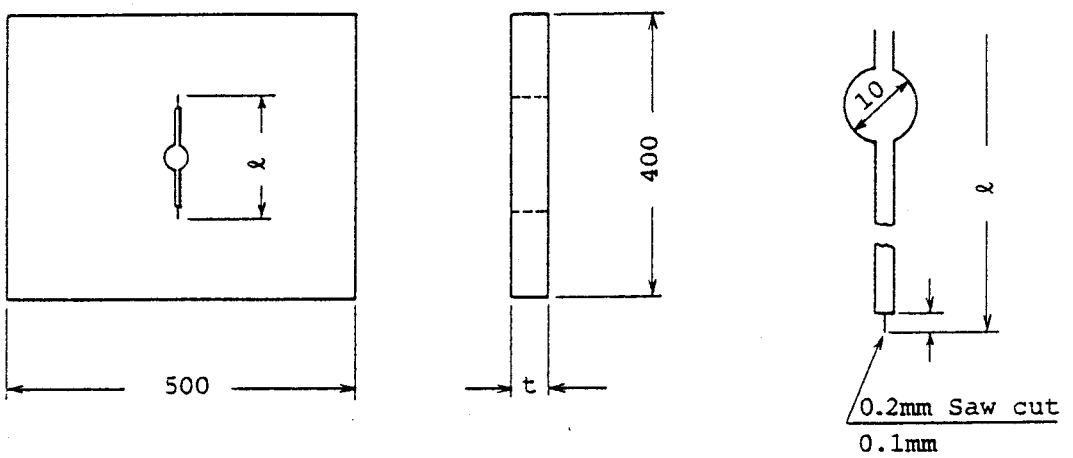

Figure 4.24: Wide plate specimens (deep center notch) tested in Japan for initiation toughness of TMCP steels

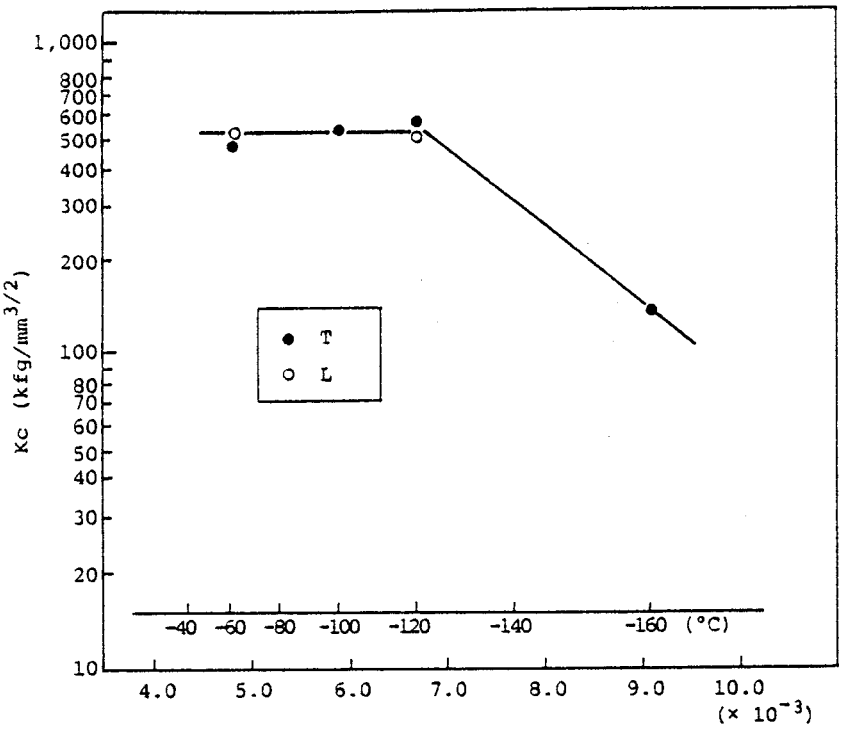

Figure 4.25: Results of wide plate tests on a TMCP steel plate Ref. [4.17]

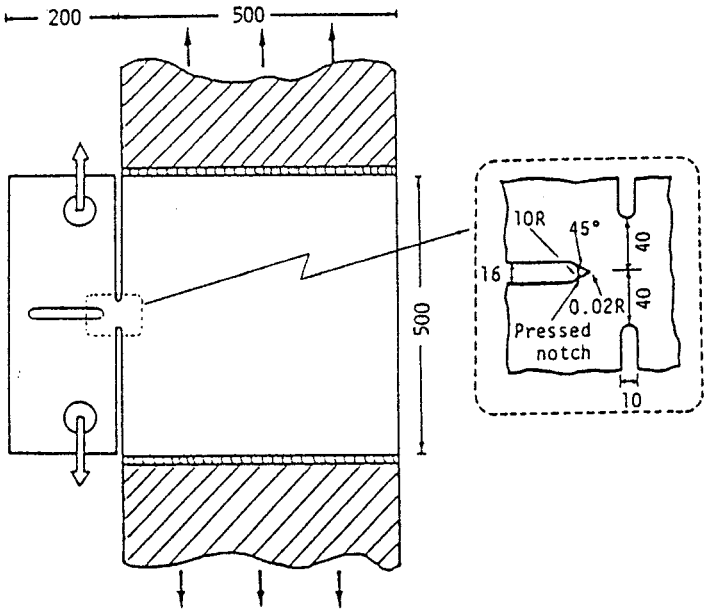

Figure 4.26: Double tension test for measuring crack arrest toughness

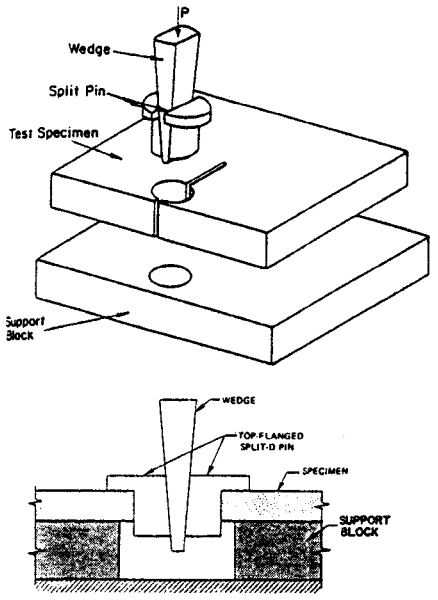

Figure 4.27: Compact crack arrest test

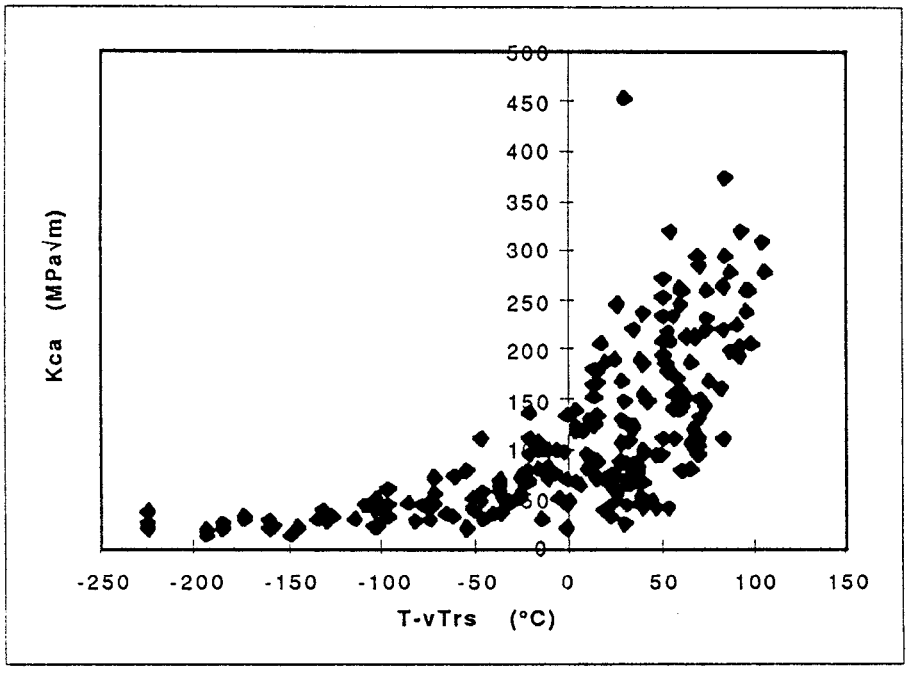

Figure 4.28: Crack arrest toughness values relative to the CVN transition temperature (all data)

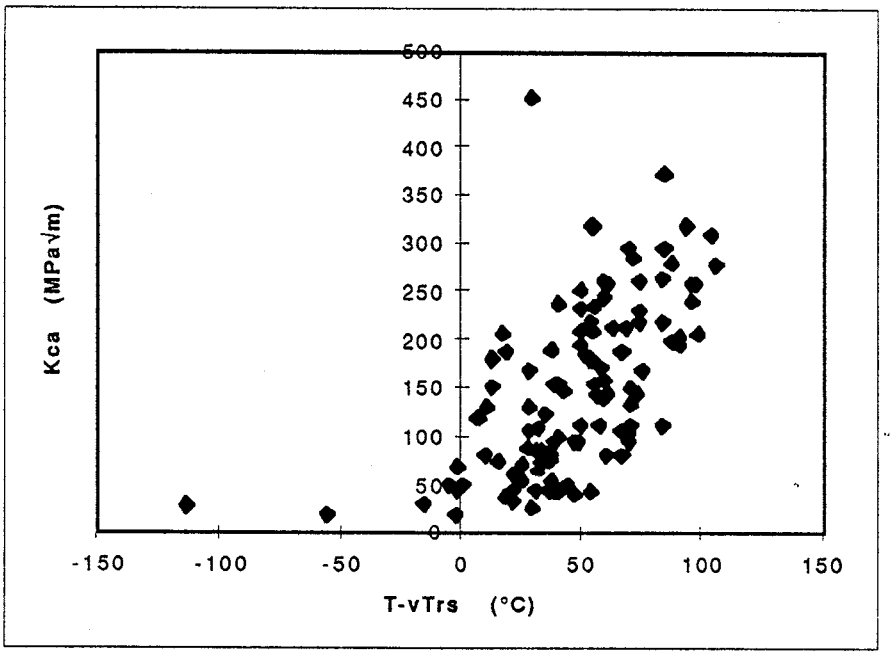

Figure 4.29: K_{ca} results for DT and Esso tests only

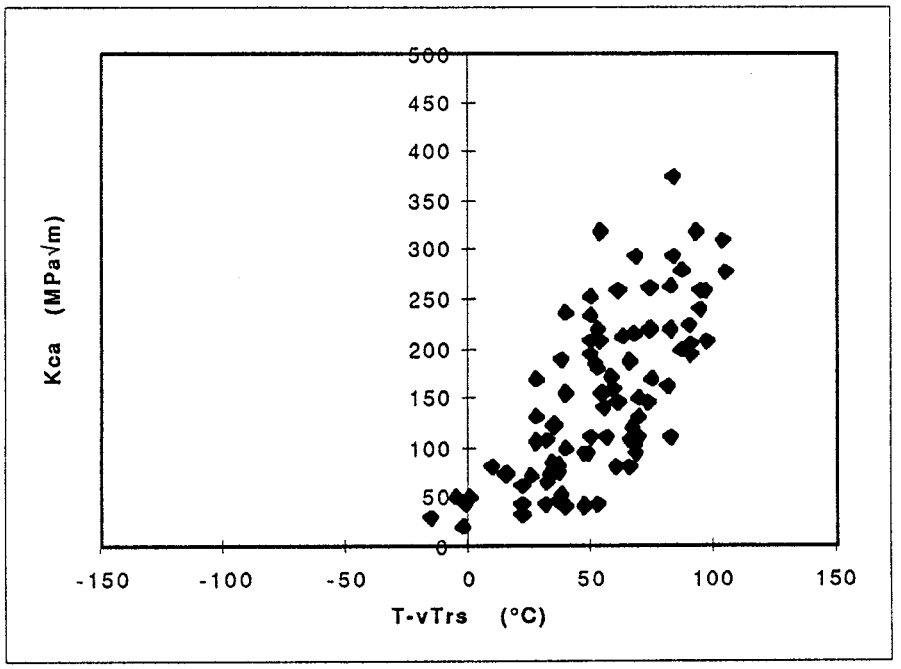

Figure 4.30: K_{ca} results in DT and Esso tests for TMCP (accelerated cooled) steels

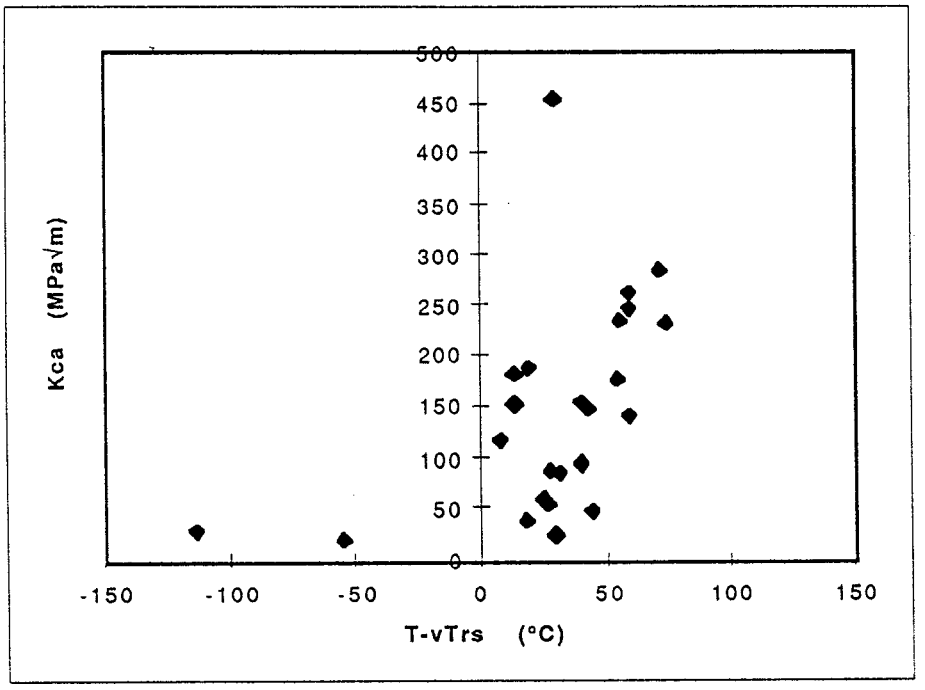

Figure 4.31: K_{ca} results in DT and Esso tests for non-TMCP steels

Steel	Type	Grade	No. of Charge	Symbol
HT50 (t=30mm)	I	KD36	2	○
	II	KA36, KD36	3	□
	III	KA36, KD36, KE36	4	△
	C.P.S.	KD32, KE32	8	•

C. P. S. : Conventional Process (Normalized) Steel

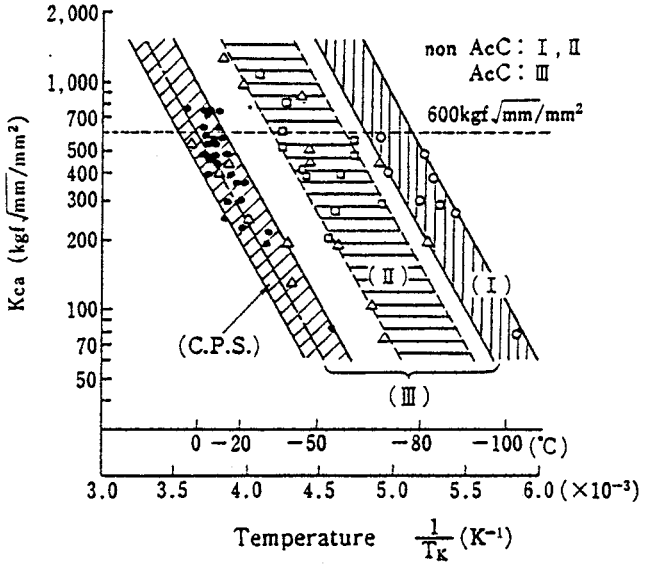

Figure 4.32: Summary of K_{ca} values from Ref. [4.19] 320-355 MPa yield strength ship steels

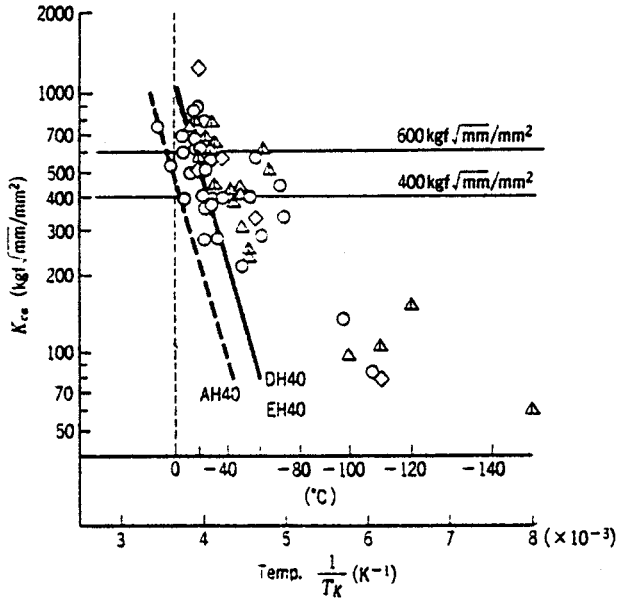

Grade	Plate thick. (mm)	Symbol	No. of charge
AH40	30	○	7
DH40		◇	1
EH40	25	◬	4
	30	△	1

Figure 4.33: Summary of K_{ca} values from Ref. [4.20] 392 MPa yield strength ship steels

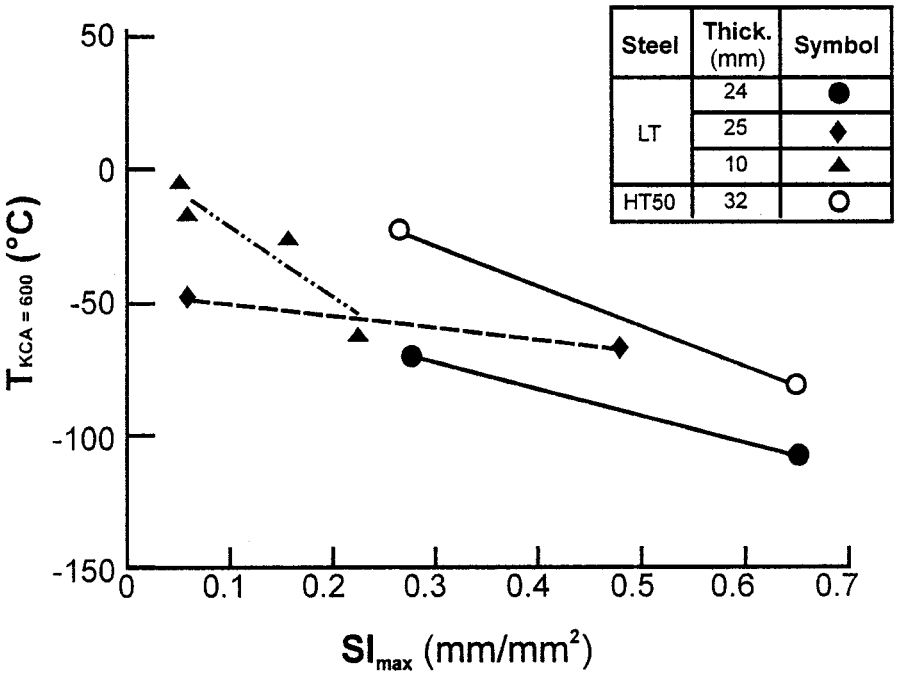

Steel	Thick. (mm)	Symbol
LT	24	●
	25	◆
	10	▲
HT50	32	○

Figure 4.34: Effect of splitting index on crack arrest toughness Ref. [4.21]

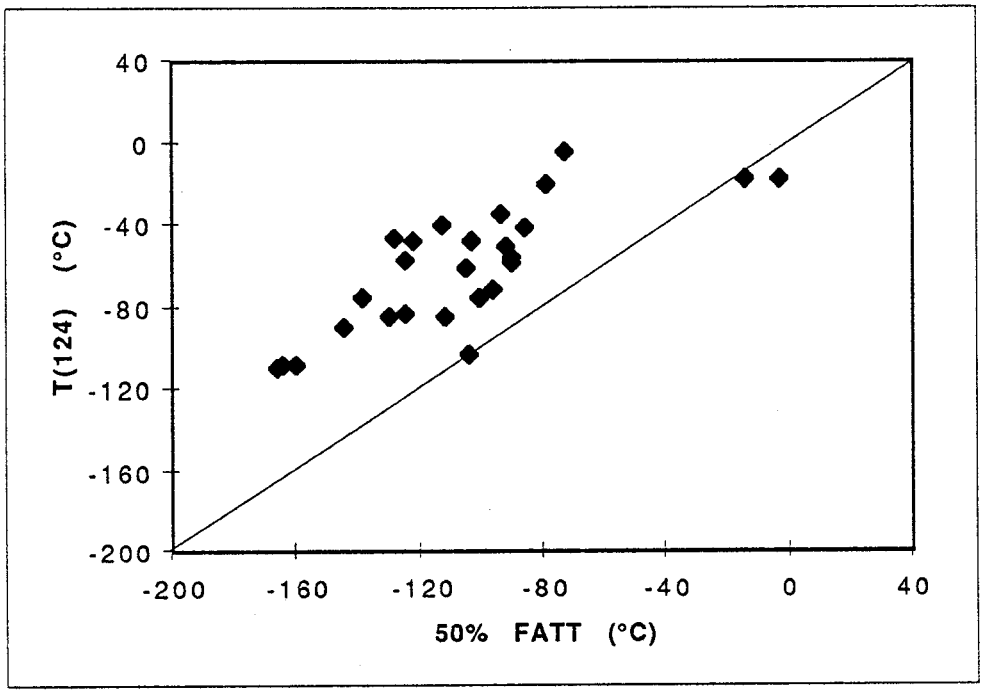

Figure 4.35: Relation between the temperature for K_{ca} = 124 MPa$\sqrt{m}$ and CVN FATT

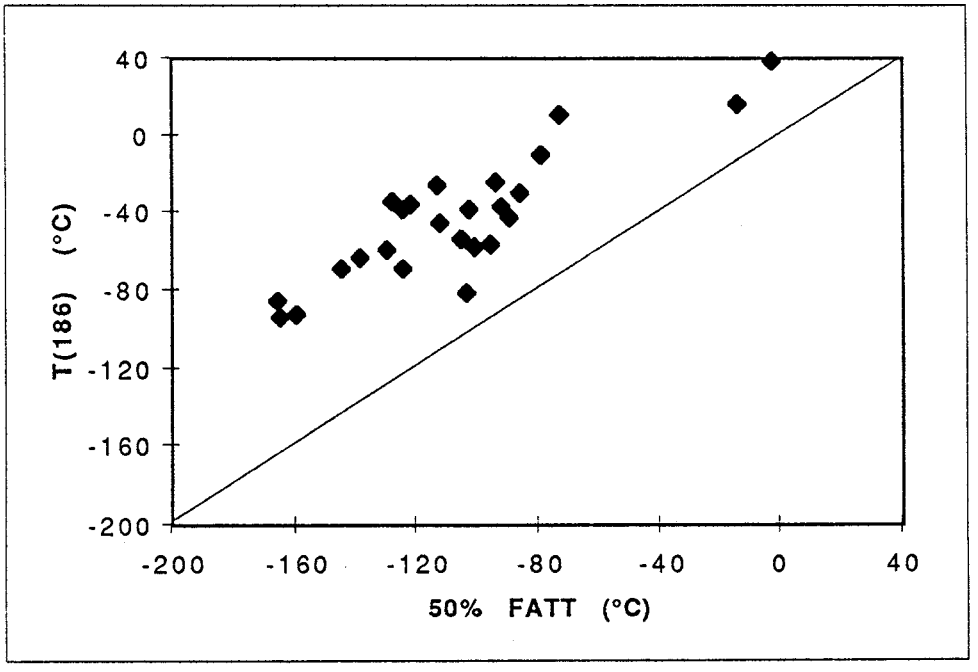

Figure 4.36: Relation between the temperature for K_{ca} = 186 MPa$\sqrt{m}$ and CVN FATT

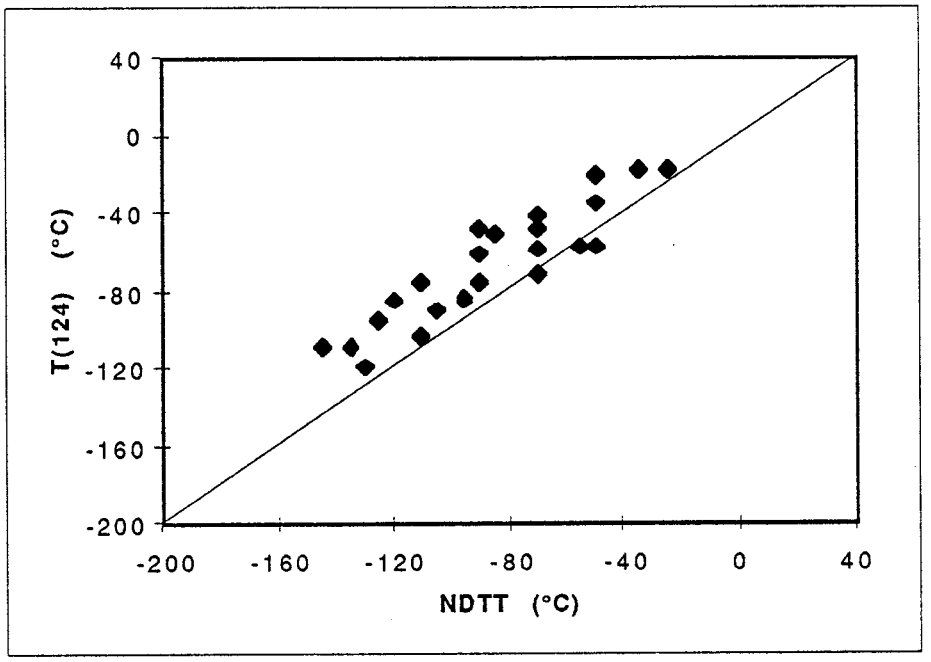

Figure 4.37: Relation of crack arrest properties (T124) to NDTT

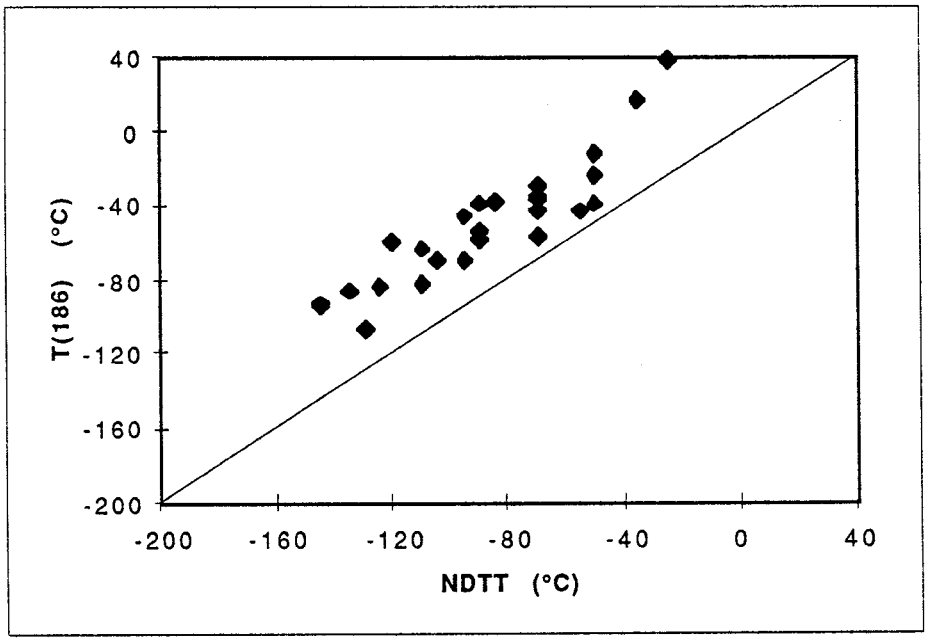

Figure 4.38: Relation of crack arrest properties (T186) to NDTT

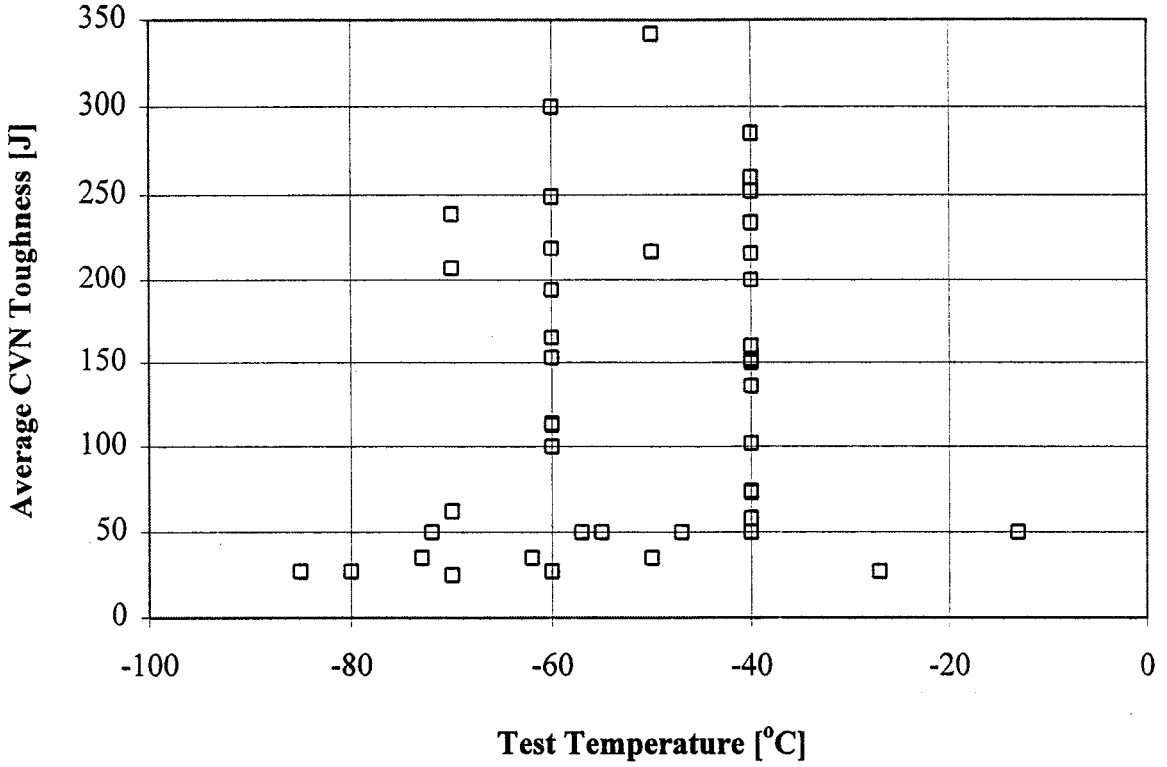

Figure 4.39: Average heat affected zone toughness determined from set of three or more CVN specimens notched at the fusion line in welds made at 3.0 kJ/mm heat input or lower

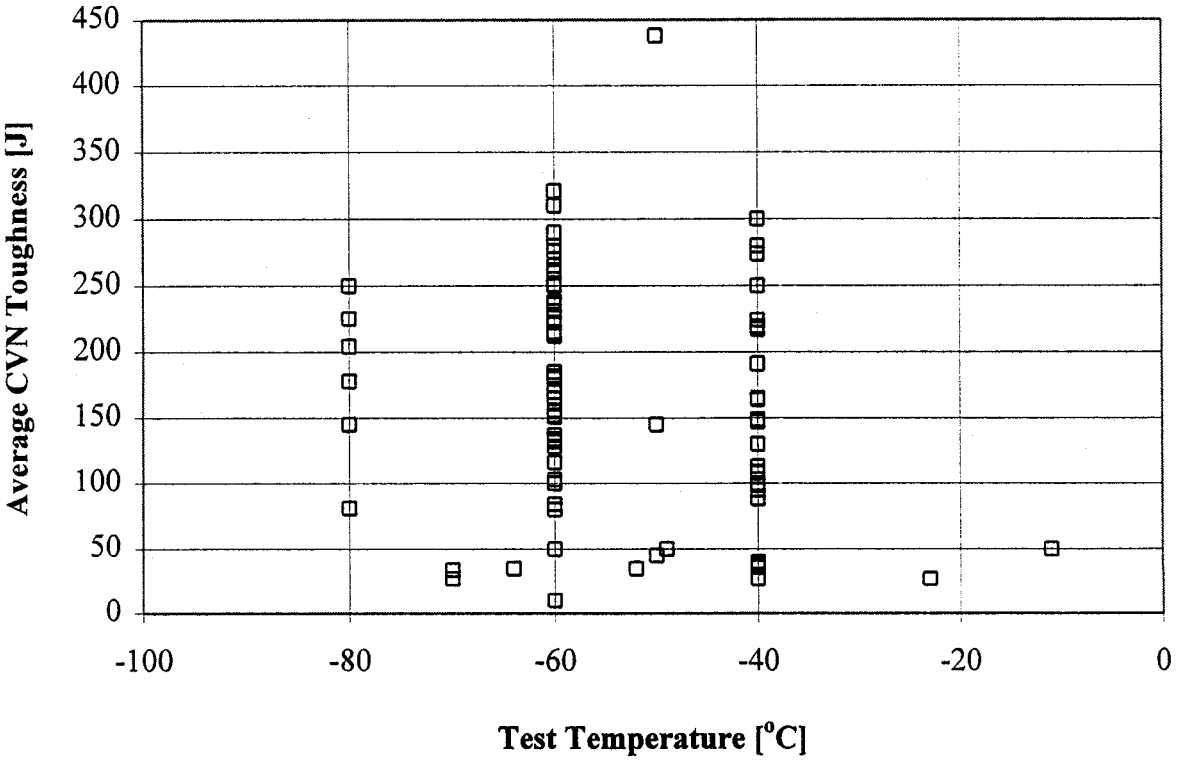

Figure 4.40: Average heat affected zone toughness determined from a set of three or more CVN specimens notched at the fusion line in welds made at heat inputs ranging from 3 to 7 kJ/mm

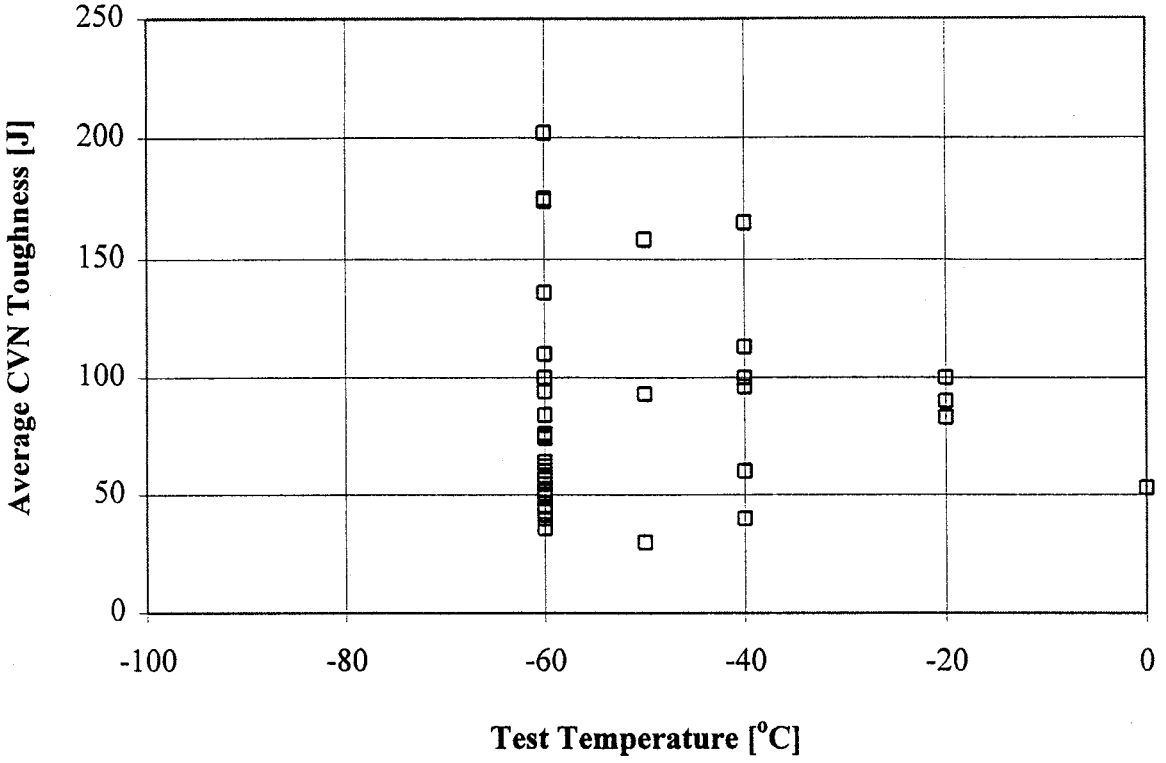

Figure 4.41: Average heat affected zone toughness determined from a set of three or more CVN specimens notched at the fusion line in welds made at heat inputs ≥ 10 kJ/mm

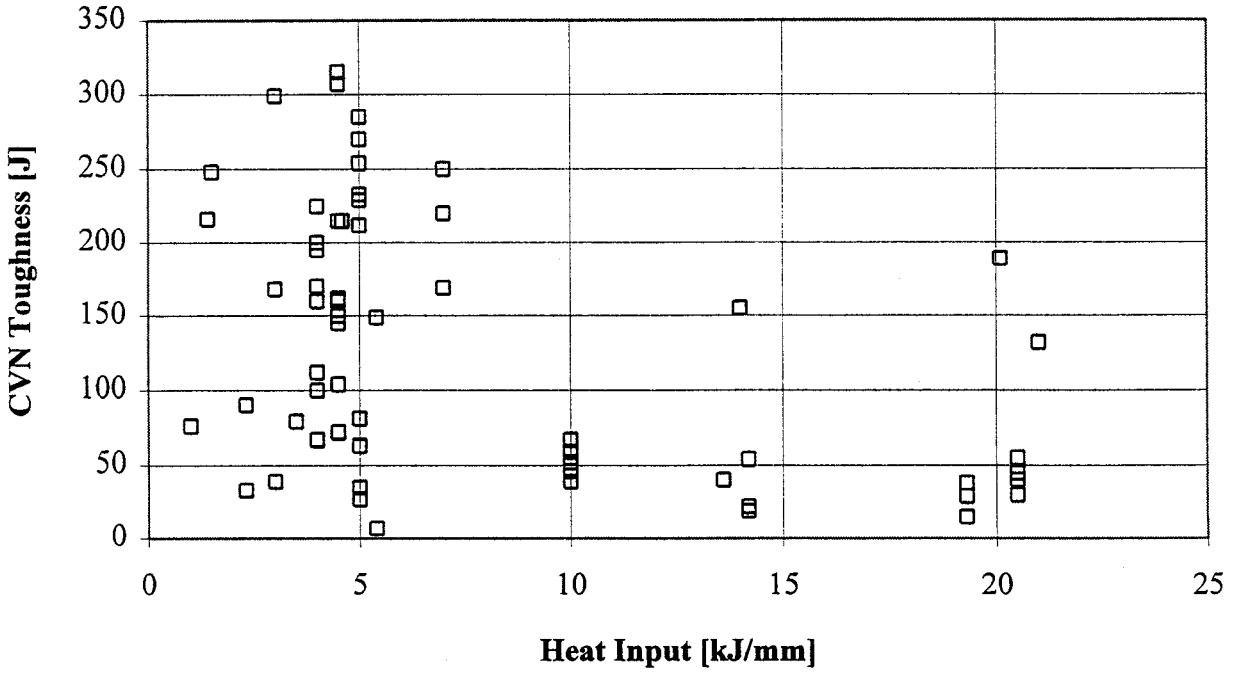

Figure 4.42: Minimum heat affected zone toughness @ -60°C in a set of three or more CVN specimens notched at fusion line

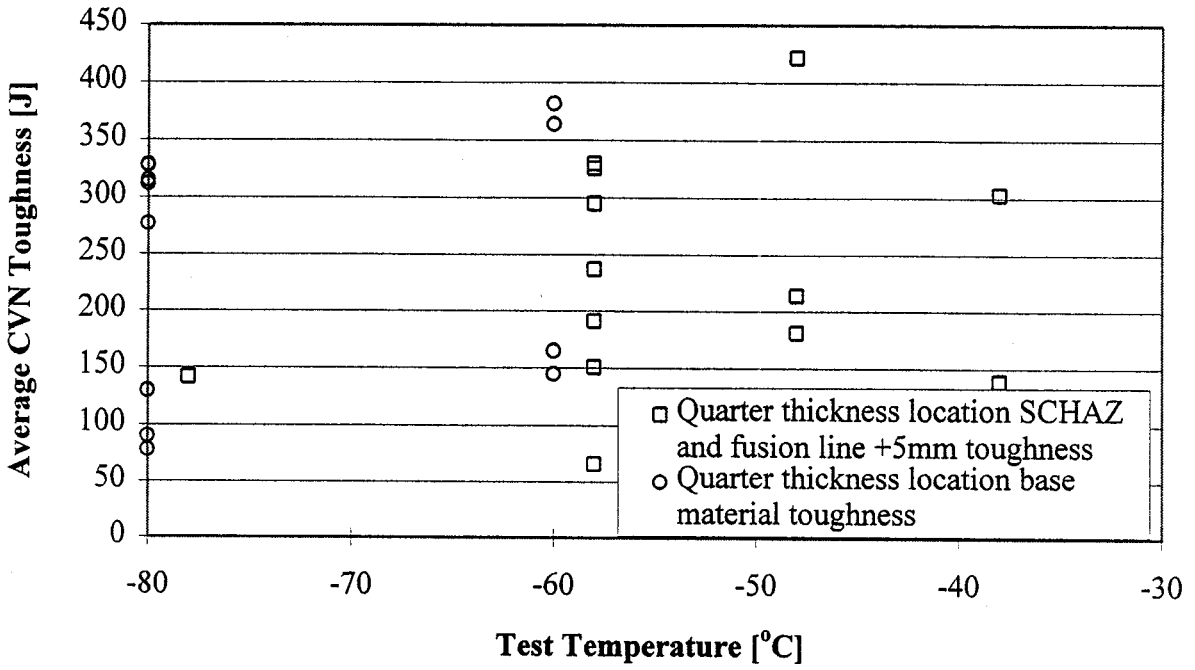

Figure 4.43: Comparison of the average CVN toughness at the subcritical heat affected zone (or fusion line + 5 mm) location with base metal toughness, at the quarter thickness location

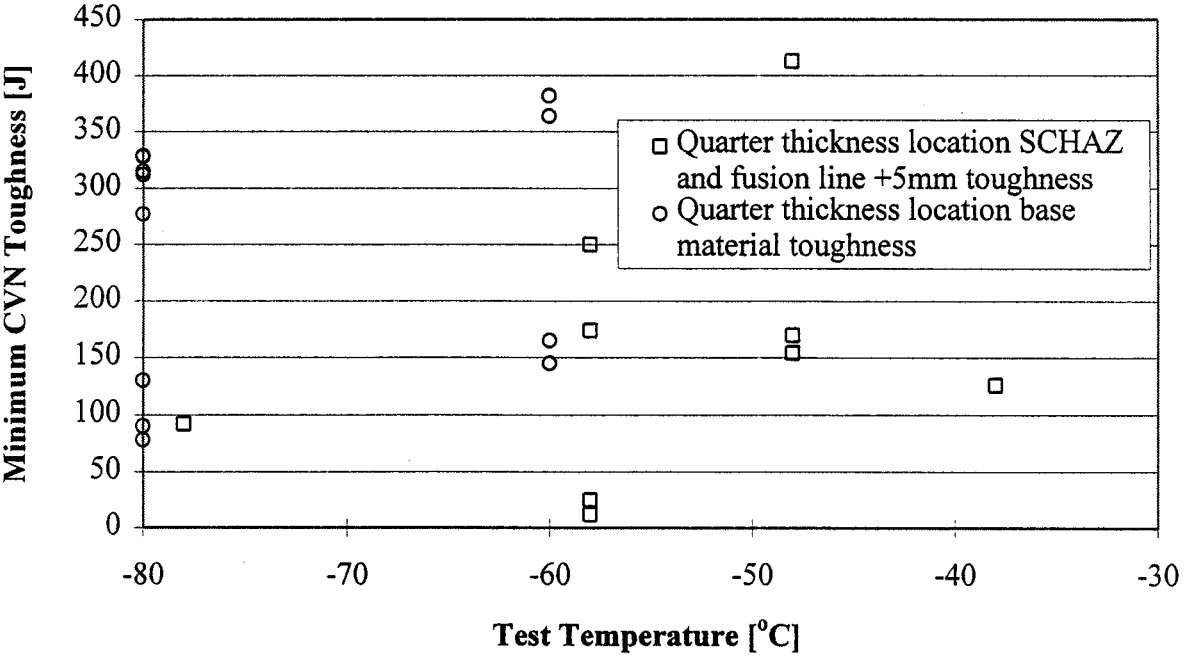

Figure 4.44: Comparison of the minimum CVN toughness (in a set of three or more specimens) at the subcritical heat affected zone (or fusion line + 5 mm) location with base metal toughness, at the quarter thickness location

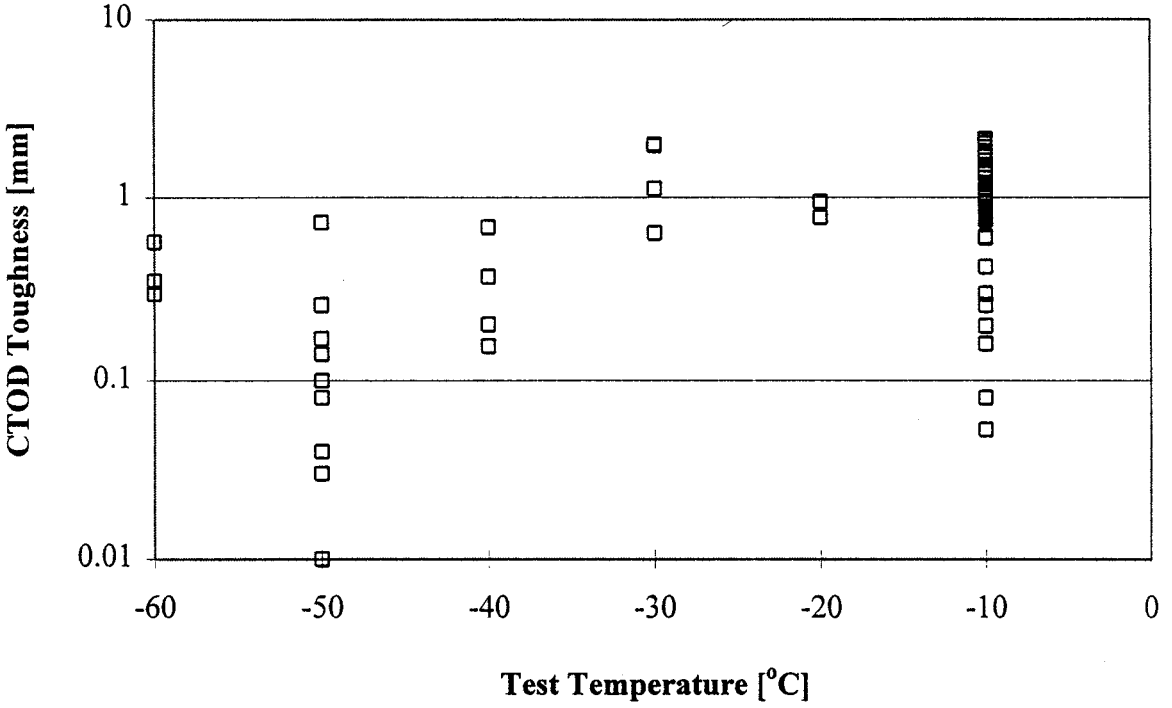

Figure 4.47: Heat affected zone fusion line CTOD toughness values reported for TMCP steels for welds made at a heat input of 3 kJ/mm or less

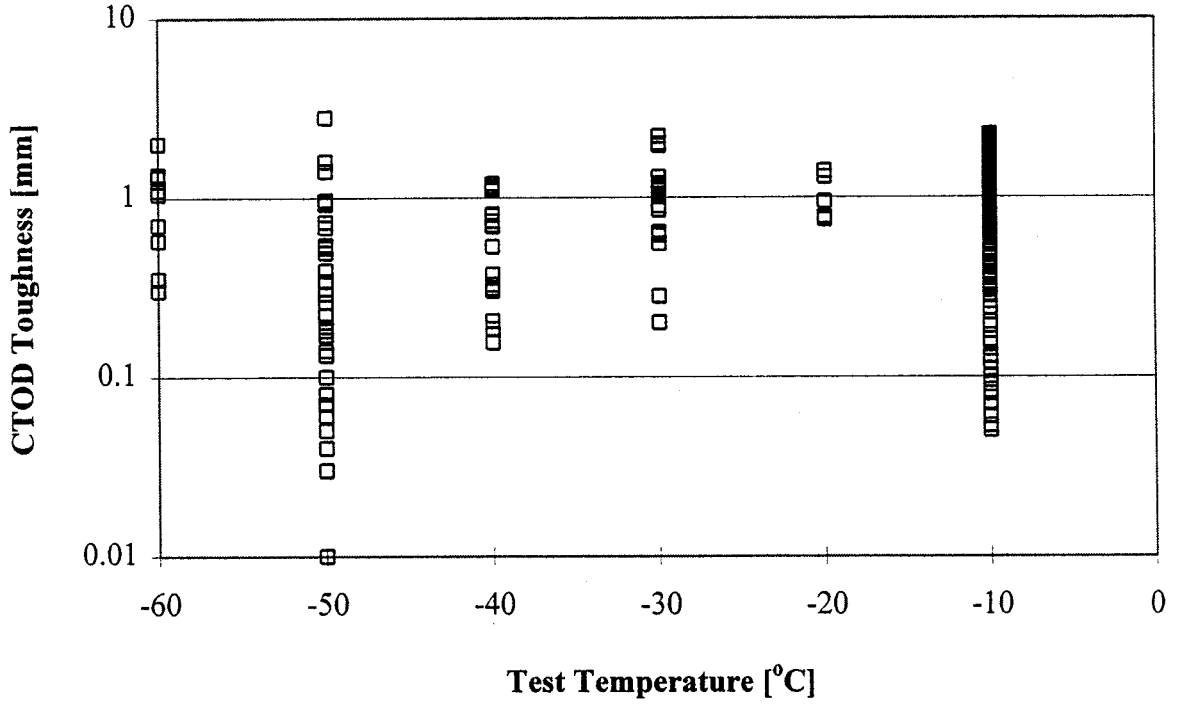

Figure 4.48: Heat affected zone fusion line CTOD toughness values reported for TMCP steels for welds made at heat inputs in the range of 3 to 7 kJ/mm

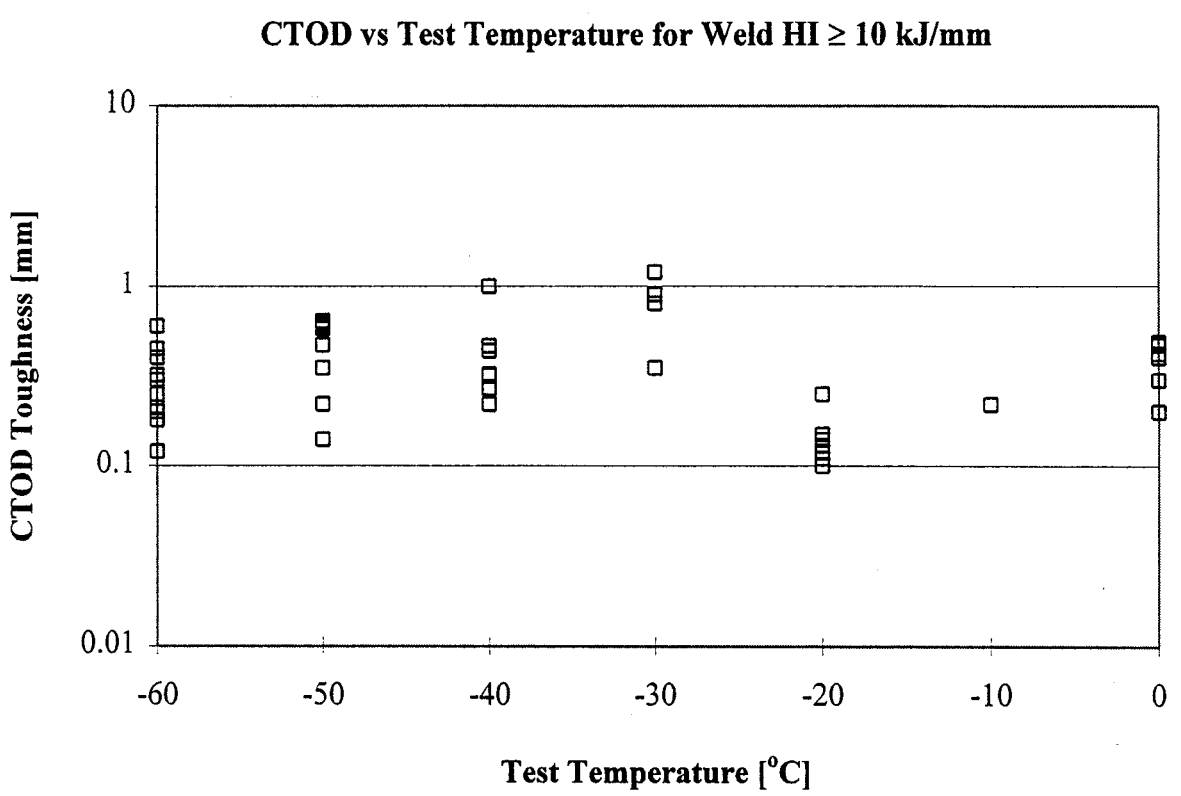

Figure 4.49: Heat affected zone fusion line CTOD toughness values reported for TMCP steels for welds made at heat inputs ≥ 10 kJ/mm

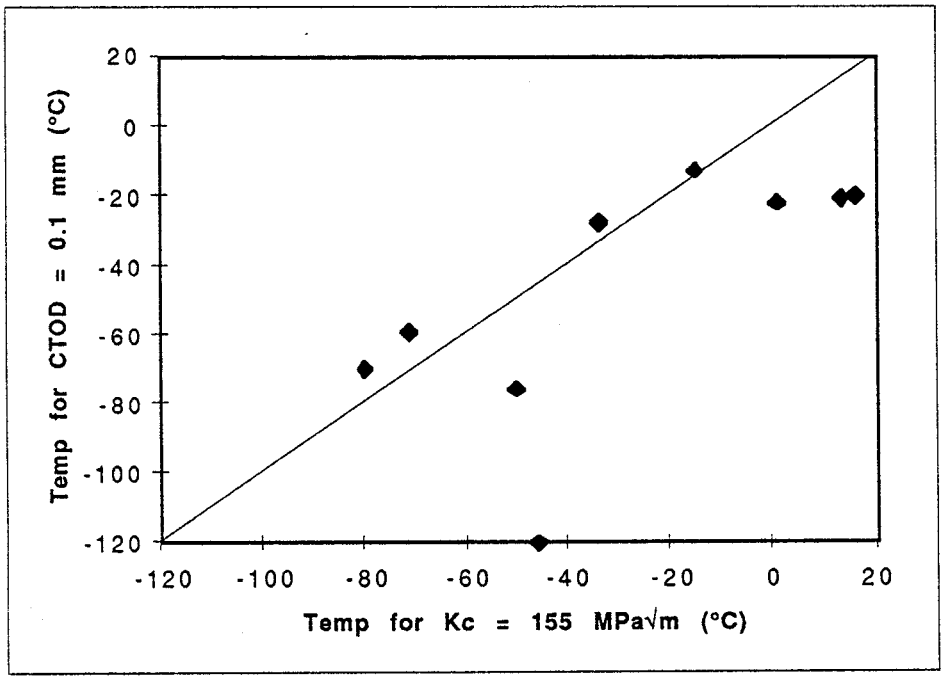

Figure 4.50: Data for machined notched centre cracked wide plate tests for fusion line (HAZ). CTOD temperature determined from lower bound of reported data (limited tests), T (155) found from regression ln K_c against $1/T^{\circ}K$

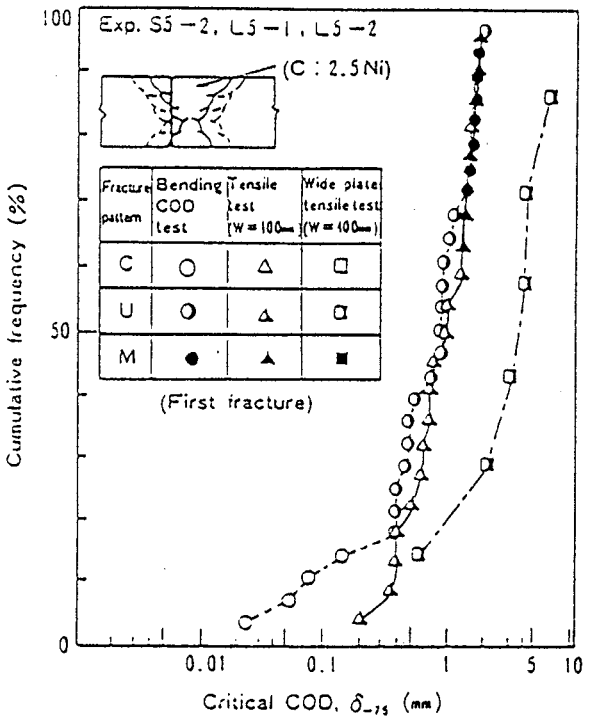

Figure 4.51: Statistical representation of CTOD data for various types of loading Ref. [4.24]

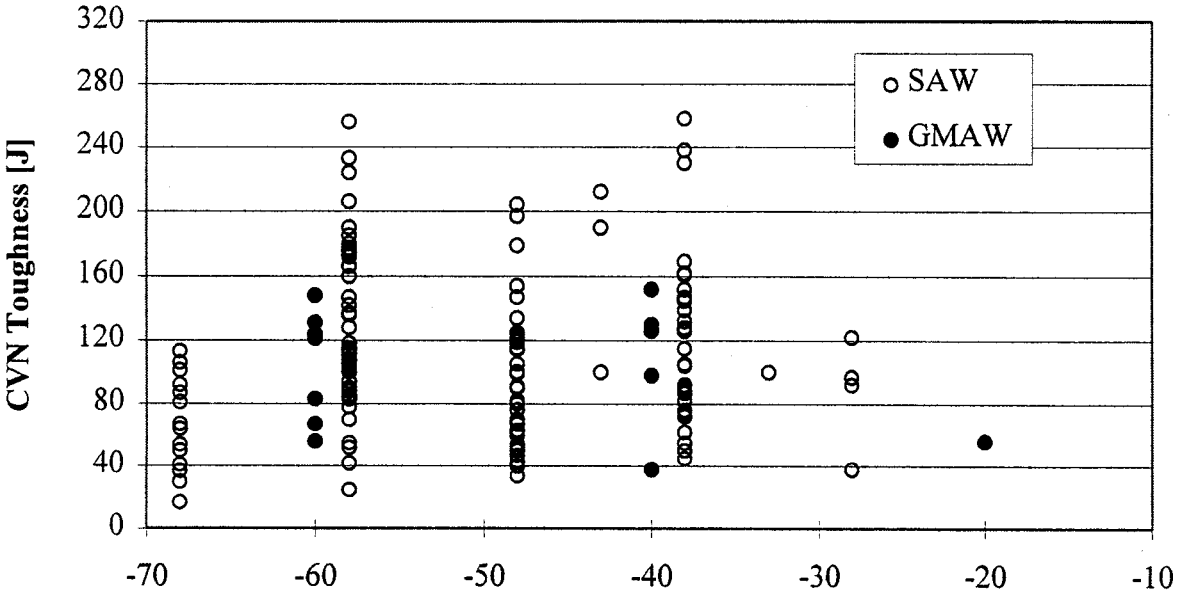

Figure 4.52: Average CVN toughness of weld metals deposited using the submerged arc and gas metal arc welding processes (data for submerged arc welds shown at a temperature 2°C higher than the actual test temperature)

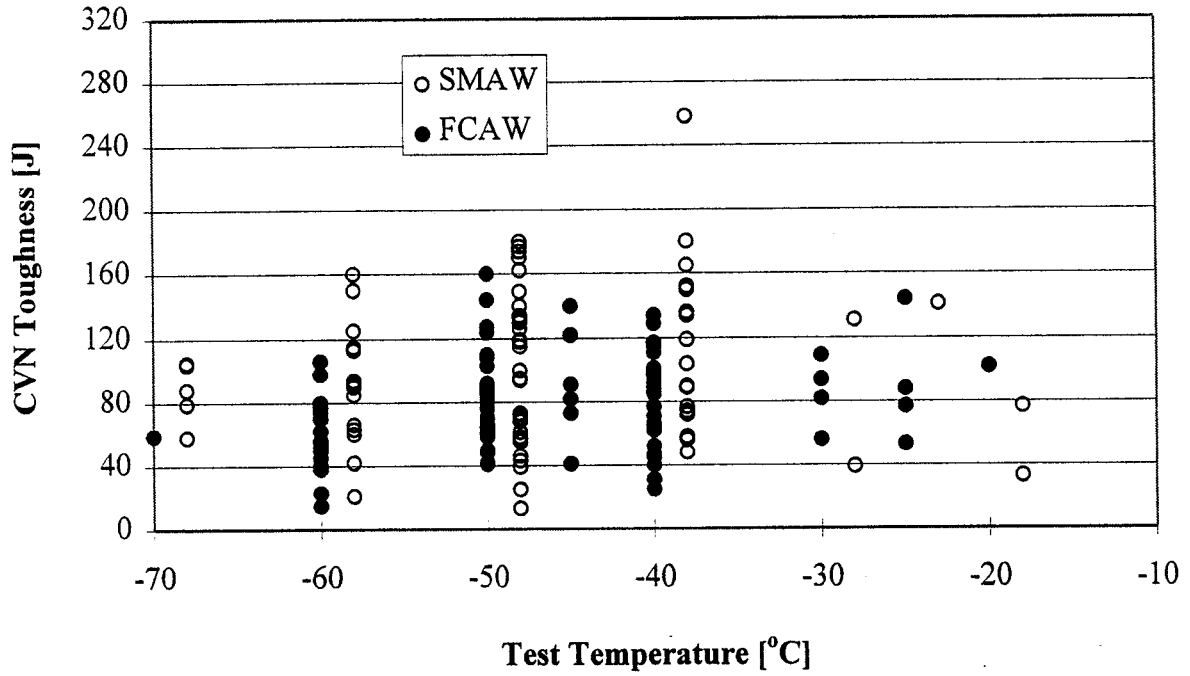

Figure 4.53: Average CVN toughness of weld metals deposited using the shielded metal arc and flux cored arc welding processes (data for shielded metal arc welds shown at a temperature 2°C higher than the actual test temperature)

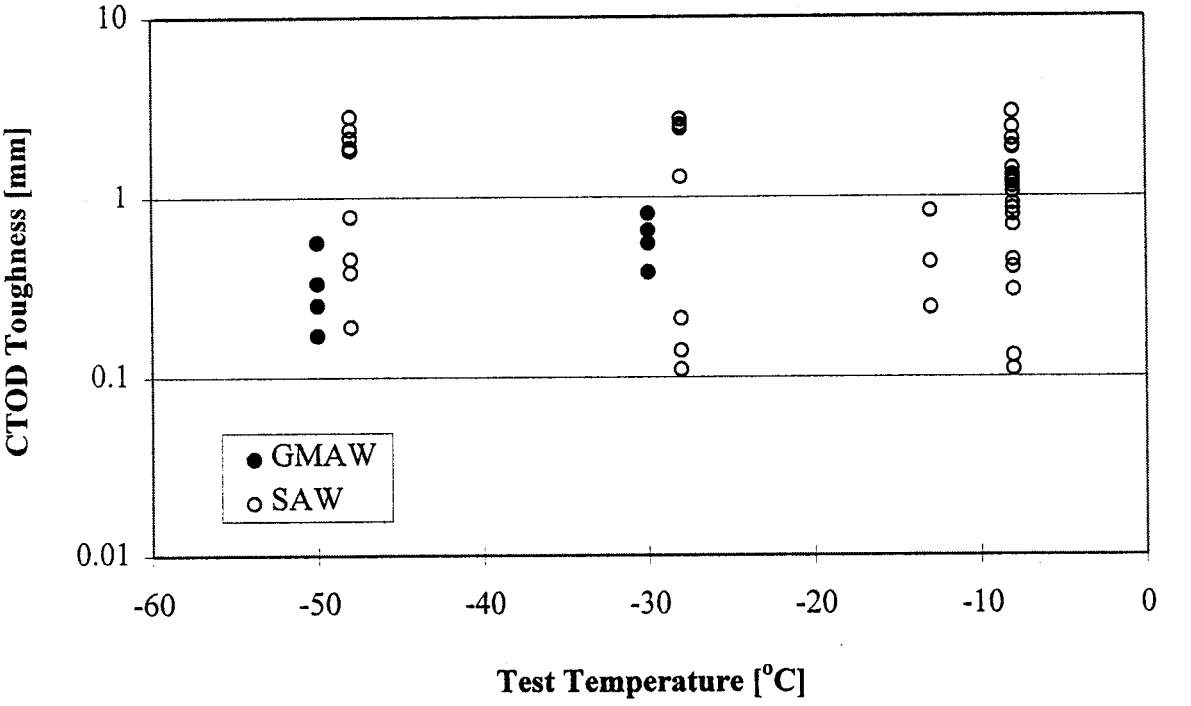

Figure 4.54: Average CTOD toughness of weld metals deposited using the gas metal arc and submerged arc welding processes (data for submerged arc welds shown at a temperature 2°C higher than the actual test temperature)

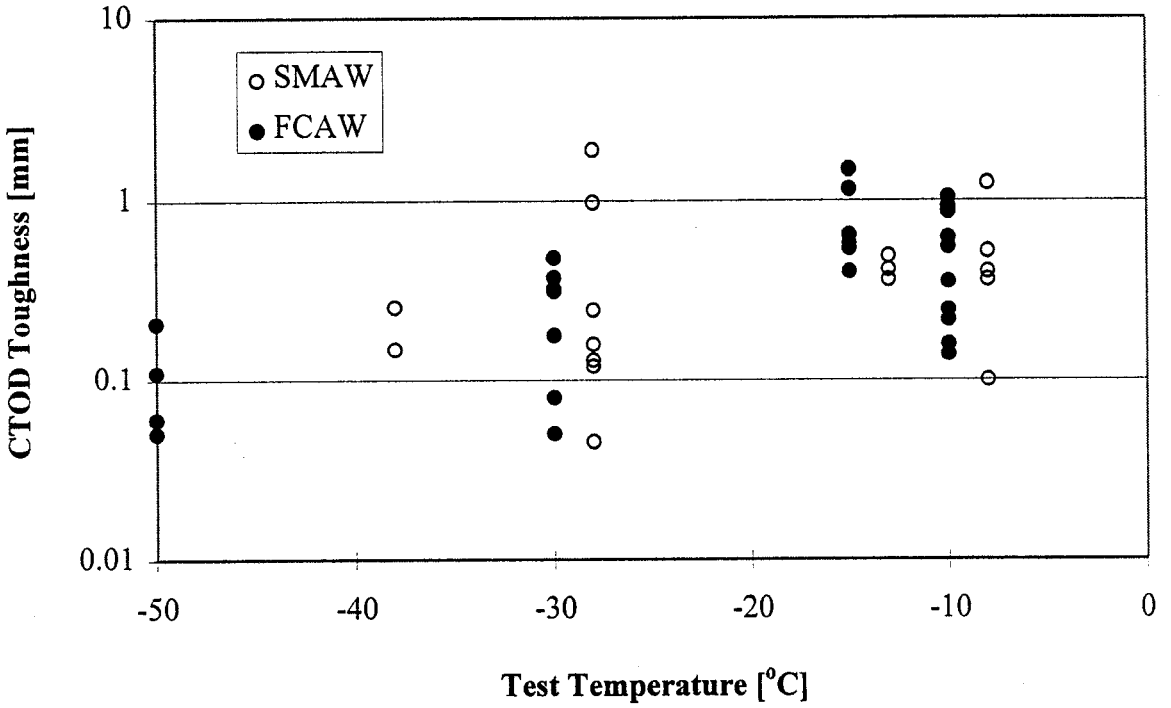

Figure 4.55: Average CTOD toughness of weld metals deposited using the shielded metal arc and flux cored arc welding processes (data for shielded metal arc welds shown at a temperature 2°C higher than the actual test temperature)

5.0 DESIGN IMPLICATIONS (STATIC STRENGTH AND FRACTURE)

5.1 Static Strength

5.1.1 Allowable Yield Strength

The lowest strength steel specified by the IACS member Classification Societies has a Specified Minimum Yield Strength (SMYS) of 235 MPa. Now referred to as ordinary strength steel, it was the only steel available in the early days of ship construction. Since then, higher strength steels have been developed and used. However, it has been known for some time that the ultimate strength of the steel, and buckling strength and fatigue performance of welded structures do not improve in the same proportion as the increase in yield strength. Therefore to maintain similar structural performance with higher yield strength steels as with 235 MPa steel, the Classification Societies, under the auspices of IACS, have incorporated common harmonized values of high tensile steel factor (Q in ABS, k in Lloyd's, f in DNV) in their respective rules for designing, building and classing steel vessels.

The high tensile steel factor (HTSF) reduces the yield strength value that can be used in design calculations, and as shown in **Table 5.1**, it has the net effect of maintaining a nearly constant difference between the specified minimum ultimate tensile strength (SMUTS) and the allowable yield strength (AYS).

Since one of the main advantages of the TMCP steels is the availability of higher SMYS (up to 500 MPa) while maintaining excellent weldability and toughness, it is useful to assess what the HTSF would be for steels with SMYS ranging from 420 to 500 MPa, following the above empirical approach, i.e., to maintain (SMUTS-AYS) equal to say 167 MPa, the average for the four lower yield strength steels. These estimates, shown in **Table 5.2**, would, of course, be applicable to all types of steels meeting the tensile property specifications.

Kitada [5.1] has offered an alternate way of deriving and justifying the existing values of the HTSF. According to this explanation,

$$HTSF = 0.5(235/SMYS + 400/SMUTS) \qquad (5.1)$$

A plot of this equation for steels with SMYS up to 500 MPa is shown in **Figure 5.1**, and the estimated values of the HTSF are shown in **Table 5.3**.

Comparing the three tables, it is observed that the Kitada approach gives slightly higher values for the HTSF, i.e., slightly lower value for the AYS and higher values for (SMUTS-AYS), especially for the 500 MPa yield strength.

Table 5.1: Effect of the high tensile steel factor (HTSF) on allowable yield stress (AYS) and safety margin with respect to the specified minimum ultimate tensile strength (SMUTS-AYS)

SMYS (MPa)	SMUTS (MPa)	HTSF	AYS=235/HTSF (MPa)	SMUTS-AYS (MPa)
235	400	1.00	235	165
315	470	0.78	301	169
355	490	0.72	326	164
390	510	0.68, 0.70 (proposed)	346, 336	164, 174

Table 5.2: Calculated HTSF values for higher strength steels to maintain a constant safety margin (SMUTS-AYS) of 167 MPa

SMYS (MPa)	SMUTS (MPa)	AYS=SMUTS-167 (MPa)	HTSF=235/AYS (MPa)
420	530	363	0.65
460	550	383	0.61
500	610	443	0.53

Table 5.3: Actual and predicted HTSF, and predicted safety margin based on Kitada's formulation

SMYS (MPa)	SMUTS (MPa)	Predicted HTSF	Class. Rule HTSF	Predicted AYS (MPa)	Actual AYS (MPa)	SMUTS - Pred. AYS (MPa)
235	400	1.00	1.00	235	235	165
315	470	0.80	0.78	294	301	176
355	490		0.72	318	326	172
390	510	0.69	0.68, 0.70 (proposed)	339	346, 336	171
420	530	0.66		358		172
460	550	0.62		380		170
500	610	0.56		418		192

5.1.2 Actual Tensile Properties of TMCP Steels

The approach followed in Section 5.1.1 to determine potential HTSF values for higher strength steels is entirely empirical and does not consider specific failure mechanisms, viz., tensile plastic collapse, fatigue and buckling. There is however increasing emphasis on explicit analysis of fatigue and buckling considerations in ship design, and in the context of high strength TMCP steels, the fatigue aspects are covered in Section 6.

From the point of view of tensile plastic collapse, the intent of minimum ductility or maximum yield ratio requirements in material specifications, and of allowable design stress in design codes is to have assurance of some undefined level of plastic deformation capacity in the welded structure and to minimize the probability of actual service stress exceeding the tensile strength.

Ductility of TMCP Steels

In the context of ductility and deformation capacity, the important parameters are uniform elongation and the strain hardening exponent though there is no existing methodology to use these in the design process.

As pointed out in the data analysis section, there is a suggestion in the limited data available that uniform elongation values for TMCP steels can be quite high, probably higher than those for conventional steels historically used in ship construction. However, there is little data available in this regard or on the strain hardening exponent for these steels. There is thus a need for further characterizing TMCP steels in this regard.

Safety Margin with respect to Design Stress

The allowable tensile stress or the design stress in a structural codes is usually specified as a fraction of the specified minimum yield strength. The difference between the actual tensile strength of the steel and the design strength can be considered as the safety margin and may be expressed as an absolute stress differential or as a proportion of the SMYS. Further, if the probabilistic distribution of service stresses is known, then the probability of exceeding the actual tensile strength can be computed and ensured to be acceptably low. To consider these aspects, **Figure 5.2** shows the actual tensile strength of the steels plotted against the SMYS. The slope of the trend line is 0.6338. (For comparison, the plot of actual tensile strength versus the actual yield strength is shown in **Figure 5.3**.)

Ignoring the HTSF, the design stress however is typically "0.7 x SMYS" (175/245=0.71 in Lloyd's rules) which means that the absolute Safety Margin would indeed decrease with increase in the specified minimum yield strength. However, as seen in **Figure 5.4**, the decrease is marginal, from about 275 MPa to 263 MPa as the SMYS increases from 315 to 500 MPa. But if the change is expressed as a fraction of the SMYS (**Figure 5.5**), then the decrease in safety margin is from 85% to 53%.

If the values computed above for the HTSF are incorporated into the calculations, the absolute safety margins would increase and be larger for the higher strength steel, increasing from 285 MPa to about 316 MPa over the same increase in the SMYS (315 to 500 MPa). On a relative basis, the corresponding numbers will change to 90% and 63%.

It is rather difficult to easily comprehend the implications of the simply calculated numbers above showing that while the absolute safety margin remains essentially constant or may even increase with increase in the SMYS, the relative safety margin certainly decreases with increase in the SYMS. Dier et al [5.2] points out that the absolute safety margin does not take into account the uncertainty or the distribution of the applied service stresses and the authors go on to assess the effect of using higher strength steels on the probability of failure for certain hypothetical distributions of the service loads. The same approach has been followed below to assess the effect of increasing the TMCP steel SMYS from 315 to 500 MPa on the probability of failure. The input data and assumptions for the analysis are as follows:

- failure probability is defined by the probability of the service stress exceeding the ultimate tensile strength of the steel;
- the ultimate strength of the TMCP steel, as a function of the SMYS is given by the trend line equation in Figure 5.2 ;
- the design stress is 70% of the SYMS or SYMS adjusted for the HTSF;
- the service stress has a normal distribution with .025 as the probability of exceeding the design stress (conservative but reasonable assumption, according to Dier et al);
- three distributions of the service stresses are considered with means of service stresses being 90, 50 and 10% of the design stress; the corresponding standard deviations are determined by the requirement that the probability of exceeding the design stress is 2.5%.

The results of this analysis are presented in the **Table 5.4**. To the extent that the assumptions made are a reasonable reflection of ship structures, and the notional failure probability of the order of 3×10^{-4} is acceptable [5.2], the above calculations indicate that the 500 MPa TMCP steel will be adequate, even without considering the HTSF and for the widest applied stress distribution assumed.

In the above approach, one need not be concerned with the some what higher yield ratio (see Section 4.1) of TMCP steels in relation to that for other steel types. The failure probability is governed by the absolute safety margin (Actual UTS-Design Stress) and design stress is determined by the specification and design codes requirements only. Therefore as long as the distribution of "Actual UTS-SMUTS" for TMCP steels is similar to or to the right (higher mean, similar or smaller standard deviation) of the distribution for conventional steels, the TMCP steels ought to be providing similar or lower failure probabilities.

In summary then, while noting the need for further experimental work to better define the strain hardening and uniform elongation characteristics of the TMCP steels, the analysis above proposes values for HTSF for higher yield strength (>390 MPa) steels following the existing approach and it also indicates that higher yield strength of the tough, weldable TMCP steels can be utilized in design while retaining acceptable structural reliability against tensile plastic collapse.

Table 5.4: Effect of higher SMYS on failure probability under various assumed distributions for the service stresses

SMYS (MPa)	Actual UTS (MPa)	Design Stress (MPa)	Service Stress Mean (MPa)	Service Stress Std. Dev. (MPa)	Probability of Failure
315	496	220	198	11	0
315	496	220	110	56	2.75E-12
315	496	220	20	110	9.77E-06
315	496	211*	190	11	0
315	496	211*	105	54	2.41E-13
315	496	211*	19	96	3.96E-07
500	613	350	315	18	0
500	613	350	175	89	4.30E-07
500	613	350	35	161	1.65E-04
500	613	300*	270	15	0
500	613	300*	150	77	9.14E-10
500	613	300*	30	138	1.20E-05

(* takes into account the HTSF)

5.2 Fracture Prevention (Base Metal)

Current Approach for Ships

Currently, fracture control in ship design is exercised indirectly through application of structural steel with appropriate level of minimum specified CVN toughness to different regions of the ship depending on the criticality of the structural component and the member thickness. For example, **Table 5.5**, reproduced from ABS Rules for Building and Classing Steel Vessels, specifies the material class that can be used for different structural members depending on location with respect to the ship length. Assuming a design temperature of 0°C, the ship steel thickness/grades that conform to a given material class are provided in **Table 5.6**, again reproduced from the ABS Rules. In Table 5.5, H denotes high tensile steel, and grades A to E imply improving steel toughness. Thus, grade EH, DH and AH are required to meet their CVN absorbed energy requirements at -40°C, -20°C and 0°C, respectively.

The application of steel, from the toughness point of view, to ship structural members is similar in other Classification Society rules. This is as a result of the efforts made in the early eighties to harmonize the requirements between the Classification Societies under the auspices of IACS. The toughness requirements are based on investigations of fracture initiation in wide plate tests and mathematical representation of the shape of typical CVN transition curves [5.3, 5.4] and the overall approach draws its strength from the fact that it is calibrated with data and experience of actual fractures in ship hulls.

Essentially, a steel conforming to any one of the five material classes must have fracture toughness (at quasistatic loading rate) that exceeds the crack driving force corresponding to predefined levels of applied and residual stresses and flaw size for that material class. The crack driving force is computed from the equation

$$\begin{aligned} K &= (\sigma_D + \sigma_R)\sqrt{(\pi a)} \\ &= (\alpha \cdot AYS + \beta \cdot SMYS)\sqrt{(\pi a)} \end{aligned} \qquad (5.2)$$

where:

K	=	crack driving force (required fracture toughness)
σ_D	=	design stress = $\alpha \cdot$ AYS
α	=	coefficient of yield strength utilization
AYS	=	allowable yield strength
σ_R	=	residual stress = $\beta \cdot$ SMYS
β	=	coefficient for residual stress = 0.6 (based on test results)
$2a$	=	assumed flaw size in a wide structural member (250 mm).

The value of α has been given as 0.2, 0.5, 0.6, 0.7 and 0.8 for the five material classes [5.4], i.e., steels conforming to material class V are subjected to the highest service stresses. Further, in the context of offshore structures, α values of 0.5, 0.6 and 0.7 are indicated to represent secondary, primary and special structural member categories.

In order then to evaluate the conformance of the steels to various material classes, their fracture toughness at the design temperature is measured using center notched ($2a$ = 250 mm) wide plate tests, based on fracture stress and the notch size. For the practical purposes of assigning different grades of ship steels to different material classes, the Japanese investigators via empirical expressions, calculated (i) the 50% fracture appearance transition temperature (vT_E) from the standard CVN absorbed energy criterion (say 27 J at -20°C); (ii) the brittle fracture transition temperature (T_i) from vT_E taking into account the effects of thickness and yield strength; (iii) fracture toughness as a function of temperature from T_i.

Comparing the required fracture toughness computed according to Equation 5.2 with the expected fracture toughness from the empirical relations, the investigators were able to assign the ship steel grades, as a function of thickness and yield strength to different material classes, culminating in tables such as those shown in Tables 5.5 and 5.6. The details of the empirical relations and the overall approach are included in **Appendix D.**

Table 5.5: ABS Material Class Requirements for Various Ship Structural Members (Design Temp; 0°C)

Structural Member	Material Class [1]	
	Within 0.4L Amidships	Outside 0.4L Amidships
Shell		
• Bottom plating including keel plate	III	I
• Bilge strake	IV [2,3,4]	III [5,6]
• Side plating	II	I
• Sheer strake at strength deck [7]	IV [3,4,8]	III [5,6]
Decks		
• Strength deck plating [9]	III	I
• Stringer plate in strength deck [7]	IV [3,4,8]	III [5,6]
• Strength deck plating within line of hatches and exposed to weather, in general	II	I
• Strength deck strake on tankers at longitudinal bulkhead [10]	IV [3,4]	III [5,6]
Longitudinal Bulkheads		
• Lowest strake in single bottom vessels	II	I
• Uppermost strake including that of the top wing tank	III	I
Other Structures in General		
• External continuous longitudinal members and bilge keels	III	I
• Stern frames, rudder horns, rudders, and shaft brackets	-	I
• Strength members not referred to in above categories and above local structures	I	I

Notes:

1. Special consideration will be given to vessels in restricted service.
2. May be of class III in vessels with a double bottom over the full breadth and with a length less than 150 m (492 ft).
3. Single strakes required to be of material class IV and V or E are to have breadths not less than 800 + 5L mm (31.5 + 0.06L in), but need not exceed 1800 mm (71 in).
4. Below 90 m (295 ft) in length this may be class III.
5. May be class II outside 0.6L amidships.
6. Below 90 m (295 ft) in length this may be class I.
7. A radius gunwale plate may be considered to meet the requirements for both the stringer plate and the sheer strake, provided it extends suitable distances inboard and vertically. For formed material see 2/3A.3.7.
8. To be class V in vessels with length exceeding 250 m (820) ft).
9. Plating at the corners of large hatch openings are to be specially considered.
10. For tankers having a breadth exceeding 70 m (230 ft) at least the center line and one strake port and starboard at the longitudinal bulkheads are to be class IV.

Table 5.6: Material Classes as defined in ABS Rules for Building and Classing Steel Vessels

Thickness mm *(in.)*	Material Class				
	I	II	III	IV	V
t ≤ 15 (t ≤ 0.60)	A, AH	A, AH	A, AH	A, AH	D, DH
15 < t ≤ 20 (0.60) < t ≤ 0.79)	A, AH	A, AH	A, AH	B, AH	D[1], DH
20 < t ≤ 25 (0.79) < t ≤ 0.98)	A, AH	A, AH	B, AH	D, DH	E, EH
25 < t ≤ 30 (0.98) < t ≤ 1.18)	A, AH	A, AH	D, DH	D[1], DH	E, EH
30 < t ≤ 35 (1.18) < t ≤ 1.38)	A, AH	B, AH	D, DH	E, EH	E, EH
35 < t ≤ 40 (1.38) < t ≤ 1.57)	A, AH	B, AH	D, DH	E, EH	E, EH
40 < t ≤ 51 (1.57) < t ≤ 2.00)	B[2], AH	D, DH	E, EH	E, EH	E, EH

Notes:
1. Grade D and DS of these thicknesses to be normalized.
2. May be Grade A for stern frames, rudder horns, rudders and shaft brackets.

The above approach has been used for steels with SMYS of 355 MPa, and in terms of required fracture toughness, would be applicable to TMCP steels as well. However, assigning the TMCP steels to the different material classes on the same premise may not be completely appropriate since the empirical relationships between CVN properties and fracture behavior derived from conventional steels are unlikely to be applicable to TMCP steels (see discussion in Section 4.2).

Nonetheless, the adequacy of the 355 MPa and higher strength TMCP steels for various material classes can be judged based on the required fracture toughness and wide plate data for these steels, noting that higher yield strength steels will need to have higher fracture toughness because of the higher assumed service and residual stresses. Such calculations have been performed by Kitada [5.1] for 390 MPa yield strength steel, however the α, β and 'a' values used are slightly different. The required fracture toughness values can be similarly calculated for higher strength TMCP steels (up to 500 MPa), and for material classes IV and V, these are shown in **Table 5.7** based on these different values for α (0.7 for material classes IV and V), β (0.5) and 'a' (200 mm and 240 mm for material class IV and V, respectively).

The base metal fracture toughness data of this type is available for steels with up to 390 MPa yield strength only, and as mentioned earlier (see Figures 4.24, 4.25), the TMCP steels with a thickness of about 30 mm, show maximum load behavior above about -100°C, with the maximum K_c value being in the neighborhood of 186 MPa$\sqrt{m}$ (600 kgf$\sqrt{mm}$/mm^2). However, by extrapolating the K_c vs $1/T(K^{-1})$ relationship, it is demonstrated that the 390 MPa yield strength steels comfortably meet the required fracture toughness at 0°C (see **Figure 5.6** [5.5]).

Table 5.7: Calculated required fracture toughness for high strength steels to meet material classes IV and V requirements

SMYS (MPa)	Assumed HTSF	Total App. Stress (235α/HTSF+βSMYS) (MPa)	Required Fracture Toughness MPa√m at 0°C	
			Class IV	Class V
390	0.68	437	245	268
420	0.65	463	260	284
460	0.61	500	280	307
500	0.53	560	314	344
500	0.47*	600	336	368

(* Assumes full utilization of yield strength.)

Table 5.8: CTOD data (three point bend specimens) for some higher strength steels

SMYS (MPa)	Thickness (mm)	Test Temperature, °C	CTOD (mm)	Comment
460	30	-50	1.55	
490	30	-40	1.2	max. load
460	30	-60	1.0, 1.4	
415	30	-60	1.3	Wide plate brittle initiation at <-140°C

Even though little similar data is available for higher strength TMCP steels, some idea of their suitability following this approach may be obtained from CTOD tests. In principle, the required fracture toughness in the table above can also be computed in terms of CTOD, using analyses of the type given in PD 6493. Suffice it to say for the time being that the requirement equivalent to 368 MPa√m will be about 2.2 mm CTOD at 0°C, i.e., the steel should display maximum (limit) load behavior at 0°C. Some of the CTOD data compiled in the data base for these higher strength steels is shown in **Table 5.8** and it is quite likely that at 0°C, these steels will meet the requirements of material class V.

Alternate Approaches for Ships

(a) Sumpter's Approach

An alternate approach proposed by Sumpter [5.6] to prevent fractures in ship structures is to ensure that the steel has a minimum fracture toughness of 125 MPa√m (actually a J integral value determined from a full thickness specimen and converted to stress intensity units) at 0°C and a loading rate appropriate to the structural member. This loading rate may vary from 10^2 MPa√m/s to simulate the effect of slamming at the midships deck to 10^4 MPa√m/s for representing the dishing of a ship bottom hull plate under local slamming. For naval ships subject to shock loading, the level of fracture toughness will need to be met at an impact loading rate.

The required level of fracture toughness assumes that the total service and residual stresses are of the order of 100 MPa and that the steel should be able to prevent fracture initiation from a meter long crack. The author goes on to add that mild steels displaying a CTOD of 0.15 mm at the appropriate loading rate or 50% fracture transition temperature of 0°C are likely to meet the stated fracture toughness requirement.

Based on this approach, the TMCP steels will comfortably meet the required fracture toughness criterion since TMCP steels with a guaranteed 50% FATT of -60°C are commercially available, and Figure 4.21 shows that TMCP steels can comfortably meet 0.15 mm CTOD requirement at 0°C, even at an impact loading rate. The exact requirement will however change if it is known that the service or residual stresses could be higher or if the tolerable flaw size changes.

(b) Crack Arrest Approach

The crack arrest approach to prevent catastrophic structures in ships can be applied in two ways. First, the Japanese researchers and NKK have proposed [5.4], based on analysis of ship fractures and damage records, that steel crack arrest toughness of 124 to 186 MPa$\sqrt{m}$ (400 to 600 kgf · $\sqrt{mm/mm^2}$) at 0°C is sufficient to arrest brittle fractures in ships. For 390 MPa yield strength TMCP steels, these levels of crack arrest toughness can be met as seen in **Figure 5.7**. For higher strength steels, the data is limited (**Table 5.9**) which nonetheless suggest that reliably meeting the target value at 0°C is quite feasible for TMCP steels.

Table 5.9: Crack arrest toughness values for two high strength steels

SMYS (MPa)	Thickness (mm)	K_{ca} (MPa$\sqrt{m}$) at °C
415	30	186 at -60
490	30	374 at -40

The second crack arrest approach is based on Pellini's drop weight NDT temperature. Notwithstanding the fact that the current specifications for Grade FH ship steels in Classification Society rules stipulate CVN tests to be performed at -60°C (absorbed energy equal to MPa/10 in Joules for the longitudinal direction), a case was made earlier in Section 4.2 that the NDTT provides a sounder basis for specifying steel toughness for qualification purposes than does the CVN based criteria. Also, a histogram of the NDTT of TMCP steels was presented in Figure 4.15 which showed that commercial steels are available to easily meet a -60°C NDTT requirement.

It is recommended, therefore, that FH grades of ship steels should require a maximum guaranteed NDTT of -60°C which in turn will assure, in terms of Pellini's fracture analysis diagram (**Figure 5.8**) that unstable brittle fracture would be virtually impossible in ships constructed for a design temperature of 0°C. From damage tolerance point of view, fracture analysis is then no longer necessary and considerations of fatigue crack growth and plastic collapse based on net section area should be enough.

Structures Operating at Lower Design Temperatures

For semi-submersibles and fixed offshore structures, the design temperatures can be substantially below 0°C. For example, the design temperature for semi-submersibles operating in the Bering Sea area is suggested to be -30°C, and the base metal for 'special' category of structural members is required to meet the following toughness requirements: 35 J CVN absorbed energy at -60°C, NDTT of -65°C (design temperature -35°C). Further, base metal quasi-static CTOD toughness of 0.2 mm at -30°C may be an additional requirement. Clearly, based on data analysis presented in Section 4.2, the NDTT requirement is the most stringent one and if it is met, then the other requirements are virtually certain to be met. The NDTT requirement of "design temperature -35°C" ensures that the structural member would be operating above the fracture transition elastic point on Pellini's fracture analysis diagram.

Looking back at the NDTT histogram in Figure 4.15, it is suggested that next tougher grade (GH?) after the FH grade should require an NDTT of -80°C. Based on the ABS requirement for "special" category structural members, such steels would be acceptable for design temperatures down to -45°C, same as usually stipulated for structures in arctic regions. Similarly, Yajima et al [5.7] have proposed a toughness requirement of 0.1 mm quasistaic CTOD at -50°C for steels employed for structures in the arctic regions. Steels with a NDTT of -80°C will comfortably meet this requirement. It should be added though that arctic structures are usually statically loaded and the structural members may not be classified as "special" in which case NDTT requirement of -80°C may be unnecessary.

5.3 Fracture Prevention (Heat affected zone)

The Japanese approach to specifying HAZ toughness requirement at the fusion line for welds in ship structures is similar to that for the base metal although flaw size, residual stress values assumed (β=0.2; assumes that transverse residual stresses acting on a flaw in the HAZ parallel to the weld axis, are considerably smaller than those in the longitudinal direction) and coefficient of yield strength utilization used to compute the required toughness are different. Following Kitada [5.1], the required fracture toughness for HAZ at the fusion line are shown in **Table 5.10**.

Table 5.10: Required fracture toughness for heat affected zone (fusion line)

SMYS (MPa)	Assumed HTSF	Total Applied Stress (235α/HTSF + βSMYS)		Required Fracture Toughness MPa$\sqrt{m}$ at 0°C	
		Side plate α=0.5	Strength Deck α=0.6	Side Plate 2a=88 mm	Strength Deck 2a=77 mm
390	0.68	251	285	93	99
420	0.65	265	301	99	105
460	0.61	285	323	106	112
500	0.53	335	366	125	127
500	0.47*	350	400	130	139

(* Assumes full utilization of yield strength)

The CTOD value corresponding to a required fracture toughness of 139 MPa$\sqrt{m}$, based on PD 6493 Level 2 analysis, would be about 0.23 mm. However, under conditions of lower constraint, as in wide plate tests, the transition temperature for 0.1 mm HAZ fusion line CTOD corresponds to a fracture toughness of 155 MPa$\sqrt{m}$ (see Figure 4.50) indicating that 0.1 mm CTOD should be an adequate requirement for HAZ fusion line toughness. Further, limited data in Figures 4.47 to 4.49 suggests that this level of CTOD could be met at temperatures as low as -30°C to -50°C, depending on the weld heat input employed. However, more data needs to be generated to have confidence that such HAZ fracture toughness in the higher strength TMCP steels (450 to 500 MPa yield strength) at low test temperatures (-30°C to -50°C) can be reliably met.

For practical procedure qualification purposes, the Kitada et al [5.1] indicate that the required fracture toughness levels for 390 MPa yield strength steels (93 to 99 MPa$\sqrt{m}$ or 309 to 320 kgf$\sqrt{mm/mm^2}$) translate into the existing CVN requirements, i.e., 27 to 40 J at a test temperature that is 20°C higher than that for the base metal. (e.g., HAZ in EH grade of steel is required to be tested at -20°C whereas the steel itself is tested at -40°C). Following this approach, for steels with base metal CVN energies specified at -60° and -80°C, the heat affected zone CVN energy requirements will need to be met at -40° and -60°C, respectively, and based on data presented in Figures 4.39 to 4.42, this should not pose a problem.

In summary, advantages of TMCP steels over conventional steels vis a vis design for fracture prevention can be stated to be as follows:

(a) higher service/applied stresses: TMCP steels and heat affected zones formed in these steels, have higher fracture toughness commensurate with increase in the allowable stress/yield strength;

(b) lower design temperature: while fixed at 0°C for merchant ships, the design temperature can be as low as -45°C for structures in the arctic and subarctic regions. TMCP steels can be furnished that will have adequate fracture toughness at these low design temperatures (NDTT = design temp. – 35°C);

(c) larger tolerable flaw size: TMCP steels could be effectively employed for those regions of the ships that are difficult to inspect; for ship structures designed for 0°C service temperature; TMCP steels with NDTT of -60°C or lower, virtually eliminate the risk of brittle fracture and tolerable flaw size is then primarily governed by plastic collapse considerations.

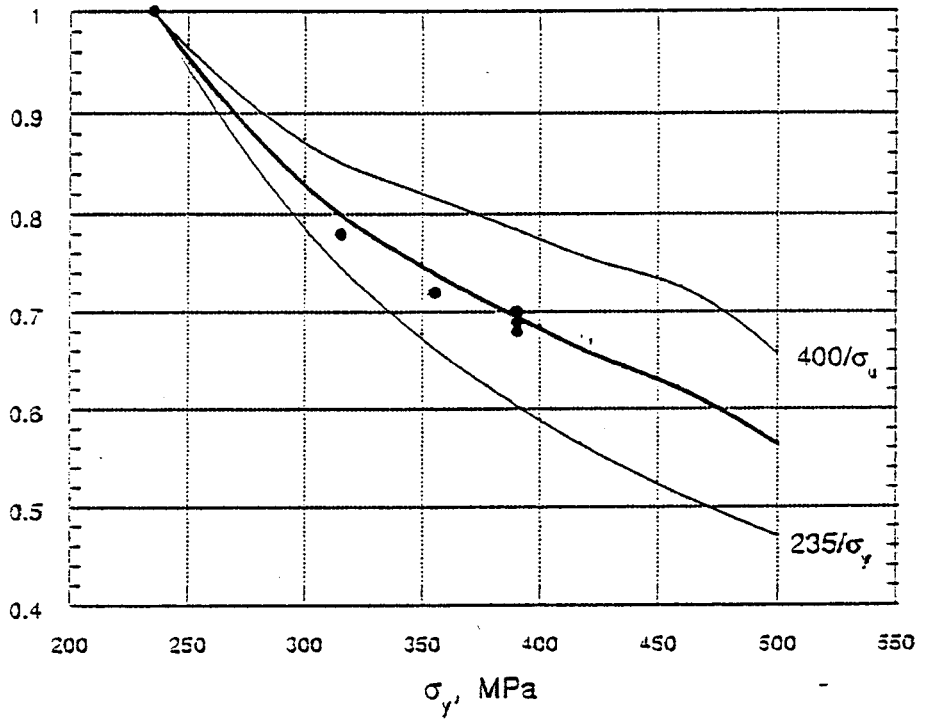

Figure 5.1: Calculation of high tensile steel factor as explained in Ref. [5.1]

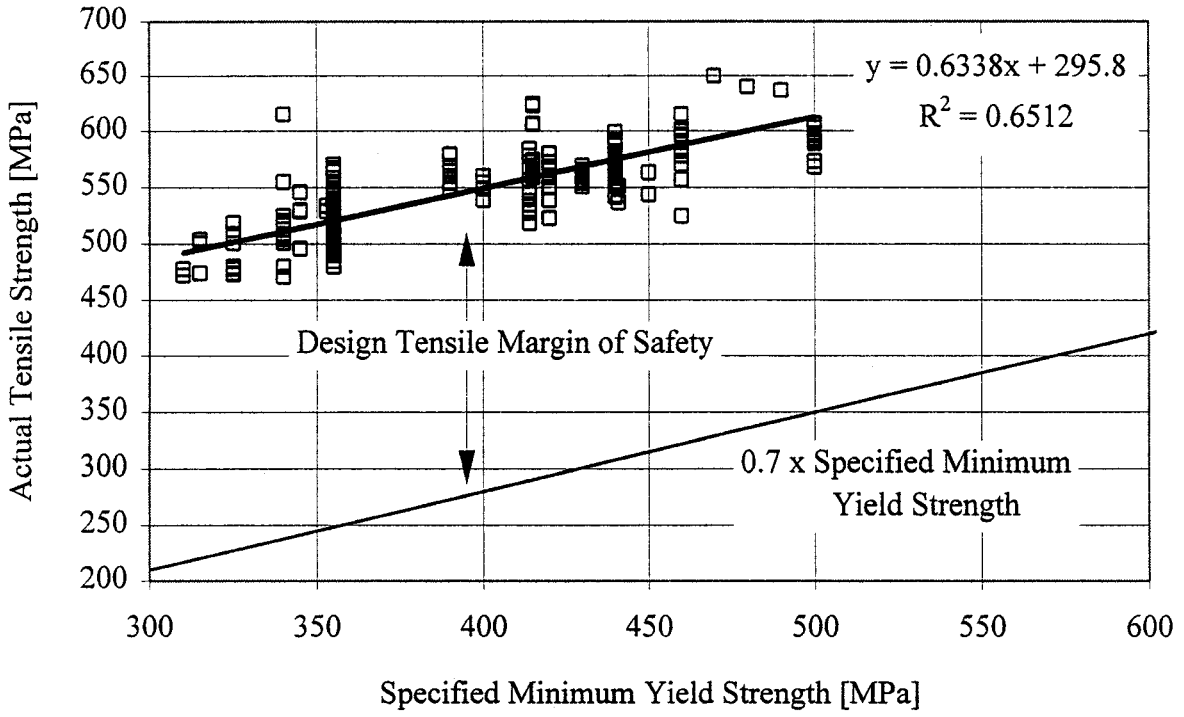

Figure 5.2: Actual tensile strength of the TMCP steel plates plotted against their specified minimum yield strength

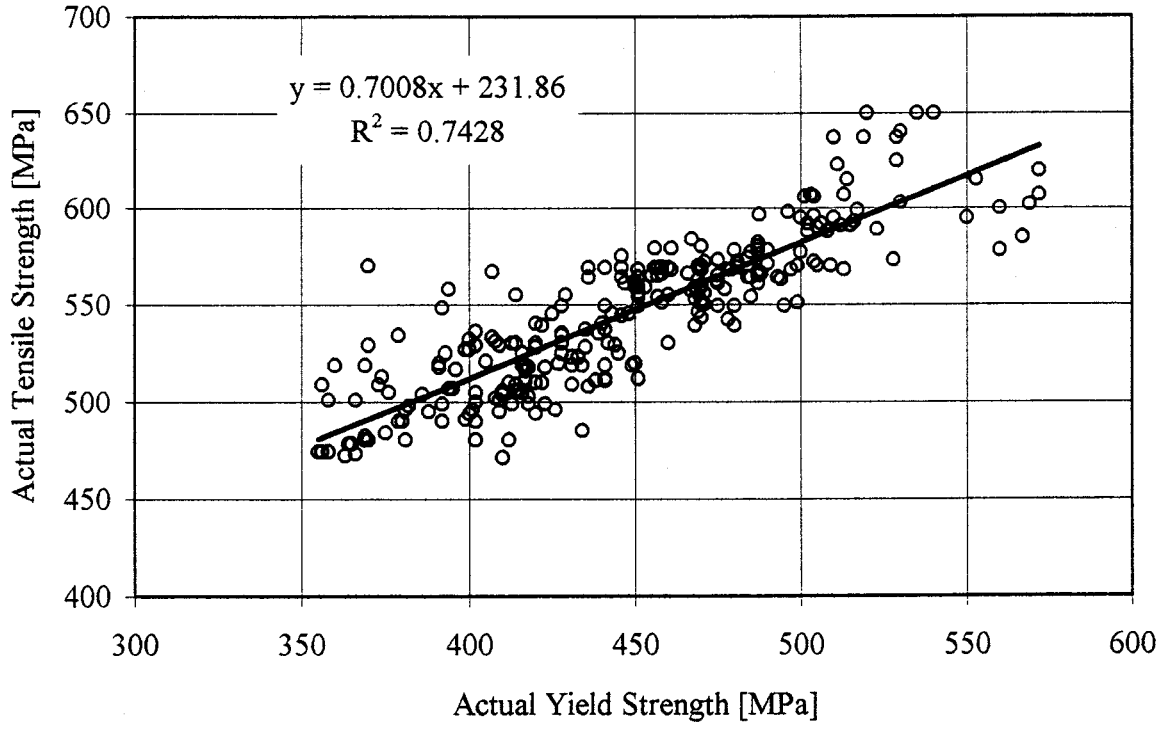

Figure 5.3: Actual tensile strength of the TMCP steel plates plotted against their actual yield strength

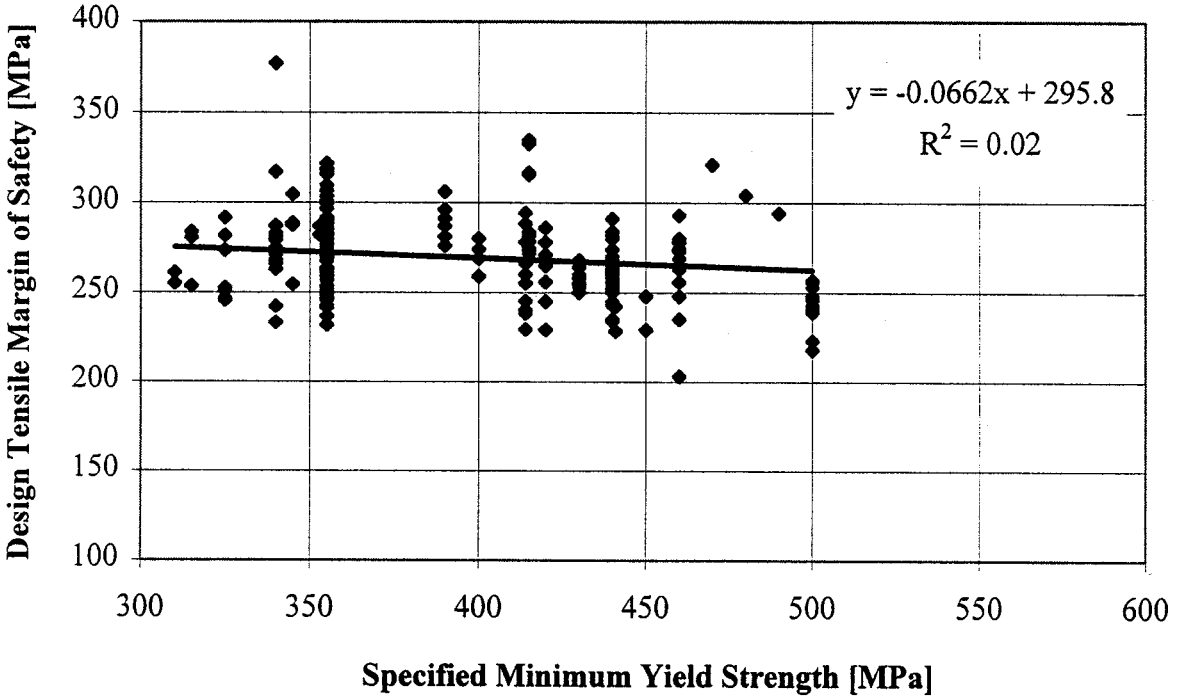

Figure 5.4: Absolute design tensile margin of safety (actual tensile strength - 0.7 x specified minimum yield strength) as a function of the specified minimum yield strength

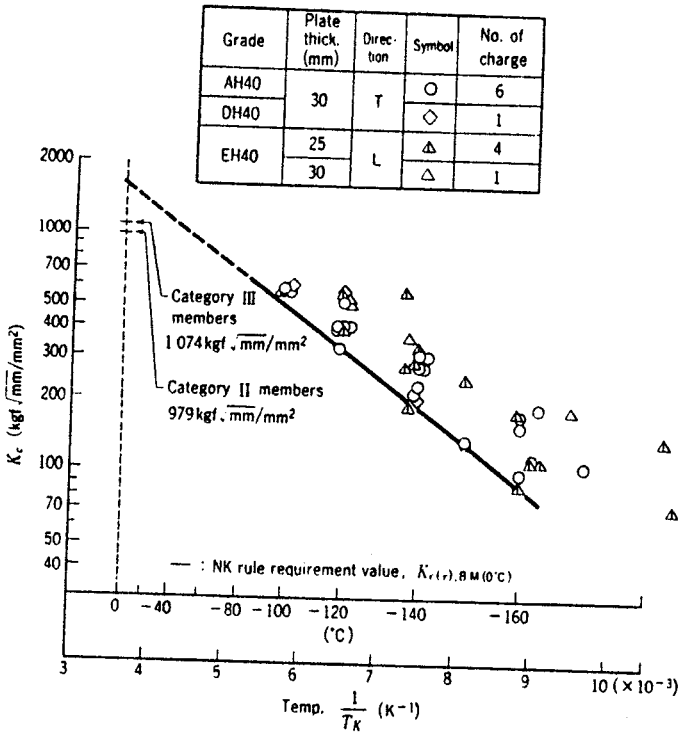

Figure 5.6: Relation between K_c (base metal) and temperature for 390 MPa yield steels

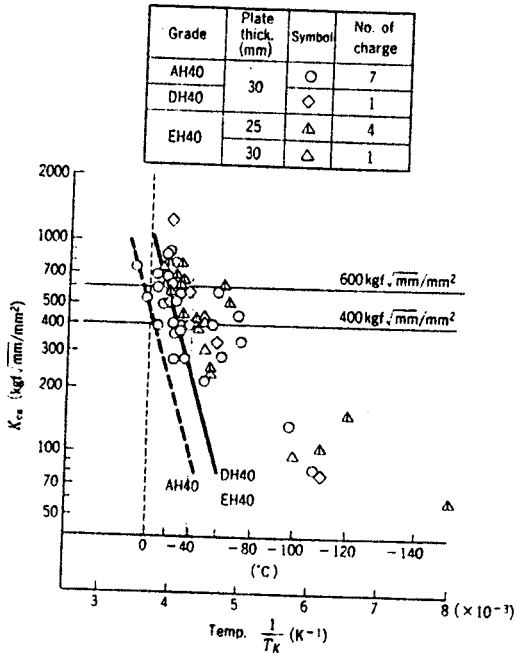

Figure 5.7: Relation between K_{ca} (base metal, L-direction) and temperature for 390 MPa yield steels

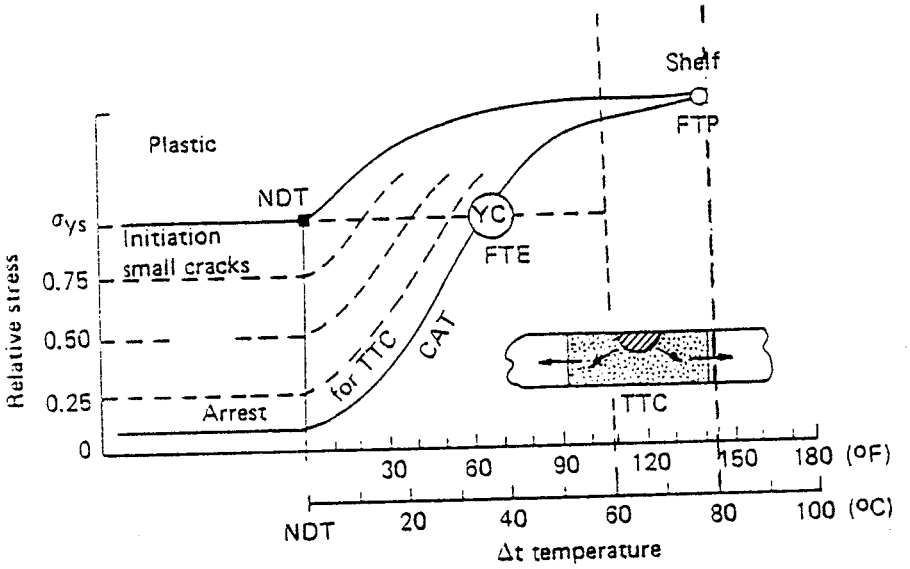

Figure 5.8: **Fracture analysis diagram as developed by Pellini. Note relation of initiation curve for small surface cracks to arrest curve for through-thickness cracks (TTCs)**

6.0 FATIGUE PROPERTIES OF TMCP STEELS

6.1 Fatigue Cracking in Ship Structures

Metal fatigue is the progressive failure of metal under cyclic loading. This type of failure can be divided into three basic stages [6.1]:

1. the initiation of microscopic cracks at microscopic or macroscopic stress concentrations;

2. the growth of microscopic cracks into macroscopic cracks; and,

3. the growth of macroscopic fatigue cracks to a critical size for failure (e.g., plastic collapse, fracture, or oil leakage).

The absolute and relative magnitudes of these stages depend on material, notch severity, structural redundancy, and environment.

Fatigue cracks in steel ships generally initiate at structural details, particularly welded ones. Fatigue-prone areas in bulk carriers include hatch corners, coamings, bracketed connections between hold frames and wing ballast tanks, the intersections of transverse corrugated bulkheads with top-side structure, and the intersections of inner bottom plating with hopper plating, while fatigue-prone areas in tankers include the intersections of side shell longitudinals and transverse structure (usually in the cargo tanks and usually between the laden water line and 2 m to 10 m below the water line), end connections for deck and bottom longitudinals, and end connections for longitudinal bulkheads [6.2-6.7].

The initiation and subsequent propagation of fatigue cracks in steel ships can be driven by several sources of cyclic loading including: (1) longitudinal bending, transverse bending, and torsion of the hull girder as a result of wave loading; (2) fluctuating hydrostatic pressure on side shell plating, cargo hold boundaries, and tank walls; and, (3) machinery and hull vibration. Exposure to corrosive media, such as sour crude oil or sea water, can accelerate the initiation and propagation of fatigue cracks, either directly through corrosion fatigue mechanisms or indirectly through the higher cyclic stresses that result from corrosion pitting and general wastage.

Although most fatigue cracks in steel ships are not detected by conventional inspection techniques until they are at least several inches long and often through the thickness of plating, catastrophic brittle fractures rarely initiate from undetected fatigue cracks because of the relatively good fracture toughness of modern ship steels, the inherent redundancy of ship structures, the use of crack arrestors, and the relatively small magnitude of normal service loads [6.3]. Nevertheless, any detected cracks are usually repaired at the earliest opportunity to prevent other problems from arising. Some of these problems are briefly described below:

1. The propagation of fatigue cracks from the internal structure of tankers to side shell plating could lead to environmental pollution.

2. Cracks at the hatch corners and coamings of bulk carriers could allow water to leak into dry cargo holds. Sloshing of the resulting slurry could introduce significant dynamic loads on cargo hold plating, and internal mixing could produce explosive gases.

3. Cracking at the hold frame ends of bulk carriers could result in the detachment of side shell from internal framing. This could eventually lead to the separation of the end brackets from the slant plate of the topside tanks or bilge hopper tanks.

In the 1960's and early 1970's, fatigue cracking was rarely detected in ships less than 10 years old, and the frequency of fatigue cracking in older ships was such that repair costs were acceptable to owners and operators. Therefore, fatigue cracking was viewed as a maintenance problem rather than a design problem, and it was not explicitly considered by ship designers [6.3].

Since the late 1970's, however, fatigue cracking has occurred more frequently in relatively new ships [6.3]. For example, fatigue cracking was detected at the intersections of side shell longitudinals and transverse bulkheads or frames in over fifteen second generation VLCC's after only 2 to 5 years of service [6.8]. Maintenance costs have risen to the point where owners and operators now recognize the need to consider fatigue at the design stage, and Classification Societies have responded by recently introducing explicit fatigue design criteria for steel ships [6.10, 6.11].

The higher frequency of fatigue cracking in steel ships over the last 15 to 20 years has been attributed to the design and construction of more structurally optimized ships with thinner scantlings [6.2-6.4, 6.9]. This optimization, which has been motivated by commercial demands to reduce the fabrication costs and weight of hull structures, has been achieved through the greater use of high strength steels and the greater exploitation of Classification Society rules which have permitted design stresses to increase with tensile strength up to a fraction of the tensile strength defined by the so-called material factor. Unfortunately, the stress concentrations of structural details have not been adequately reduced to compensate for the higher design stresses and higher local bending stresses associated with thinner scantlings. Furthermore, the fatigue strength of as-welded steel joints is essentially independent of tensile strength. Therefore, local cyclic stresses at structural details have been permitted to increase without a matching increase in the fatigue strength of these details. In certain cases, corrosive environments have probably exacerbated this mis-match since the flexibility of thin structure promotes the flaking of rust which accelerates the wastage process and further increases the flexibility of thin structure in a self-perpetuating manner.

As explained at the beginning of this report, the development of TMCP steels has contributed significantly to the greater use of high strength steels in ship construction over the last 15 to 20 years, and there has been an on-going effort to characterize the fatigue properties of TMCP steels and their welds. This effort has included:

1. quantifying the resistance of TMCP steels to the initiation and propagation of fatigue cracks in air, sea water, and sour crude oil;

2. quantifying the effects of plate thickness, weld profile, and weld toe treatment on the fatigue strength of TMCP steel welded joints;

3. quantifying the effects of sea water and sour crude oil on the corrosion fatigue strength of TMCP steel welded joints;

4. quantifying the effect of welding heat input on the fatigue strength of TMCP welded joints and the resistance of the heat affected zone (HAZ) in such joints to the initiation and propagation of fatigue cracks; and,

5. comparing the fatigue properties of TMCP steels and their welds to the fatigue properties of conventional high strength steels and their welds.

The available results of this work are presented in the remainder of this section.

6.2 Fatigue Crack Growth in Air

The resistance of a metal to fatigue crack propagation in air at ambient temperature is usually characterized by a log-log plot of crack growth rate (da/dN) versus stress intensity factor range (ΔK) for a specific R-ratio[1] where da/dN is measured during constant amplitude fatigue tests of standardized specimens with long initial fatigue cracks (typically several mm long), ΔK for tensile cyclic loading is defined as the difference between the maximum and the minimum calculated stress intensity factors (K_{max} and K_{min}), and ΔK for partly compressive cyclic loading is defined[2] as the maximum calculated stress intensity factor (K_{max}).

[1] The ratio of the minimum applied load to the maximum applied load.

[2] A crack is assumed to be fully closed during the compressive portion of a loading cycle. Since the stress intensity factor has no physical meaning for a closed crack, ΔK for partly compressive cyclic loading is defined as K_{max}.

The correlation of da/dN against ΔK is predicated upon the existence of identical stress-strain fields at the tips of cracks of different size in different bodies subjected to different external loads if the magnitude of the crack tip stress intensity factor (K) remains the same. The latter parameter quantifies the magnitude of the asymptotic stress-strain field at a crack tip (i.e., K-field) in a linear elastic material. Although a plastic zone inevitably exists at the tip of a crack, similitude is maintained if the plastic zone is small compared to crack size and surrounded by the elastic K-field.

A typical log-log plot of da/dN versus ΔK data has a sigmoidal shape which can be divided into three regions (**Figure 6.1**):

Region I - Crack growth in Region I involves non-continuum mechanisms, and associated crack growth rates ($<10^{-5}$ mm/cycle) can be strongly influenced by microstructure and R-ratio. These rates diminish rapidly with decreasing ΔK, and fatigue cracks are assumed to be non-propagating below a threshold value of the stress intensity factor range (ΔK_{th}) which is usually defined at a growth rate of 10^{-7} mm/cycle to 10^{-8} mm/cycle.

Region II - Crack growth in Region II is characterized by a nearly linear relationship between log da/dN and log ΔK. This relationship is usually approximated by the Paris equation

$$\frac{da}{dN} = C\Delta K^m \qquad (6.1)$$

where C and m are empirical constants. Crack growth occurs by continuum mechanisms (usually a transgranular striation mechanism), and the associated crack growth rates (10^{-5} mm/cycle to 10^{-3} mm/cycle) are less sensitive to microstructure and R-ratio than crack growth rates in Region I.

Region III - Crack growth rates in Region III increase asymptotically with increasing ΔK. This acceleration of crack growth is related to the emergence of static failure modes such as cleavage and microvoid coalescence, and it is accompanied by an increased sensitivity of crack growth rates to microstructure and R-ratio.

Of these three regions, Regions I and II have received the most attention from researchers because they dominate the crack propagation life of most engineering structures. Region III crack growth is only of interest when the crack propagation life is in the order of 10^3 cycles or less, and this crack growth can be ignored in many engineering structures because it does not significantly affect the total crack propagation life.

6.2.1 *Region I Crack Growth in Steels*

ΔK_{th} values for non-TMCP steels are essentially independent of R-ratio for R-ratios less than 0.1, but tend to decrease with increasing R-ratio for R-ratios above 0.1. Several investigators have compiled ΔK_{th} values for a wide range of non-TMCP steels [6.13, 6.14], and Rolfe and Barsom [6.16] have found that the following equations

$$\Delta K_{th} = 6 \text{ MPa}\sqrt{m} \qquad \text{for } R < 0. \tag{6.2}$$

$$\Delta K_{th} = 7(1 - 0.85R) \text{ MPa}\sqrt{m} \qquad \text{for } R \geq 0.1 \tag{6.3}$$

define a reasonable lower bound on this data (**Figure 6.2**). The range of compiled ΔK_{th} values for a given R-ratio is nearly 10 MPa$\sqrt{m}$ at R-ratios less than 0.1, but narrows with increasing R-ratio to about 2 MPa$\sqrt{m}$ at an R-ratio of 0.9. The greater range of ΔK_{th} values at low R-ratios appears to be related to the strong influence of microstructure on ΔK_{th} for some steels loaded at low R-ratios. In particular, Taylor [6.16] and Ritchie [6.17] noted that ΔK_{th} values for martensitic, bainitic, and ferritic-pearlitic steels with high ferrite content decrease significantly with increasing yield strength at low R-ratios, whereas ΔK_{th} values for ferritic-pearlitic steels with high pearlite content are relatively insensitive to yield strength. In addition, several investigators [6.17] reported a marked increase in ΔK_{th} for various low strength ferritic-pearlitic steels loaded at low R-ratios when ferrite grain size was increased, while other investigators [6.15] found little effect of prior austenite grain size on ΔK_{th} values for martensitic and bainitic high strength steels loaded at low R-ratios.

The data base for this project includes six sets of da/dN versus ΔK data for Region I crack growth in TMCP steels (**Figures 6.3-6.5**). Two sets are for steels with measured yield strengths of about 400 MPa, while the remaining four sets are for steels with measured yield strengths of about 500 MPa. The lower strength steels were tested at an R-ratio of 0.028, while the higher strength steels were tested at R-ratios of 0.5 and 0.8. Only one set included crack growth rates much less than 10^{-6} mm/cycles. Therefore, a reliable comparison of ΔK_{th} values for these TMCP steels and the ΔK_{th} values compiled for non-TMCP steels is not possible. However, it is worth noting that ΔK_{th} values obtained by linear extrapolation of the available crack growth data for TMCP steels to a growth rate of 10^{-7} mm/cycle fall within the scatter band of ΔK_{th} values for non-TMCP steels in **Figure 6.2**. Moreover, the extrapolated ΔK_{th} values for the TMCP steels tested at low R-ratios fall on the upper part of that scatter band. The latter observation is consistent with the fine ferritic-pearlitic or fine ferritic-bainitic microstructure of TMCP steels.

6.2.2 *Region II Crack Growth in Steels*

Although Region II crack growth rates for non-TMCP steels tend to increase with increasing R-ratio, this dependency is small compared to the dependency of Region I crack growth on R-ratio and it is usually ignored in comparisons of Region II crack growth rates for different steels. For example, Rolfe and Barsom [6.16] compiled da/dN versus ΔK data for Region II crack growth in a wide range of steels tested at various R-ratios, and divided this data into three groups according to microstructural differences (viz., martensitic, ferritic-pearlitic, or austenitic). They found that most of the measured crack growth rates within each group varied by less than a factor

of two at any given ΔK value.Considering the wide range of mechanical properties and chemical compositions represented within each group, Rolfe and Barsom suggested that engineering estimates of crack growth rates in martensitic, austenitic, and ferritic-pearlitic steels could be obtained from the following upper bound relationships[3] :

martensitic steels

$$\frac{da}{dN} = 1.36 \times 10^{-10} \Delta K^{2.25} \qquad (6.4)$$

ferritic-pearlitic steels

$$\frac{da}{dN} = 6.89 \times 10^{-12} \Delta K^{3} \qquad (6.5)$$

austenitic steels

$$\frac{da}{dN} = 5.61 \times 10^{-12} \Delta K^{3.25} \qquad (6.6)$$

Most investigations of fatigue crack growth in non-TMCP steels have not been accompanied by fractographic examinations of fatigue crack growth mechanisms. The few studies [6.22] that have involved such examinations have shown that Region II fatigue crack growth in a wide range of microstructures occurs by a transgranular striation mechanism, and that crack growth rates associated with this mechanism fall within a common scatter band regardless of R-ratio and tensile strength. Departures from the striation mechanism (e.g., microcleavage in coarse pearlitic steels and steels with brittle second phase particles such as spheroidized carbides, intergranular cracking in tempered martensite tested at low ΔK, void coalescence in tempered martensitic steels tested at high ΔK) are invariably associated with higher crack growth rates that tend to increase with increasing tensile strength and R-ratio (**Figure 6.6**).

BS7608 [6.23] and PD6493 [6.24] recommend the following relationship for engineering analysis in the absence of specific data for ferritic steels[4] :

$$\frac{da}{dN} = 9.5 \times 10^{-12} \Delta K^{3} \qquad (6.7)$$

[3] Units for da/dN and ΔK are m/cycle and MPa$\sqrt{m}$ respectively.

[4] Units for crack growth rate and ΔK are m/cycle and MPa$\sqrt{m}$.

This relationship represents an upper bound on published da/dN versus ΔK data for crack growth by a striation mechanism. If there is a potential for crack growth by non-striation mechanisms, then both references recommend the following equation

$$\frac{da}{dN} = 1.9 \times 10^{-11} \Delta K^3 \qquad (6.8)$$

The former equation may be overly conservative for certain steels since the rate of crack growth rate by a striation mechanism in different steels can vary by as much as factor of five for a given ΔK value, while the latter equation should be used with caution since it is less conservative than Rolfe and Barsom's upper bound relationship (**Equation 6.4**) for martensitic steels.

Ten sets of da/dN versus ΔK data for Region II crack growth in TMCP steels were found in the open literature and included in the data base for this project (**Figures 6.3-6.10**). These steels were tested at R-ratios between 0.028 to 0.1, and the measured yield strengths of these steels ranged from 375 MPa to 520 MPa. In several of the publications from which these data sets were obtained, the da/dN versus ΔK data for TMCP steels was compared to data for specific grades of non-TMCP steels. In some cases, there was no obvious difference between crack growth rates in the non-TMCP steels and TMCP steels. In other cases, the crack growth rates in the TMCP steels were either lower or higher than those in the non-TMCP steels. However, all of the TMCP steel data fall within the scatter band of da/dN versus ΔK data for crack growth by a striation mechanism in non-TMCP steels and fall below Rolfe and Barsom's upper bound relationship for ferritic-pearlitic steels (**Equation 6.5**). Although crack growth mechanisms in the TMCP steels were not confirmed by fractographic examination, crack growth by a striation mechanism would be expected given the fine ferritic-pearlitic or fine ferritic-bainitic microstructures of these steels.

6.2.3 Region III Crack Growth In Steels

The transition from Region II crack growth to Region III crack growth in non-TMCP steels with low fracture toughness occurs at a ΔK value that increases with increasing fracture toughness and decreasing R-ratio, whereas the transition from Region II crack growth to Region III crack growth in non-TMCP steels with high fracture toughness occurs at a ΔK value that is independent of fracture toughness and increases with increasing yield strength and decreasing R-ratio. The transition in steels with low fracture toughness is associated with the emergence of brittle fracture mechanisms such as intergranular cracking and cleavage, which dominate over striation crack growth mechanisms as K_{max} approaches the critical value for brittle fracture; whereas the transition in steels with high fracture toughness is associated with the emergence of ductile fracture mechanisms such as microvoid coalescence, which become increasingly prominent as the critical load for plastic collapse or ductile tearing is approached.

In the latter case, the stress intensity factor loses its physical significance and it may be better to correlate crack growth against an elasto-plastic parameter such as ΔJ. Nevertheless, Rolfe and Barsom [6.16] have analyzed Region III crack growth data for various steels subjected to pulsating tension (i.e., $\Delta K = K_{max}$ or R-ratio = 0), and found that the Region II-Region III transition in steels with high fracture toughness occurs at a critical K_{max} value (K_T) that is estimated to an acceptable degree of accuracy by the following relationship:

$$K_T = 0.0064\sqrt{E\,\sigma_f} \qquad (6.9)$$

where σ_f is the flow stress defined as the average of yield strength and ultimate tensile strength (MPa) , E is Young's Modulus (MPa) and K_T is in MPa$\sqrt{m}$.

The transition from Region II crack growth to Region III crack growth in TMCP steels is expected to occur at a ΔK value that is independent of fracture toughness and that increases with increasing yield strength and decreasing R-ratio, given the high fracture toughness of these steels. Furthermore, one would expect **Equation 6.9** to be applicable to TMCP steels subjected to pulsating tension loading. This is supported by the only data set in the open literature for Region III crack growth in TMCP steels (**Figure 6.34**). The Region II-Region III transition in this data , which is for a TMCP steel (yield strength = 477 MPa and ultimate tensile strength = 588 MPa) tested at an R-ratio of .05, occurs at a K_{max} value of about 60 MPa$\sqrt{m}$ as predicted by **Equation 6.9**.

6.2.4 Short Crack Growth in Steels

Recent research [6.29-6.31] has led to a growing awareness of the apparently anomalous behavior of fatigue cracks less than a few mm long in metals when da/dN is correlated against ΔK in Region I. This behavior includes crack propagation at ΔK values below the threshold value of ΔK for long cracks (ΔK_{th}), and higher crack growth rates than those for long cracks at ΔK values above ΔK_{th} (**Figure 6.11**). Kitigawa and Takahashi [6.31] have also examined ΔK_{th} for long and short cracks in a wide range of ductile metals and demonstrated that there exists a critical crack size above which ΔK_{th} is independent of crack size. For crack lengths below this critical size, ΔK_{th} decreases with decreasing crack length, and the corresponding threshold stress range ($\Delta\sigma_{th}$) approaches the endurance limit in smooth specimens. The fatigue limit of steels tends to increase with increasing tensile strength and decreasing grain size, whereas ΔK_{th} for long cracks in certain steels decreases with increasing tensile strength strength and decreasing grain size. A transition between these extremes occurs in the short crack regime.

It is now understood that different types of short cracks can exhibit the aforementioned behavior, and researchers [6.33] have classified these cracks according to the following definitions or slight variations of these definitions:

> **Microstructurally short cracks** are comparable in size to microstructural dimensions such as grain size or inter-particle spacing. The path and growth rate of such cracks is strongly influenced by the crystallographic orientation of grains and microscopic discontinuities such as grain boundaries and inclusions. The effects of these microstructural factors on crack growth cannot be quantified by parameters based on continuum mechanics such as ΔK.

Mechanically short cracks are cracks for which the near-tip stress-strain field is no longer uniquely characterized by the elastic K-field. These cracks include cracks that are comparable in size to their own crack tip plastic zone and cracks that are embedded within the plastic zones of notches.

Physically short cracks are less than a few mm long but longer than microstructurally short cracks and mechanically short cracks. Such cracks are too small for significant crack closure to occur.

Short crack behavior in welded steel structures has received little attention from researchers because it is believed that the fatigue life of such structures is controlled by the existence of welding flaws and that only a small portion of the total life is spent in the initiation and propagation of short fatigue cracks. In recent years, however, researchers at Florida Atlantic University [6.34, 6.35] have studied the behaviour of short cracks in high strength steels suitable for offshore structures. This research has been conducted in response to growing interest in the use of high strength steel threaded connections in offshore structures and improving the fatigue strength of high strength steel welded connections in such structures through the use of weld improvement techniques. Crack initiation and short crack growth can occupy a significant fraction of the fatigue lives of such connections. Most of the research has focused on the behavior of short cracks in sea water environments. This work is discussed later in this report. The work on short crack behavior in air is discussed below.

Kim and Hartt [6.34, 6.35] have studied the growth behavior of short cracks in two TMCP steels and three non-TMCP steels. The yield strengths of the TMCP steels were about 500 MPa, while the yield strengths of the non-TMCP steels ranged from 371 MPa to 571 MPa. The da/dN versus ΔK data for each steel was obtained from three-point bending tests ($R = 0.5$) of single edge notch specimens with 0.1 mm deep initial fatigue cracks. This data was compared to da/dN versus ΔK data for long cracks in the same steel loaded at the same R-ratio. The long crack data had been obtained in previous tests of tapered compact tension specimens with 2 to 3 mm long initial fatigue cracks. As evident in **Figure 6.12**, the two data sets for each steel merged once crack lengths exceeded a certain value (0.8 to 0.9 mm for the TMCP steels and 1.2 to 1.3 mm for the non-TMCP steels). Immediately below this transition, the slope of the da/dN versus ΔK data for the three-point bending specimens decreased abruptly below the slope of the da/dN versus ΔK data for the tapered compact tension specimens, and crack growth rates in the former specimens became increasingly greater than crack growth rates in the latter specimens with decreasing ΔK. Eventually, the crack growth rates in the three-point bending specimens diminished rapidly with decreasing ΔK, and the corresponding ΔK values appeared to approach a threshold between 5 to 6 $MPa\sqrt{m}$, regardless of steel grade. Direct comparisons between near-threshold crack growth rates in the three-point bending specimens and tapered compact tension specimens were not possible because of insufficient crack growth data for the latter specimens in the near-threshold regime. However, it is worth noting that the apparent ΔK_{th} values for short cracks in the three-point bending specimens fall on the upper part of the scatter band of ΔK_{th} compiled by Lindley and Richards for non-TMCP steels (**Figure 6.2**). Furthermore, Kim and Hartt extrapolated the da/dN versus ΔK data for long cracks in the tapered compact tension specimens into the near-threshold region and noted that the

ratio of the measured crack growth rates for short cracks to the extrapolated crack growth rates for long cracks at a given ΔK value reached a maximum value of 3 to 4 in the TMCP steels and 10 to 20 in the non-TMCP steel. It is not clear if these differences in crack growth rates and the differences in transition crack lengths reflect experimental scatter or real differences in the behavior of short cracks in TMCP steels and non-TMCP steels.

6.3 Crack Initiation In Steels in Air

6.3.1 S-N Data

The relative fatigue performance of steels subjected to predominantly elastic cyclic stresses has traditionally been characterized by load-controlled tests of polished rotating beam specimens or polished pulsating tension specimens under constant amplitude loading. The number of loading cycles to failure in these tests is usually plotted against the applied nominal stress range on a log-log plot. A characteristic feature of this so-called S-N data for steels is a threshold stress range (or amplitude), called the endurance limit or fatigue limit, below which fatigue life is considered to be infinite. Above this limit, fatigue life is finite and the proportion of this life spent in crack initiation decreases with increasing stress range. For engineering purposes, the fatigue limit is usually defined at a life of about 10^6 loading cycles.

Several investigators [6.36-6.39] have compiled endurance limits for polished rotating beam specimens and polished pulsating tension specimens fabricated from various mild steels and conventional high strength steels (**Figure 6.13**). The compiled endurance limits (in terms of stress amplitude) for rotating beam specimens fabricated from steels with ultimate tensile strengths (UTS) less than 1380 MPa range from 0.35 UTS to 0.61 UTS (about 0.5 UTS on average), whereas the compiled endurance limits (in terms of stress range) for pulsating tension specimens fabricated from steels with ultimate tensile strengths less than 600 MPa vary from 0.65 to 0.9. The compiled endurance limits for specimens fabricated from higher strength steels are widely scattered with no clear dependency on tensile strength. The lower bound and upper bound ratios of endurance limit to ultimate tensile strength for low strength steels are generally associated with coarse pearlitic microstructures and fine ferritic microstructures, respectively, whereas the lower bound and upper bound ratios for high strength steels are generally associated with untempered martensitic microstructures and tempered martensitic microstructures, respectively.

Only three sets of S-N data for smooth pulsating tension specimens fabricated from TMCP steels were found in the open literature (**Figure 6.14**). These data sets were generated by Lim et al. [6.26] for three grades of TMCP steel: AH32, DH36, and EH36. The measured ultimate tensile strengths of the AH32, DH36, and EH36 steels were 500 MPa, 540 MPa, and 480 MPa respectively. The AH32 and EH36 steels both had predominantly bainitic and ferritic microstructures with some localized pearlite, but the EH36 steel had finer grains and less pearlite. In contrast, the DH36 steel had a banded ferritic-pearlitic microstructure. Lim et al argued that the banded microstructure is indicative of a steel that has not undergone proper accelerated cooling. However, it should be noted that a certain amount of banding is be expected in all TMCP steels. The DH36 steel had the highest endurance limit and the highest fatigue strengths for finite lives,

whereas the AH32 steel had the lowest endurance limit and the lowest fatigue strength for finite lives for a given nominal stress range. However, the differences between the endurance limits and fatigue strengths of these two steels were less than 10%, and the ratio of the endurance limit to ultimate tensile strength for all three steels (0.65 to 0.71) fell within the scatter band of ratios for non-TMCP steels. Furthermore, there was no systematic influence of microstructure or tensile strength on the endurance limit and fatigue strengths of the TMCP steels.

Even fewer sets of S-N data were found in the open literature for smooth rotating beam specimens fabricated from TMCP steels (Figure 6.15). These sets were found in a technical brochure for two grades of Dillinger Hutte TMCP steel with nominal yield strengths of 355 MPa and 460 MPa [6.40]. An accelerated cooled process is used to produce plates thicker than 40 mm. Compared to the banded ferritic-pearlitic microstructure of normalized steels, the TMCP steels have a finer, more homogeneous microstructure with less pearlite. The specimens for the lower strength steel were machined from 20 mm and 40 mm thick steel plates, whereas the specimens for the higher strength steel were machined from 20 mm and 50 mm thick steel plates. The S-N data for these specimens were compared to S-N data for normalized steels with the same nominal tensile strength. The endurance limits and the fatigue strengths of the specimens fabricated from the higher strength TMCP steels were about 10% higher than the endurance limits and fatigue strengths of the specimens fabricated from the lower strength TMCP steels. Furthermore, there were no obvious differences between the fatigue strengths of the specimens machined from accelerated-cooled TMCP steels, non-accelerated-cooled TMCP steels, and normalized steels with the same nominal tensile strength. The ratio of the endurance limit to ultimate tensile strength for the different TMCP steel specimens ranged from 0.28 to 0.33. These ratios are significantly lower than those reported for rotating beam specimens fabricated from non-TMCP steels. However, the latter specimens were tested at an R-ratio of -1, whereas the Dillinger Hutte specimens were tested at an R-ratio of 0. If the well known Goodman equation [6.36] is used to correct the endurance limits of the Dillinger Hutte specimens for mean stress effects, then the corrected ratios fall within the scatter band of ratios for non-TMCP steels.

It is worth noting that Rowe [6.41] demonstrated a better correlation between the fatigue limit of steels in rotating bending with the true stress-strain parameters of these steels. He found that the least squares regression equation

$$\log S_f{}^n = .0059951 + .911 \log(\sigma^n{}_{1.0}) \qquad (6.10)$$

expressed the correlation quite adequately for polished rotating beam specimens for a variety of steels and microstructure, where $\sigma_{1.0}$ is the true stress at a true strain of unity, S_f is the fatigue limit, and n is the strain hardening exponent. Reemsnyder [6.42] found a similar correlation between the fatigue limit of flat axially loaded specimens of low to intermediate strength steels with a work hardening exponent exceeding 0.1.

$$\log S_f{}^n = .0148736 + .788883 \log(\sigma^n{}_{1.0}) \qquad (6.11)$$

More recently, Reemsnyder [6.43] has shown that better correlation can be obtained between cyclic stress-strain properties and the fatigue lives of smooth steel specimens, including TMCP steel specimens tested in the U.S. Title III program. Unfortunately, the TMCP data was not available for this project.

6.3.2 $\Delta\varepsilon$ vs N Data

Until the 1950's, little attention was given to the low cycle fatigue performance of metals as structures and machine components were usually designed to withstand a large number of load cycles over expected service lives. In fact, a common practice was to design machine components for an infinite life by keeping cyclic stresses below the fatigue limit. It was then realized that only a short fatigue life is required for some pressure vessels and certain parts of aerospace structures and that a certain amount of gross-section cyclic plasticity could be permitted in these structures. Consequently, tests of axially-loaded polished specimens subjected to fully reversing strain cycles of constant amplitude were developed to characterize the relative low cycle fatigue performance of different metals.

During initial loading of such strain-controlled specimens, stress and strain follow the monotonic stress-strain curve up to the maximum applied tensile strain. Upon unloading, yielding begins in compression at a stress that is lower in magnitude than the tensile yield strength due to the Bauschinger effect (**Figure 6.16**). Re-loading to the maximum applied tensile strain forms a hysteresis loop, the size of which is characterized by the total strain range ($\Delta\varepsilon$) and total stress range ($\Delta\sigma$). The stress range usually changes with increasing load cycles before stabilizing. Initially, hard and cold worked metals tend to cyclically soften (i.e., $\Delta\sigma$ decreases under initial strain cycling), whereas initially, soft and annealed metals tend to cyclically harden (i.e., $\Delta\sigma$ increases under initial strain cycling). Certain metals, including steels, cyclically soften under low cyclic strains but cyclically harden under high cyclic strains.

The usual way to present low cycle fatigue data is to plot either the plastic strain amplitude ($\Delta\varepsilon_p/2$) or total strain amplitude ($\Delta\varepsilon/2$) against the number of strain cycles (N) or strain reversals (2N) to failure on a log-log plot, where failure may be defined as fracture, some percentage drop in the applied load, or the initiation of a certain sized crack. The following equations are usually fitted to these plots

$$\frac{\Delta\varepsilon_p}{2} = \varepsilon_f'(2N)^c \tag{6.12}$$

$$\frac{\Delta\varepsilon}{2} = \frac{\sigma_f'}{E}(2N)^b + \varepsilon_f'(2N)^c \tag{6.13}$$

where ε_f' is the fatigue ductility coefficient, c is the fatigue ductility exponent, σ_f' is the fatigue strength coefficient and b is the fatigue strength exponent. Typical values of σ_f', ε_f', b, and c for various steels and other metals are given in [6.44]. **Equations 6.12 and 6.13** show that the number of strain cycles or reversals to failure increases with decreasing total strain amplitude or decreasing plastic strain amplitude. In general, fatigue lives around 10^3 to 10^4 cycles for strain-controlled specimens tend to be relatively independent of material properties. Shorter fatigue lives tend to decrease with increasing tensile strength and decreasing ductility, whereas longer fatigue lives tend to increase with increasing tensile strength and decreasing ductility.

Only three sets of fatigue data for smooth strain-controlled specimens fabricated from TMCP steels were found in the open literature (**Figure 6.17**). This data was generated by Lim et al. [6.26] for AH 32, DH 36, and EH 36 TMCP steels with fatigue lives ranging from 500 to 5000 cycles. All the data fell above the design curve specified by the ASME Pressure Vessel Code for carbon and low alloy steels with ultimate tensile strength less than 550 MPa (80 ksi) at temperatures less than 370°C (700°F). There was no systematic effect of ductility or tensile strength on fatigue lives. However, it should be noted that most of the fatigue lives fell within the range where the effects of material properties are minimized.

6.3.4 ($\Delta K_{eq}/\sqrt{\rho}$) vs N Data

Fatigue cracks in structures and machine components invariably initiate at notches which act as stress raisers. S-N data for smooth specimens has historically been used to predict fatigue crack initiation at notches, but it is now generally accepted that $\Delta\varepsilon$-N data for smooth specimens is more appropriate for predicting fatigue crack initiation at notches with significant localized cyclic plasticity. The basic premise of both approaches is that the number of cycles to initiate a fatigue crack at a notch is equal to the fatigue life of a smooth specimen subjected to the same stress-strain history as the root of the notch. Since stresses and strains decrease more rapidly with increasing distance from sharper notches, both approaches tend to overpredict fatigue crack initiation lives at sharp notches. For such notches, some researchers have advocated the correlation of fatigue crack initiation lives against $\Delta K_{eq}/\sqrt{\rho}$ where ρ is the notch radius and K_{eq} is the equivalent stress intensity factor for a sharp crack equal in length to the sharp notch and subjected to the same loading conditions as the notch.

Creager [6.45] has shown that $K_{eq}/\sqrt{\rho}$ is directly proportional to the maximum stress (σ_{max}) at the root of a sharp elliptical notch or a sharp hyperbolic notch in a body subjected to tensile stresses normal to the notch.

$$\rho_{max} = \frac{2\,K_{eq}}{\sqrt{\rho\pi}} \qquad (6.14)$$

Although this relationship is only exact when ρ approaches zero, finite element analyses of compact tension specimens of blunt notches much greater in length than the notch radius have shown that the relationship is accurate to within 10% for notch radii up to 4.6 mm. For larger radii, maximum stresses are underestimated with increasing notch radius.

Barsom and McNicol [6.46] investigated fatigue crack initiation behavior in single edge notch specimens that were fabricated from various steels and cyclically loaded in three-point bending at an R-ratio of 0.1. The tensile strengths ranged from 531 to 1606 MPa (77 to 233 ksi) and covered a wide range of chemical compositions and mechanical properties. The fatigue crack initiation lives were plotted against $\Delta K_{eq}/\sqrt{\rho}$. Because the same nominal notch length and tip radius were used for all specimens of the steels investigated, the differences in the fatigue crack initiation behavior are related to inherent differences in the fatigue crack initiation characteristics of the steels. The data show that fatigue cracks do not initiate in steel structural components when the body configuration, the notch geometry, and the nominal stress fluctuations are such that the magnitude of $\Delta K_{eq}/\sqrt{\rho}$ is less than a characteristic threshold value for the material. In general, the threshold $\Delta K_{eq}/\sqrt{\rho}$ values increased with increasing ultimate tensile strength (UTS) for UTS values less than 1035 MPa (150) ksi. Above this point, the threshold values were relatively independent of ultimate tensile strength. Rolfe has suggested the following relationship for single edge notch specimens fabricated from steels with UTS less than 1035 MPa and tested at an R-ratio of 0.1

$$\left(\frac{\Delta K_{eq}}{\sqrt{\rho}}\right)_{th} = 0.9UTS \qquad (6.15)$$

where the units for ΔK_{eq} and UTS are ksi$\sqrt{in}$ and ksi respectively.

Rajpathak and Hartt [6.50] have correlated fatigue crack initiation lives for several TMCP steels in sea water with and without cathodic protection. This data is presented later in this report along with other fatigue data for TMCP steels in a sea water environment. Unfortunately, no $\Delta K_{eq}/\sqrt{\rho}$ vs N data for TMCP steels in air was found in the open literature for comparison against **Equation 6.15**.

6.4 Corrosion Fatigue of Steels in Sea Water

Unprotected areas of steel marine structures are prone to general corrosion as a result of exposure to sea water. Wastage can lead to higher stresses as a result of reductions in net section and load re-distribution away from severely corroded structure, and gross corrosion pitting can introduce significant stress concentrations in plating. In addition to these factors, which effectively increase the driving force for fatigue crack propagation, the resistance of steels to crack initiation and propagation can be reduced by various corrosion fatigue mechanisms.

6.4.1 Growth of Long Fatigue Cracks

Various laboratory studies [6.47-6.49] have shown that the fatigue crack growth resistance of freely corroding non-TMCP steels immersed in sea water differs from that in air. Fatigue crack growth rates under free corrosion conditions are similar to those in air at near-threshold ΔK values (<10 MPa$\sqrt{m}$) and at high ΔK values (60 to 80 MPa$\sqrt{m}$). At intermediate ΔK values, however, crack growth under free corrosion conditions is faster than crack growth in air and can be characterized by a bi-linear relationship between log da/dN and log ΔK (**Figure 6.18a**). The accelerated crack growth has been attributed to anodic dissolution at the crack tip which is

enhanced by higher temperatures, lower loading frequency, and higher oxygen content. It is also believed that the diffusion of hydrogen to the crack tip may contribute to the acceleration of crack growth, but it is not clear whether this is through an embrittlement mechanism or through some other form of hydrogen-assisted cracking. The ΔK value at which the knee of this relationship occurs increases with decreasing frequency (~10 to 20 MPa$\sqrt{m}$ for frequencies in the order of 1 Hz and ~20 to 40 MPa$\sqrt{m}$ for frequencies in the order of 0.1 Hz). Furthermore, crack growth rates above this knee increase with increasing frequency. In contrast, crack growth rates at near-threshold ΔK values seem to be independent of frequency although there is relatively little data on frequency effects in this regime. The difference between crack growth rates in air and under free conditions is highest at the knee and increases with decreasing loading frequency, increasing temperature, and increasing oxygen content. For example, it has been observed that growth rates under free corrosion conditions in 0°C sea water are only marginally higher than crack growth rates in air at room temperature, whereas growth rates under free corrosion conditions in sea water at room temperature can be 3 to 4 times faster than those in air at room temperature.

Cathodic protection is used to control the general corrosion process in steel marine structures, whereby the structure is held at an electrochemical potential to make steel behave as a cathode in the environmental system. It is believed that cathodic protection also nullifies the anodic dissolution process at a crack tip. However, experimental studies indicate that cathodic protection does not restore fatigue crack growth rates in non-TMCP steels to in-air values [6.47-6.49]. In the near-threshold ΔK regime, cathodic protection reduces crack growth rates in sea water below crack growth rates in air and increases ΔK_{th} values in sea water above ΔK_{th} values in air. Increasing the negativity of impressed potentials increases ΔK_{th} and decreases crack growth rates. These beneficial effects of cathodic protection have been attributed to the precipitation of calcareous deposits which wedge the crack closed at near-threshold ΔK values. In the intermediate ΔK regime, crack growth approaches a plateau of constant rate (**Figure 6.18b**). Above this plateau, growth rates approach in-air values. Crack growth rates along this plateau increase with increasing impressed potential, decreasing loading frequency, and increasing R-ratio. Impressed potentials of -0.7V to -0.8V (Ag/AgCl) have been found to reduce fatigue crack growth rates in sea water close to air values, whereas highly negative impressed potentials (-1.1 V) have been found to elevate crack growth rates in sea water above growth rates under free corrosion conditions. It is believed that the more negative potentials increase the amount of hydrogen available for adsorption and diffusion to the crack tip and therefore, promotes hydrogen-assisted cracking.

Recommendations of da/dN versus ΔK relationships for engineering predictions of crack propagation lives in steels in a marine environment, in the absence of specific corrosion fatigue data, have been complicated by the sensitivity of crack growth rates to impressed potential, loading frequency, R-ratio, and the complex relationship between da/dN and ΔK. For example, PD6493 recommends the following equations for estimating ΔK_{th} and crack growth[5] for structural ferritic steels in a marine environment in the absence of specific corrosion fatigue data:

[5] Units for da/dN and ΔK are m/cycle and MPa$\sqrt{m}$ respectively.

$$\Delta K_{th} = 1.992 \qquad \text{for } R > 0.5 \qquad (6.16)$$

$$\Delta K_{th} = 5.38 - 6.77R \qquad \text{for } 0 \leq R \leq 0.5 \qquad (6.17)$$

$$\Delta K_{th} = 5.38 \qquad \text{for } R > 0.5 \qquad (6.18)$$

$$da/dN = 7.27 \times 10^{11} \Delta K^3 \qquad \text{for } \Delta K > \Delta K_{th} \qquad (6.19)$$

Equations 6.16 to **6.18** may be overly conservative for steels that are cathodically protected with highly negative impressed potentials since they are intended to be lower bounds on ΔK_{th} values for structural ferritic steels in air and in sea water. **Equation 6.19**, on the other hand, can lead to overly conservative predictions of crack propagation lives in steels that are loaded at low R-ratios and cathodically protected at optimum potentials of -0.7V to -0.8V since this equation defines an upper bound for crack growth rates over a wide range of intermediate ΔK values in structural ferritic steels that are loaded at high R-ratios and cathodically protected at highly negative impressed potentials[6].

Hartt and Yang [6.20,6.21] investigated the effects of sea water on long fatigue crack growth rates at ΔK values less than 20 MPa$\sqrt{m}$ in two TMCP steels and two non-TMCP steels. These steels were tested at two different R-ratios (0.5 and 0.8) in air, in sea water without cathodic protection, and in sea water with three different levels of cathodic protection (-0.8V, -0.95V, and -1.1V). The two TMCP steels had measured yield strengths of 500 MPa, while the non-TMCP steels had measured strengths of 371 MPa and 537 MPa. As evident in **Figure 6.5**, crack growth data for steels that were tested at the same R-ratio and in the same environment fell within common narrow scatter bands. These scatter bands manifested the various corrosion fatigue characteristics that have been observed in other non-TMCP steels. ΔK_{th} values for freely corroding steels in sea water were similar to ΔK_{th} values in air. ΔK_{th} values for cathodically protected steels were higher than ΔK_{th} values for steels in air and freely corroding steels in sea water. Increasing the negativity of the impressed potential in cathodically protected steels increased ΔK_{th} values and crack growth rates at the transition from the near-threshold regime to the intermediate ΔK regime. Crack growth rates in freely corroding steels in sea water were about a factor of two higher than crack growth rates in air at this transition, but lower than crack growth rates in steels that were cathodically protected with highly negative impressed potentials.

Nakano et al.[6.27], on the other hand, investigated the effect of sea water on the growth of long fatigue cracks in a TMCP and a normalized steel at an R-ratio of 0.05 and intermediate ΔK values. The TMCP steel had a measured yield strength of 465 MPa, while the normalized steel had a measured yield strength of 372 MPa. These steels were tested in air, in sea water without cathodic protection, and in sea water with three different levels of cathodic protection (-0.8V, -0.95V, and -1.1V). Crack growth rates in freely corroding TMCP steel in sea water were about a

[6] Equation 6.19 does not clear all experimental data for cathodically protected steels in the plateau region.

factor of two higher than in-air crack growth rates for the TMCP steel, whereas crack growth rates in freely corroding normalized steel in sea water were similar to in-air crack growth rates (**Figure 6.7**). In both steels, crack growth rates increased with increasing cathodic polarization although the effect was more pronounced in the normalized steel. Plateaus were evident in the da/dN versus ΔK data for cathodically protected TMCP steels and cathodically protected normalized steels but the plateaus for the TMCP steels were more distinct.

6.4.2 Growth of Short Fatigue Cracks

As explained earlier, recent research has led to a growing awareness of the apparently anomalous behavior of fatigue cracks less than a few mm long in metals in air when da/dN is correlated against ΔK in Region I. This behavior includes, for long cracks, decelerating crack propagation at ΔK values below ΔK_{th} and higher crack growth rates at ΔK values above ΔK_{th}. This anomalous behavior has also been observed in freely corroding non-TMCP steels immersed in sea water or sodium chloride solutions [6.33]. In these studies, fatigue crack growth rates for short cracks were faster than crack growth rates for long cracks by as much as a factor of 2 to 4 in steels with yield strengths between 300 MPa and 800 MPa and by as much as a factor of 500 in high strength steels with yield strengths greater than 1000 MPa. The transition from short crack behavior to long crack behaviour in this environment typically occurred at crack lengths less than 3 mm.

More recently, researchers at Florida Atlantic University have reported on short crack behaviour in modern weldable high strength steels including TMCP steels. In particular, Kim and Hartt [6.34 and 6.35] studied the growth behavior of short cracks in two TMCP steels and three non-TMCP steels in natural sea water under freely corroding conditions. The yield strengths of the TMCP steels were about 500 MPa, while the yield strengths of the non-TMCP steels ranged from 371 MPa to 571 MPa. The da/dN versus ΔK data for each steel was obtained from three-point bending tests ($R = 0.5$) of single edge notch specimens with 0.1 mm deep initial fatigue cracks. This data was compared to da/dN versus ΔK data for short cracks in the same steels that were tested at the same R-ratio but in air (**Figure 6.12**). Like the short crack behavior that was observed in air, the slope of the da/dN versus ΔK data for each steel increased abruptly for crack lengths above a certain value, the ΔK value at this transition was relatively independent of the transition crack length, and the crack growth rate at this transition decreased with increasing transition crack length. However, the range of transition crack lengths for the different steels in sea water (0.25 mm to 1.6 mm) was wider than the range of transition crack lengths in air (0.8 mm to 1.3 mm), and the corresponding ΔK values in sea water (8 to 11.5 MPa$\sqrt{m}$) were about 35% lower than those in air (14.3 to 18 MPa$\sqrt{m}$). Furthermore, there was no apparent difference between the transition crack lengths for the TMCP and non-TMCP steels immersed in sea water, whereas the transition crack lengths for the TMCP steels in air (0.8 mm to 0.9 mm) were consistently lower than those in the non-TMCP steels in air (1.2 mm to 1.3 mm). Immediately below the transition, measured crack growth rates for steels in both environments became increasingly greater than the crack growth rates predicted by extrapolating crack growth rates for ΔK values above the transition to ΔK values below the transition. Eventually, the crack growth rates for steels in both environments diminished rapidly with decreasing ΔK, and the corresponding ΔK values appeared to approach a threshold that

appeared to be independent of steel grade. As observed in other studies of long crack growth in freely corroding steels in sea water, the short cracks in the freely corroding steels in sea water grew faster than the short cracks in air at ΔK values above ΔK_{th}. However, the ratio of measured crack growth rates to extrapolated crack growth rates for steels in sea water reached a maximum value of 2 to 6 at ΔK values above the transition , whereas the ratio of measured crack growth rates to extrapolated crack growth rates for steels in air reached a maximum value of 3 to 20 at ΔK values below the transition. Furthermore, the apparent ΔK_{th} values for steels in sea water (3 to 4 MPa$\sqrt{m}$) were lower than the apparent ΔK_{th} values for steels in air (5 to 6 MPa$\sqrt{m}$), whereas ΔK_{th} values for long cracks in freely corroding steels in sea water are similar to those in air. These differences between short cracks and long cracks in sea water were attributed to the greater sensitivity of short cracks to crack closure from the wedging action of corrosion products.

Kim and Hartt also studied the effect of cathodic protection on the growth of short cracks in the aforementioned steels. The experimental procedure for this work was identical to the procedure used to study short crack growth under free corrosion conditions, except that three different cathodic potentials were impressed on the test specimens (-0.8V, -0.9V, and -1.1 V). The da/dN versus ΔK data for the cathodically protected specimens manifested the same abrupt transition in slope as the da/dN data versus ΔK data for freely corroding specimens and specimens in air. However, the apparent ΔK_{th} values for different steels cathodically polarized to -0.95V (6 to 8 MPa$\sqrt{m}$) were equal to or higher than those in air (5 to 6 MPa$\sqrt{m}$), whereas the apparent values for different steels cathodically polarized to -0.8V and -1.1 (6 to 8 MPa$\sqrt{m}$) were equal to or lower than those in air. Furthermore, near-threshold crack growth rates at the former level of cathodic polarization were less than or equal to those in air, whereas the near-threshold crack growth rates for the latter levels of cathodic polarization were less than or equal to those in air. This differs from the observed behavior of long cracks in cathodically protected steels. As explained earlier, ΔK_{th} values for such cracks are higher than those in air and increase with increasing cathodic polarization, and near-threshold crack growth rates decrease with increasing cathodic polarization. No explanation was cited for these differences.

6.4.3 Crack Initiation in Steels

Prior to the 1990's, the understanding of the resistance of steels to fatigue crack initiation at low cyclic stresses in a marine environment was largely based on S-N data for simple smooth specimens and simple notched specimens that were fabricated from low to medium strength structural steels, loaded in tension, cantilever bending, or rotating bending, and immersed in sea water or sodium chloride solution [6.47, 6.48]. The few high strength steels that were considered in these studies were seldom used in marine structures because of their poor weldability and fracture toughness. It was usually reported that the fatigue lives of free corroding specimens in either sea water or sodium chloride solutions were significantly reduced with respect to the fatigue lives of in-air specimens with the magnitude of this difference increasing with decreasing stress range and decreasing test frequency. Furthermore, the fatigue lives of freely corroding specimens continued to decrease with increasing cyclic stress below the in-air fatigue limit with no evidence of a fatigue limit even at 10^8 cycles. Moderate cathodic polarization (-0.8V to -0.95V) was found to restore high cycle fatigue lives to in-air values, but more negative impressed potentials were

found to have little effect on fatigue performance. The reduced resistance of freely corroding steels to fatigue crack initiation was attributed to several factors including the stress concentration effect of microscopic corrosion pits and the anodic dissolution of iron at nascent crack tips, but the mechanisms of fatigue crack initiation in cathodically protected steels were not clearly understood.

Recently, Rajpathak and Hartt [6.50] studied the resistance of several modern weldable high strength steels to fatigue crack initiation in sea water at low cyclic stresses. These steels included two TMCP steels with respective yield strengths of 450 MPa and 500 MPa and seven non-TMCP steels with yield strengths ranging from 370 MPa to 985 MPa. Keyhole compact tension specimens were tested at an R-ratio of 0.5 in natural sea water with and without cathodic protection. A high cathodic polarization (-1.1V) was impressed on cathodically protected specimens. Unlike the investigators in previous studies of fatigue crack initiation in freely corroding and cathodically protected steels, Rajpathak and Hartt correlated their experimental fatigue crack initiation lives against $\Delta K_{eq}/\sqrt{\rho}$ **(Figure 6.19)**. The fatigue crack initiation lives for each freely corroding steel increased with decreasing $\Delta K_{eq}/\rho$ with no evidence of a threshold $\Delta K_{eq}/\rho$ value at fatigue lives of 10^6, and the free corrosion data for the different steels fell within a common scatter band irrespective of microstructure and composition. Cathodic protection consistently improved the fatigue crack initiation lives in each steel despite the high cathodic polarization used in this study. The magnitude of this improvement increased with decreasing $\Delta K_{eq}/\sqrt{\rho}$, and most steels exhibited a threshold $\Delta K_{eq}/\sqrt{\rho}$ value after 10^6 to 10^7 loading cycles. The threshold value was found to increase in proportion to tensile strength up to a tensile strength of approximately 720 MPa. Beyond this limit, the threshold value was essentially independent of tensile strength. As discussed earlier in this report, Rolfe and Barsom [6.16] found a similar relationship between $\Delta K_{eq}/\rho$ and tensile strength for a wide range of non-TMCP steels in air at an R-ratio of 0.1.

Only one other study has been conducted on fatigue crack initiation in TMCP steels in sea water. Matsumoto et al. [6.51] produced S-N data for four steel plates in air and in sea water under freely corroding conditions, including two TMCP steel plates with yield strengths of 465 and 481 MPa, a normalized steel plate with a yield strength of 372 MPa, and a quenched and tempered steel plate with a yield strength of 764 MPa **(Figure 6.20)**. The fatigue strengths of freely corroding plates were 1.4 to 1.8 times lower than the fatigue strengths of steels in air at a fatigue life of 10^6 cycles. This factor tended to decrease with increasing stress range, with the fatigue strength of the freely normalized steel plate approaching the fatigue strength of the normalized steel plate in air at 10^5 cycles. All of the steels exhibited an endurance limit in air but only the lower strength TMCP steel exhibited an endurance limit under free corrosion conditions. This difference is inconsistent with the results of Rajpathak and Hartt's study. Further studies are needed to determine whether there is, in fact, a real difference between the resistance of TMCP steels and conventional steels to crack initiation under free corrosion conditions.

6.5 The Effect of Sour Crude Oil

As mentioned earlier, some of the most fatigue-prone areas in oil tankers have been the intersections of longitudinals and transverse structure in cargo tanks. Various studies [6.2-6.7] have attributed fatigue cracking in these areas to high local cyclic stresses resulting from fluctuating hydrostatic loading on tank boundaries, hull girder bending, the use of high strength steel, and poor detail design. However, there have also been concerns that sour crude oil (i.e., crude oil containing a high concentration of H_2S) has a deleterious effect on the fatigue strength of steel structural members in oil tankers.

Although the MARPOL requirements for segregated ballast tank systems were adopted back in 1975, no studies were performed on the effect of sour crude oil on the fatigue strength of steel members in oil tankers throughout the 1980's, largely because of the difficulty of conducting fatigue tests in a crude oil environment. The only relevant studies from outside the shipping industry were by Vosikovsky [6.52] on the effect of sour crude oil on the growth of long fatigue cracks at intermediate ΔK values in freely corroding X65 pipeline steels. He observed that fatigue crack growth rates in a sour crude environment were accelerated with respect to fatigue crack growth rates in air and that these increased with increasing H_2S concentration. For example, fatigue crack growth rates in sour crude oil with a H_2S concentration of 100 ppm were over a factor of four higher than crack growth rates in air at ΔK value of 30 MPa$\sqrt{m}$, and increasing the H_2S concentration in sour crude oil from 100 ppm to 1000 ppm nearly doubled crack growth rates at a ΔK value of 30 MPa$\sqrt{m}$. The accelerated crack growth in sour crude oil was attributed to hydrogen embrittlement of the crack tip plastic zone as a result of absorption of atomic hydrogen from the breakdown of H_2S to the crack tip.

In the interim, several Japanese investigators [6.18, 6.19, 6.53] have studied the effects of sour crude oil on the growth of long fatigue cracks in ship steels including TMCP steels with yield strengths of about 400 MPa and mild steels with yield strengths of about 300 MPa. These studies were restricted to low R-ratios (0.028 to 0.05) and ΔK values less than 50 MPa$\sqrt{m}$. There were no significant differences between the crack growth rates for the TMCP steels and the mild steels in a given environment (**Figures 6.3, 6.4,** and **6.21**). Like Vosikovsky, the Japanese investigators observed that fatigue crack growth rates in a sour crude environment were significantly higher than fatigue crack growth rates in air at intermediate ΔK values (20 to 50 MPa$\sqrt{m}$) and that fatigue crack growth rates at intermediate ΔK values in a sour crude oil environment increased with increasing H_2S concentration. The magnitudes of the accelerated effects were similar to those reported by Vosikovsky. However, the Japanese investigators also observed that crack growth rates in sour crude oil rapidly approached crack growth rates in air at ΔK values less than 20 MPa$\sqrt{m}$. Observations of brittle striations on the surfaces of cracks loaded in sour crude oil at high ΔK values but ductile striation mechanisms on the surfaces of cracks loaded in sour crude oil at low ΔK values have lead to the hypothesis that hydrogen molecules are produced by the reaction of H_2O and H_2S in the crude oil and that atomic hydrogen broken down from the hydrogen molecules diffuses to and embrittles the crack tip plastic zone. The hydrogen embrittlement is more pronounced at high ΔK values because of the large plastic zone.

The Japanese investigators have also examined the effect of sour crude oil on the resistance of the aforementioned TMCP steels to fatigue crack initiation. S-N data was generated for axially-loaded round notched specimens that were tested at an R-ratio of 0.05 in air and sour crude oil (**Figure 6.22** and **6.23**). In the intermediate life regime (10^4 to 10^5 cycles), the fatigue strengths of the TMCP steel specimens in sour crude oil were similar to the fatigue strengths of the TMCP steel specimens in air. In the high cycle regime (>10^5 cycles), fatigue strengths in sour crude oil were higher than those in air, and this difference increased with decreasing nominal stress range. Opposite trends were observed in the low cycle regime (<10^4 cycles). The lower fatigue strengths of specimens in sour crude oil in the low cycle regime is consistent with the argument that the crack growth in sour crude oil is accelerated by hydrogen embrittlement and the fact that fatigue lives in this regime are mainly spent in crack propagation. The higher fatigue strengths of specimens in sour crude oil in the high cycle regime has been attributed to the reduced effect of hydrogen embrittlement because of the smaller plastic zone at the crack tip and to crack closure as a result of the wedging action of the crude oil and corrosion products. More studies, however, are needed to confirm the aforementioned trends.

6.6 S-N Data for Welded Joints

Fatigue design rules for welded plate joints in steel bridges and offshore structures are based on an S-N design curve approach [6.23, 6.54]. This approach, which also forms the basis of fatigue design procedures developed by Classification Societies, Hughes [6.55], and Munse et al. [6.56] for ship structures for welded plate joints in ship structures, identifies potential crack initiation sites in typical welded joints and classifies these sites into different categories of fatigue performance. An S-N design curve is specified for each category; where S is the allowable design stress range at the anticipated crack initiation site in a joint, and N is the number of constant amplitude load cycles to initiate what is typically a through-thickness crack several inches long. These curves are used in conjunction with Miner's damage summation rule to assess the fatigue performance of welded details subjected to variable amplitude loading. The relevant design stress is based on local nominal stresses at the anticipated crack initiation site, and excludes stress concentrations and residual stresses already built into the classified joints.

The aforementioned S-N design curves are largely based on S-N design curves that were generated more than twenty years ago from S-N data for small laboratory welded joints (typically 100 to 10 mm wide with 10 to 30 mm thick plates) in air and include factors of safety to account for scatter in this data. S-N data for welded joints fabricated from a wide range of structural steels were included in the data base for the S-N design curves, and the curves were assumed to be independent of material tensile strength. Although it was well known that the fatigue strength of machined and forged components tended to increase with increasing tensile strength, there was substantial S-N data showing that the high cycle fatigue strength of as-welded steel joints is essentially independent of tensile strength. At the time, there was also an emerging consensus that high tensile welding residual stresses are initially present along the weld toes of steel structures and that a significant portion of the fatigue life of steel welded joints is spent in crack propagation from initial crack-like welding flaws along weld toes. It was assumed that the residual stresses are only partially relaxed by local yielding at peak service loads (i.e., shake-down), and that post-shake-down residual stresses are sufficiently high for the weld toe to remain in tension during the compressive portions

of applied loading cycles. Since most of the available S-N data had been obtained from tests of laboratory specimens that were probably too small to develop significant welding residual stresses, only data for joints under uniaxial tension or in the flanges of beams in bending were included in the data bases for the S-N design curves. These curves were assumed to be independent of mean stress.

In the late 1970's, a few experimental studies and theoretical studies indicated that the fatigue strength of a fillet-welded joint between a base plate and a transverse attachment plate decreases with increasing joint size if attachment plate thickness and weld size are scaled in proportion to base plate thickness. This size effect was attributed to the effect of plate thickness on the stress concentration along a weld toe and the stress gradient through the thickness of a plate. Since existing S-N design curves for welded plate details were largely based on experimental data for small welded joints between 10 to 30 mm thick plates, there was concern that these design curves would not be sufficiently conservative for large welded details in steel offshore structures.

In 1979, Gurney [6.57] proposed the following penalty on the fatigue strength of a wide range of welded details with plate thickness exceeding a reference thickness T_r (22 mm)

$$\left(\frac{S}{S_r}\right)=\left(\frac{T_r}{T}\right)^{.25} \tag{6.20}$$

where T is the thickness of the plate through which fatigue cracks propagate, S_r is the design stress range allowed by the relevant S-N design curve, and S is the corrected design stress range. This penalty was incorporated into a number of fatigue design standards for offshore structures in the early 1980's. This penalty remains in effect in current editions of these standards despite theoretical predictions and experimental evidence, including a few sets of S-N data for TMCP steel welded joints (**Figures 6.24-6.26**), that it is unconservative for fillet-welded joints with transverse attachments and welds that scale in proportion to base plate thickness but overly conservative for some types of welded joints (e.g., butt joints, fillet-welded joints with longitudinal attachments, fillet-welded transverse attachments that do not scale in proportion to base plate thickness, and fillet-welded transverse attachments with concave weld profiles achieved by grinding or special welding techniques).

The offshore industry and its regulators have also sponsored considerable research over the past 15 years on the fatigue performance of welded steel joints in a sea water environment [6.47,6.49]. A large part of this work has involved the generation of S-N data for welded plate joints with transverse attachments immersed in sea water with and without cathodic protection. The following trends were observed in initial studies:

1. The fatigue lives of freely corroding test specimens were up to a factor of two lower than the high cycle fatigue lives of test specimens in air. Accelerated crack initiation along weld toes as a result of local corrosion pitting and accelerated crack propagation as a result of anodic dissolution and hydrogen-assisted mechanisms at the crack tip were cited as possible explanations for this reduction in fatigue life.

2. Optimum cathodic protection restored the fatigue lives of test specimens in sea water to close to in-air values. This beneficial effect of cathodic protection was attributed to reduced corrosion pitting and crack closure induced by the formation of calcareous deposits in cracks.

As a result of these initial observations, several fatigue design guidance notes for steel offshore structures imposed a factor of 2 penalty on the design life of freely corroding welded joints [6.54]. However, more recent S-N data, including limited S-N data for TMCP steel joints (**Figures 6.26-6.28**), has indicated that a factor of 3 penalty on the design life of freely corroding joints is more appropriate and that the beneficial effect of cathodic protection diminishes with increasing stress range, particularly for joints with excessive cathodic polarization [6.60]. The reduced effectiveness of cathodic protection at higher cyclic stresses has been attributed to accelerated crack growth as a result of hydrogen embrittlement at the crack tip.

The available S-N data for TMCP steel welded joints, including data for joints with soft heat affected zones, fall within the scatter bands of S-N data for similar types of joints fabricated from non-TMCP steels. For example, Yajima et al. [6.61, 6.62] generated S-N data for butt welded joints that were fabricated from either a normalized HT50 steel, an accelerated-cooled TMCP HT50 steel, a non-accelerated-cooled TMCP HT50 steel, or an accelerated-cooled TMCP AH40 steel. The HT50 steels had minimum specified yield strengths between 320 MPa and 360 MPa, whereas the AH40 steel had a minimum specified yield strength of 400 MPa. All of these specimens were tested under pulsating tension with intact reinforcements. Some of the accelerated-cooled TMCP steel joints were welded with a high heat input process (submerged arc welding-SAW) to deliberately soften heat affected zones, while the remaining accelerated-cooled TMCP steel joints were welded with a low heat input process (gas metal arc welding-GMAW) to avoid softened heat affected zones. The non-accelerated-cooled TMCP steel joints and the normalized steel joints were produced with a manual shielded metal arc welding process (SMAW). As is evident in **Figures 6.29** and **6.30**, the S-N data for all the joints fell within a common scatter band with no significant difference between the fatigue strengths of joints with and without softened heat affected zones.

Yajima et al also generated S-N data for T-joints and cruciform joints with non-load-carrying transverse attachments that were fillet-welded to base plates loaded in pulsating tension. These joints were fabricated from a normalized HT50, an accelerated-cooled TMCP HT50, or an non-accelerated-cooled TMCP HT50 steel. The fillet welds for the non-accelerated-cooled TMCP steels and normalized steels were produced with a shielded metal arc process, whereas the fillet welds for the accelerated-cooled TMCP steels were produced with a low heat input GMAW process. The toes of some of the latter fillet welds were located in softened heat affected zones that were deliberately introduced in the base plate by a high heat input SAW process before the fillet welding process. Again, there were no significant differences between the fatigue strengths of the joints with weld toes located in the softened heat affected zone and the remaining fillet-welded joints (**Figures 6.31** and **6.32**). Although there were sometimes consistent differences between the S-N data for the two types of joints, these differences were no more significant than typical differences between S-N data for welded joints fabricated from different batches of the same material, fabricated by different welders, and/or tested at different laboratories.

It is generally accepted that a significant portion of the fatigue life of as-welded joints is spent in Region II crack propagation. The apparent insensitivity of the high cycle fatigue life of TMCP steel as-welded joints to the presence of softened heat affected zones is consistent with limited da/dN versus ΔK data indicating that Region II crack growth rates in the weld metal and heat affected zone of TMCP steel welds are similar to those in base metal (**Figures 6.8, 6.10 , 6.21, 6.33,** and **6.34**). For example, Lim et al [6.26] generated da/dN versus ΔK data for Region II crack growth in the weld metal and heat affected zone metal of butt joints fabricated by low and high heat input from AH 32, DH 36, and EH 36 grades of TMCP steel. They found that the crack growth data for the weld metal and heat affected zone fell within the scatter band of crack growth data for the base metals.

The insensitivity of the high cycle fatigue life of as-welded steel joints to material tensile strength has also been attributed to the large fraction of life spent in Region II crack growth. This implies that the fatigue strength of welded joints can be improved and made to increase with increasing tensile strength by using weld improvement techniques such as shot-peening, hammer-peening, grinding, and TIG dressing to introduce a significant crack initiation period. Recent S-N data for welded joints fabricated from non-TMCP steel joints show that the aforementioned techniques can improve the fatigue strength of welded joints in air and in sea water with and without cathodic protection by 20% to 100% with the magnitude of improvement increasing with increasing tensile strength. Similar improvements have also been observed in limited tests of TMCP steel welded joints by NKK (**Figure 6.28**). However, limited S-N data indicates that high heat input can reduce the endurance limit of heat affected zone in TMCP steel welds (**Figure 6.14**), and limited da/dN versus ΔK data indicates that Region I crack growth in the softened heat affected zone of TMCP steels welds is faster than that in the base metal (**Figure 6.34**). This data suggests that the effectiveness of weld improvement techniques could be reduced if crack initiation occurs in soft heat affected zone and the presence of soft heat affected zones could reduce the fatigue strength of ground butt joints.

Most of the available S-N data for steel welded joints corresponds to nominal stress ranges less than the yield strength of the parent material. The majority of fatigue damage in welded steel structures is sustained at such cyclic load levels, but extreme wave loads can produce significant cyclic plasticity in certain areas of ships and offshore structures. Available low cycle fatigue data for steel welded joints indicate that the S-N design curves for steel welded joints can be extrapolated to cyclic stress ranges up to four times the yield strength of the parent material. Although most fatigue design rules restrict this upper limit to twice the yield strength, significant cyclic plasticity can still occur at structural details at these stress ranges. Under such conditions, soft heat affected zones in TMCP welded joints could act as strain concentrators. Such strain concentrations could act as preferred crack initiation sites although this tendency would be offset to some extent by the greater resistance to crack initiation of softer metals for a given cyclic strain range. Such strain concentrations could also cause cracks initiating outside the softened heat

affected zone to propagate into that softened zone where the resistance to Region III crack growth would be expected to be lower than that in harder metal. Youn and Kim [6.62] have observed that Region III crack growth in softened heat affected zone of TMCP welds tends to be faster than that in base metal (**Figure 6.34**), and Lim et al [6.26] observed that high heat input tends to reduce the low cycle fatigue life of smooth strain-controlled specimens machined from the heat affected zone of butt joints (**Figure 6.17**). Unfortunately, no low cycle S-N data for TMCP steel welded joints was found in the open literature.

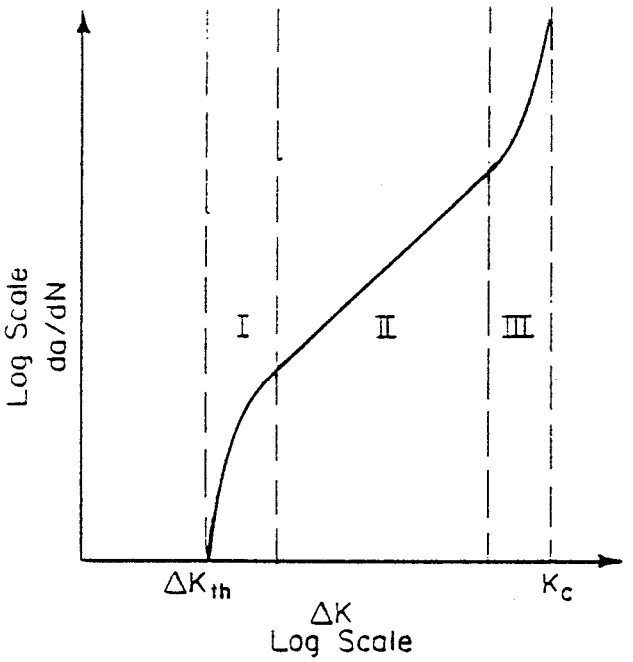

Figure 6.1: Basic shape of da/dN vs ΔK curve

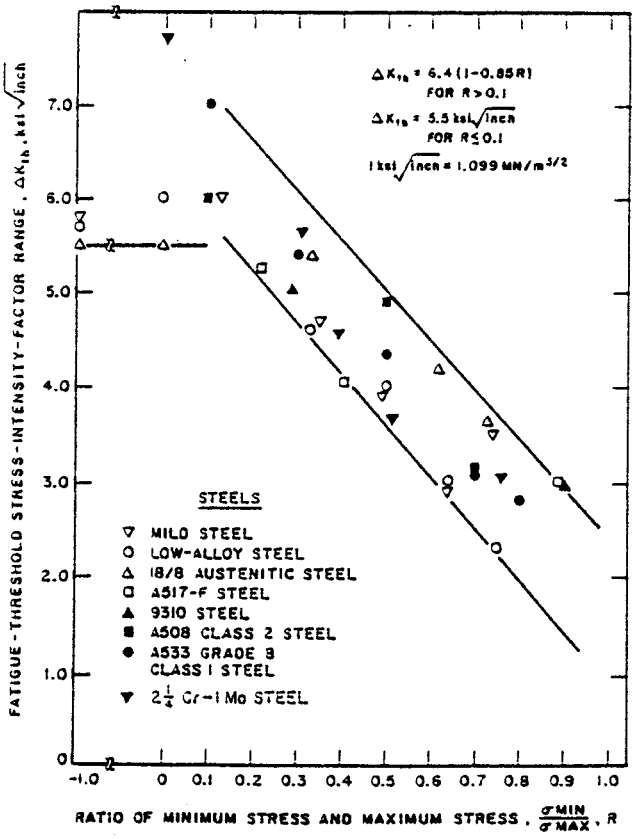

Figure 6.2: Plot of ΔK_{th} vs R-ratio for different steels from [6.16]

Ebara et al. [6.18]

Data Type:	da/dN vs ΔK data for long cracks
Material:	HT50 TMCP steel
Environments:	air, sour crude oil (400 ppm H_2S)
Specimen Type:	compact tension (CT)
Specimen Size:	B=12 mm, W = 50 mm
Specimen Orientation:	machined from center of 25 mm thick plates in L-T orientation
Pre-Cracking:	1 mm long fatigue crack at tip of 27 mm long notch
Loading:	R = .028, f_{oil} = .17 Hz , f_{air} = .25 Hz

Steel	Chemical Composition (wt. %)											YS	UTS	El.
Grade	C	Si	Mn	P	S	Cu	Ni	Cr	Nb	Al	Ti	(MPa)	(MPa)	%
HT50	.14	.41	1.19	.15	.005	.01	.02	.01	.006	.034	.016	412	527	22

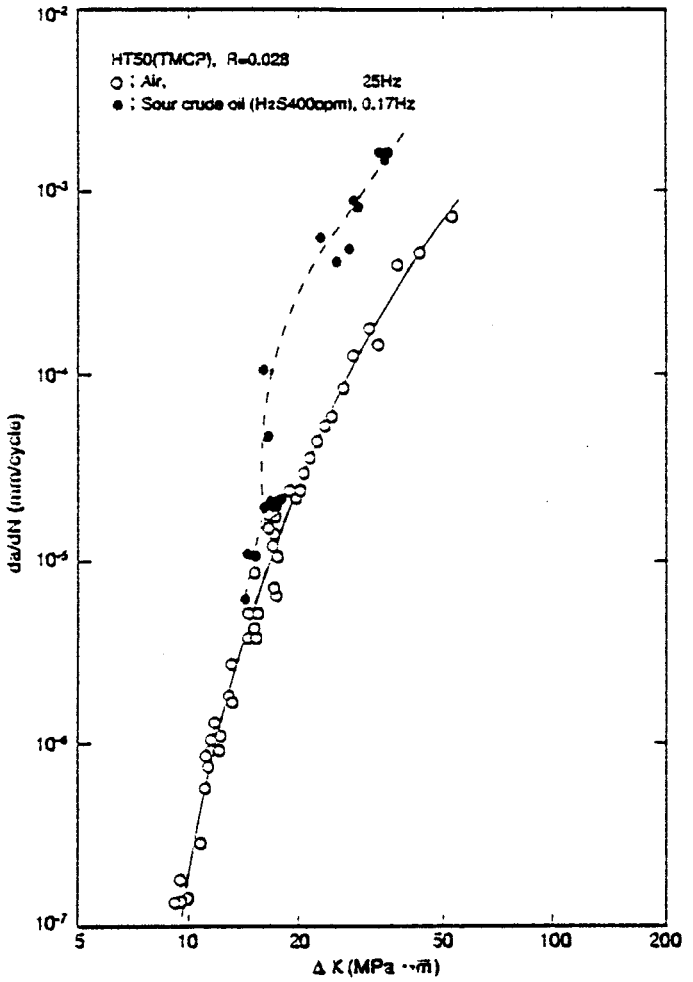

Figure 6.3

Ouchi et al. [6.19]

Data Type:	da/dN vs ΔK for long cracks
Material:	KA36 TMCP steel and KAS TMCP steel
Environments:	air, sour crude oil (400 ppm H_2S)
Specimen Type:	compact tension (CT)
Specimen Size:	B = 12 mm, W = 50 mm or 50.8 mm
Specimen Orientation:	machined from center of 25 mm plate plates in L-T orientation
Pre-cracking:	1 mm long fatigue crack at tip of 27 mm long notch or 3 mm long fatigue crack at tip of 23 mm long notch
Loading:	R = .028, f = .17 Hz (.25 Hz for some in-air tests)

Steel Grade	Chemical Composition (wt. %)					YS (MPa)	UTS (MPa)	El. %
	C	Si	Mn	P	S			
K36	.14-.15	.20-.41	1.13-1.19	.015	.005	375-426	512-555	22-26
KAS	.12-.15	.19-.20	.94-1.22	.014-.017	.005-.007	285-291	429-457	27-36

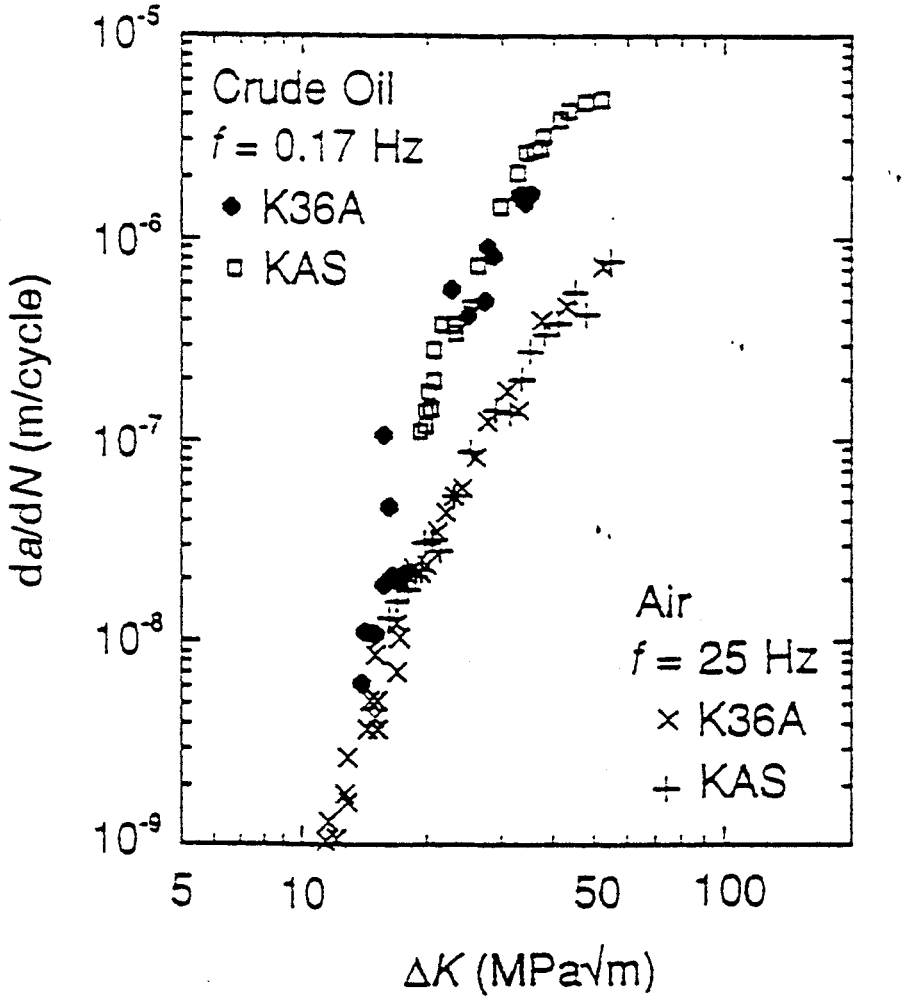

Figure 6.4

Yang and Hartt [6.20 and 6.21]

Data Type:	da/dN vs ΔK for long cracks
Materials:	AC70 TMCP steel (accelerated cooled) and A537 TMCP steel (direct quenched)
Environments:	air, natural sea water with and without cathodic protection
Specimen Type:	tapered compact tension (TCT)
Loading:	R = .5 and .8, f_{air} = 3 Hz , $f_{seawater}$ = .3 Hz

Steel Grade	Chemical Composition (wt. %)											YS (MPa)	UTS (MPa)
	C	Si	Mn	P	S	Cu	Ni	Cr	Mo	Nb	V		
A537-DQ	.12	.41	1.3	.014	.003	.01	.03	.04	.05		.044	500	598
AC70	09	.30	1.5	.007	.003	.18	.40			.016		503	618

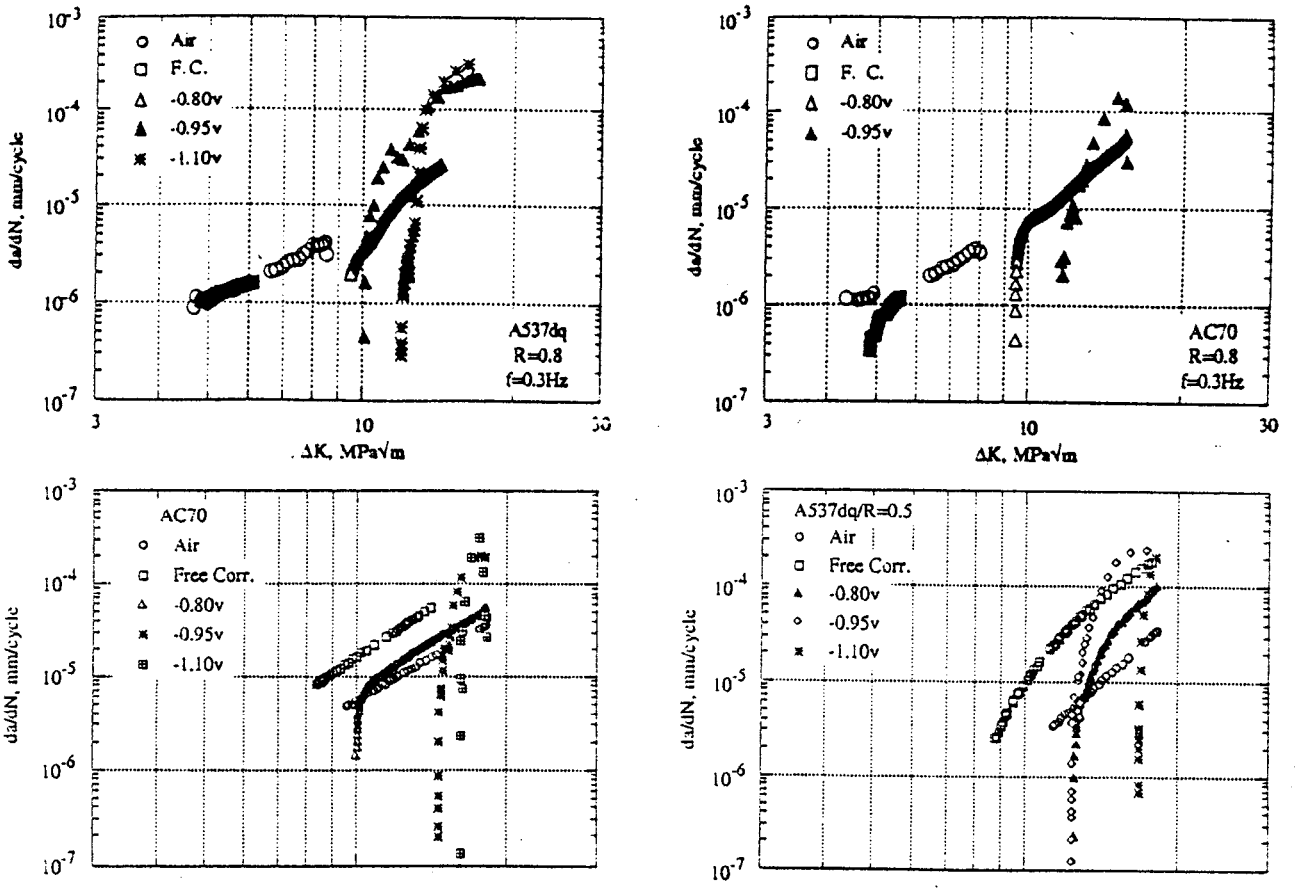

Figure 6.5

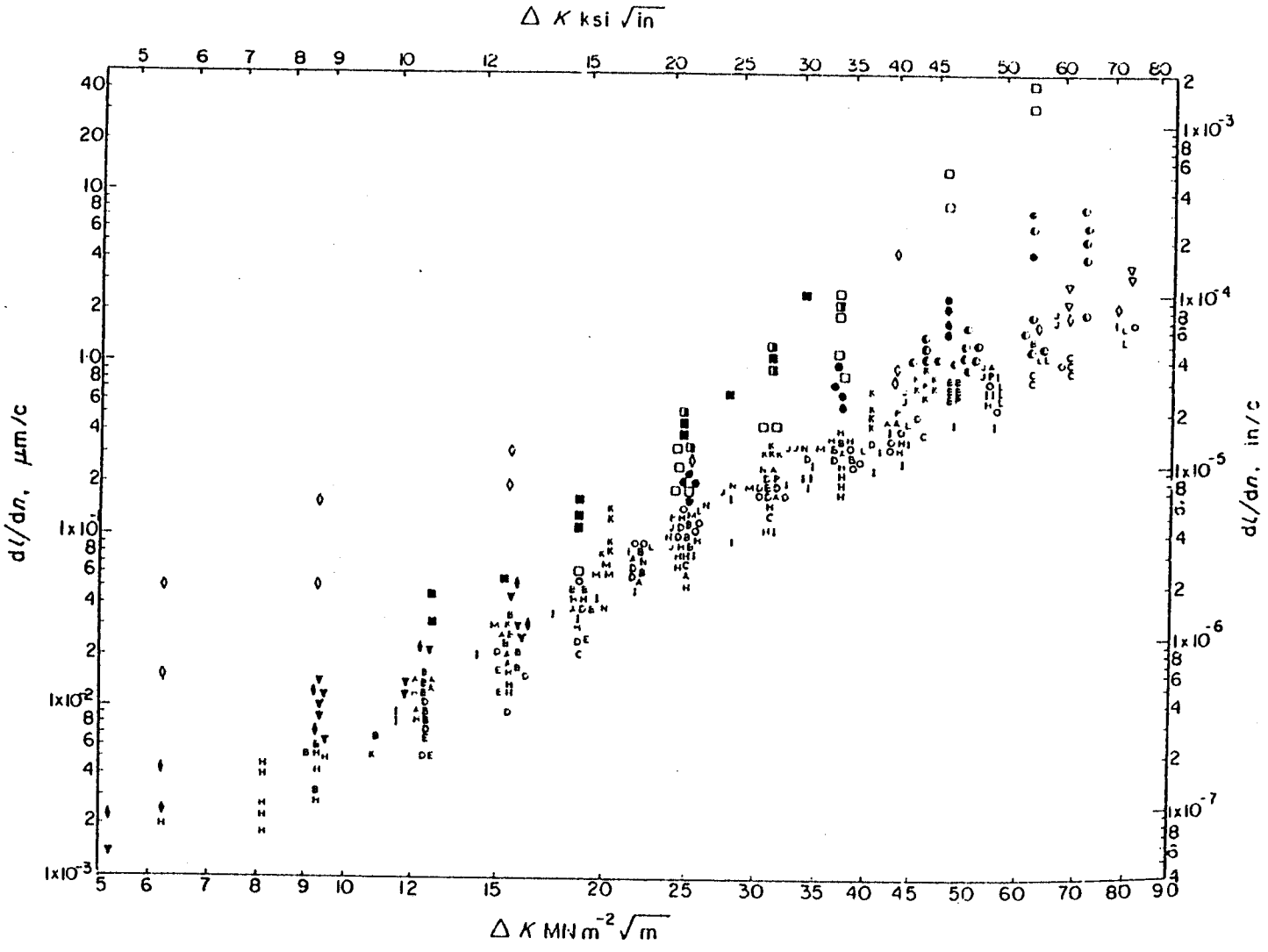

Figure 6.6: da/dN vs ΔK data for various steels, weld metals and heat affected zone metal from [6.22]. Letters indicate growth by striation mechanism

Spurrier et al. [6.25]

Data Type:	da/dN vs ΔK
Materials:	Grade 55F TMCP steels (OLAC)
Environments:	air
Specimen Type:	single edge notch bending (SENB)
Specimen Size:	B = 12 mm, W = 24 mm
Loading:	three-point bending, R = .1, f = 10 Hz

Steel Grade	Thickness (mm)	Chemical Composition (wt. %)										YS (MPa)
		C	Si	P	S	Cu	Ni	N	Ti	Nb	S.Al	
55F	32	07	.34	.007	.001	.26	.45			.01		506

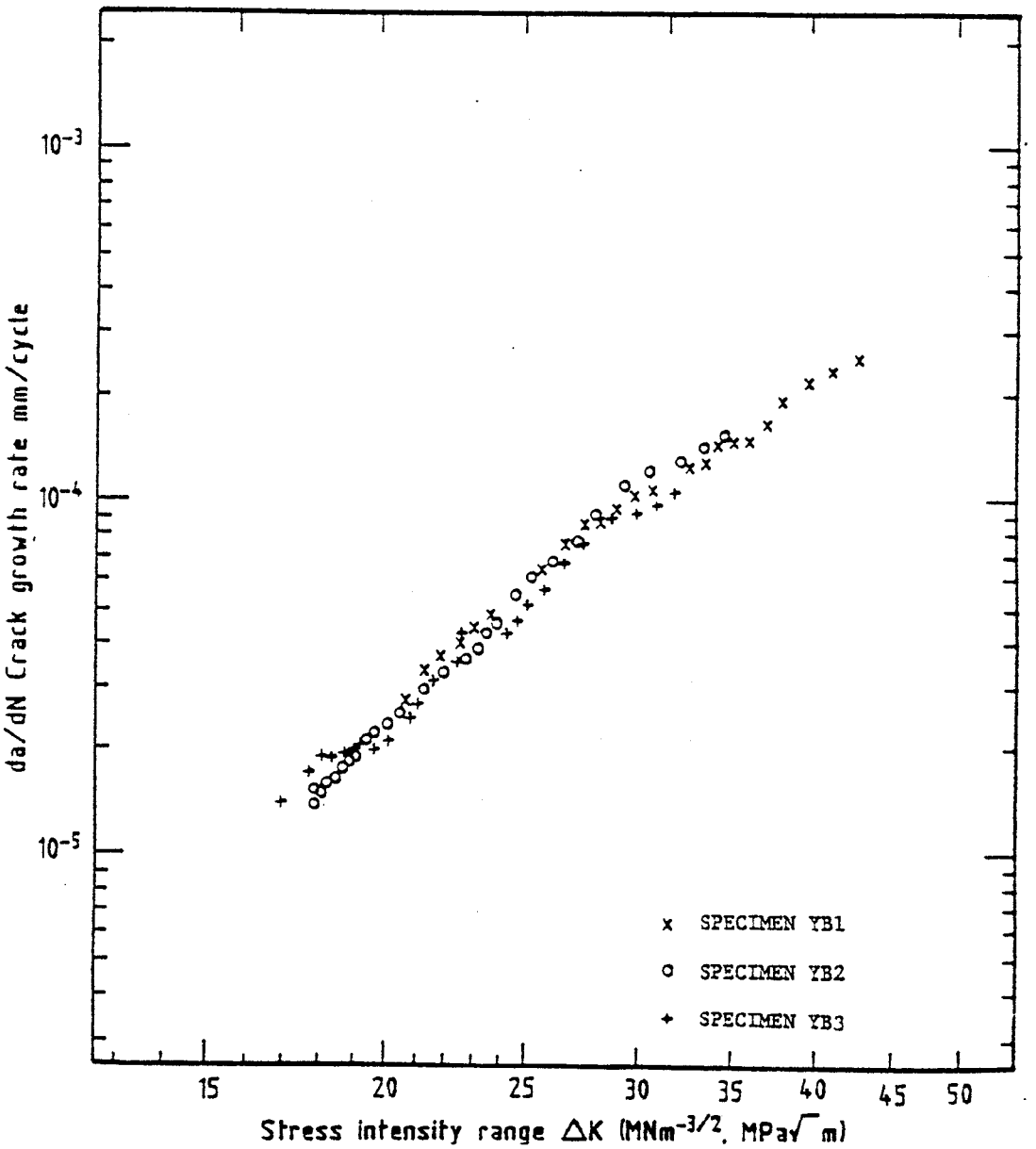

Figure 6.7

Lim et al. 1990

Data Type: da/dN vs ΔK data for long cracks
Materials: base metal, HAZ, and weld metal of AH 32, DH 36, and EH 36 TMCP steels
Environment: air
Specimen Type: compact tension specimens machined from base metal
compact tension specimens machined from butt joints produced by SAW process (80 kJ/cm or 180 kJ/cm of heat input) with notch running parallel to weld and located in weld metal or HAZ
Loading: R = .1, f = 20 Hz

Steel Grade	Thickness (mm)	Chemical Composition (wt. %)							YS (MPa)	UTS (MPa)	El. %
		C	Si	Mn	P	S	Sol. Al	Ti			
AH 32	18	.147	.246	1.030	.020	.004	.020		370	510	39.7
DH 36	25	.141	.329	1.214	.022	.004	.027	.010	415	550	35.4
EH 36	20	.086	.285	1.400	.017	.006	.048	.016	398	490	42.8

Steel Grade	Specimen	YS (MPa)	UTS (MPa)	El. %	% Area Reduction	YS/UTS %	True Fracture Stress (MPa)	True Strain Fracture
AH 32	base metal	370	510	39.7	73	73	112	1.309
	weld (180 kJ /cm)	360	509	25.4	69	71	105.5	1.171
	weld (80 kJ/cm)	356	515	32.8	73	69	116	1.309
DH 36	base metal	415	550	35.4	75	75	129.9	1.386
	weld (180 kJ/cm)	373	529	27.2	74	71	127.3	1.347
	weld (80 kJ/cm)	392	527	30	73	74	123.9	1.309
EH 36	base metal	398	490	42.8	82	81	133.5	1.715
	weld (180 kJ/cm)	357	459	23.4	79	78	127.3	1.561
	weld (80 kJ/cm)	342	460	32.4	77	74	120.3	1.47

Figure 6.8a

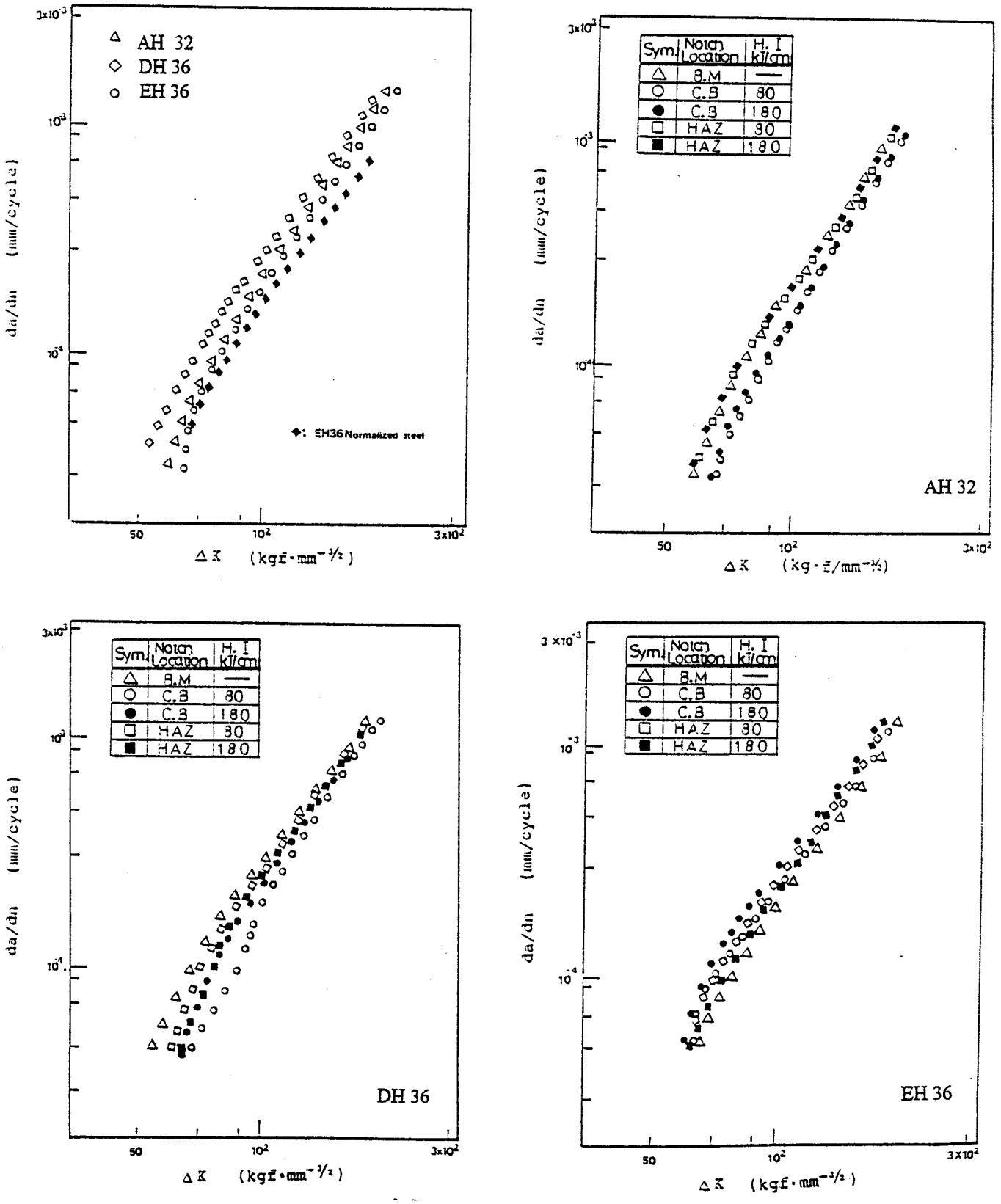
△ AH 32
◇ DH 36
○ EH 36
◆: SH36 Normalized steel
da/dn (mm/cycle)
ΔK (kgf·mm^-3/2)
Sym. | Notch Location | H.I kJ/cm
△ | B.M | —
○ | C.B | 80
● | C.B | 180
□ | HAZ | 30
■ | HAZ | 180
AH 32
DH 36
EH 36
ΔK (kg·f/mm^-3/2)

Figure 6.8b

Nakano et al. [6.27]

Data Type:	da/dN vs ΔK for long cracks
Materials:	YS36 TMCP steel (accelerated cooled), YS46 TMCP steel (control rolled and accelerated cooled), YS36 normalized steel
Environments:	air, artificial sea water with and without cathodic protection
Specimen Type:	compact tension (TCT)
Specimen Orientation:	T-L for YS36 TMCP steel and YS 36 normalized steel L-S for YS 46 TMCP steel
Specimen Size:	B_{T-L} = 12.5 mm, B_{L-S} = 6 mm, W = 2B
Pre-cracking:	not specified
Loading:	R = .05, $f_{seawater}$ = .167 Hz, f_{air} = not specified

Steel Grade	Thick (mm)	Chemical Composition (wt. %)									YS (MPa)	UTS (MPa)	El %
		C	Si	Mn	P	S	Cr	V	Nb	Al			
YS36 norm.	25	.14	.35	1.31	.022	..006	.02	.034	.016	.028	385	523	25
YS36 norm.	30	.15	.40	1.32	.016	.004			.026		372	523	30
YS36 TMCP	30	.07	.26	1.32	.006	.002			.017	.032	465	520	26
YS46 TMCP	25	.054	.30	1.50	.006	.003	.55	.031	.038	.027	520	571	42

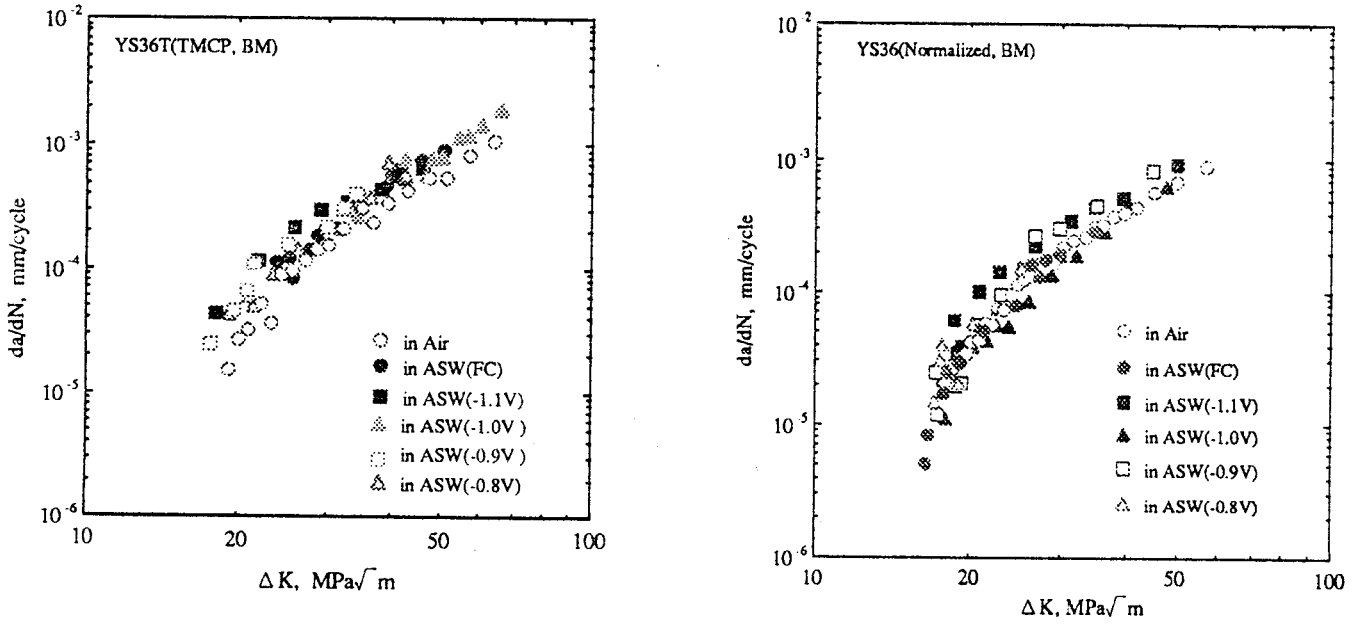

Figure 6.9a

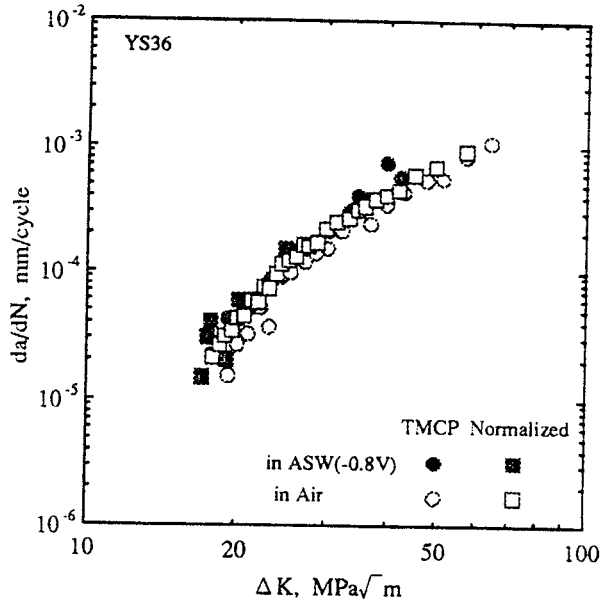
YS36
da/dN, mm/cycle
ΔK, MPa√m
TMCP Normalized
in ASW(-0.8V)
in Air

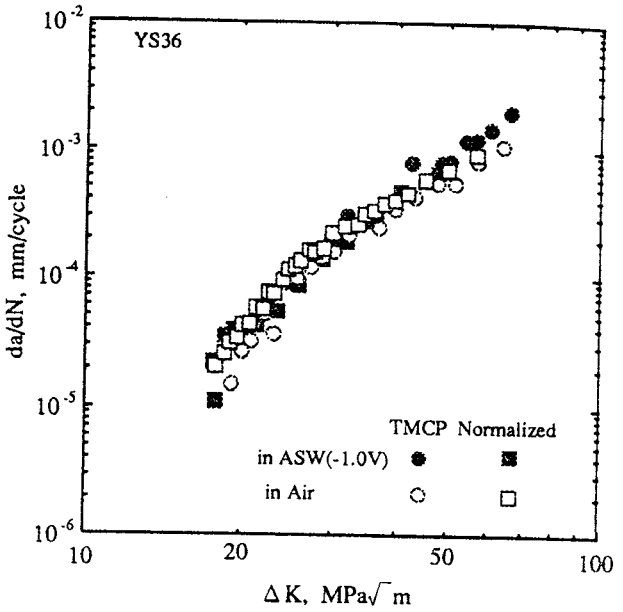
YS36
da/dN, mm/cycle
ΔK, MPa√m
TMCP Normalized
in ASW(-1.0V)
in Air

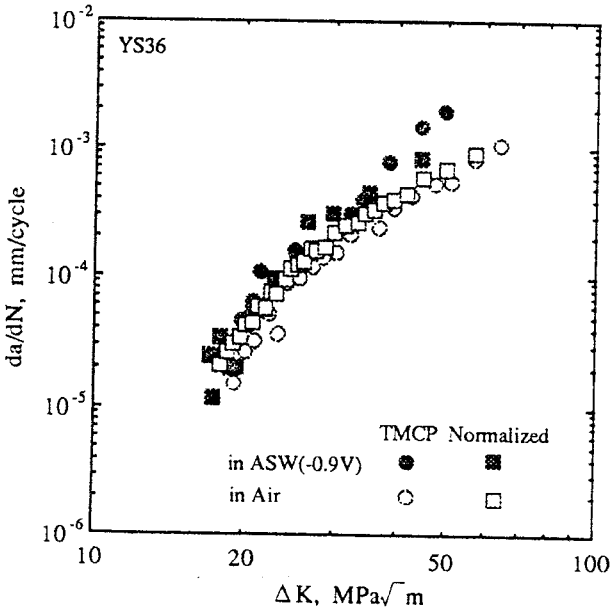
YS36
da/dN, mm/cycle
ΔK, MPa√m
TMCP Normalized
in ASW(-0.9V)
in Air

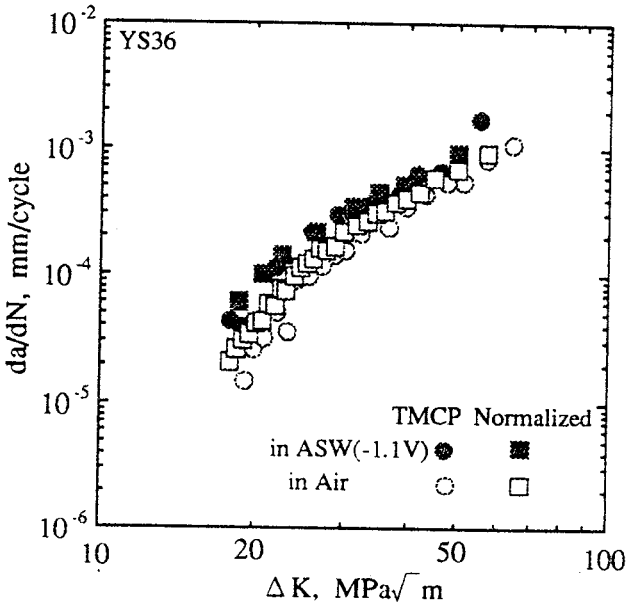
YS36
da/dN, mm/cycle
ΔK, MPa√m
TMCP Normalized
in ASW(-1.1V)
in Air

Figure 6.9b

Tubby and Booth [6.28]

Data Type:	da/dN vs ΔK for long cracks
Materials:	base metal and HAZ of YS36 Grade MACS steel
Environments:	air, artificial sea water @ 5°C without cathodic protection
Specimen Type:	single edge notch bending (SENB)
Specimen Size:	B = 19 mm , W = 38 mm
Specimen Orientation:	base metal specimens machined in L-T orientation HAZ metal specimens machined from K-grooved butt joints with notch located parallel to straight side of K-groove, 1mm from fusion line
Pre-cracking:	2 mm fatigue crack at tip of 3 mm deep, 2mm wide starter notch
Loading:	three-point bending, R = .7, $f_{seawater}$ = .167 Hz

Chemical Composition (wt. %)

C	Mn	Si	Ni	Cr	P	Mo	Cu	Nb	Ti	Al	S	V	B
.10	1.33	.30	.26	.02	.007	.005	.27	.016	.007	.03	<.002	.002	<.0003

Mechanical Properties

YS (MPa)	UTS (MPa)	El. %
431	556	25

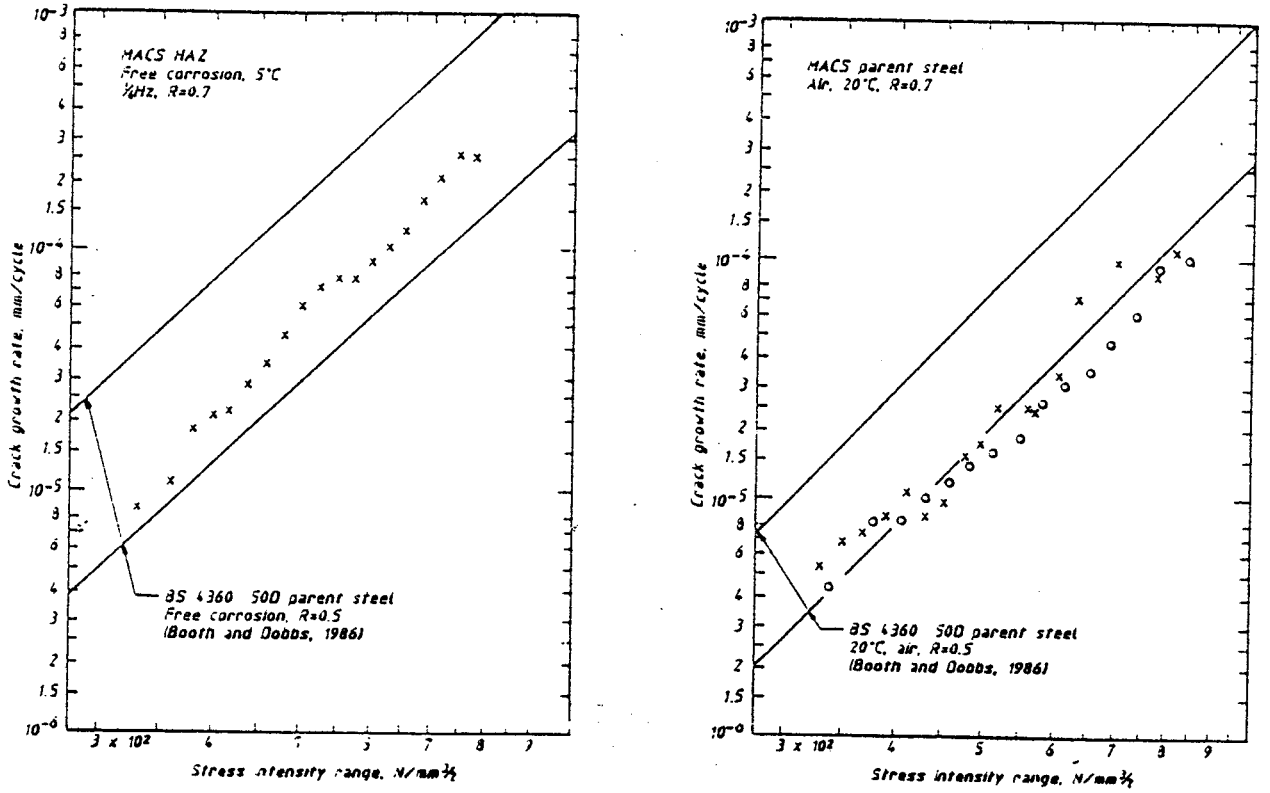

Figure 6.10

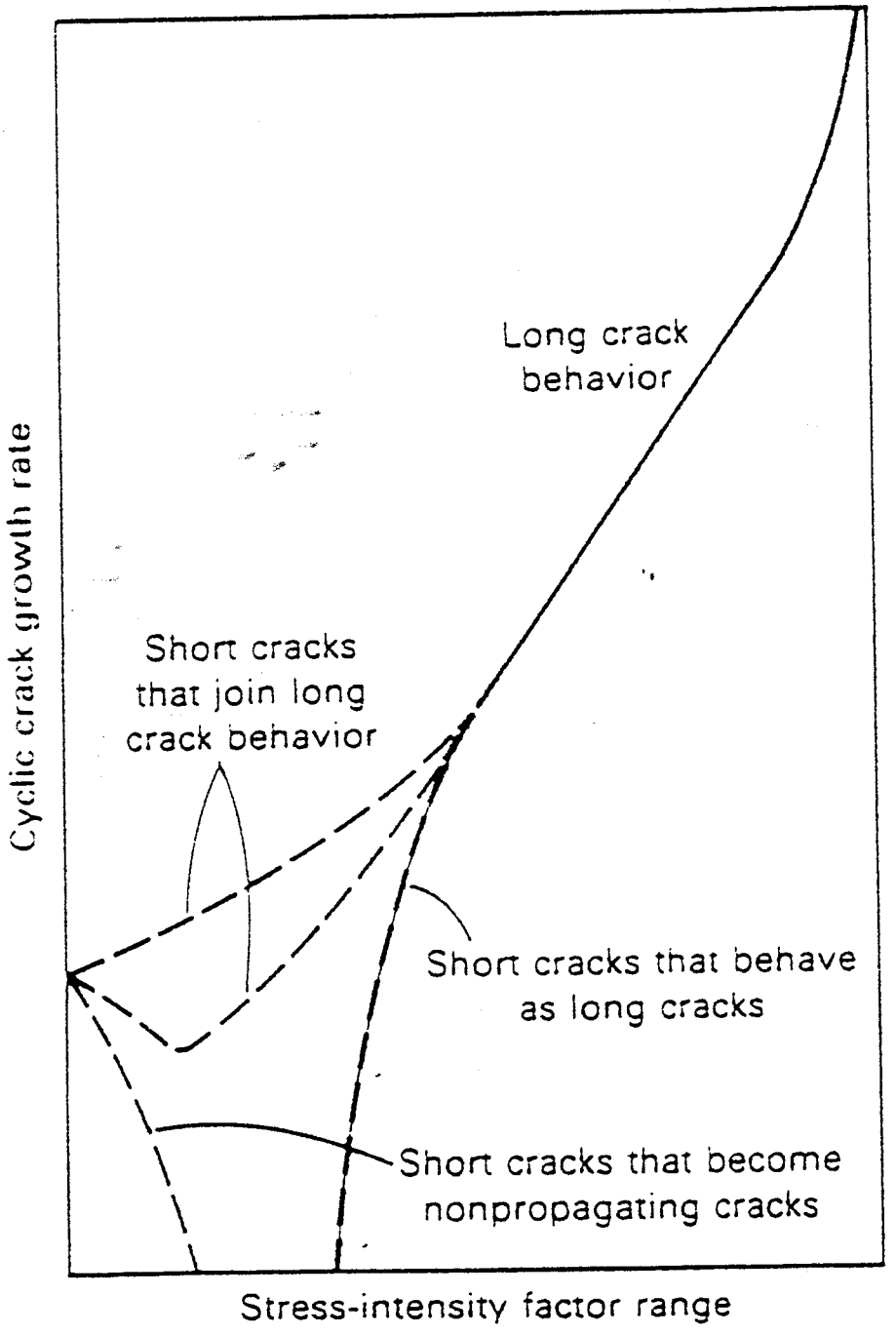

Figure 6.11: Schematic representation of short crack behaviour from [6.32]

Kim and Hartt [6.34 and 6.35]

Data Type:	da/dN vs ΔK for short cracks
Materials:	AC70 TMCP steel (accelerated cooled) and A537 TMCP steel (direct quenched)
Environments:	air, natural sea water with and without cathodic protection
Specimen Type:	single edge notch bending (SENB)
Specimen Orientation:	L-T
Pre-cracking:	.1 mm deep EDM starter notch
Loading:	three-point bending, R = .5, f_{air} = 3 Hz , $f_{seawater}$ = .1 Hz

Steel Grade	Chemical Composition (wt. %)											YS (MPa)	UTS (MPa)
	C	Si	Mn	P	S	Cu	Ni	Cr	Mo	Nb	V		
A537-DQ	.12	.41	1.3	.014	.003	.01	.03	.04	.05		.044	500	598
AC70	09	.30	1.5	.007	.003	.18	.40			.016		503	618

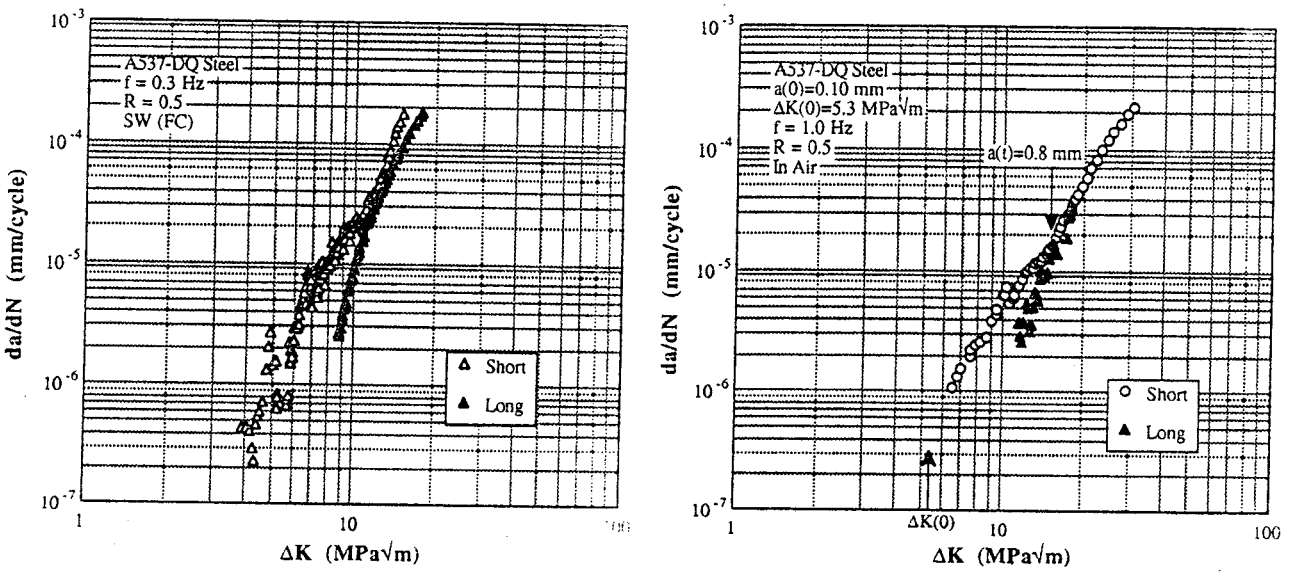

Figure 6.12a

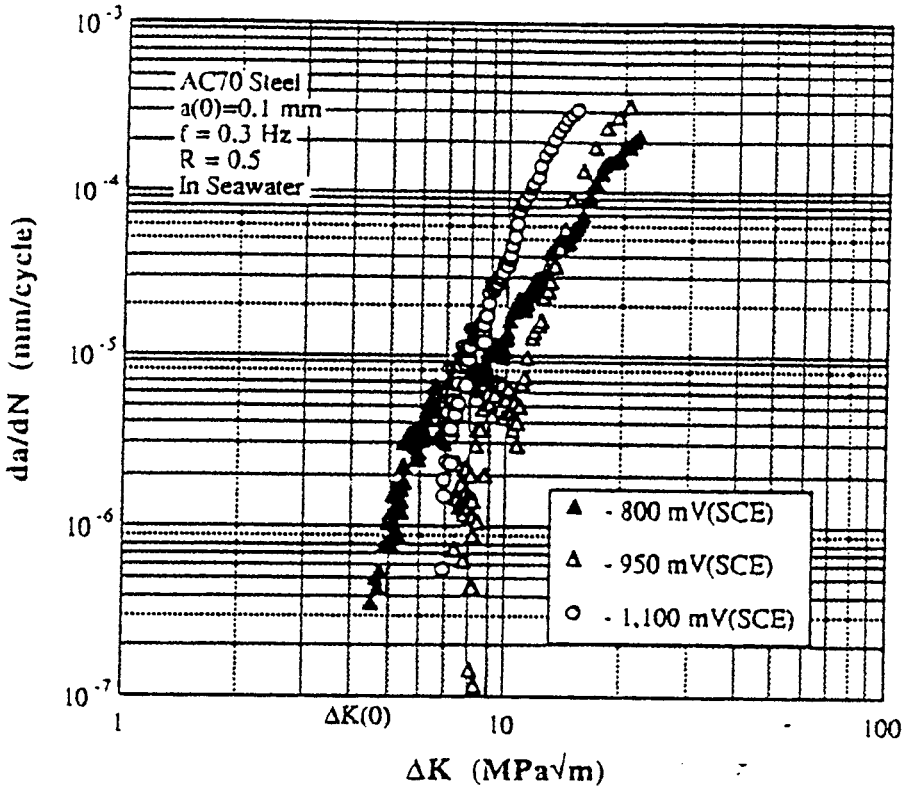
AC70 Steel
a(0)=0.1 mm
f = 0.3 Hz
R = 0.5
In Seawater
- 800 mV(SCE)
- 950 mV(SCE)
- 1,100 mV(SCE)
da/dN (mm/cycle)
ΔK(0)
ΔK (MPa√m)

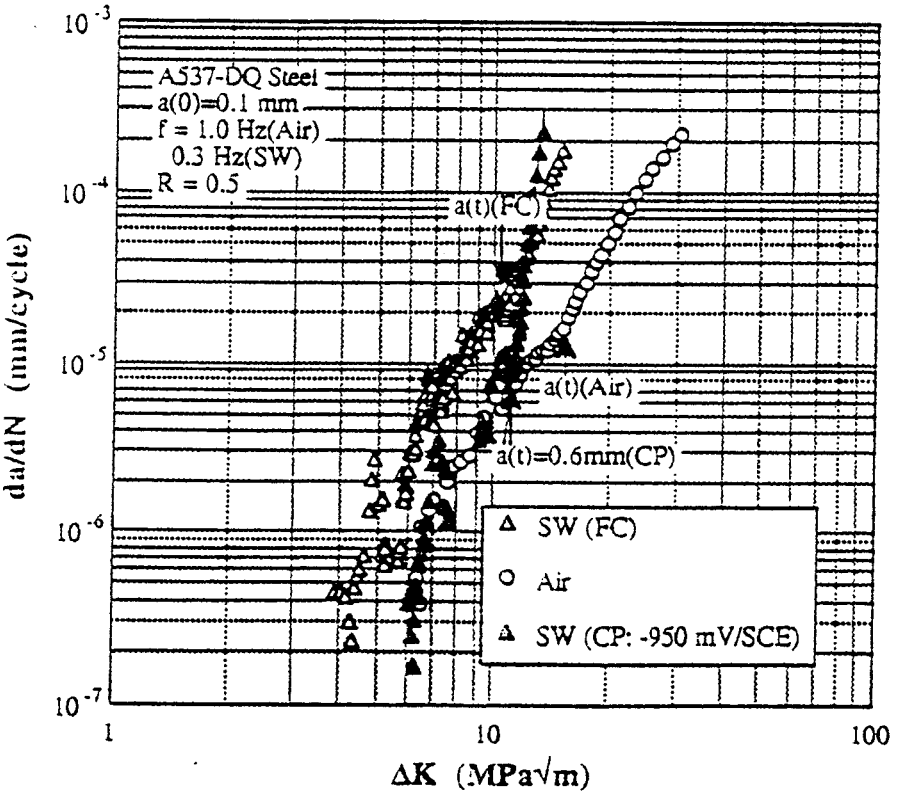
A537-DQ Steel
a(0)=0.1 mm
f = 1.0 Hz(Air)
0.3 Hz(SW)
R = 0.5
a(t)(FC)
a(t)(Air)
a(t)=0.6mm(CP)
SW (FC)
Air
SW (CP: -950 mV/SCE)
da/dN (mm/cycle)
ΔK (MPa√m)

Figure 6.12b

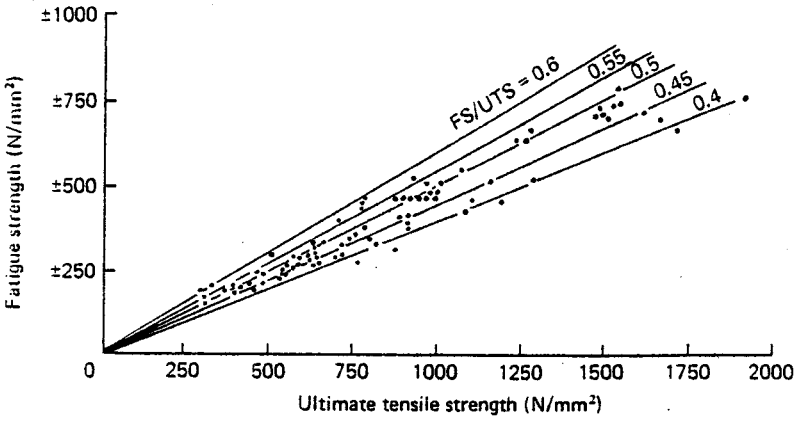

(a)

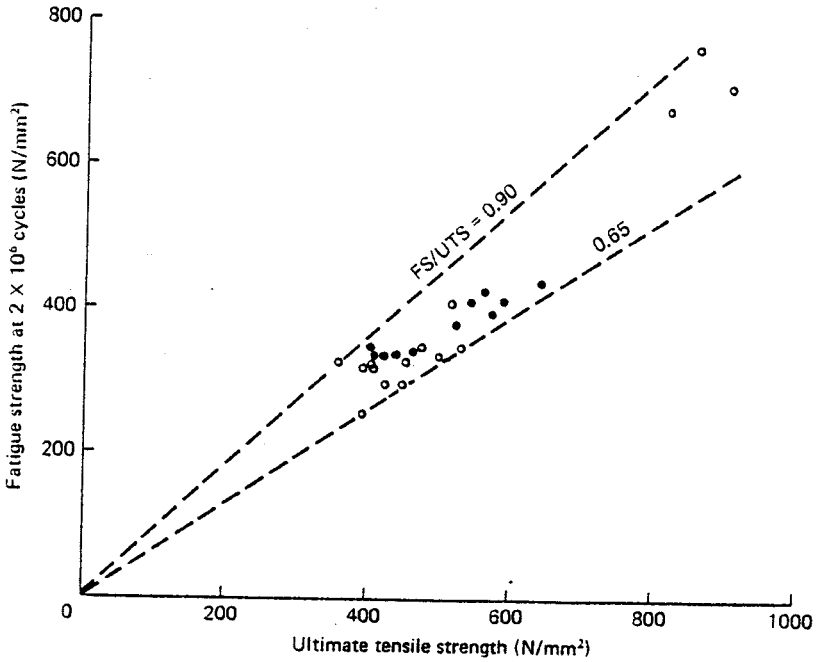

(b)

Figure 6.13: Fatigue limit vs ultimate tensile strength data for: (a) smooth steel rotating beam specimens [6.38]; and (b) smooth steel pulsating tension specimens [6.39]

Lim et al. [6.26]

Data Type: S-N data
Materials: base metal, HAZ, and weld metal of AH 32, DH 36, and EH 36 TMCP steels
Environment: air
Specimen Type: tensile test specimens machined from base metal
tensile test specimens achined from butt joints produced by SAW prcess (80 kJ/cm or 180 kJ/cm of heat input) with weld metal located I in the center of gauge section
Loading: axial, R = .1, f = 20 Hz

Steel Grade	Thickness (mm)	Chemical Composition (wt. %)							YS (MPa)	UTS (MPa)	El. %
		C	Si	Mn	P	S	Sol. Al	Ti			
AH 32	18	.147	.246	1.030	.020	.004	.020		370	510	39.7
DH 36	25	.141	.329	1.214	.022	.004	.027	.010	415	550	35.4
EH 36	20	.086	.285	1.400	.017	.006	.048	.016	398	490	42.8

Steel Grade	Specimen	YS (MPa)	UTS (MPa)	El. %	% Area Reduction	YS/UTS %	True Fracture Stress (MPa)	True Strain Fracture
AH 32	base metal	370	510	39.7	73	73	112	1.309
	weld (180 kJ /cm)	360	509	25.4	69	71	105.5	1.171
	weld (80 kJ/cm)	356	515	32.8	73	69	116	1.309
DH 36	base metal	415	550	35.4	75	75	129.9	1.386
	weld (180 kJ/cm)	373	529	27.2	74	71	127.3	1.347
	weld (80 kJ/cm)	392	527	30	73	74	123.9	1.309
EH 36	base metal	398	490	42.8	82	81	133.5	1.715
	weld (180 kJ/cm)	357	459	23.4	79	78	127.3	1.561
	weld (80 kJ/cm)	342	460	32.4	77	74	120.3	1.47

Figure 6.14a

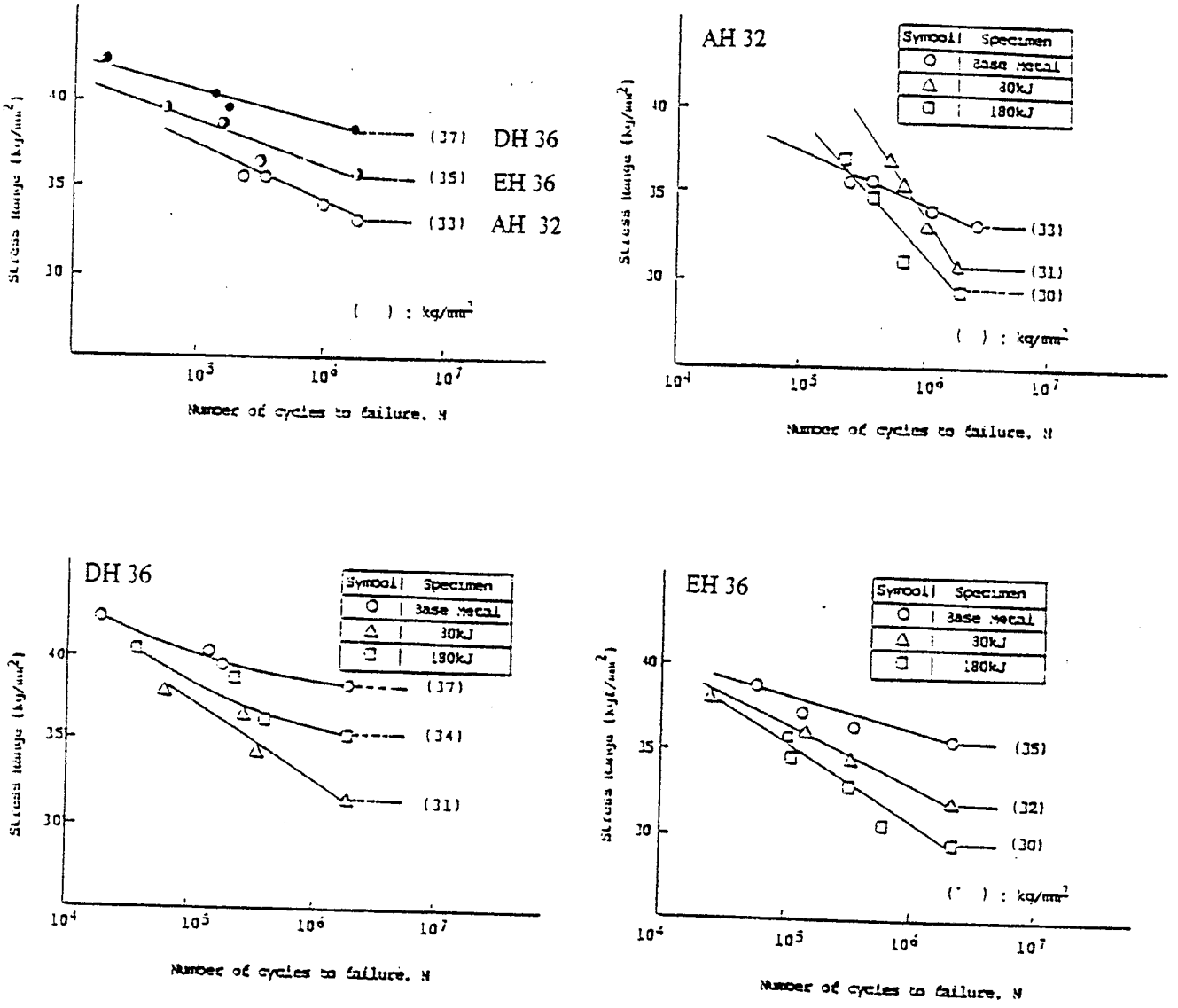
(37) DH 36
(35) EH 36
(33) AH 32
( ) : kg/mm²
Number of cycles to failure, N
AH 32
Symbol | Specimen
○ | Base metal
△ | 30kJ
□ | 180kJ
(33)
(31)
(30)
DH 36
(37)
(34)
(31)
EH 36
(35)
(32)
(30)

Figure 6.14b

Dillinger Hutte GTS [6.40]

Data Type:	S-N data
Materials:	D-MC 355 and D-MC 460 TMCP steel (accelerated cooled and non-accelerated cooled) Fe 510 and Fe E 460 normalized steels
Environments:	air
Specimen Type:	rotating beam
Loading:	R = 0

Steel Grade	Thickness (mm)	YS (MPa)	UTS (MPa)
D-MC 355 non-accelerated cooled	20	462	528
D-MC 355 accelerated cooled	40	426	545
Fe 510 D1 normalized	14	419	564
D-MC 460 non-accelerated cooled	20	530	631
D-MC 460 accelerated cooled	50	450	550
Fe E 460 normalized	30	494	646

Figure 31: Fatigue characteristics of DI-MC 355 and DI-MC 460 (TM and TM-ACC) in comparison with normalized steel of the same strength class

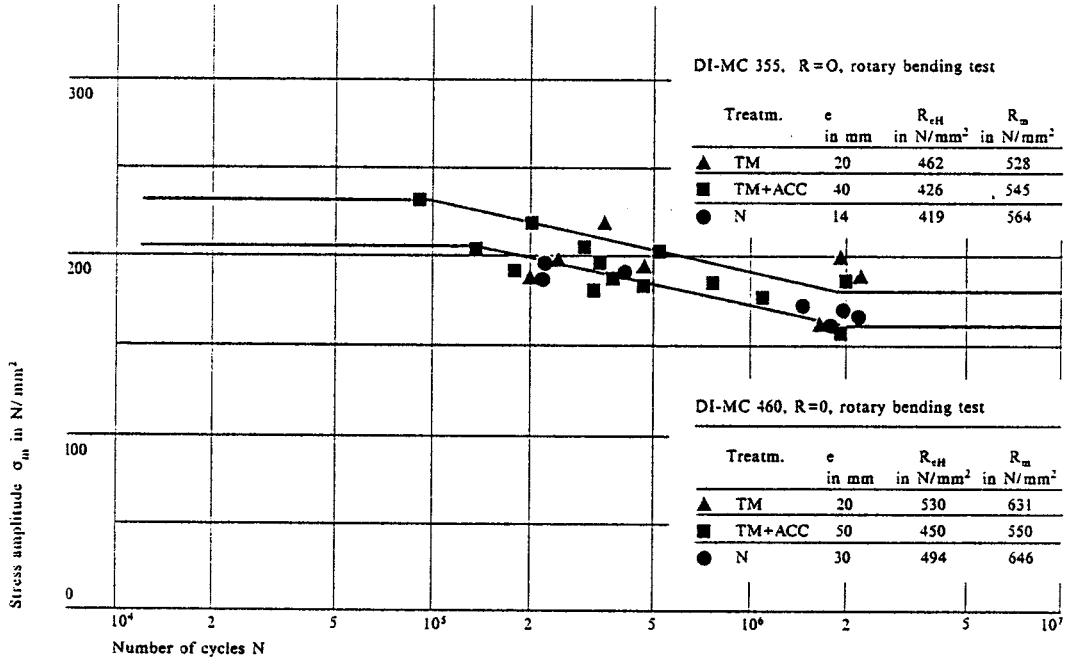

Figure 6.15

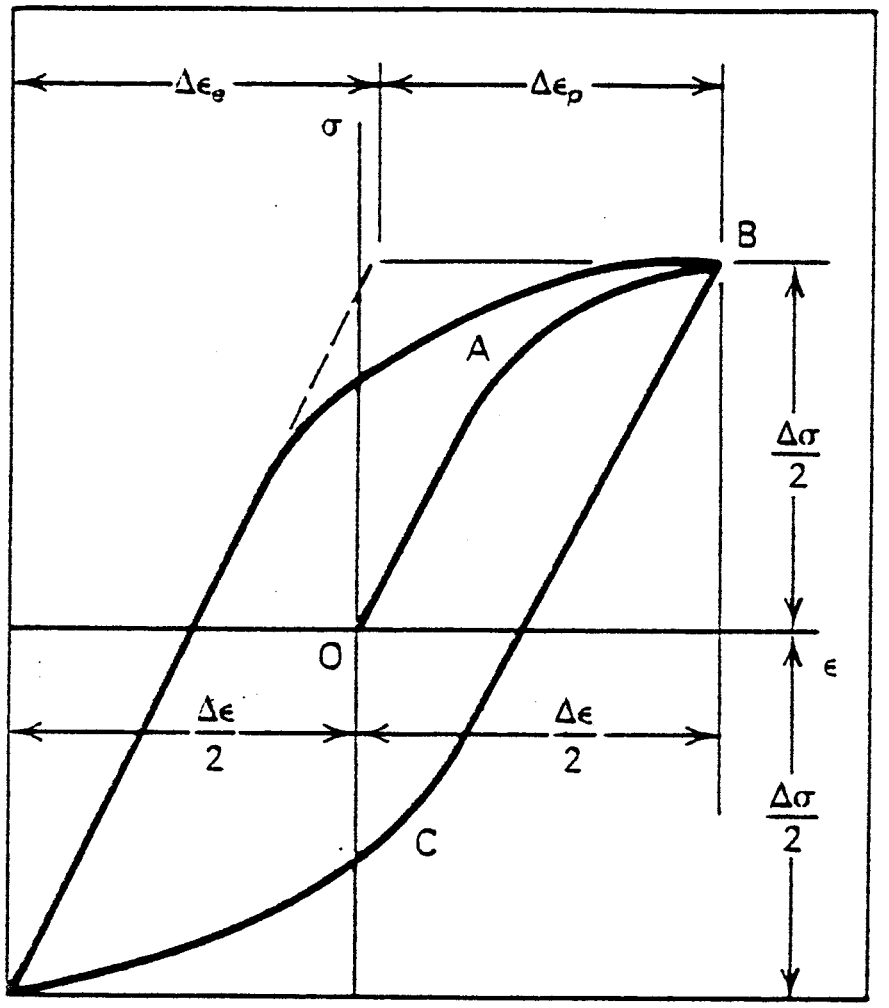

Figure 6.16: Hysteresis stress-strain loop for strain-controlled specimen [6.32]

Lim et al. 1990

Data Type: ε-N data
Materials: base metal, HAZ, and weld metal of AH 32, DH 36, and EH 36 TMCP steels
Environment: air
Specimen Type: tensile test specimens machined from base metal
tensile test specimens machined from butt joints produced by SAW process (80 kJ/cm or 180 kJ/cm of heat input) with weld metal located in the center of gauge section
Loading: axial, R = -1, f = .1-1 Hz

Steel Grade	Thickness (mm)	Chemical Composition (wt. %)							YS (MPa)	UTS (MPa)	El. %
		C	Si	Mn	P	S	Sol. Al	Ti			
AH 32	18	.147	.246	1.030	.020	.004	.020		370	510	39.7
DH 36	25	.141	.329	1.214	.022	.004	.027	.010	415	550	35.4
EH 36	20	.086	.285	1.400	.017	.006	.048	.016	398	490	42.8

Steel Grade	Specimen	YS (MPa)	UTS (MPa)	El. %	% Area Reduction	YS/UTS %	True Fracture Stress (MPa)	True Strain Fracture
AH 32	base metal	370	510	39.7	73	73	112	1.309
	weld (180 kJ /cm)	360	509	25.4	69	71	105.5	1.171
	weld (80 kJ/cm)	356	515	32.8	73	69	116	1.309
DH 36	base metal	415	550	35.4	75	75	129.9	1.386
	weld (180 kJ/cm)	373	529	27.2	74	71	127.3	1.347
	weld (80 kJ/cm)	392	527	30	73	74	123.9	1.309
EH 36	base metal	398	490	42.8	82	81	133.5	1.715
	weld (180 kJ/cm)	357	459	23.4	79	78	127.3	1.561
	weld (80 kJ/cm)	342	460	32.4	77	74	120.3	1.47

Figure 6.17a

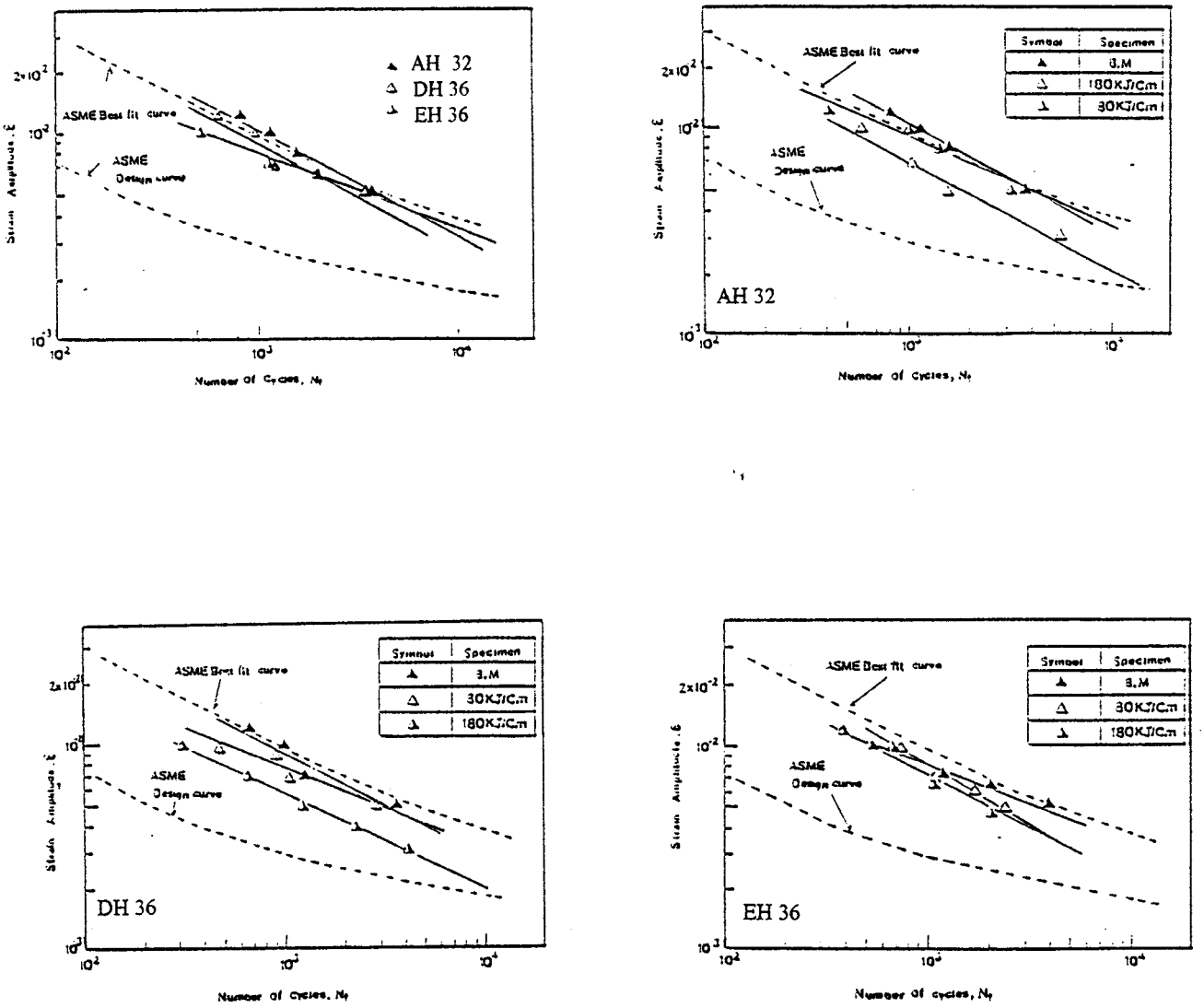
AH 32
DH 36
EH 36
ASME Best fit curve
ASME
Design curve
Symbol
Specimen
B.M
180KJ/Cm
30KJ/Cm
AH 32
DH 36
EH 36
Number of Cycles, Nf

Figure 6.17b

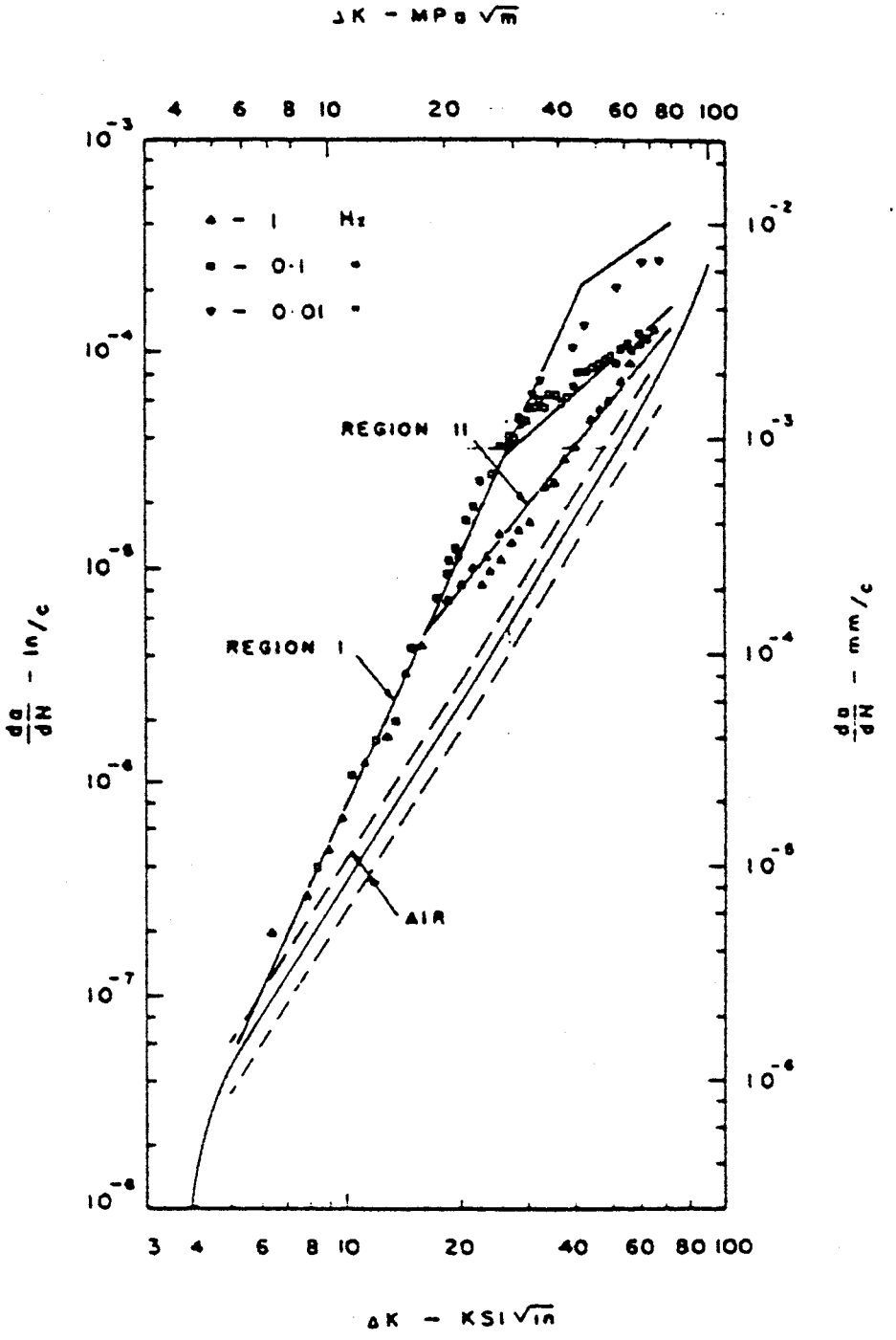

Figure 6.18a: Typical da/dN vs ΔK data for steels in sea water without cathodic protection [6.47]

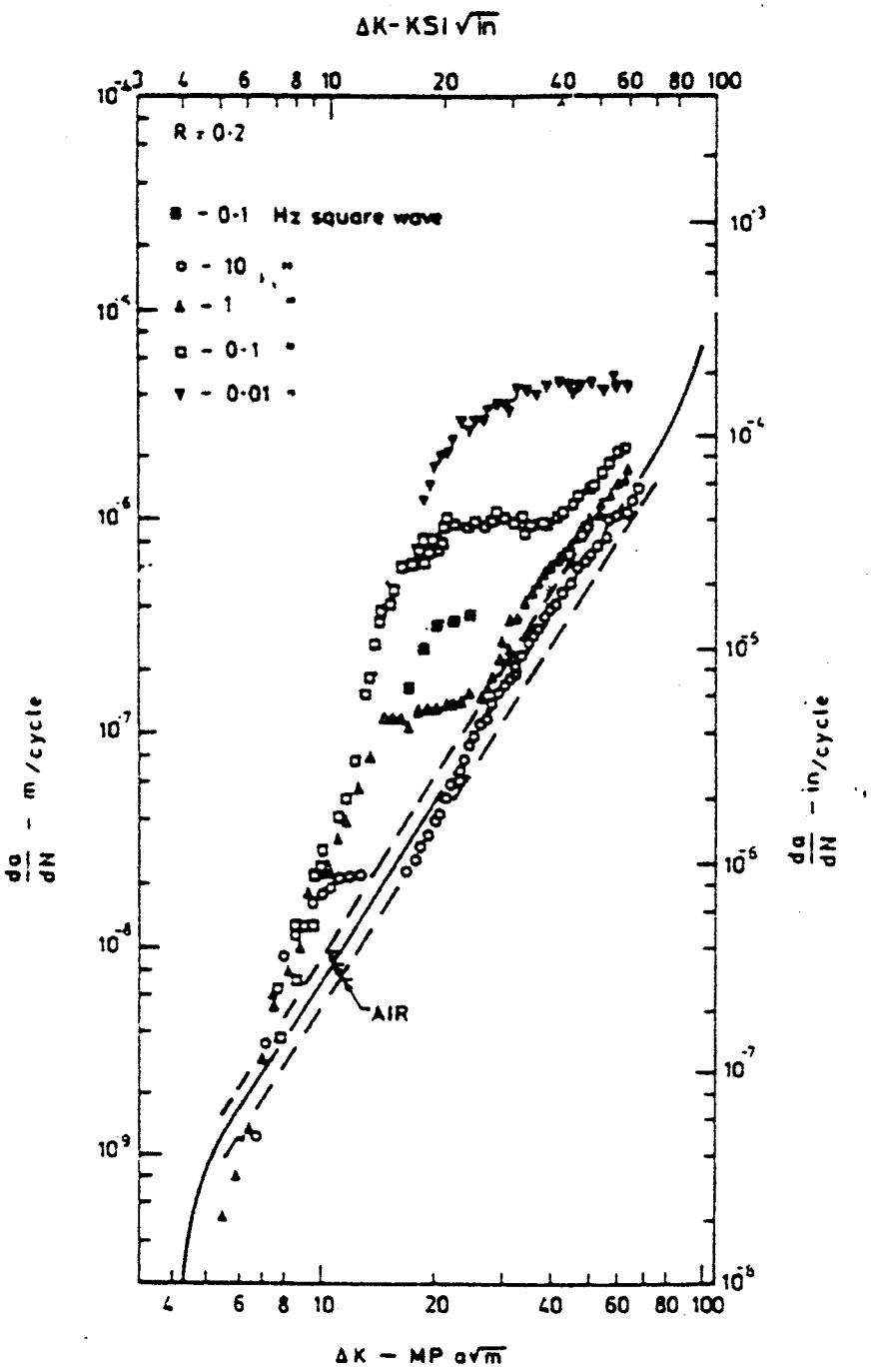

Figure 6.18b: Typical da/dN vs ΔK data for steels in sea water with cathodic protection [6.47]

Rajpathak and Hartt [6.50]

Data Type:	$\Delta K/\sqrt{\rho}$ vs N
Materials:	AC70 TMCP steel (accelerated cooled) and A537 TMCP steel (direct quenched)
Environments:	natural sea water with or without cathodic protection (-1.1V SCE)
Specimen Type:	keyhole compact tension (KCT)
Specimen Size:	B = 25.4 mm, W = 101.6 mm , keyhole radius = 3.2 mm
Specimen Orientation:	machined from 25.4 mm thick plates in L-T orientation
Definition of Failure:	initiation of 1mm long crack
Loading:	R = .5, f = 1 Hz

Steel Grade	Chemical Composition (wt. %)											YS (MPa)	UTS (MPa)
	C	Si	Mn	P	S	Cu	Ni	Cr	Mo	Nb	V		
A537-DQ	.12	.41	1.3	.014	.003	.01	.03	.04	.05		.044	500	598
AC70	09	.30	1.5	.007	.003	.18	.40			.016		503	618

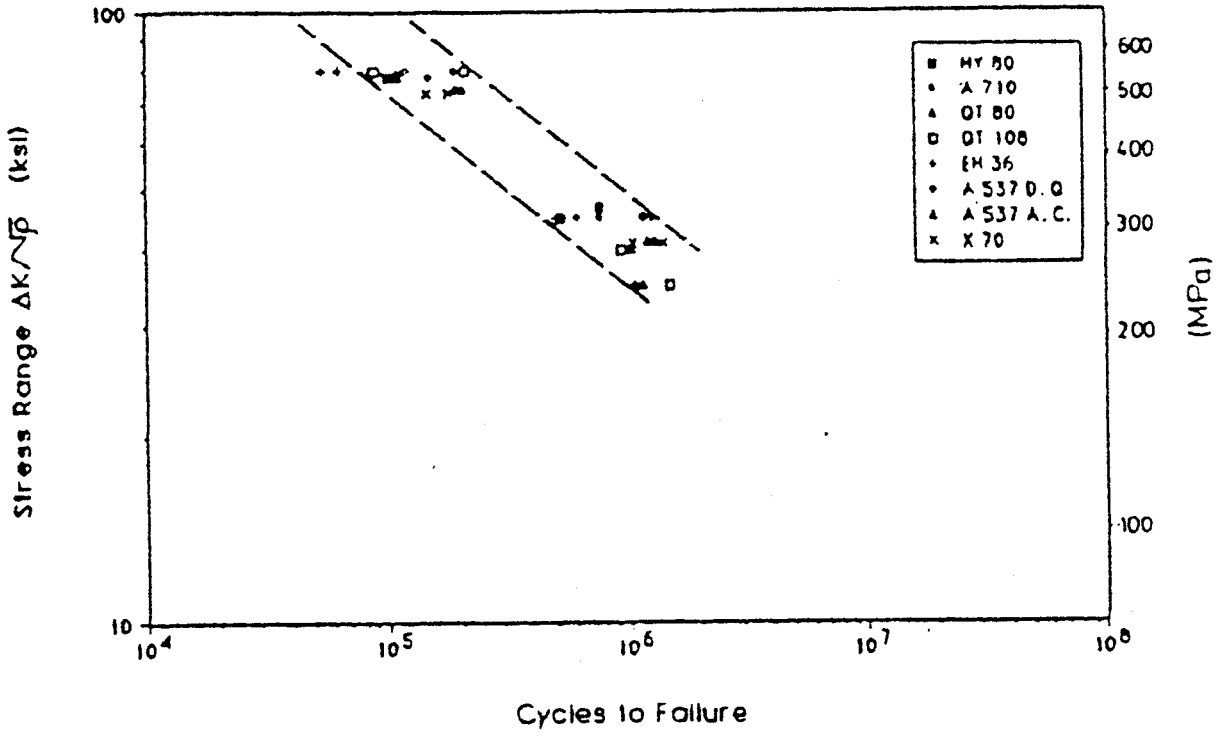

Figure 6.19a: Free corrosion data

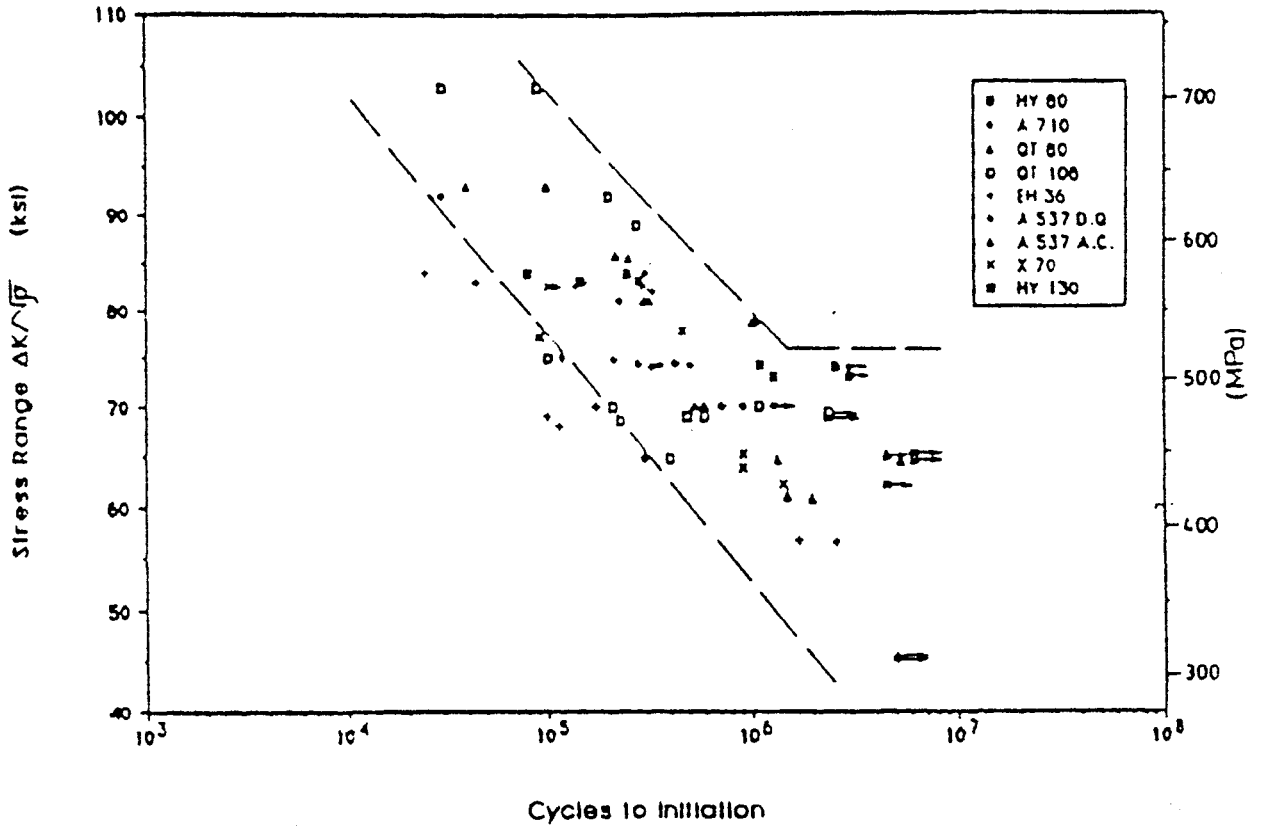

Figure 6.19b: Data for cathodically protected specimens

Matsumoto et al. [6.51]

Data Type:	S-N data for steel plates
Materials:	YS36 and YS46 TMCP steels (accelerated cooled), YS36 normalized steel, and YS70 QT steel
Environments:	air and artificial sea water without cathodic protection
Specimen Type:	cruciform joints with non-load-carrying fillet welds
Specimen Size:	30 mm thick x 100 mm wide plates
Welding Process:	SMAW
Loading:	cantilever bending, R = 0, f = .167 Hz

Steel Grade	Chemical Composition (wt. %)							YS (MPa)	UTS (MPa)	El. %
	C	Si	Mn	P	S	Nb	Cu			
YS36 -1 norm.	.15	.40	1.32	.016	.004	.026		372	523	30
YS46-TMCP	.09	.30	1.5	.007	.003	.016	.18	481	579	30
YS70-QT	.11	.25	.93	.014	.003		.22	764	813	23
YS36 -2 TMCP	.07	.26	1.32	.006	.002	.017		465	520	26

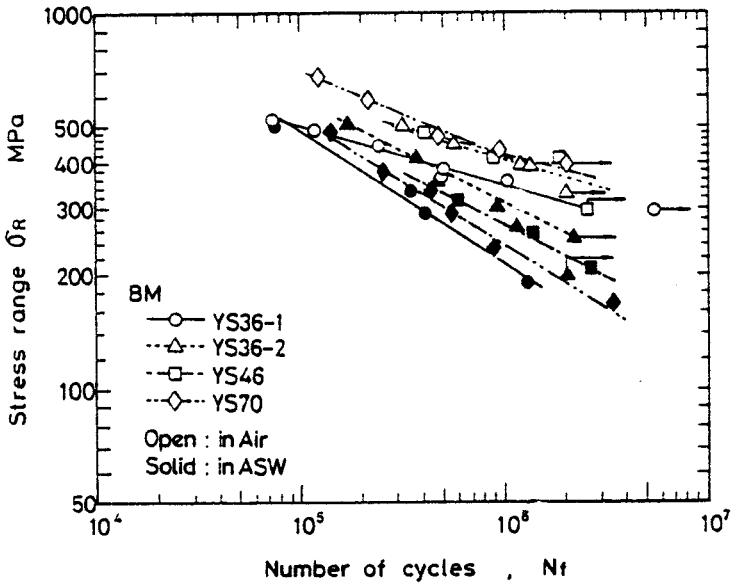

Figure 6.20

Watanabe et al. [6.53]

Data Type:	da/dN vs ΔK for long cracks
Material:	base metal , weld metal, and HAZ metal of KA36 TMCP steel
Environments:	air, sour crude oil (400 ppm H_2S)
Specimen Type:	compact tension (CT) machined from GMAW butt joints
Specimen Size:	B = 12 mm, W = 50 mm or 50.8 mm
Specimen Orientation:	not specified
Pre-cracking:	2 mm long fatigue crack at tip of starter notch in targetted region
Loading:	R = .028, f = .17 Hz (.25 Hz for some in-air tests)

Steel Grade	Chemical Composition (wt. %)					YS (MPa)	UTS (MPa)	El. %
	C	Si	Mn	P	S			
K36	.14-.15	.20-.41	1.13-1.19	.015	.005	375-426	512-555	22-26
KAS	.12-.15	.19-.20	.94-1.22	.014-.017	.005-.007	285-291	429-457	27-36

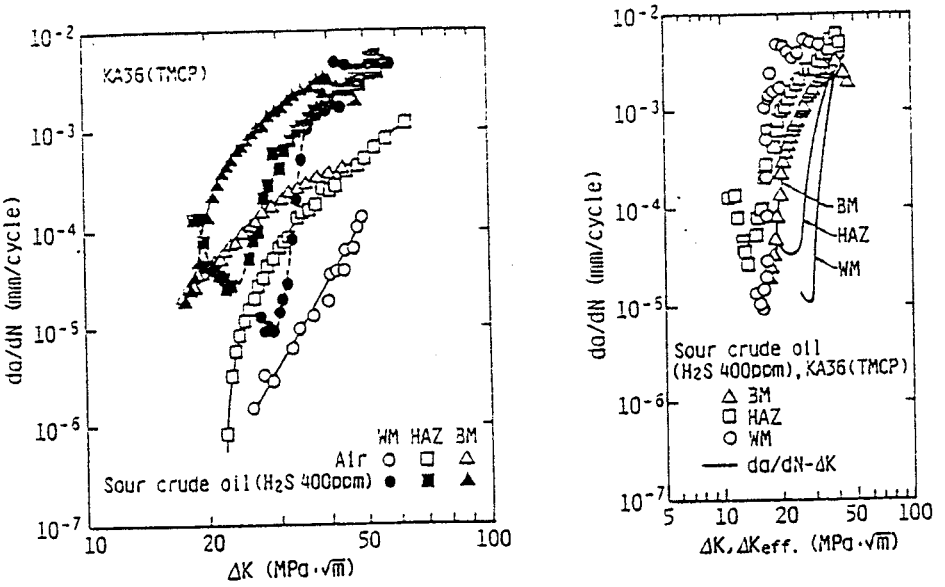

Figure 6.21

Ebara et al. [6.18]

Data Type:	S-N data
Material:	HT50 TMCP steel
Environments:	air, sour crude oil (400 ppm H_2S)
Specimen Type:	round notched bars (K_t = 4.1)
Specimen Size:	not specified
Specimen Orientation:	not specified
Loading:	axial, R = .05, f_{oil} = .17 Hz , f_{air} = .25 Hz

Steel Grade	Chemical Composition (wt. %)											YS (MPa)	UTS (MPa)	El. %
	C	Si	Mn	P	S	Cu	Ni	Cr	Nb	Al	Ti			
HT50	.14	.41	1.19	.15	.005	.01	.02	.01	.006	.034	.016	412	527	22

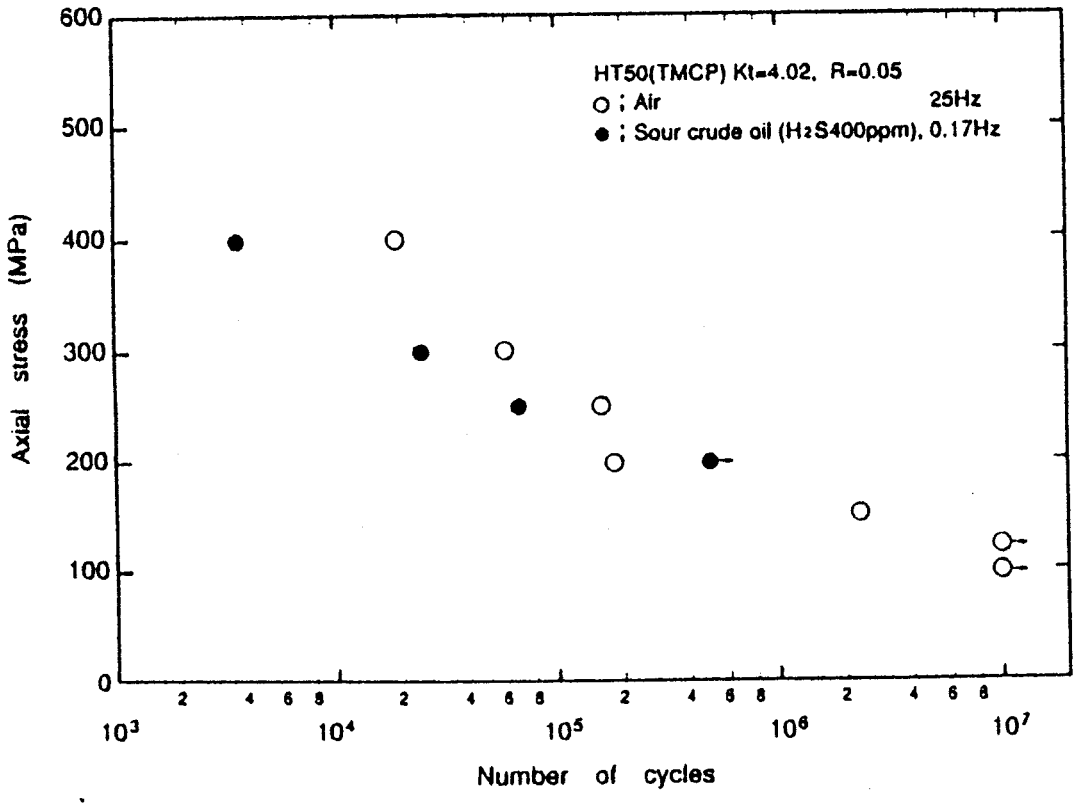

Figure 6.22

Ouchi et al. [6.19]

Data Type:	S-N data
Material:	K36A TMCP steel and KAS mild steel
Environments:	air, sour crude oil (400 ppm H_2S), hydrogen-charged electrolyte with applied potential of -1.2 V (SCE)
Specimen Type:	round notched bars (K_t = 4.02)
Specimen Size:	16 mm diameter, notch depth = 4 mm, notch radius = .24 mm
Specimen Orientation:	machined from center of 25 mm thick plates with longitudinal axis aligned with rolling direction
Loading:	axial, R = .05, f = .17 Hz

Steel Grade	Chemical Composition (wt. %)					YS (MPa)	UTS (MPa)	El. %
	C	Si	Mn	P	S			
K36	.14-.15	.20-.41	1.13-1.19	.015	.005	375-426	512-555	22-26
KAS	.12-.15	.19-.20	.94-1.22	.014-.017	.005-.007	285-291	429-457	27-36

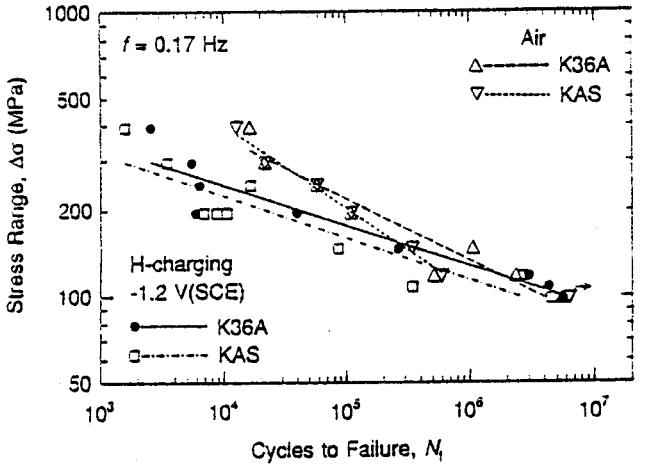

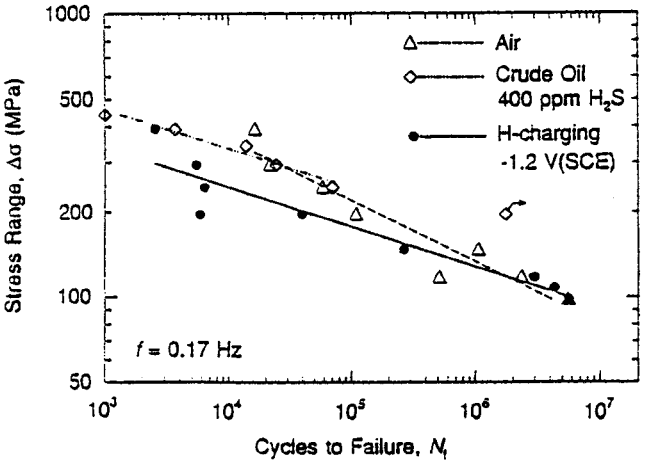

Figure 6.23

Yagi et al. [6.64]

Data Type:	S-N_f and S-N_i data for welded joints where N_f is the number of cycles to final failure and N_i is the number of cycles to initiation of 1 to 2 mm deep crack
Materials:	YP36 TMCP steel
Environment:	air
Specimen Type:	T-joints and cruciform joints with non-load-carrying fillet welds
Specimen Size:	attachment plate thickness = 10 mm, 22 mm, 40 mm, or 80 mm base plate thickness = 10 mm, 22 mm, 40 mm, or 80 mm width of T-joints = 100 mm width of cruciform joints = 80 mm
Welding Process:	SMAW
Loading:	base plates of cruciform joints loaded axially base plates of T-joints loaded in three-point bending R = 0

Thickness (MPa)	YS (MPa)	UTS (MPa)
10	402-455	500-547
22	421-466	500-571
40	392-471	459-552
80	403-449	510-560

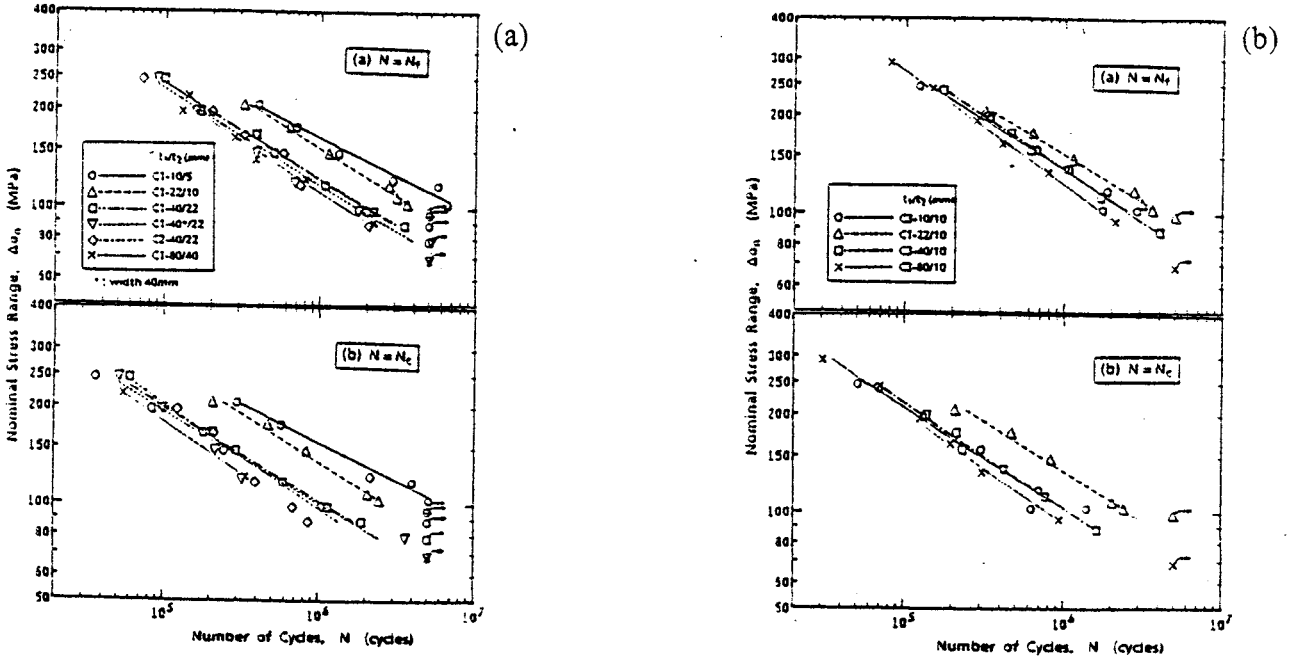

Figure 6.24: Cruciform joints: (a) with constant ratio of attachment plate thickness to plate thickness; (b) constant attachment plate thickness

NK 1988 [6.59]

Data Type:	S-N data for welded joints
Materials:	BS 4360 Grade 50E OLAC steel
Environments:	air and artificial sea water without cathodic protection
Specimen Type:	cruciform joints with non-load-carrying fillet welds
Specimen Size:	50 mm thick attachment plate, 50 mm or 100 mm thick base plate
Welding Process:	SMAW
Loading:	four-point bending, R = .1, f_{air} = 5 Hz, $f_{seawater}$ = .167 Hz

Thickness (mm)	Chemical Composition (wt. %)												YS (MPa)	UTS (MPa)	El. %
	C	Si	Mn	P	S	Cu	Ni	Cr	Nb	Ti	SAl	N			
50	.08	.30	1.55	.003	.001	.16	.23	.01		.006	.048	.003	404	479	36.9
100	.08	.15	1.55	.004	.001	.25	.44		.01	.009	.040	.004	365	478	31.6

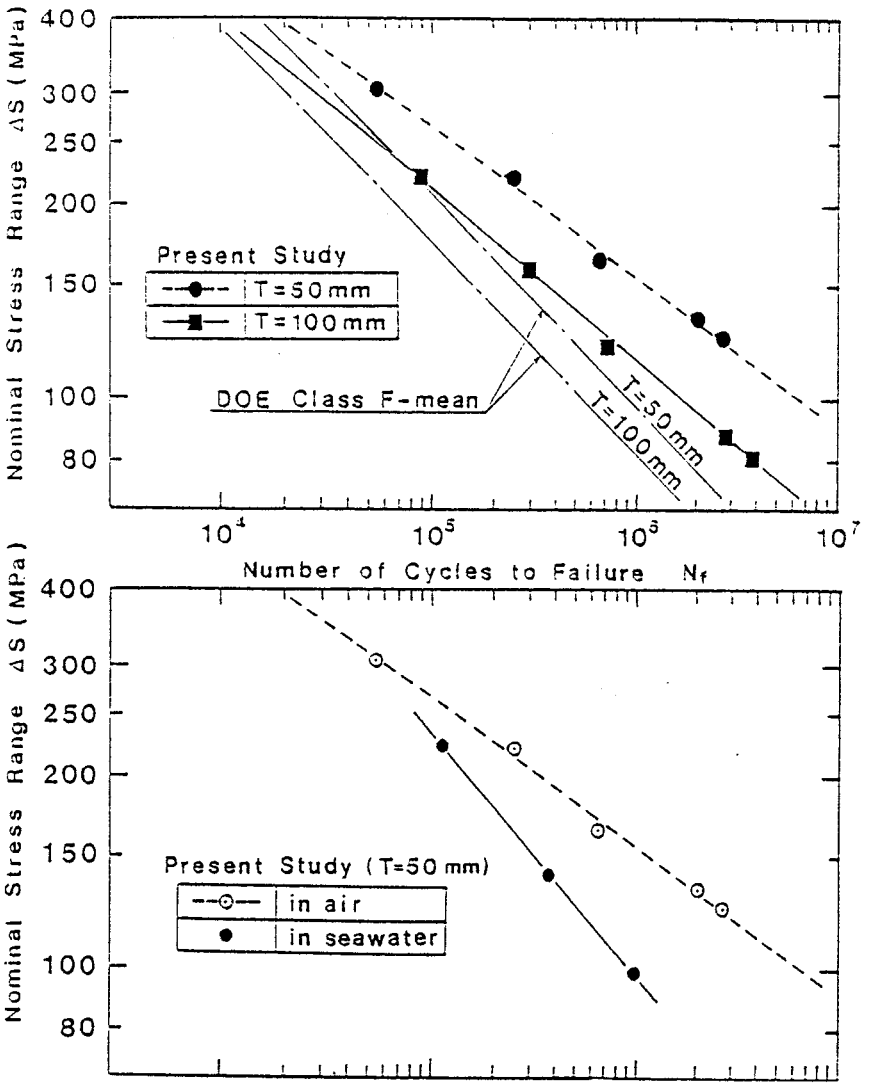

Figure 6.25

Cole et al. [6.58]

Data Type: S-N data for welded joints
Material: normalized steel, controlled rolled steel, and accelerated cooled TMCP steel
Specimen Type: Plate T-butt joints and tubular X- joints
Environment: air, sea water with cathodic protection (-.85V)
Loading: four point bending for T-joints, axial and in-plane bending for tubular joint, R=.1

STEEL	C	Mn	Si	P	S	Cr	Mo	Ni	Cu	V	Nb	Al	N	Ti	Ceq (IIW)
N.	.10	1.38	.30	.009	.007	.14	–	.38	.10	.05	.02	.025	.011	–	0.40
C.R.	.14	1.23	.26	.015	.0044	–	–	–	–	.042	.039	.031	.009	–	0.34
A.C.	.050	1.60	.228	.016	.0025	.01	–	.36	.017	.006	.024	.02	.010	.02	0.34

Composition of steels

STEEL	Y.S. (MPa)	U.T.S. (MPa)	E%	R.A.%	T.T.R.A.%	K_{VT}(-20°) (J)	K_{VT}(-40°) (J)
N.	403	547	28	64	65	200	154
C.R.	388	547	29	—	58	97	70
A.C.	450	547	25	—	—	273	265

Mechanical properties

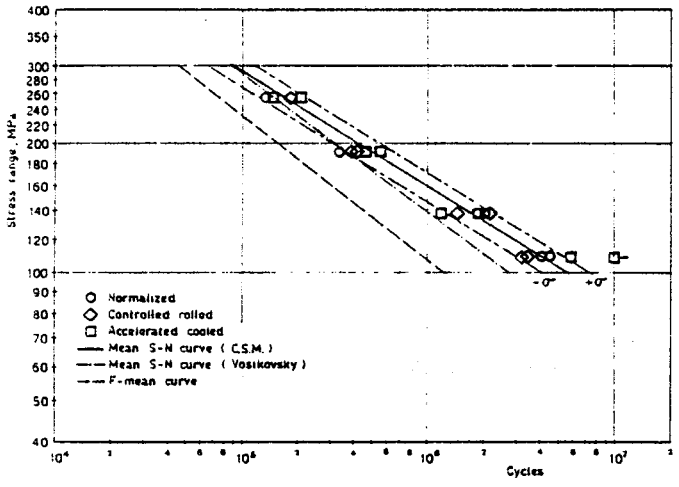

Results from T-butt tests in air

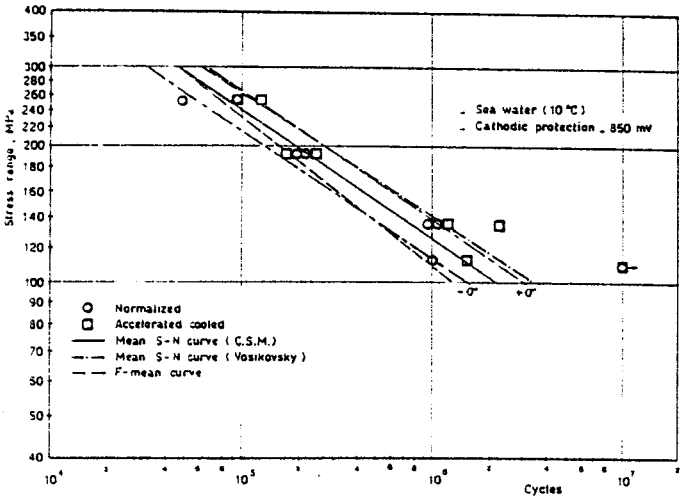

Results from T-butt tests in sea water with cathodic protection

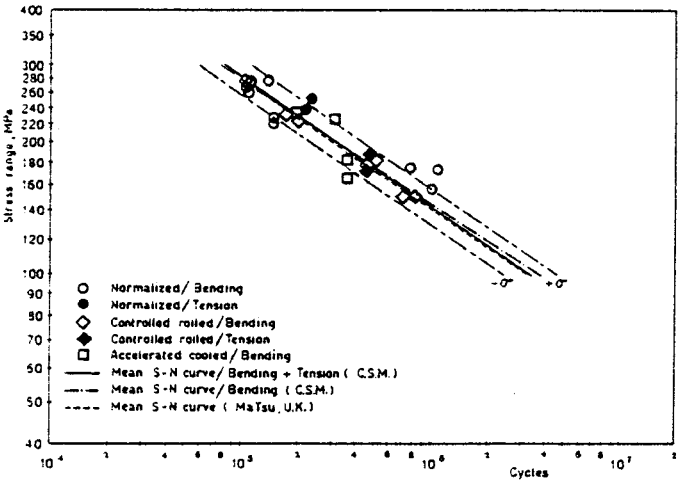

Results from X-joint tests in sea water with cathodic protection

Figure 6.26

Nakano et al. 1993

Data Type:	S-N data for welded joints
Materials:	YS36 TMCP steel (accelerated cooled) and YS36 normalized steel
Environments:	air and artificial sea water without cathodic protection
Specimen Type:	cruciform joints with non-load-carrying fillet welds
Specimen Size:	30 mm thick x 100 mm wide plates
Welding Process:	SMAW
Loading:	cantilever bending, R = 0, f = .167 Hz

Steel Grade	Chemical Composition (wt. %)							YS (MPa)	UTS (MPa)	El. %
	C	Si	Mn	P	S	Nb	Al			
YS36 normalized	.15	.40	1.32	.016	.004	.026		372	523	30
YS36 TMCP	.07	.26	1.32	.006	.002	.017	.032	465	520	26

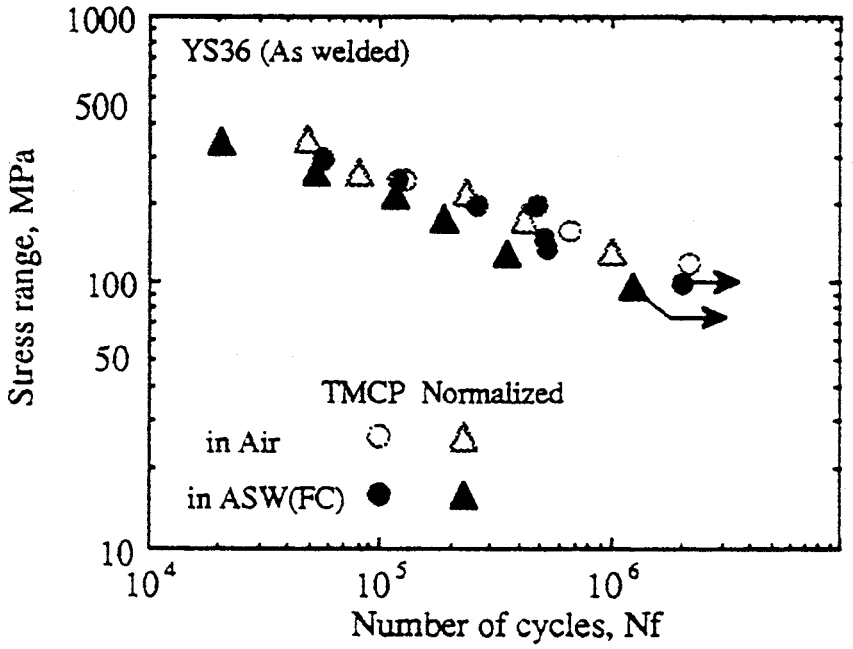

Figure 6.27

Matsumoto et al. [6.51]

Data Type:	S-N data for welded joints
Materials:	YS36 TMCP steel (accelerated cooled), YS46 TMCP steel (control rolled and accelerated cooled), YS36 normalized steel, YS70 QT steel
Environments:	artificial sea water @ 5°C with and without cathodic
Specimen Type:	cruciform joints with non-load-carrying fillet welds in as-welded, ground toe, hammer-peened, or TIG-dressed condition
Specimen Size:	plate width = 100 mm, plate thickness = 30 mm or 50 mm
Loading:	cantilever bending, R = 0, f = .167 Hz

Steel Grade	Thickness (mm)	Chemical Composition (wt. %)											
		C	Si	Mn	P	S	Cu	Ni	Nb	Cr	Mo	V	B
YS36 norm.	30	.15	.40	1.32	.016	.004			.026				
YS36 TMCP	30	.07	.26	1.32	.006	.002			.017				
YS46 TMCP	50	.09	.30	1.50	.007	.003	.18	.40	.016				
YS70 QT	30	.054	.30	1.50	.006	.003	.22	.85		.048	.42	.029	.0012

Steel Grade	Thickness (mm)	YS (MPa)	UTS (MPa)	El. %
YS36 norm.	30	372	523	30
YS36 TMCP	30	465	520	26
YS46 TMCP	50	481	579	30
YS70 QT	30	764	813	23

Figure 6.28a

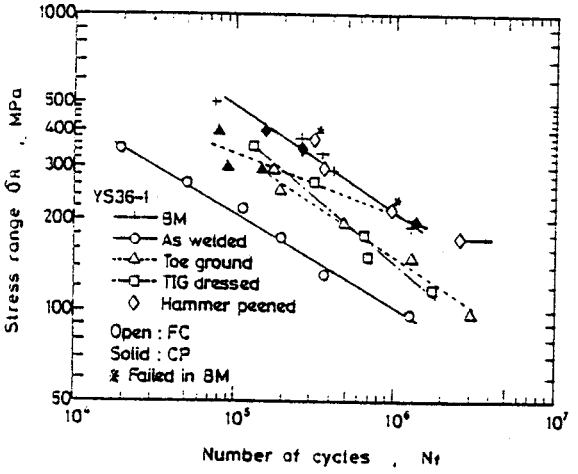

Effect of weld toe treatment on the fatigue strength of the YS36-1 steel in the artificial sea water

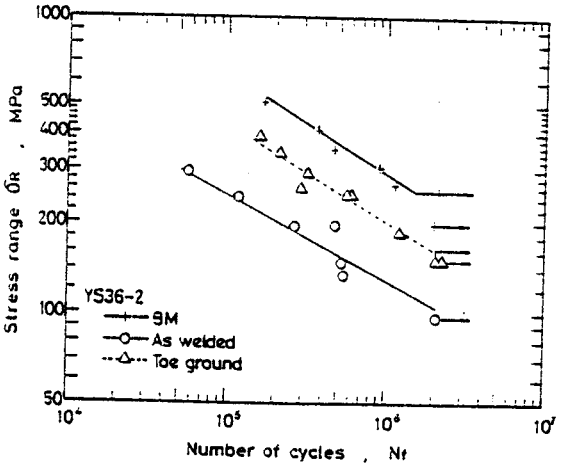

Effect of weld toe treatment on the fatigue strength of the YS36-2 steel in the artificial sea water

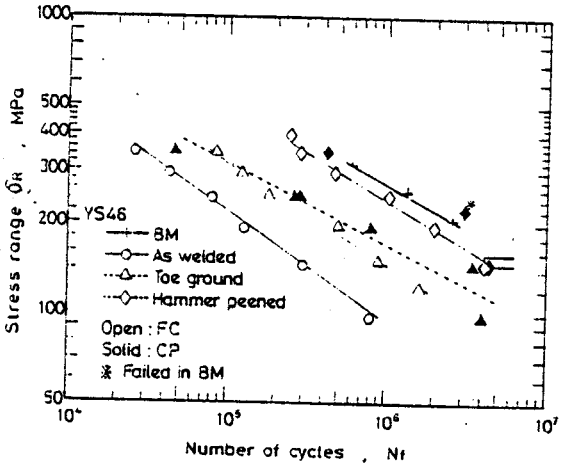

Effect of weld toe treatment on the fatigue strength of the YS46 steel in the artificial sea water

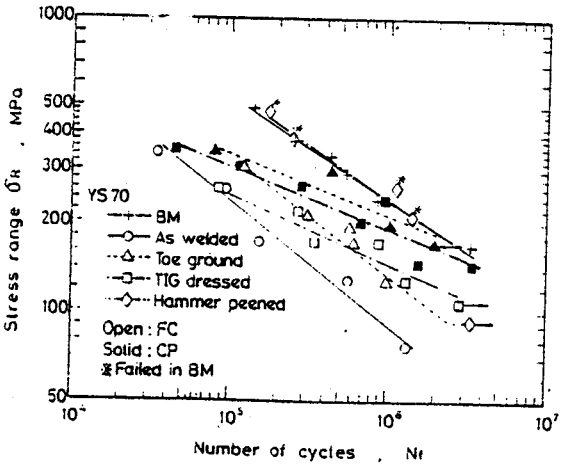

Effect of weld toe treatment on the fatigue strength of the YS70 steel in the artificial sea water

Figure 6.28b

Yajima et al. [6.61]

Data Type:	S-N data for welded joints
Environments:	air
Specimen Type A:	butt joints fabricated by GMAW from 20 mm to 40 mm thick HT50 TMCP steel plates (accelerated cooled and non-accelerated cooled)
Specimen Type B:	butt joints fabricated by SAW from 20 to 40 mm thick HT50 TMCP steel plates (accelerated cooled and non-accelerated cooled) with softened HAZ
Specimen Type C :	butt joints fabricated by SMAW from 20 or 25 mm thick conventional HT50 steel plates
Loading:	axial, R=0

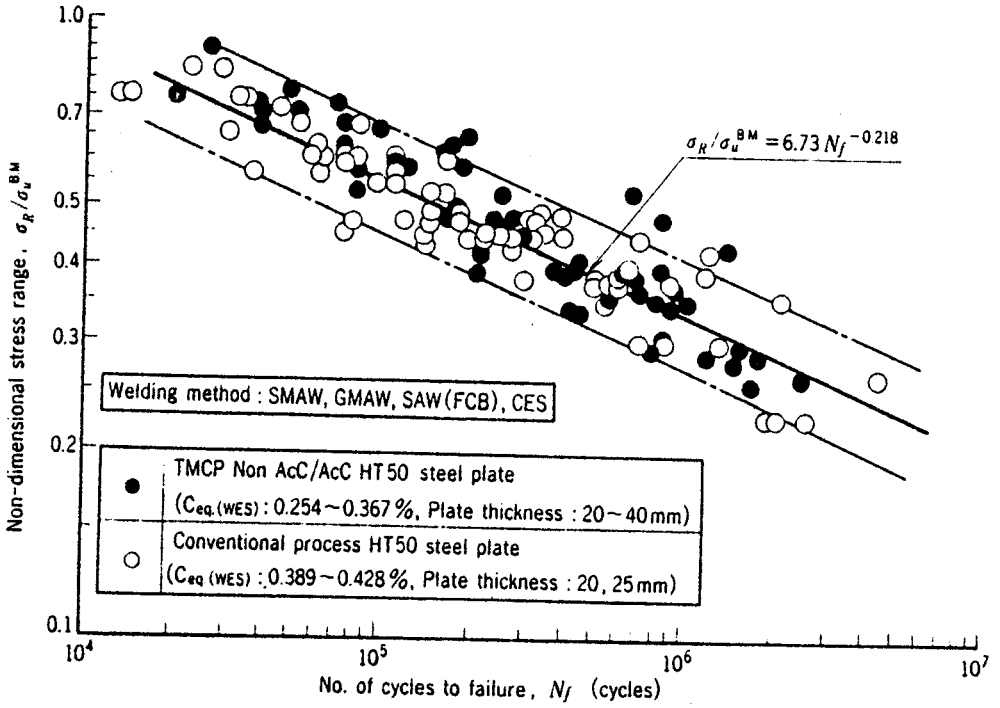

Figure 6.29

Yajima et al. [6.60]

Data Type:	S-N data for welded joints
Environments:	air
Specimen Type A:	butt joints fabricated by GMAW from 30 mm thick AH40 TMCP steel plates (accelerated cooled)
Specimen Type B:	butt joints fabricated by SAW from 30 mm thick AH40 TMCP steel plates (accelerated cooled)
Specimen Type C:	butt joints fabricated by SAW from 25 mm thick AH40 TMCP steel plates (accelerated cooled)
Loading:	axial, R = 0

Chemical Composition (wt. %)							YS	UTS	El.
C	Si	Mn	P	S	Nb	Ti	(MPa)	(MPa)	%
.10-.15	.20-.36	1.18-1.42	.011-.020	.001-.006	0-.016	0-.015	> 400	540-660	> 20

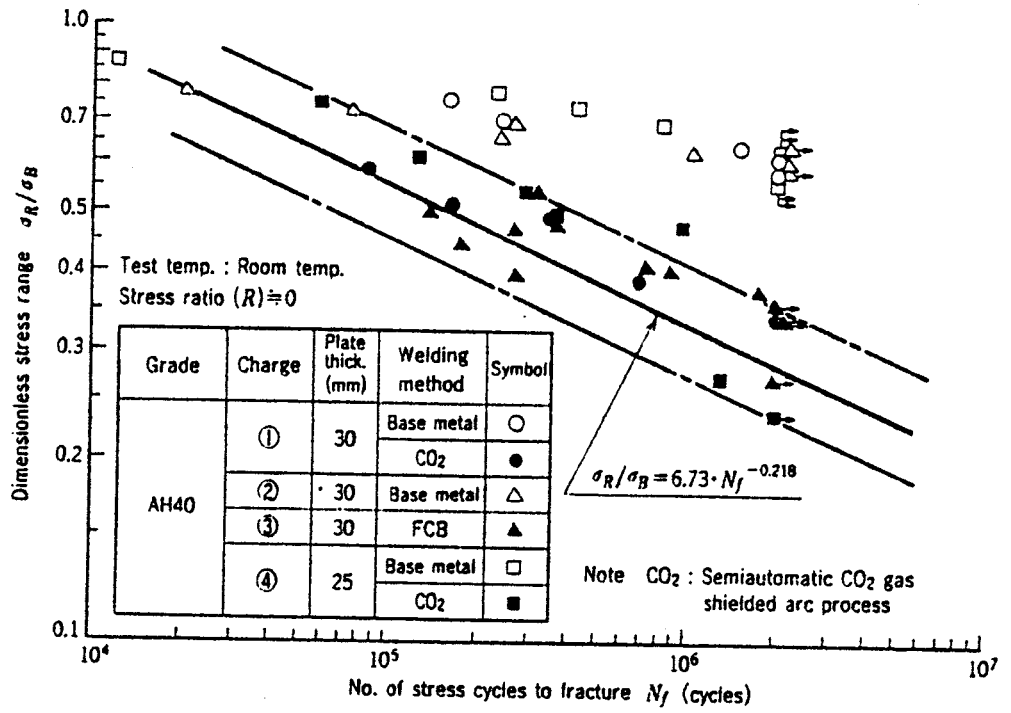

Figure 6.30

Yajima et al. [6.61]

Data Type:	S-N data for welded joints
Environments:	air
Specimen Type A:	non-load-carrying fillet welded T- joints fabricated by SAW from 25 mm thick HT50 TMCP steel plate (accelerated cooled) with weld toes in softened HAZ
Specimen Type B:	non-load-carrying fillet welded T-joints and cruciform joints fabricated by GMAW from 25 to 40 mm thick HT50 TMCP steel plates (accelerated cooled and non-accelerated cooled) with weld toes in base metal with weld toes in softened HAZ
Specimen Type C:	non-load-carrying fillet welded T-joints and cruciform joints fabricated by GMAW from 12 to 25 mm thick conventional HT50 steel plates with weld toes in base metal
Loading:	axial, R=0

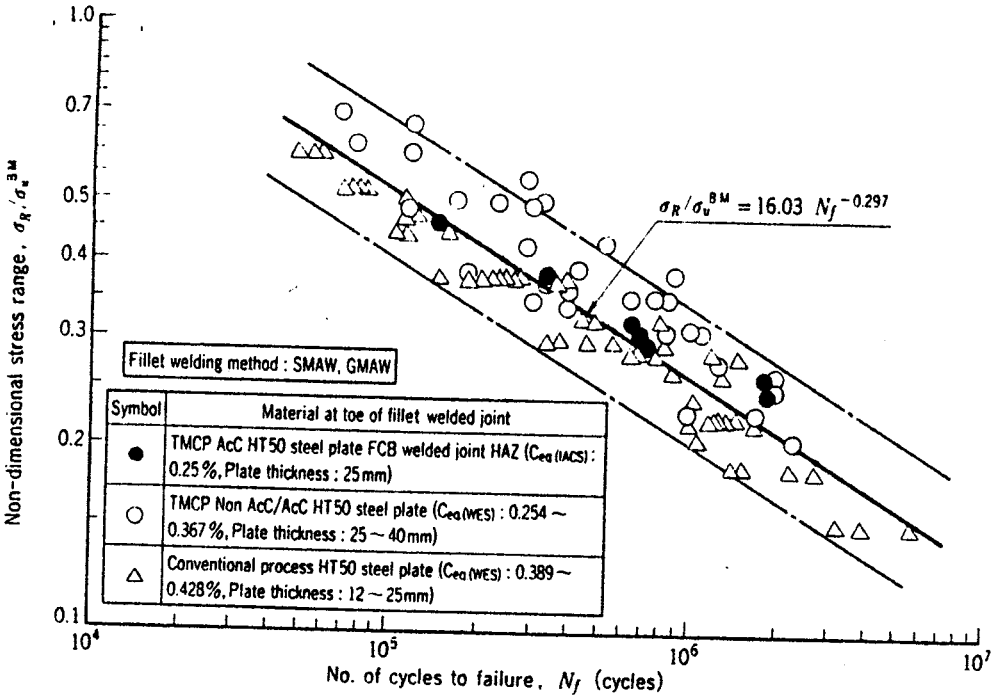

Figure 6.31

Yajima et al. [6.60]

Data Type:	S-N data for welded joints
Environments:	air
Specimen Type A:	non-load-carrying fillet welded T-joints fabricated by gravity welding process from 30 mm thick AH40 TMCP steel plates (accelerated cooled)
Specimen Type B:	non-load-carrying fillet welded T-joints fabricated by SMAW process from 30 mm thick AH40 TMCP steel plates (accelerated cooled)
Specimen Type C:	non-load-carrying fillet welded T-joints fabricated by SMAW process from 25 mm thick AH40 TMCP steel plates (accelerated cooled)
Loading:	axial, R = 0

Chemical Composition (wt. %)							YS	UTS	El.
C	Si	Mn	P	S	Nb	Ti	(MPa)	(MPa)	%
.10-.15	.20-.36	1.18-1.42	.011-.020	.001-.006	0-.016	0-.015	> 400	540-660	> 20

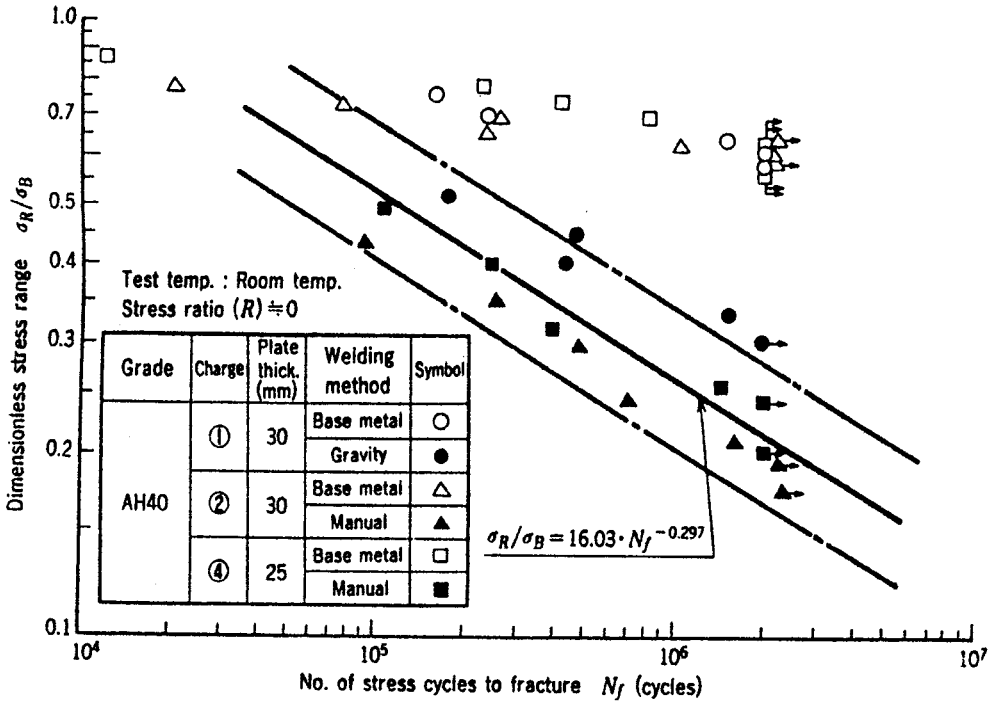

Figure 6.32

Yajima et al. [6.61]

Data Type:	da/dN vs ΔK data for long cracks
Material:	HAZ of TMCP and conventional HT50 steels
Environment:	air
Specimen Type:	plate with center notch
Specimen Orientation:	machined from SAW butt joints with weld running across the width of the specimen
Starter Notch:	centered through-thickness notch in the softened part of the HAZ
Loading:	axial, R=0

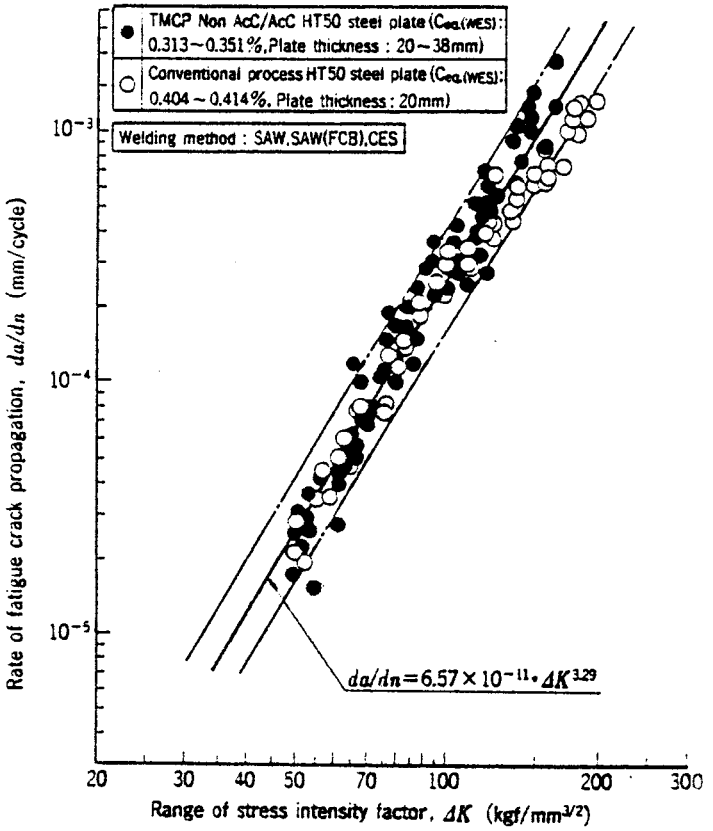

Figure 6.33

Youn and Kim [6.62]

Data Type: da/dN vs ΔK data for long cracks
Material: softened HAZ and base metal of EH36 accelerated cooled TMCP steel
Environment: air
Specimen Type: compact tension

Chemical Composition (wt.%)									
C	Si	Mn	P	S	Cu	Ni	Cr	Nb	Al
0.06	0.14	1.33	0.010	0.001	0.31	0.31	0.05	0.015	0.034

Mechanical Properties		
Yield Strength (MPa)	UTS (MPa)	Elongation (%)
477	589	27.0

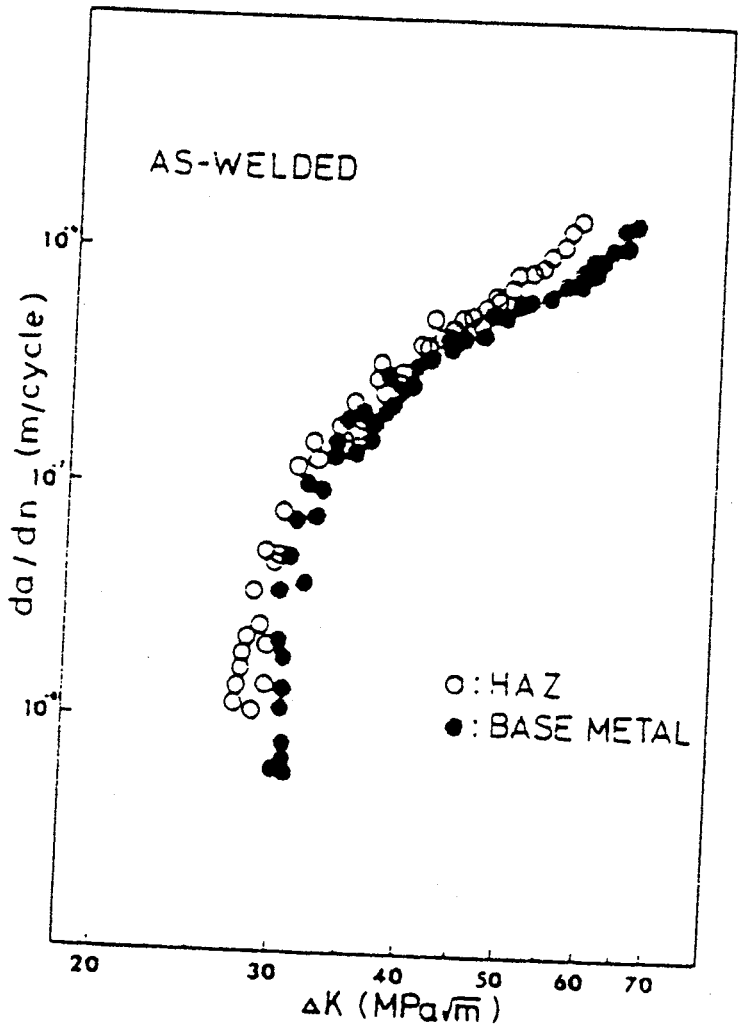

Figure 6.34

7.0 FABRICATION CONSIDERATIONS IN THE USE OF TMCP STEELS

7.1 Weldability

At the time of steel procurement, adequate weldability (resistance to hydrogen induced heat affected zone cracking) is one of the prime considerations, and it is usually specified by placing upper limits on one or both of two commonly used carbon equivalents. These equivalents are as follows:

$$CE\ (IIW) = C + Mn/6 + (Cr + Mo + V)/5 + (Ni + Cu)/15$$

$$P_{cm} = C + Si/6 + Mn/20 + Cu/20 + Ni/60 + Cr/20 + Mo/15 + V/10 + 5B$$

P_{cm} has been increasingly used in specifications, particularly for the lower carbon steels. The maximum limits placed on CE (IIW) and P_{cm} are typically 0.45 and 0.25, respectively. **Figures 7.1** and **7.2** show that a vast majority of the TMCP steels for which data has been collected, would meet this requirement, even for steels with 500 MPa SMYS.

AWS D1.1 Structural Welding Code provides guidelines on selecting preheat requirements based on the carbon equivalent P_{cm} and the hydrogen potential of the welding consumable. These two factors determine the susceptibility Index, and an index of "B" permits low restraint joints to be welded in any thickness without preheat. Susceptibility Index B is maintained when weld metal hydrogen content is low and the steel P_{cm} is ≤ 0.23. As seen from Figure 7.1 and 7.2, a P_{cm} less than 0.23 can be readily achieved in TMCP steels..

7.2 Fabrication Concerns

Softening in the Heat Affected Zone

As mentioned earlier, the TMCP steels rely upon fine grain size, precipitation hardening and possibly substructure strengthening for their strength. Such microstructures are thermally unstable and as a result the thermal cycles associated with welding can lead to decrease in strength of the heat affected zone. Past research [7.1, 7.2] has shown that depending on the steel chemistry and processing, maximum softening is expected in the intercritical or the subcritical heat affected zone. The magnitude of decrease in yield or tensile strength at any location is, however, hard to measure or predict since the heat affected zones are relatively narrow, weld thermal gradients are rather steep and one must deal with the cumulative effect of multipass weld thermal cycles. Predictive equations proposed by Kluken [7.3] and Liu [7.4] are not directly relevant since these focus on the properties of the coarse grain heat affected zone, next to the fusion boundary.

Since several of the documents reviewed in the present study provided hardness traverses across the heat affected zones, an attempt was made to relate the minimum HAZ hardness, reduction in hardness with respect to the base metal and the width of softened HAZ to weld heat input and base metal composition (carbon equivalent), however, no meaningful relationship could be developed.

The other assessment approach used in this context was to plot the ratio of the cross weld tensile strength to the average base metal tensile strength as a function of weld heat input. The data base covers steels with up to 600 MPa actual tensile strength. As seen in **Figure 7.3**, with increasing heat input, the likelihood of cross weld tensile strength meeting or exceeding the base metal strength decreases. The local tensile strength of the softened heat affected zone determined is generally lower than that inferred from Figure 7.3. Presumably, there is some constraint effect from the stronger weld metal and the shoulders of the relatively small gauge length cross weld tensile specimens, so that the strength reduction in these tests is limited to about 5%.

In wider structural welds, the joint tensile strength can apparently be still higher. Japanese research [7.5] has demonstrated this as seen in **Figure 7.4** which shows that although the HAZ tensile strength based on small round specimens is rather low (about 470 MPa) for the high heat input welds employed (>13.8 kJ/mm), the cross weld tensile strength is about 480 MPa for small specimens and about 515 MPa for 400 mm wide specimens, compared to 530 MPa for the base metal. The research document goes on to show the actual HAZ tensile strength and relative width of the softened HAZ as a function of the steel composition (**Figures 7.5** and **7.6**) for very high heat input welds in 355 MPa SMYS steels.

From the fracture point of view, Inoue et al [7.6] and de Lede et al [7.2] have tested wide plate specimens, and concluded that softened zones are not a concern in the respective steels examined. Inoue and Hagiwara [7.6] conducted wide plate tests, with and without a stress concentrator in the form of load transmitted through a plate welded at right angles to the wide plate. The softened HAZ was produced in the wide plate by welding a TMCP steel (510 MPa yield, 570 MPa ultimate tensile strength) at a heat input of 5 kJ/mm and the results were compared with those from specimens fabricated from a normalized steel which in fact exhibited some HAZ hardening instead of softening. Based on the results, the authors concluded that the overall strain in the wide plate tests depended on the fracture toughness of the softened zone rather than the degree of softening.

In de Lede's study [7.2], the steel examined had yield and ultimate tensile strengths of 470 and 580 MPa., respectively. For the weld made at 4.46 kJ/mm heat input, the softened heat affected zone fracture toughness transition behavior was similar to that of the base metal and superior to that of the coarse grain heat affected zone, next to the fusion boundary. In the double edge notched, wide plate tests too, the specimens notched in the softened HAZ performed as well as the base metal and superior to the coarse grain heat affected zone.

Earlier in Section 4.3, it was concluded that some degradation in toughness at the FL5/SCHAZ location does occur, and then the actual behavior would depend on the relative locations of the softened and toughness degraded areas, and the extent of toughness degradation. No studies could be found in literature that examined the fracture behaviour of HAZ that has suffered lowering of local strength and toughness. The importance of this particular aspect depends on the likelihood of finding flaws in such a region.

Line Heating and Flame Straightening Effects

Line heating and flame straightening are commonly used in shipyards to introduce desired curvature in the steel plates and for correcting distortion in the welded assembly and structure. These techniques apply heat to one surface of the steel plate and then rely upon through thickness temperature gradients to introduce the desired deformations. However, there has been a concern that procedures applicable to conventional hot rolled and normalized steels may not be applicable to TMCP steels as there is potential for microstructure changes, especially grain growth, leading to degradation of mechanical properties. Keeping the temperatures below about 600°C, as has been occasionally suggested, would limit the degree of bending/straightening that could be achieved in practice.

This issue has been studied by a Research Committee of the Shipbuilding Research Association of Japan [7.7] which made the following recommendations regarding the line heating practice appropriate to TMCP steels:

SMYS ≤ 355 MPa and CVN toughness requirement at -20°C or a higher test temperature:
Heat to 1000°C, followed by air or water cooling; 3 cycles maximum.

SMYS ≤ 355 MPa and CVN toughness requirement at -40°C :
Heat to 900°C followed by air or water cooling; 2 cycles maximum.

Some of the data which formed the basis of these recommendations is given in the **Table 7.1** [7.7] and shows that the average increase in transition temperature with the optimum procedure (900°C followed by air or water cooling) is about 17 to 18°C although in individual cases, it might approach 45°C.

Data (**Figure 7.7**) also shows that applying the same guidelines to 400 MPa minimum specified yield strength steels [7.8] leads to a similar increase in transition temperature (about 15°C for the EH grade of steel). From the point of view of maintaining the tensile strength above the design minimum, however, it is recommended to water cool after line heating in the case of steels with lean compositions. Conversely, if the steel carbon equivalent is relatively high, it may be prudent to air cool after line heating in order to prevent excessive hardening of the surface layers.

Table 7.1: Change in CVN transition temperature due to line heating thermal cycles

Line Heating Cycle	Change in Transition Temp., °C	Min. Kc (MPa.√m) at 0°C
1000°C, water cool	0 to +32; avg. 16	236 for DH grade of steel
1000°C, air cool	-8 to +31; avg. 9	233 for DH grade of steel
950°C, water cool	+7 to 45; avg. 26	237 for AH grade of steel
950°C air cool, 650°C water cool	+6	
900°C, water cool	-9 to +45; avg. 17	291 for EH grade of steel
900°C air cool, 850/800°C water cool	+8 to 45; avg. 31	263 for EH grade of steel
900°C air cool, 750/700°C water cool	+24 to 45; avg. 30	255 for EH grade of steel
900°C air cool, 650/600°C water cool	+15 to 45; avg. 30	260 for EH grade of steel
900°C air cool	-3 to +39; avg. 18	342 for EH grade of steel
850°C water cool	+9C	
700°C, water cool	16 to 27; avg. 21	

More recently, data has been reported by Nippon Steel Corporation [7.9] and Dillinger Hutte [7.10, 7.11] on the effect of line heating/flame straightening on their respective 355 MPa steels. The Nippon data shows that indeed beyond 900°C, there is a steep decline in the steel toughness (**Figure 7.8**). When the maximum temperature is kept below 900°C, the increase in transition temperature is of the order of 20°C.

The study from Dillinger by Hanus is a more detailed one and it examines the effect of flame straightening on the strength and toughness properties of 355 MPa yield strength in two different thicknesses (non-accelerated cooled 15 mm and accelerated cooled 50 mm). Line heating simulations (furnace heat treatments, heat to peak temp in 60 s, hold for 60 s, cool so that $t_{8/5}$ = 20s) carried out by the author show that once the lower critical temperature is exceeded, there is potential for drop in yield strength (**Table 7.2**), especially when three cycles are employed and the peak temperature is below the upper critical temperature, A_{c3}. The maximum drop in yield strength under these conditions was observed to be 39 MPa, however, the minimum requirement was still met. Similarly, the 50 J transition temp increases by as much as 41°C, however, the initial transition temperature is sufficiently low so that typical requirement of 50 J at -60°C is still met.

Table 7.2: Mechanical properties of 385 MPa yield strength TMCP Steel. Ref. [7.11] after simulated heat treatment (thermal conditions, 60S heating, 60S holding at T_{max}, cooling according to $t_{8/5}$ 20S) for 15 mm test plate material

Temperature O°C	Cycles	Hardness HV10	Yield Strength MPa	Tensile Strength MPa	Impact Trans Temperature 50J	100J
750	1	166	427	534	-88	-75
750	3	163	393	533	-92	-75
850	1	161	397	550	-105	-100
850	3	163	377	548	-82	-76
950	1	169	432	533	-76	-72
950	3	167	401	523	-85	-80
base material		165	416	537	-117	-108

In actual line heating trials, Hanus changed the flame travel speed such that the 2 mm subsurface temperatures reached would have been 650 to 950°C (based on prior trial instrumented tests). The surface temperatures would have been 100 to 150°C higher. The plates were allowed to cool freely in air or water cooled once the temperature had fallen down to 600°C. The tensile properties were assessed using 3 mm thick surface specimens as well as full thickness specimens. Based on results shown in **Figures 7.9** and **7.10,** it seems that the surface layer, if anything, increases in yield and tensile strength and it is in the subsurface region that some softening occurs (drop in yield strength only), especially when the aimed subsurface temperature was 850°C for the 15 mm plate. The 50 J transition temperature also increases (**Table7.3**), the maximum changes corresponding to a peak temperature of 850°C followed by water cooling for the 15 mm plate (about 22°C), and 750°C peak temperature followed by free cooling for the 50 mm plate (about 11°C).

In summary, the available evidence indicates that TMCP steel plates with up to 400 MPa minimum specified yield strength can be formed by line heating and flame straightened, keeping in mind that: (i) the maximum surface temperature must not exceed 900°C; (ii) the optimum cooling after heating may depend on the steel composition; (iii) some degradation in steel toughness can be expected, however, the initial toughness is usually far superior to the minimum requirements so that even after the degradation, the minimum requirements are easily met. For ship applications, therefore, it will be desirable to obtain optimum line heating guidelines and procedures from the steel manufacturer at the time of purchasing the steel.

Table 7.3: Influence of different line heating conditions on the impact transition temperatures of 15 mm and 50 mm thick plates

Tmax (°C)	Cooling	Cycles	15mm Plate		50mm Plate	
			TT50J	TT100J	TT50J	TT100J
650	free	1	-114	-110	-90	-80
750	free	1	-115	-106	-79	-65
850	free	1	-113	-100	-85	-76
950	free	1	-118	-112	-86	-78
850	water	1	-98	-94	-80	-68
950	water	1	-99	-95	-81	-72
850	free	3	-116	-110	-94	-86
850	water	3	-92	-95	-112	-99

7.3 Other Applications of TMCP Steels

The data presentation and discussion in the previous sections have been in the context of ship structures, and references have been made to offshore structural application where appropriate. Two of the main advantages in the use of TMCP steels in place of the conventional normalized steel are their higher strength (up to 500 MPa), and improved weldability as indicated by susceptibility to hydrogen cold cracking and broader weld heat input range over which the specified heat affected zone toughness could be met (see **Figure 7.11**, adapted from Ref [7.12]).

In practical terms, these advantages can be reflected in cost savings due to:

(i) in a lighter structure requiring reduced welding, especially when buckling and fatigue are not critical considerations;
(ii) reduction, if not elimination of preheat, leading to reduced repairs, delays and documentation costs;
(iii) greater in-service reliability due to better base metal and heat affected zone toughness.

Due to these potential advantages, TMCP steels have been considered for bridges buildings and construction machinery applications. Some specific instances of cost savings attributed to the use of TMCP steels are as follows:

- It has been estimated that for an offshore structure requiring 17,000 tons of steel, a saving of $1.4 million was realized by virtue of not having to preheat the TMCP steel procured for the project [7.13].

- Savings of $200,000. were realized by substituting 3000 tons of greater than 25 mm thick normalized steel requiring preheat by TMCP steel in a 13,000 ton steel bridge. The increased cost of the steel was $134,000. In addition, the fabrication time was reduced by about three weeks [7.12].

- For offshore structures, the use of higher strength, weldable steels can frequently reduce the thickness sufficiently so that postweld heat treatment is no longer necessary, and it is estimated that accompanying cost saving are of the order of $125 per meter of weld length.

- With frequent specification for hydrogen induced cracking (HIC) resistance in sour environment, line pipe with greater than 550 MPa yield strength is difficult to produce economically without the accelerated cooling technology.

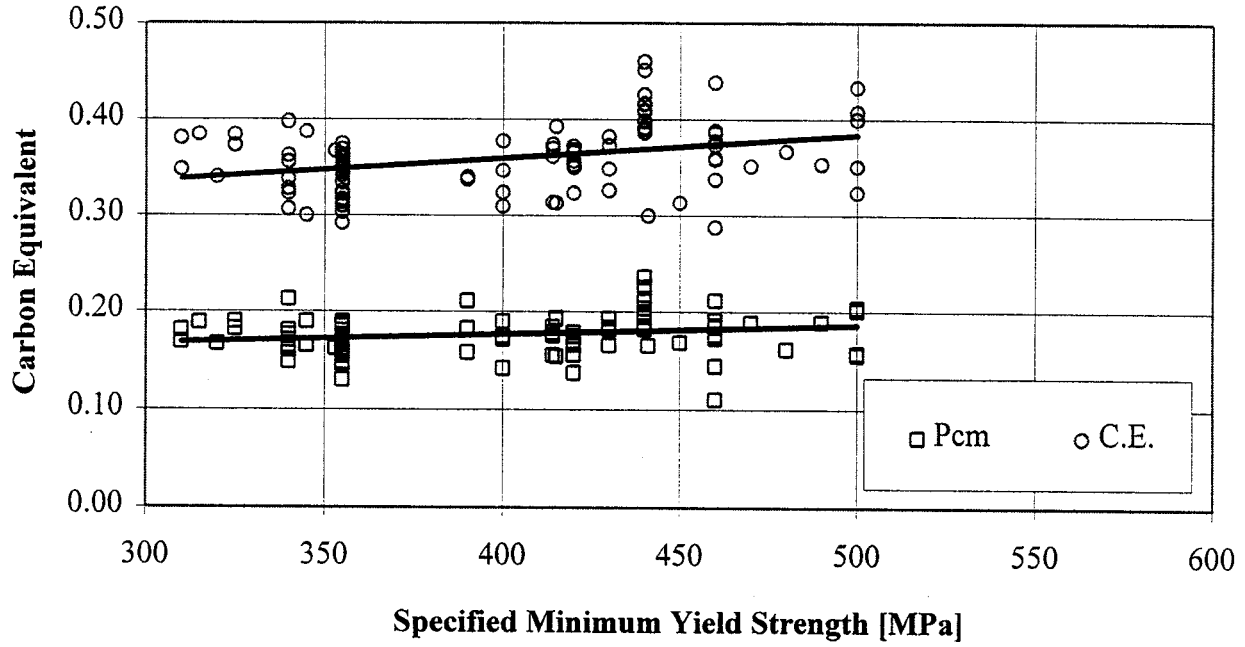

Figure 7.1: **CE (IIW) and P_{cm} for TMCP steels plotted against the specified minimum yield strength**

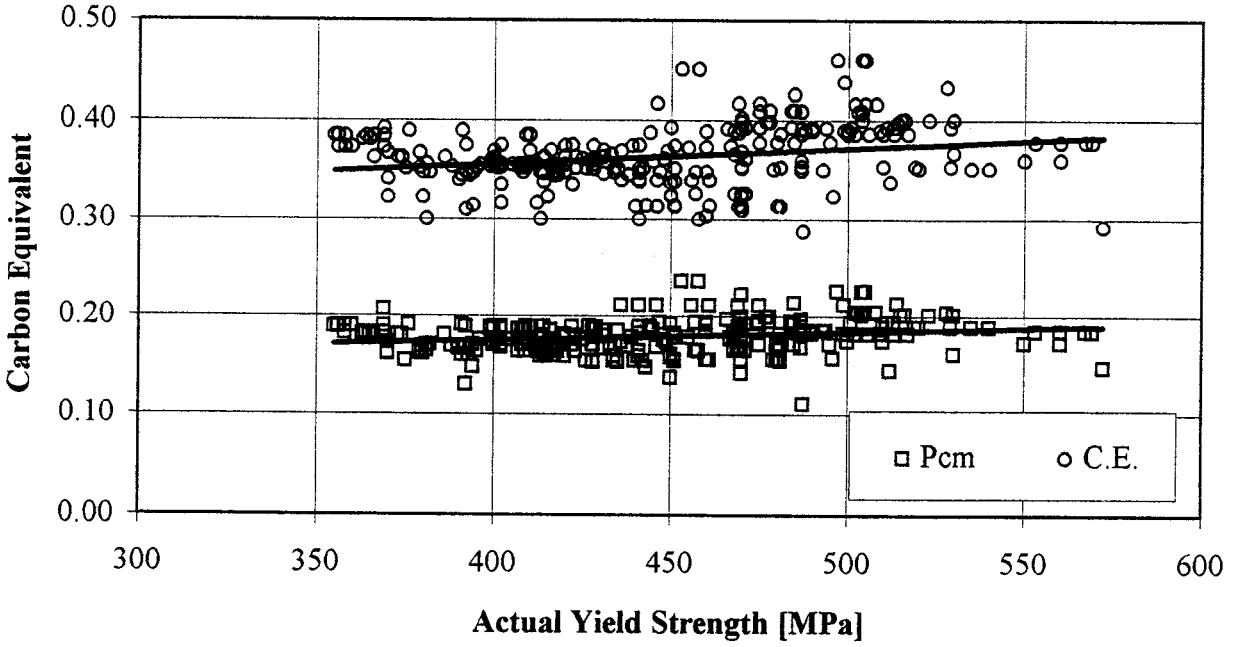

Figure 7.2: **CE (IIW) and P_{cm} for TMCP steels plotted against their actual yield strength**

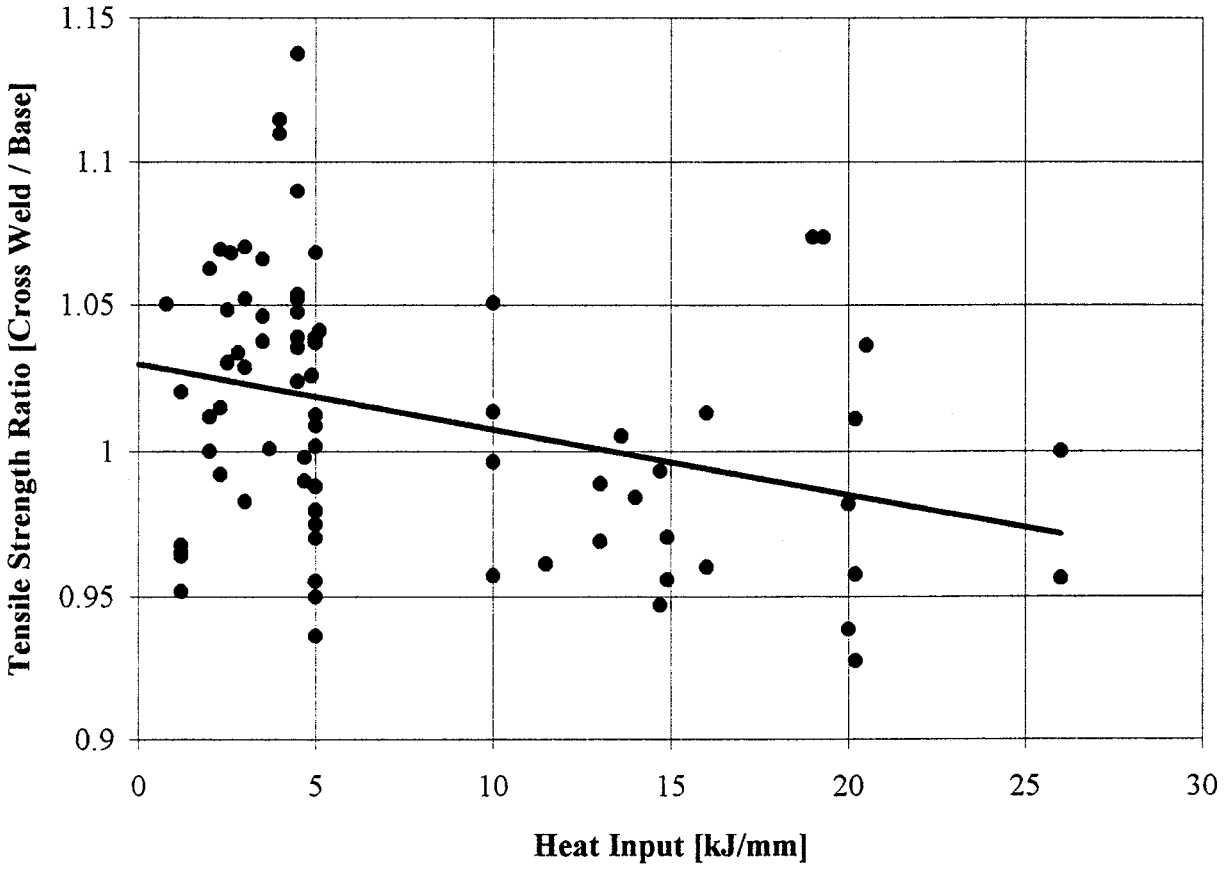

Figure 7.3: Ratio of tensile strengths determined in cross-weld and base metal tensile tests plotted against the weld heat input

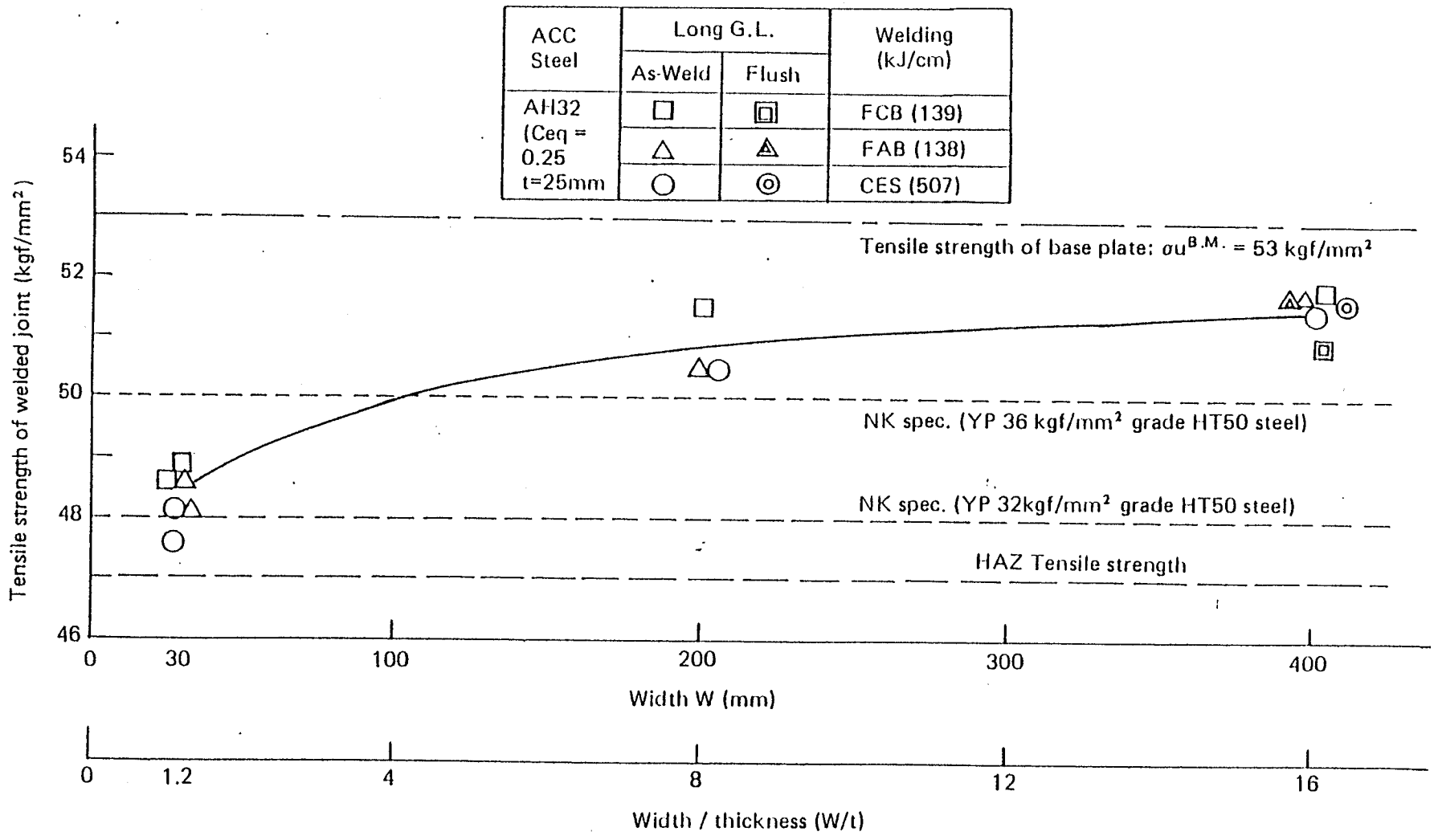

Figure 7.4: Effect of specimen width on tensile strength of welded joint. Ref. [7.6]

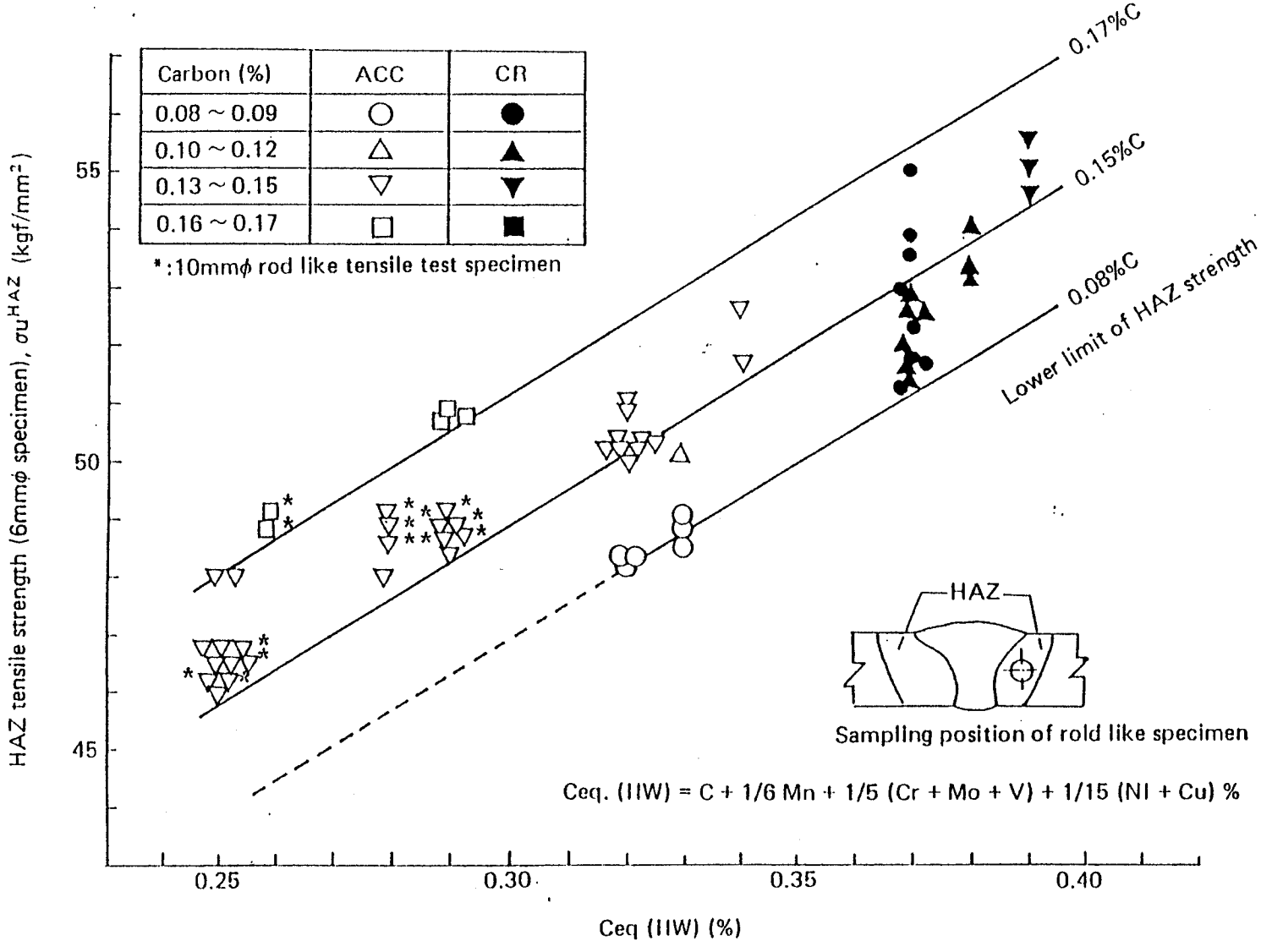

Figure 7.5: Relationship between HAZ tensile strength and carbon equivalent (Ceq). Ref. [7.6]

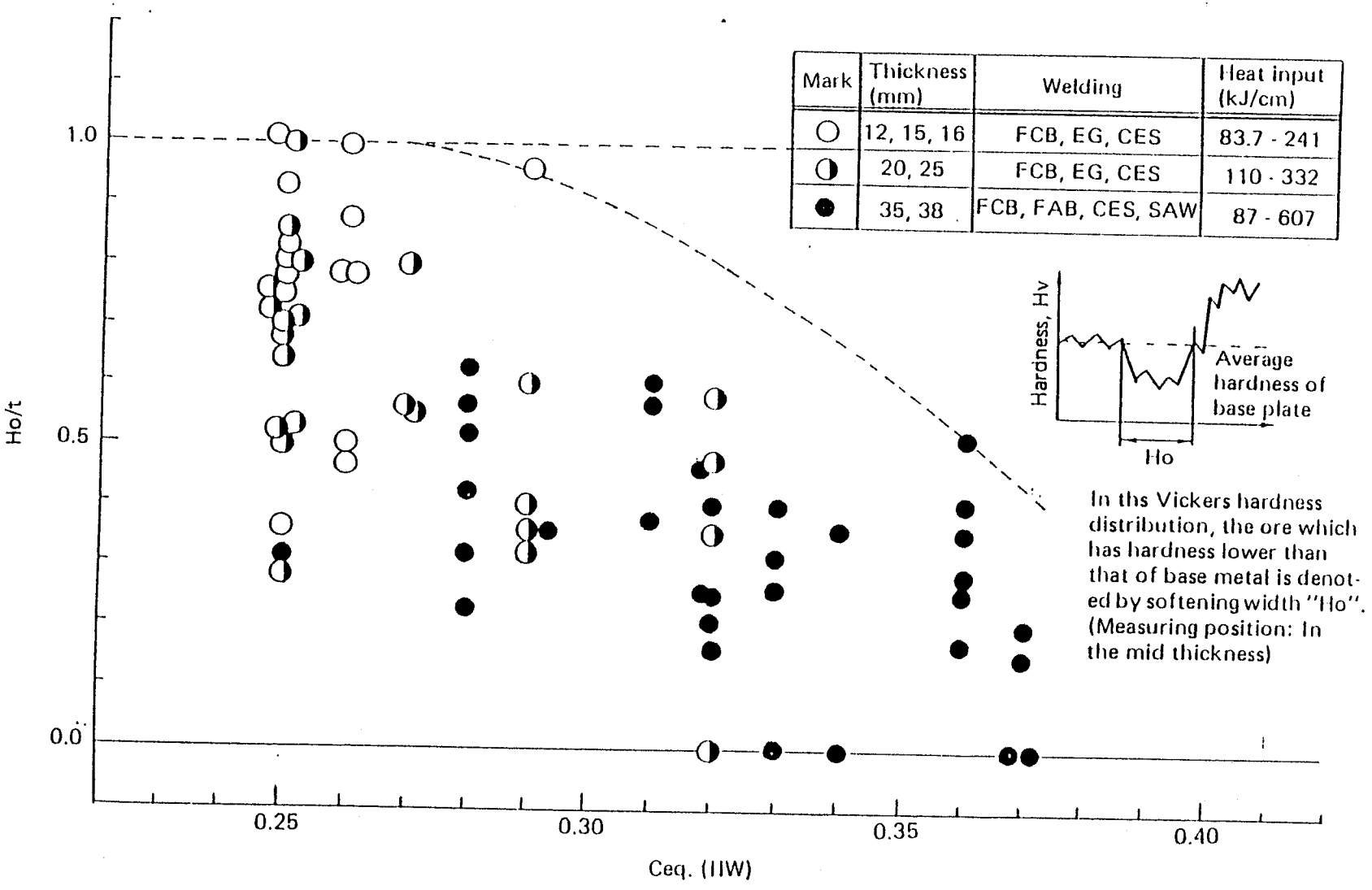

Figure 7.6: Relationship between Ho/t and Ceq (Ref. [7.6])

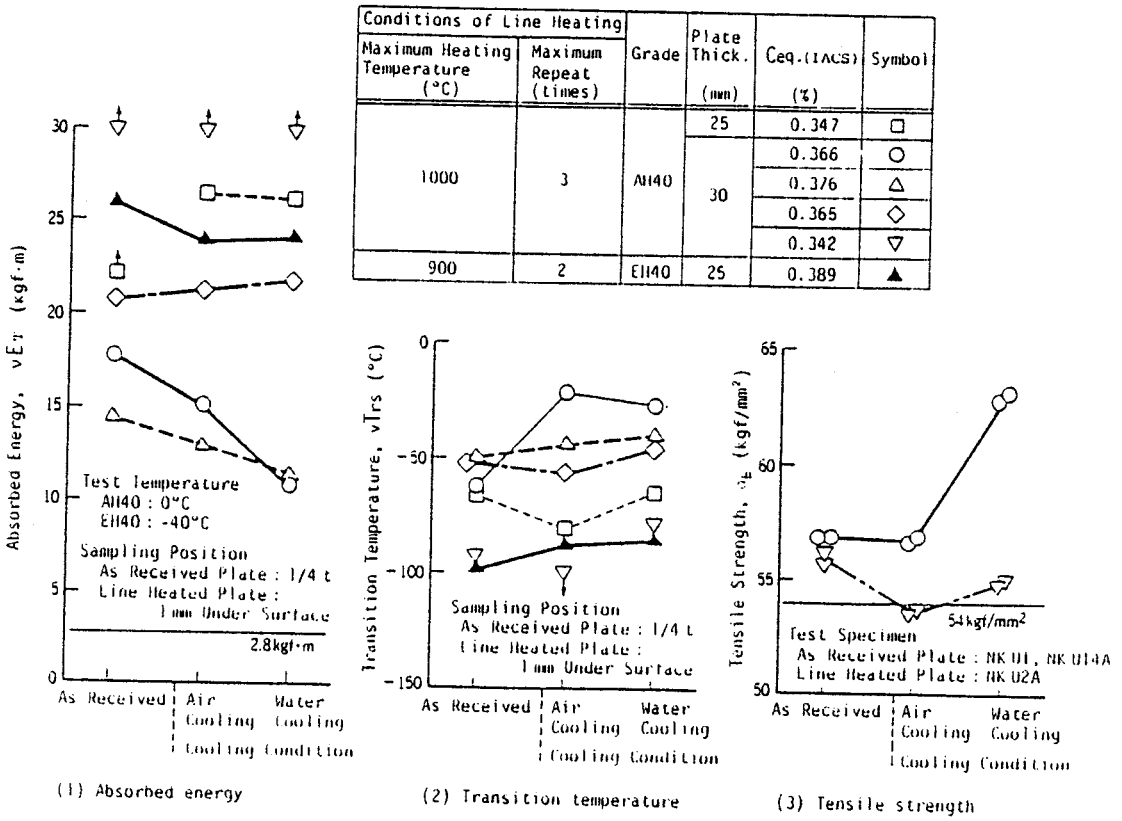

Figure 7.7: Mechanical properties of plates after line-heating (transverse direction). Ref. [7.9]

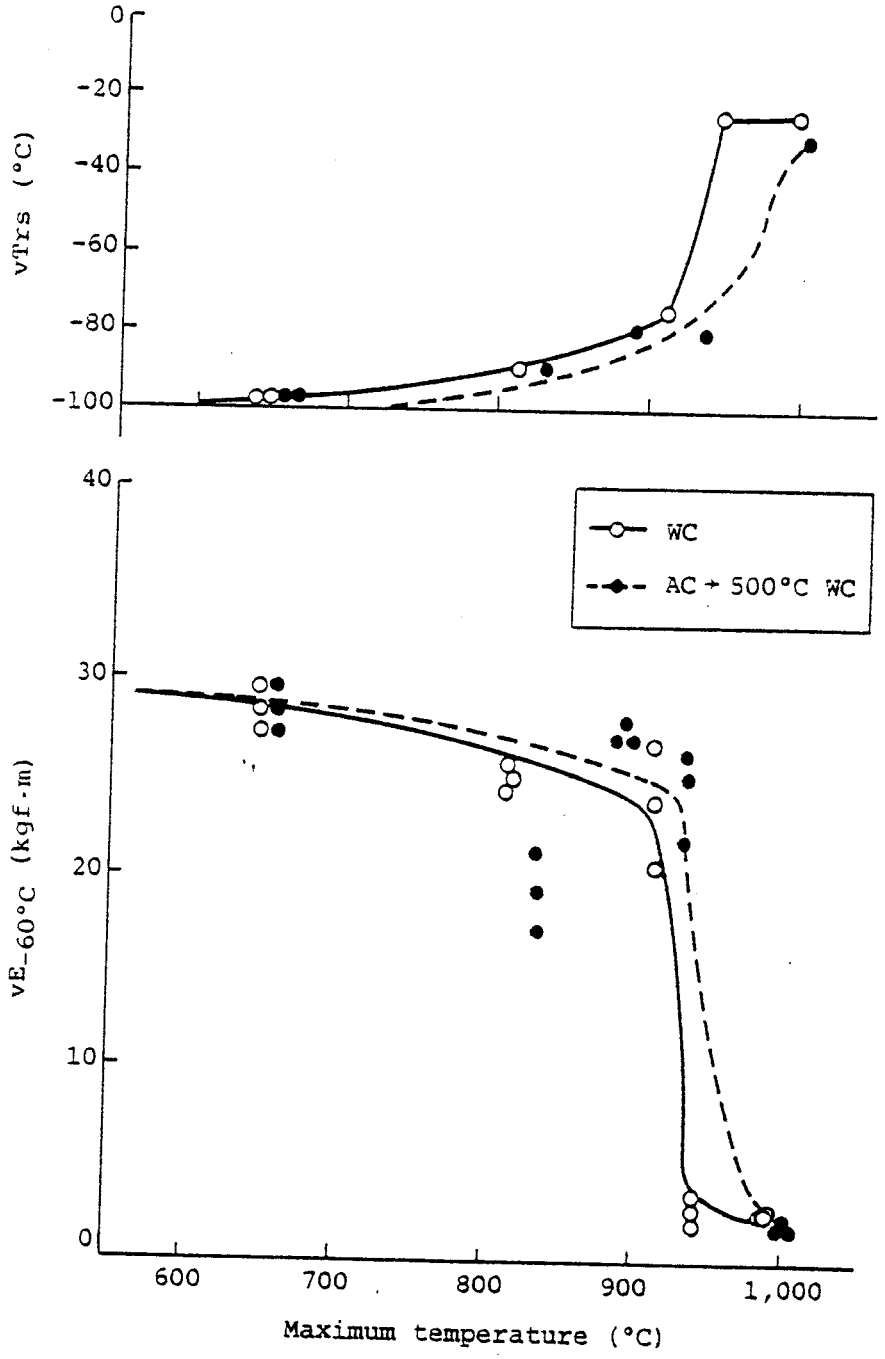

Figure 7.8: **CVN toughness of a 40 mm thick TMCP steel as a function of peak temperature during flame straightening Ref. [7.10]**

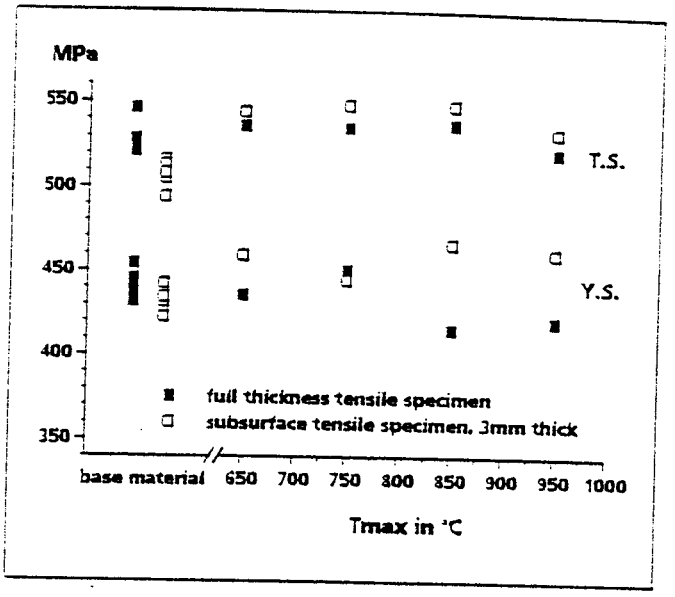

Figure 7.9: Tensile properties of line heated 15 mm thick panels

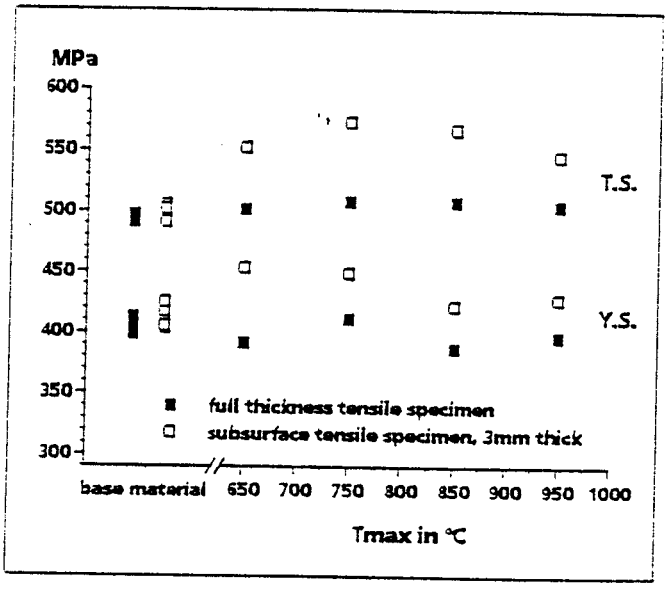

Figure 7.10: Tensile properties of line heated 50 mm thick panels

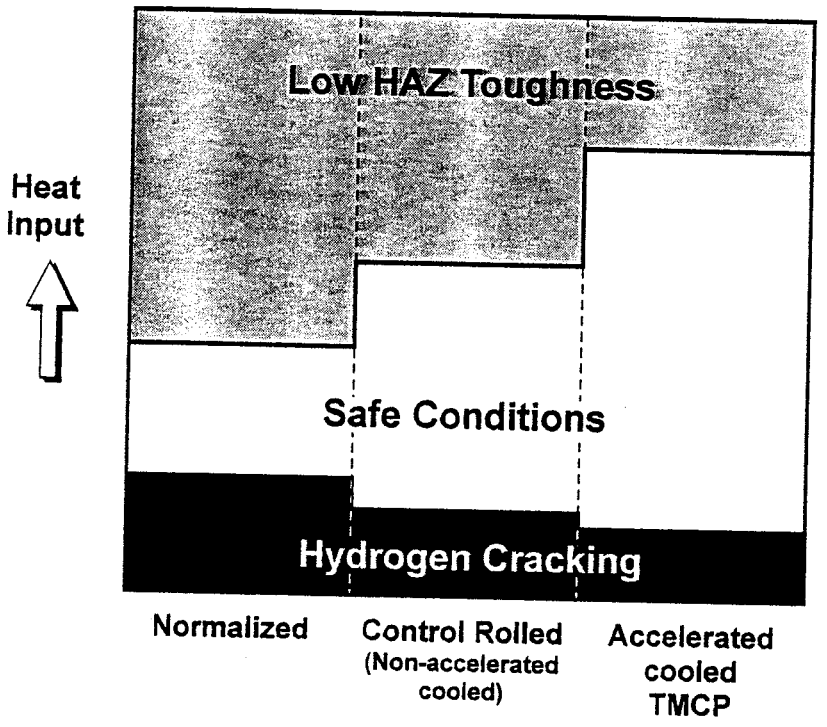

Figure 7.11: Improved weldability of accelerated cooled TMCP steels

8.0 SUMMARY AND RECOMMENDATIONS FOR FURTHER WORK

A data base of mechanical properties relevant for ship design has been compiled for welded TMCP (**accelerated cooled**) steels. The mechanical properties considered include tensile properties, base metal and heat affected zone toughness, and fatigue crack initiation and propagation characteristics. The data has been analyzed to examine if certain type of mechanical property data is lacking, if any changes in material specifications are warranted and if ship designers can take advantage of some of their unique properties, mainly excellent base metal and heat affected zone toughness, and their ability to be welded without preheat for a large number of applications besides those in ships. In addition, weld metal toughness data for welding consumables that can be used in conjunction with TMCP steels have been collected and the fabrication characteristics of these steels have also been reviewed.

Static Strength Properties

The available data indicates that TMCP steels are available in thickness up to 50 mm at the 500 MPa minimum specified yield strength level while maintaining excellent weldability and ductility as measured by uniform elongation in a tensile test. For lower yield strength steels, the maximum thicknesses available are much larger.

The compiled strength data suggests that for TMCP steels, the yield strength is higher in the transverse direction than in the longitudinal. For specification and qualification purposes, it is preferable, therefore, to assess tensile properties based on longitudinal specimens.

The work hardening behaviour of TMCP steels which influences the fracture behaviour in the presence of flaws and which can be important for structures designed using plastic design based procedures, is however not well characterized. Using the Ludwik model, the relatively large uniform elongations observed in tensile tests do not seem consistent with the yield to ultimate tensile strength ratio of these steels. **Further experimental work to investigate the work hardening behaviour of TMCP steels is therefore warranted.**

The steel property of most concern to a naval architect or structural designer is the specified minimum yield strength. In this regard, there is no particular advantage or disadvantage of accelerated cooled TMCP steels as compared with other types of steels (i.e., hot rolled, control rolled, normalized, quenched or tempered). Whatever the selected minimum yield strength in light of weight requirements, the supplied steel is likely to comfortably meet it. However, the plate to plate variation in yield strength of TMCP steels is likely to be less than that for hot rolled or normalized steels. Also, while the yield to ultimate tensile strength ratio for TMCP steels seems to be slightly higher than that for other types of steel, sample calculations suggest that the higher strength TMCP steels can be utilized in design while retaining acceptable structural reliability against tensile plastic collapse.

The allowable yield strength stipulated in various Classification Society rules for ship design is less than the specified minimum yield strength by a factor called the high tensile steel factor (HTSF). Following the existing approach for steels up to 390 MPa yield strength, HTSF values are proposed for steels with yield strengths in the range 420 to 500 MPa. These, of course, are equally valid for high strength steels produced by processes other than the accelerated cooled TMCP approach.

Base Metal Toughness

The base metal toughness is most commonly measured and specified using the Charpy Vee Notch test and the data base compiled indicates that virtually all TMCP steels meet a transition temperature requirement (corresponding to 50% FATT, or 35 to 50 J absorbed energy) at -60°C for specimens extracted from the quarter thickness location. There can be, however, a through thickness heterogeneity in the CVN toughness with the transition temperature being higher by as much as 35°C at the half thickness location, compared with that at the quarter thickness location.

The base metal toughness can also be assessed using Pellini's drop weight test to determine the nil-ductility transition temperature. Performed customarily on specimens that include one original surface of the steel plate, a vast majority of the TMCP steels tested to date have their NDT temperature at or below -60°C.

Examination of the empirical relationships between CVN properties and NDT temperature on the one hand, and steel fracture toughness as assessed by elevated loading rate CTOD tests and crack arrest tests, indicates that NDT temperature provides a better indication of the steel's fracture toughness than does the CVN transition temperature.

It is recommended, therefore, that the primary toughness requirement for Grade F steels in the Classification Society rules (and other specifications for similar steels) should be changed from a CVN transition temperature of -60°C maximum (at subsurface or quarter thickness location) to an NDT temperature of -60°C maximum. A CVN transition temperature of -60°C, however, should still be required for specimens extracted from the half thickness location to limit toughness variation with thickness and to guard against potentially harmful centreline segregation.

According to the reported data, several of the TMCP steels have NDT temperature of -80°C or below. **Therefore, if a specification were to be written for steel with toughness that is superior to that of Grade F (a Grade G?), then it is suggested that the primary toughness requirement should be an NDT temperature of -80°C.**

From the design point of view, the use of the TMCP steels (all strength levels) meeting the above toughness levels (NDTT = -60°C to -80°C) will minimize the potential for brittle fracture propagation in the base metal, depending on the design temperature (usually between 0°C and -45°C). The TMCP steels could be used effectively in locations that are hard to inspect since the tolerable flaw size will likely be governed by plastic collapse considerations which, in turn, are likely to be sufficiently large so as to be easily detected.

The above conclusion is based on NDT temperature-crack arrest toughness correlations derived from a relatively limited data base. **It is suggested, therefore, that further experimental work should be undertaken to assess the short crack arrest toughness and crack size tolerance of the TMCP steels with reference to the steel's NDT temperature.**

Also, based on experience with conventional steels, the NDT temperature is believed to be insensitive to the specimen orientation with respect to rolling direction. However, in one of the publications in the technical literature, there was a significant difference between the NDT temperatures for the two orientations. **It is suggested, therefore, that a small study to assess the effect of specimen orientation on the NDT temperature should be undertaken.**

The excellent base metal toughness of accelerated cooled TMCP steels documented in this report stems from their other underlying characteristics, viz., the use of clean steel technology to make the steel, lower carbon and alloy content (lower carbon equivalent) for any given strength level (see Figure 1.4) compared to hot rolled, normalized and control rolled steels, and finally, its fine microstructure obtained by controlled rolling and accelerated cooling. Thus, Figure 4.32 showed the superior crack arrest toughness of accelerated cooled steels compared to conventional steels, and Figure 4.15 demonstrates that TMCP steels with drop weight nil-ductility transition temperature as low as -80°C can be procured. The significance of procuring steels with such low nil-ductility transition temperatures can be judged from the observation that at NDTT +40°C, the steel's crack arrest toughness is typically 186 MPa$\sqrt{m}$, a level that Japanese investigators have found to be adequate to prevent brittle fracture propagation in ships. Clearly, brittle fracture is unlikely to occur in such steels at a design temperature of 0°C, and perhaps not even at temperatures down to -40°C.

It is also worth noting that the carbon equivalent of accelerated cooled TMCP steels does not increase significantly with increases in yield strength (see Figures 7.1 and 7.2) so that TMCP steels with specified minimum yield strengths up to 500 MPa retain excellent weldability (greater resistance to hydrogen induced cold cracking in the heat affected zone). This, in turn, reduces fabrication costs (lower preheat requirements) and enhances structural integrity by virtue of reduced repairs/undetected flaws remaining in the structure.

Heat Affected Zone Toughness

The clean steel technology and steel's lower carbon content mentioned previously are also instrumental in achieving improved heat affected zone fracture toughness in accelerated cooled TMCP steels. Conversely, when the heat affected zone toughness requirements are not very demanding, the TMCP steels may be welded using higher weld heat inputs, once again reducing fabrication costs (see Figure 7.11).

The heat affected zone toughness requirements for welds in ships, normally specified in terms of the CVN transition temperature, tend to be less demanding than those for the base metal, primarily due to the assumption of a smaller tolerable (welding related) flaw size compared to that in the base metal (longer fatigue cracks). The required CVN transition temperature for heat affected zones is typically 20°C higher than that for the base metal. Based on this empirical shift and underlying fracture mechanics calculations, the assembled data indicates that the heat affected zones in TMCP steels would be able to meet the CVN requirements in a vast majority of cases, especially if the heat input is maintained below about 5.0 kJ/mm.

For some welded structures, such as offshore structures, the minimum HAZ toughness is frequently specified in terms of CTOD as obtained from specially welded joints. Some of the available literature suggests that a 0.1 mm HAZ CTOD requirement could be met at -50°C as long as the heat input was maintained below 5.0 kJ/mm. However, there is usually a large scatter in the results and the data base is limited. **Therefore, more data needs to be generated to have confidence that adequate HAZ fracture toughness can be achieved reliably in the higher strength TMCP steels (450 to 500 MPa yield strength) at low test temperatures (-30°C to -50°C).**

The required base metal and heat affected zone fracture toughness for TMCP steels must increase with the steel's yield strength (and, therefore, the allowable stress) in order to maintain the same degree of flaw tolerance. Following the existing approach to estimate the required base metal and heat affected zone toughness, corresponding values for higher strength steels were estimated and the data base assembled as part of this project indicates that the higher strength TMCP steels will comfortably meet these requirements for ship structures at a design temperature of 0°C.

Finally, it should be added that several steel mills today employ clean steel technology for the production of conventional steels and, therefore, any associated advantages mentioned above in terms of better base metal or heat affected zone toughness, in principle, would be achievable in conventional steels as well, but for the synergistic benefits from the lower carbon equivalent. And, as far as the carbon equivalent of the conventional steels is concerned, it can be progressively reduced as one goes from hot rolling to normalizing to control rolling and finally to quenched and tempered steels. In practice though, controlled rolled steels are the only economic alternative to accelerated cooled TMCP steels when the specified minimum yield strength is 350 MPa. Still, the thickness range available is likely to be smaller and at best, the control rolled

steel properties might approach those of the accelerated cooled TMCP steels. Similarly, for a specified minimum yield strength of say 450 to 500 MPa, quenched and tempered steels are the main alternative to accelerated cooled steels and limited direct comparataive evaluation of these two groups of steels indicates that their toughness properties (base metal and heat affected zone) can be comparable.

Fatigue Properties

Fatigue cracks in steel ships generally initiate at welded structural details. The initiation and subsequent propagation of fatigue cracks is driven by: (i) bending and torsion of the hull girder as a result of wave loading; (ii) fluctuating hydrostatic pressure on side shell plating and tank boundaries: and/or, (iii) machinery and hull vibration. Exposure to corrosive media, such as sour crude oil or sea water, can also accelerate the initiation and propagation of fatigue cracks, either directly through corrosion fatigue mechanisms or indirectly through the higher cyclic stresses that result from corrosion pitting and general wastage.

Historically, fatigue cracking in steel ships has been viewed as a maintenance problem rather than a design problem. In the past 15 to 20 years, however, more structurally optimized ships with thinner scantlings have been designed and constructed. This optimization has been achieved through the greater use of high strength steels and the greater exploitation of Classification Society rules which have permitted design stresses to increase with tensile strength up to a fraction of the tensile strength defined by the so-called material factor. The development of TMCP steels with superior weldability to conventional high strength steels has contributed significantly to this greater use of high strength steels in ship construction. Unfortunately, the stress concentrations of many structural details have not been adequately reduced to compensate for the higher design stresses and higher local bending stresses associated with thinner scantlings. Furthermore, the fatigue strength of as-welded steel joints is essentially independent of tensile strength. Therefore, local cyclic stresses at many structural details have been permitted to increase without a matching increase in the fatigue strength of these details. As a result, fatigue cracking has occurred more frequently in relatively new and older ships since the late 1970's. Maintenance costs have risen to the point where owners and operators now recognize the need for more direct control of fatigue cracking at the design stage.

Classification Societies have responded by recently adapting S-N design procedures for as-welded joints in bridges and offshore structures to steel ships. These procedures are based on S-N data for the high cycle fatigue lives of welded joints fabricated from non-TMCP structural steels and reflect the following characteristics of these joints: (i) the fatigue strength of as-welded joints is essentially independent of tensile strength; (ii) the fatigue lives of freely corroding joints in sea water is, on average, a factor of two to three lower than the fatigue lives of joints in air; (iii) cathodic protection can restore the fatigue lives of joints in sea water to in-air values at low stress levels, but the beneficial effect of cathodic protection diminishes with increasing stress level and increasing cathodic polarization; and, (iv) the fatigue lives of fillet-welded joints with transverse attachments decrease with increasing base plate thickness if attachment plate thickness and weld size are scaled in proportion to base plate thickness.

Limited S-N data for butt joints and fillet-welded joints fabricated from TMCP steels indicate that such joints share the aforementioned characteristics of non-TMCP steel joints, and that there is no difference between the fatigue lives of as-welded joints fabricated from TMCP and non-TMCP steels, even if soft heat affected zones are present in the TMCP steel joints. Therefore, **it is recommended that designers continue to apply the new fatigue design criteria for welded joints in steel ships to as-welded joints fabricated from TMCP steels until additional S-N data for such joints becomes available and indicates otherwise.**

Fatigue cracking will continue to occur in existing ships designed without explicit consideration of fatigue cracking. Limited fatigue cracking is also to be expected at properly designed and well fabricated structural details in future ships, since the new fatigue design procedures allow for a low probability of fatigue crack initiation at welded structural details over a ship's design life. In addition, premature cracking could occur in new ships as a result of poor workmanship and design errors.

Fatigue cracks detected in service are generally repaired at the earliest opportunity even though some cracks do not pose an immediate threat to the structural integrity or functionality of a ship. Consideration is now being given to the use of damage tolerance assessments to optimize a ship's through-life maintenance costs without compromising safety. A key component of such assessments is the prediction of Region II crack growth by linear elastic fracture mechanics analysis. Available da/dN versus ΔK data for Region II crack growth in the base metal, weld metal, and heat affected zone of TMCP steel welded joints falls within the scatter band of da/dN versus ΔK data for Region II crack growth in the base metal, weld metal, and heat affected zones of non-TMCP ferritic-pearlitic steel joints in the same environment (in air or in sea water with or without cathodic protection). Therefore, **it is recommended that well-established upper bounds on the latter data be used for damage tolerance assessments in the absence of specific da/dN versus ΔK data for Region II crack growth in the base metal, weld metal, and heat affected zones of TMCP steel joints in a given environment.**

Most of the available S-N data for steel welded joints corresponds to nominal stress ranges less than the yield strength of the parent material. The majority of fatigue damage in welded steel structures is sustained at such cyclic load levels, but extreme wave loads can produce significant cyclic plasticity in certain areas of ships and offshore structures. Available low cycle S-N data for steel welded joints indicates that the S-N design curves for steel welded joints can be extrapolated to cyclic stress ranges up to four times the yield strength of the parent material. Although most fatigue design rules restrict this upper limit to 2 times the yield strength, significant cyclic plasticity can still occur at structural details at these stress ranges. Under such conditions, soft heat affected zones in TMCP welded joints could act as strain concentrators. Such strain concentrations could act as preferred crack initiation sites although this tendency would be offset to some extent by the greater resistance to crack initiation of softer metals for a given cyclic strain range. Such strain concentrations could also cause cracks initiating outside soft heat affected zones to propagate into

these zones where the resistance to Region III crack growth would be expected to be lower than that in harder metal. Limited data suggests that Region III crack growth in soft heat affected zones of TMCP welds tends to be faster than in base metal and that high heat input tends to reduce the low cycle fatigue life of smooth strain-controlled specimens machined from soft heat affected zones of butt joints. **Low cycle S-N data for TMCP steel welded joints is needed to assess the net effect of these two factors on fatigue life.**

Some of the most fatigue-prone areas in oil tankers have been the intersections of longitudinals and transverse structure in cargo tanks. Various studies have attributed fatigue cracking in these areas to high local cyclic stresses resulting from fluctuating hydrostatic loading on tank boundaries, hull girder bending, the use of high strength steel, and poor detail design. However, limited S-N data for simple notched specimens fabricated from TMCP and non-TMCP steels and limited da/dN versus ΔK data for Region II crack growth in these steels indicate that exposure to sour crude oil (i.e., crude oil containing a high concentration of H_2S) can have a deleterious effect on the initiation and propagation of fatigue cracks at high cyclic stress levels. **S-N data for TMCP and non-TMCP steel joints immersed in sour crude oil is needed to determine whether special fatigue design measures are required for welded details exposed to sour crude oil.**

The growth of short cracks in welded steel structures has received little attention from researchers because it is believed that the fatigue life of such structures is controlled by the existence of welding defects and that only a small portion of the total life is spent in the initiation and propagation of short fatigue cracks. In recent years, however, there has been growing interest in the use of high strength steel threaded connections in offshore structures and weld improvement techniques to increase the fatigue strength of high strength steel welded connections in such structures. Crack initiation and short crack growth could occupy a significant fraction of the fatigue lives of such connections. Available experimental data indicates that the resistance of available TMCP steels in air to fatigue crack initiation increases with increasing tensile strength (like the resistance of non-TMCP steels to fatigue crack initiaiton), and it is comparable to that of non-TMCP steels with comparable tensile strength and microstructure. However, **limited studies suggest that short crack behaviour may be more pronounced in TMCP steels than non-TMCP steels for both air and sea water environments. Further studies are required to confirm this difference.**

The insensitivity of the high cycle fatigue life of as-welded steel joints to material tensile strength has also been attributed to the large fraction of life spent in Region II crack growth. This implies that the fatigue strength of welded joints can be improved and made to increase with increasing tensile strength by using weld improvement techniques such as shot-peening, hammer-peening, grinding, and TIG dressing to introduce a significant crack initiation period. Recent S-N data for welded joints fabricated from non-TMCP steel joints shows that the aforementioned techniques can improve the fatigue strength of welded joints in air and in sea water, with and without, cathodic protection by 20% to 100% with the magnitude of improvement increasing with

increasing tensile strength. Similar improvements have also been observed in limited tests of TMCP steel welded joints. However, **limited S-N data indicates that high heat input can reduce the endurance limit of heat affected zone metal in TMCP steel welds , and limited da/dN versus ΔK data indicates that Region I crack growth in soft heat affected zones of TMCP steels welds is faster than that in the base metal. This data suggests that the effectiveness of weld improvement techniques could be reduced if crack initiation occurs in soft heat affected zones and that the presence of soft heat affected zones could reduce the fatigue strength of ground butt joints. Further studies are required to quantify and assess the likelihood of these reductions.**

9.0 REFERENCES

1.1 Pickering, F.B.; "High strength, low-alloy steels - a decade of progress"; MicroAlloying'75 Conference; Oct. 1975; Washington, D.C.; pub. Union Carbide Corp. 1977; p 9.

1.2 Gray, J.M., and Post, J.W.; "Steels for offshore structures - Materials Engineering concerns"; OMAE 1994 Conference Workshop on Steel and Weldment Testing and Data Analysis; 1994; Houston, Texas.

1.3 "Rules for Building and Classing Steel Vessels"; published by the American Bureau of Shipping; New York; 1992.

1.4 Kitada, H.; "Recent ship steels and some considerations in their welding-TMCP steel"; Technical Bulletin of Nippon Kaiji Kyokai; V4; 1986; p53.

1.5 API RP 2Z (1987); "Recommended practice for preproduction qualification for steel plates for offshore structures"; American Petroleum Institute.

1.6 Personal Communication with H. Sueoka (Mitsubishi Heavy Industries) at SSC Symposium on Ship Structure Fracture; Washington, DC; March 1995.

1.7 Personal Communication with K. Ishida (IHI, Japan); ibid.

1.8 Kim, H.J., et al; "Application of TMCP steels for shipbuilding and offshore structures"; Conf. Proceedings ' Microalloyed HSLA Steels'; ASM World Materials Congress; 1988; p 131.

1.9 Personal Communication between J. McCallum (Canarctic Shipping, Ottawa) and Odense Shipyard in Denmark.

1.10 Tanaka, T.; "Science and technology of hot rolling process of steel"; Proc. Intl. Conf. Microalloying '95; Pittsburgh, USA; June 1995; p 165.

1.11 Haze, T., et al; "Steel Plate with superior HAZ toughness for offshore structures"; Seitetsu Kenkyu; (326); 1987; p 36-44.

1.12 Shiga, C, and Saito, Y.; "Toughness improvement in HAZ of HSLA steels by TMCP in Japan"; Proc. of the 1st United States-Japan Symposium on Advances in WeldingMetallurgy; (AWS, JWS and JWES); p 177-205; 1990.

1.13 Terada, Y., et al; "Titanium -oxide bearing steels for offshore structures"; presented at Intl. Conf. On HSLA Steels: Processing, Properties and Applications; Eds. G. Tither and Z. Shouhua; Beijing, China; Nov, 1990; p 519.

1.14 Commision of European Communities. High Strength Structural Steels - A European Review. Final Report EUR 1176. EN 1998.

4.1 Meksi, K.; "High strength steels in offshore engineering-The question of high yield to ultimate ratio in high strength steels"; M.Sc. Thesis; Cranfield Institute of Technology; 1992.

4.2 Dier, A.F., et al; "The influence of the uniaxial stress-strain curve on the use of materials offshore and on structural integrity"; Paper 7496 presented ast the 26th Annual OTC; Houston; 1994; p 285.

4.3 Healy, J., et al; "Metallurgical considerations of the high yield to ultimate ratio in high strength steels for use in offshore engineering"; presented at the Annual OMAE Conference; Stockholm; 1995.

4.4 Ohnishi, K., et al; "Development of low yield ratio 60 kgf/mm2 class steel plate for skyscrapers"; The Sumitomo Search; No. 41; Jan. 1990; p 71.

4.5 Shikani, N., et al; "Development of high strength steels with low yield ratio for large scale steel structures"; Proc. Of Microalloying'88; Chicago; Sept. 1988; p 481.

4.6 Reemsnyder, H.S.; "Determination of strain hardening exponent from yield and tensile strengths"; Technical Report prepared for Research Department, Bethlehem Steel Corporation; Oct. 1994.

4.7 Dobi, D., et al; "Evaluation of fracture properties of cold deformed 450YS TMCP steel"; Proc. Of the 13th OMAE Conf.; V III; p 315.

4.8 Bannister, A.C., et al; "A comparative study of wide plate behavior of a range of structural steels using the failure assessment diagram"; Proc. Of the 14th OMAE Conf.; V III; p 65.

4.9 "EH36Mod steel plates produced by OLAC for arctic marine use structures"; NKK Technical Bulletin; July 1990.

4.10 Huther, M., et al; "Statistical representation of steel mechanical properties for probabilistic analysis of structures"; European Safety and Reliability Conference'92; Copenhagen; June 1992.

4.11 Personal Communication with Dr. Zettlemoyer (Exxon Production Research Co.); 1994.

4.12 Kurihara, M, et al; "Coarse grain HAZ toughness evaluation on heavy gauge TMCP steel plate by wide plate tests"; 8th OMAE Conf.; 1989; p 649.

4.13 Graville, B.A., et al; "Toughness requirements for welded structures in the arctic"; Welding Journal; V71; Nov. 1992; p 437s.

4.14 ASTM Standard E208; "Conducting drop-weight test to determine nil-ductility transition temperature of ferritic steels"; published by ASTM (Philadelphia.

4.15 Tagawa, H., et al; "Development of YS460MPa grade steel plate for offshore structures with thermo-mechanically processed copper bearing age hardenable steel"; Nippon Kokan Technical Report; Overseas No. 50; 1987.

4.16 Pussegoda, L.N., et al; "Strain rate effects on fracture toughness of ship plate steels"; submitted to OMAE for publication.

4.17 "Nippon Steel's high strength steel plate series for ice breaker and frozen-sea structure"; Technical data presented by Nippon Steel Corporation; Jan., 1994.

4.18 Graville, B.A.; "Crack arrest requirements for arctic structures"; CANMET Contract Report 23440-8-9-9190/01-SQ; march 1989.

4.19 Yajima, H., et al; "Extensive application of TMCP manufactured high tensile steel plate to ship hulls and offshore structures"; Mitsubishi Heavy Industries Ltd. Technical Review; V24; No. 1; Feb. 1987; p 12.

4.20 Yajima, H., et al; "Extensive application of TMCP manufactured high tensile steel plate 40 kgf/mm2 class in yield point to ship hulls"; Mitsubishi Heavy Industries Ltd. Technical Review; V25; No. 2; June 1988; p 130.

4.21 Japan Pressure Vessel Research Council, "Review of properties of TMCP steel-pressure vessel steels for low temperature service"; Welding Research Council Bulletin. No 334, June 1988.

4.22 Barnes, A. M., et al; "Determination of the cause of low HAZ Charpy impact properties in structural steels at the "fusion line + 5 mm" location"; OMAE Conf.; V3; 1995.

4.23 Yajima, H., et al; "Toughness required of frigid zone offshore structure steel plate 400 MPa in yield point and a newly developed heavy thickness plate"; Proc.of the 2nd Intl. Offshore and Polar Engineering Conf.; San Francisco; June 1992; p 116. (Also, Kawasaki Steel/Mitsubishi Joint Report on YP 390 class, 60 mm thick MACS (TMCP) steel for icy water marine applications")

4.24 Toyoda, M.; "Fracture toughness evaluation of steel welds - Review"; published by Osaka University; July 1986.

4.25 Spurrier, J.; "Being tough with the wide plate test"; OMAE Conf. 1994; Vol III; p 37.

4.26 Tanigawa, O., et al; "420 and 500 MPa yield strength steel plates with high HAZ toughness produced by TMCP for offshore structures"; Kawasaki Technical Report No. 29; Nov. 1993.

4.27 Mottate, H., et al; "High strength steel plates manufactures by MACS for offshore structures"; data supplied by Kawasaki Steel; 1993. (Also, Kawasaki Steel/Mitsubishi Joint Report on YP 460 class, 30 mm thick MACS (TMCP) steel for icy water marine structure applications")

5.1 Kitada, H., et al; "Application of YP 40 TMCP steel plates to hull structural members-Material selection and notch toughness in welded joints"; Journal of the Society of Naval Arhitects of Japan; V162; 1986; p408.

5.2 Dier, A.F., et al; "The influence of the uniaxial stress-strain curve on the use of materials offshore and on structural integrity"; Paper 7496 presented ast the 26th Annual OTC; Houston; 1994; p 285.

5.3 Nippon Kaiji Kyokai Document submitted to IACS; "Guide of minimum service temperature of hul structural steels"; Study Reort for Agenda Item 3 of the IACS Working Party on Materials and Welding; July 1979.

5.4 Kitada, H.; "Recent ship steels and some considerations in their welding-TMCP steel"; Technical Bulletin of Nippon Kaiji Kyokai; V 4; 1986; p 53.

5.5 Yajima, H., et al; "Extensive application of TMCP manufactured high tensile steel plate 40 kgf/mm2 class in yield point to ship hulls"; Mitsubishi Heavy Industries Ltd. Technical Review; V25; No. 2; June 1988; p 130.

5.6 Sumpter, J.D.G., et al; "Recommended facture toughness for ship hull steel and weld"; Marine Structures; V8 (1995); p 345.

5.7 Yajima, H., et al; "Toughness required of frigid zone offshore structure steel plate 400 MPa in yield point and a newly developed heavy thickness plate"; Proc.of the 2nd Intl. Offshore and Polar Engineering Conf.; San Francisco; June 1992; p 116. (Also, Kawasaki Steel/Mitsubishi Joint Report on YP 390 class, 60 mm thick MACS (TMCP) steel for icy water marine applications").

6.1 Reemsnyder, H., " Fatigue and Fracture of Ship Structures", Symposium and Workshop on The Prevention of Fracture in Ship Structure, March 30-31, 1995, Washington, D.C..

6.2 "Bulk Carriers: Seeking Solutions to the Safety Problem", 100A1, The Magazine of Lloyd's Register, Issue 3, 1991, pp 6-9.

6.3 "A Guide to Combatting Fatigue", Surveyor, Dec. 1992, pp 24-31.

6.4 "HTS - Something For Nothing ?", 1001A1, The Magazine of Lloyd's Register, Issue 3, 1992, pp 11-14.

6.5 Card, J.C., "Safelife for Ships", Proc. Symposium and Workshop on the Prevention of Fracture in Ship Structure, March 30-31, 1995, Washington, DC.

6.6 Jordan, C.R. and Cochrane, C.S., In-Service Performance of Structural Details, Ship Structure Committee Report SSC-272, 1978.

6.7 Jordan, C.R. and Cochrane, C.S., Further Survey of In-Service Performance of Structural Details, Ship Structure Committee Report SSC-294, 1980.

6.8 Sucharski, D., " Crude Oil Tanker Hull Structure Fracturing - An Operator's Perspective", Proc. Symposium and Workshop on the Prevention of Fracture in Ship Structure, March 30-31, 1995, Washington, DC.

6.9 Liu, D. and Thayambali, A., " Local Cracking in Ships - Causes, Consequences, and Control", Proc. Symposium and Workshop on the Prevention of Fracture in Ship Structure, March 30-31, 1995, Washington, DC.

6.10 Nakijima, Y., Iino, N., Neki, I., Ushirokawa, O., Maeda, M., and Sasajima, H., "Fatigue Strength Design of Ship Structure", IHI Engineering Review, Vol. 26, No. 2, April, 1993.

6.11 Cramer, E., Gran, S., Holtsmark, G., Lotsberg, I., Loseth, R., Olaisen, K., Valsgard, S., "Fatigue Assessment of Ship Structures", Det Norske Veritas Report No. 93-0432, Jan., 1995.

6.12 "Guide for the Fatigue Strength Assessment of Tankers", ABS, June, 1992.

6.13 Lindley, T.C., Richards, C.E., "Near-Threshold Fatigue Crack Growth in Materials Used in the Electricity Supply Industry", Fatigue Thresholds - Fundamentals and Engineering Applications, EMAS, U,K, 1982, pp 1087-1113.

6.14 Priddle, E.K., The Threshold Stress Intensity Factor for Fatigue Crack Growth in Mild Steel Plate and Weld Metal: Some Effects of Temperature and Environment", Fatigue Thresholds - Fundamentals and Engineering Applications, EMAS, U.K. ,1982, pp 581-600.

6.15 Taylor, D., Fatigue Thresholds, Buterworth, London, 1989.

6.16 Barsom, J.M. and Rolfe, S.T., Fracture and Fatigue Control in Structures, Prentice-Hall, Englewood Cliffs, New Jersey, 1987.

6.17 Ritchie, R.O., "Near-threshold Fatigue-Crack Propagation in Steels", International Metals Reviews, Review 245, No. 5 and 6, 1979.

6.18 Ebara, R., Yamada, Y., Zama, M., Sakai, D., Fushimi, A., and Yajima, H., "Fatigue Strength of HT50 Steel Plates in Sour Crude Oil", Proc. 11th Int. Conf. Offshore Mechanics and Arctic Engineering (OMAE'92), Calgary, Canada, June 7-12, 1992, Vol. III-B, pp 509-512.

6.19 Ouchi, H., Kobayashi, J., Ishikawa, T., Takezawa, H., Ebara, R., and Yamada, Y., "Effects of Sour Crude Oil on Fatigue Properties of Steel Plates for Shipbuilding", Proc. of Corrosion'94, Paper 218.

6.20 Yang, J. and Hartt, W.H., "Near-Threshold Fatigue Crack Growth of High Strength Steels In Seawater", Proc. of 12th Int. Conf. on Offshore Mechanics and Arctic Engineering (OMAE'93), Stavangar, Norway, Vol. III-B, 1993, pp 463-471.

6.21 Yang, J. and Hartt, W.H., "High R-Ratio Near-Threshold Fatigue Crack Growth Rates of High Strength Steels in Seawater", Proc. of 13th Int. Conf. on Offshore Mechanics and Arctic Engineering (OMAE'94), Glasgow, 1994.

6.22 Richards, C.E. and Lindley, T.C., "The Influence of Stress Intensity and Microstructure n Fatigue Crack Propagation in Ferritic Materials", Engineering Fracture Mechanics, Vol.4, 1977, pp951-978.

6.23 BS7608, Code of Practice for Fatigue Design and Assessment of Steel Structures, 1993.

6.24 PD6493:1991,"Guidance on Methods for Assessing the Acceptability of Flaws in Fusion Welded Structures",British Standards Institution.

6.25 Spurrier, J., Billingham, J., Hockenhull, B.S., "Fatigue Performance of Intermediate Strength Accelerated Cooled Steels with Emphasis on HAZ Behaviour", Cranfield Report Project No. CIT 12 (828).

6.26 Lim, C.B., Kweon, Y.G., Chang, R.W., "Fatigue Behaviour og TMCP Steel Welds", Proc. 9th Int. Con. Offshore Mechanics and Arctic Engineering (OMAE'90), Houston, TX, Feb. 18-23, 1990, edited by S.K. Chakrabarti, H. Maeda, C. Aage, and F.G. Nielsen, Vol. III, pp 433-442.

6.27 Nakano, Y., Matsumoto, S., Watanabe, 0., and Hatomura, T., "Corrosion Fatigue Crack Propagation Behaviour of TMCP Steels", Proc. 12th Int. Conf. on Offshore Mechanics and Arctic Engineering (OMAE'93), Stavangar, Norway, 1993, pp 215-223.

6.28 Tubby, P. and Booth, G.S., "Corrosion Fatigue Crack Growth Studies in Two Weldable High Strength Steels", Proc. 11th Int. Conf. on Offshore Mechanics and Arctic Engineering (OMAE'92), Volume III-B, Materials Engineering, Calgary, Canada, June 7-12, 1992, pp 539-546.

6.29 Dowling, N.E., "Crack Growth During Low Cycle Fatigue of Smooth Axial Specimens", Cyclic Stress-Strain and Plastic Deformation Aspects of Fatigue Crack Growth, STP 637, ASTM, Philadelphia, 1977, pp97-121.

6.30 Pearson, S., "Initiation of Fatigue Cracks in Commercial Aluminum Alloys and the Subsequent Propagation of Very Short Cracks", Engineering Fracture Mechanics, Vol.7, 1975, pp235- 247.

6.31 Kitigawa, H. and Takahashi, S., "Applicability of Fracture Mechanisms to Very Small Cracks of the Cracks in the Early Stage", Proc. 2nd Int. Conf. Mech. Behaviour of Materials, 1979, pp627-631.

6.32 ASM Metals Handbook, Mechanical Testing, Vol.8, 9th edition, American Society for Metals,1985.

6.33 Ouchi, H., "Definition and Behaviour of Small Cracks in Corrosion Fatigue", Corrosion Engineering, 42, 1993, pp 299-313.

6.34 Kim, K. and Hartt, W.H., "Growth Rate of Short Fatigue Cracks as Relevant to Higher Strength Steels for Offshore Structures in Seawater", Proc. 11th Int. Conf. on Offshore Mechanics and Arctic Engineering (OMAE'92), Volume III-B, Materials Engineering, pp 565-575.

6.35 Kim, K. and Hartt, W.H., "Corrosion Fatigue of Short Cracks for Higher Strength Steels in Seawater with Cathodic Protection", Proc. 12th Int. Conf. on Offshore Mechanics and Arctic Engineering (OMAE'93), Stavangar, Norway, 1993.

6.36 Bannitine, J.A., Comer, J.J., and Handrock, J.L., Fundamentals of Metal Fatigue Analysis, Prentice Hall, Englewood Cliffs, New Jersey, 1990.

6.37 Frost, N.E., Marsh, K.J., and Pook, L.P., Metal Fatigue, Clarendon Press, Oxford, 1974.

6.38 Gough, H.J., The Fatigue of Metals and Structures, Scott, Greenwood, and Son, 1924.

6.39 Funck, A., "Fatigue Tests on Basic Bessemer and Open Hearth Steels", Acier Stahl Steel, Vol. 23, No. 1, 1958, pp 19-24.

6.40 "Structural Steels - DI-MC", Dillinger Hütte GTS Technical Information No. 1/1993.

6.41 Rowe, G.H., "Correlation of High Cycle Fatigue Strength with True Stress-True Strain Behaviour", Journal of Materials, Vol. 1, No. 3, Sept. 1966, pp 689-715.

6.42 Reemsnyder, H.S., "Correlation of Fatigue Limit with True Stress-Strain Behaviour", Materials Research and Standards, Vol. 7, No. 9, Sept. 1967, pp.390-392.

6.43 Reemsnyder, H.S.,"Effect of Cold Forming on the Strain Controlled Fatigue Resistance of Automotive Steels", SAE 1992 Trans. J. of Materials and Manufacturung, Section 5, pp 554-566.

6.44 Fuchs, H.O. and Stephens, R.I., Metal Fatigue in Engineering, John Wiley & Sons, New York, 1980.

6.45 Creager, M., "The Elastic Stress-Field Near the Tip of a Blunt Crack", Master of Science Thesis, Lehigh University, Bethlehem, Pa., 1966.

6.46 Barsom, J.M. and McNicol, R.C., "Effect of Stress Concentration on Fatigue Crack Initiation in HY-130 Steel", ASTM STP 559, American Society For Testing and Materials, Philadelphia, 1974.

6.47 Bignonnet, A., "Corrosion Fatigue of Steel in Marine Structures - A Decade of Progress", Proc. of 3rd Int. Conf. on Steel in Marine Structures (SIMS'87), Delft, The Netherlands, June 15-18, 1987, Paper PS5, pp 119-135.

6.48 Jaske, C.E., Broek, D., Slater, J.E., and Anderson, W.E., "Corrosion Fatigue of Structural Steels in Seawater and for Offshore Applications", Corrosion Fatigue Technology, ASTM STP 642, edited by H.L. Craig, T.W., Crooker, and D.W. Hoeppner, American Society for Testing and Materials, 1978, pp 19-47.

6.49 Burnside, O.H., Jr. Hudak, S.J., Oelkers, E., Chan, K., and Dexter, R.J., "Long-Term Corrosion Fatigue of Welded Marine Steels", Ship Structure Committee report SSC-326, 1984.

6.50 Rajpathak, S.S. and Hartt, W.H., "Fatigue Crack Initiation of Selected High Strength Steels in Sea Water", Proc. 7th Int. Conf. Offshore Mechanics and Arctic Engineering (OMAE'88), Houston, TX, Feb. 7-12, 1988, edited by J.S. Chung and S.K. Chakrabarti, Vol. III, pp 323-331.

6.51 Matsumoto, S., Nakano, Y., Shia, C., Narumoto, A., and Kikukawa, S., "Improvement of Corrosion Fatigue Strength of Cruciform Fillet Welded Joints of Steel Plates for Offshore Structures", Proc. Int. Conf. Evaluation of Materials Perforamnce in Severe Environments (EVALMAT'89), Nov.20-23, 1989, Kobe, Japan, pp 159-166.

6.52 Vosikovsky, O., "Frequency, Stress Ratio, an dPotential Effects on Fatigue Crack growth of HY130 Steel in Salt Water", J. Testing and Evaluation, 6(3), pp175-182, 1978.

6.53 Watanabe, E., Yajima, H., Ebara, R., Sakai, D., Matsumoto, S., Nakano, S., and Sugie, E., "Corrosion Fatigue Strength of Ship Structural Steel Plates and Their Welded Joints in Sour Crude Oil", Proc. 13th Int. Conf. Offshore Mechanics and Arctic Engineering (OMAE'94), pp 151-158.

6.54 Offshore Installations: Guidance on Design and Construction, U.K. Department of Energy, HMS, London, 1984.

6.55 Hughes, O., Ship Structural Design, John Wiley and Sons, USA.

6.56 Munse, W.H., Wilbur, T.W., Tellalia, M.L., Nicoll, K., and Wilson, K., "Fatigue Characterization of Fabricated Ship Details for Design", Ship Structure Committe Report SCC-318, 1983.

6.57 Gurney, T.R., "The Influence of Thickness on the Fatigue Strength of Welded Joints, proc. of 2nd Int. Conf. on Behaviour of Offshore Structures (BOSS'79), Paper 41, 1979, BHRA Fluid Engineering, Cranfield, England, pp 523-534

6.58 Cole, I., Pietrosanti, C., Vittori, O., Bufalini, P., and Rizzi, L., "Welded Joints in Offshore Structures: The Significance of Data Derived From Small and Full Scale Tests", Proc. 9th Int. Conf. Offshore Structures and Arctic Engineering, Vol. III, Part A, pp 419-424.

6.59 "Fatigue Strength of Heavy Sectioned Welded Joints Fabricated From OLAC Processed Plates", NKK Technical Bulletin No. 243-224, June, 1988.

6.60 Stacey, A. and Sharp, J.V., "The Revised HSE Fatigue Guidance", Proc. 14th Conf. Offshore Mechanics and Arctic Engineering, Volume III, Materials Engineering, 1995, pp1-16.

6.61 Yajima, H., Kawamura, A., Hayashida, T., Tada, M., and Noda, S., "Extensive Application of TMCP-Manufactured High-Tensile Steel Plates 40kgf/mm^2 Class in Yield Point to Ship Hulls", Mitsubishi Heavy Industries Technical Review, Vol. 25, No. 2, June 1988.

6.62 Yajima, H., Kawamura, A., Hayashida, T., Tada, M., and Noda, S., "Extensive Application of TMCP-Manufactured High-Tensile Steel Plates to Ship Hulls and Offshore Structures", Mitsubishi Heavy Industries Technical Review, Vol. 24, No. 1, Feb. 1987..

6.63 Youn, J.G. and Kim, H.J., "Characteristics of TMCP Steel and Its Softening", Proc. Conf. on Welding Metallurgy of Structural Steels, pp 157-168

6.64 Yagi, J., Tomita, Y., Machida, S., Matoba, M., and Soya, I., "Influencing Factors on the Thickness Effect of Fatigue Strength in As-Welded Joints for Steel Structures", Proc. 10th Int. Conf. on Offshore Mechanics and Arctic Engineering (OMAE'91), Vol. III-B, pp 305-313.

7.1 Toyoda, M.; "Significance of Mismatching of steel welds: Over/undermatch versus evenmatch"; OMAE Conf.; 1993; Vol III-A; p9.

7.2 de Lede, F., et al; "Fracture behavior of weldments containing softened zones"; International Conf. Welding-90

7.3 Kluken, A.O., et al; "Use of predictive equations for arctic steel heat affected zone properties"; OMAE Conf.; 1992; Vol III-A; p 1.

7.4 Liu, S., et al; "Assessment of Microstructural and property prediction equations in structural welding"; paper 7497; presented at the 1994 OTC; Houston, 1994.

7.5 "Tensile strength of welded joint with HAZ softening"; Report of the Shipbuilding Research Association of Japan by the 193 Research Committee; Tokyo; (provided by Kawasaki Steel); MArch 1987.

7.6 Inoue, T., et al; "Fracture behavior of welded joints with HAZ undermatching";

7.7 Kitada, H.; "Recent ship steels and some considerations in their welding-TMCP steel"; Technical Bulletin of Nippon Kaiji Kyokai; V 4; 1986; p 53.

7.8 Machida, S., et al; "Extensive application of TMCP steel plate to ship hulls:40kgf/mm2 class high yield stress steel"; Marine Structures; V1; No. 3; 21988; p219.

7.9 "Nippon Steel's high strength steel plate series for ice breaker and frozen-sea structure"; Technical data presented by Nippon Steel Corporation; Jan., 1994.

7.10 Hanus, F.E.; "Flame straightening thermomechanically rolled structural steels"; Welding and Cutting; No 4, V 46; 1994: p E56

7.11 Hanus, F.E.; "Flame straightening shape control of TMCP steels"; 14th OMAE Conference; 1995; VIII; p 371.

7.12 Myllykoski, L., et al; "Advances in the accelerated cooling of plates"; presented at Microalloying'95; Pittsburgh, U.S.A.; June 1995.

7.13 Personal Communication with Dr. M. Miglin; Babcock and Wilcox; Alliance, Ohio; 1995.

APPENDIX A

LIST OF PERSONS/ORGANIZATIONS THAT RESPONDED TO REQUEST FOR TECHNICAL INFORMATION AND DATA

APPENDIX A

List of Persons and Organizations Contacted

*Algoma Steel Corp., Canada; (Mr.M. McLean)
*Amoco Corporation, U.S.A.; (Dr. J. Ibarra)
*Babcock & Wilcox - a McDermott Company; USA (Dr. M. Miglin)
*Bethlehem Steel Corp., U.S.A.; (Dr. H. Reemsnyder)
BHP Research, Australia; (Dr. P.D. Hodgson)
*Canadian Liquid Air, Canada; (Mr.V. Vaidya)
*Canarctic Shipping Company, Canada (Mr. John McCallum)
*CANMAR, Canada (Mr. W.A. Brydon)
*ClassNK - Nippon Kaiji Kyokai, Tokyo, Japan; (Messers Y. Ino; H. Kitada)
*Conoco Inc., U.S.A.; (Dr. M. Salama)
*Cranfield Institute of Technology (Drs. J. Billingham and
*Exxon Production Research Co., U.S.A.; (Dr. N. Zettlemoyer)
*GTS Industries, France (Mr. J. Vigo)
Italsider, Italy; (C. Jannone)
*Kawasaki Steel U.S.A., (Mr. T. Miyake)
*Lincoln Electric Company, Canada; (Mr. B. Clark)
Lukens Steel, U.S.A.; (Mr. A. Wilson)
Professor S. Machida, University of Tokyo, Japan
Mannesmannrohren-Werke, Germany; (Mr. M.K.Graf)
*Marathon Oil Company, U.S.A.; (Mr. P. Sandy)
*Professor K. Masubuchi, M.I.T., U.S.A.
*Metals Technology Laboratories, CANMET, Canada (Mr. J. Gianetto)
Mitsubishi Heavy Industries, Japan (Dr. H. Yajima)
*Nippon Steel U.S.A., Inc.; (Dr.N. Suzuki)
*NKK Corporation, Vancouver Office (Mr. H. Sugimara)
*Norske Hydro Research Centre, Norway (Dr. I. Harneshaug)
*NSWC Carderock Division, U.S.A; (Dr. E. Czyryca)
Shell Offshore Inc., U.S.A.; (Mr. J.D. Smith)
*Sumitomo Metal Industries, Japan; (Dr. K. Bessyo)
Svenskt Stal, Sweden; (Dr. B. Ahlblom)
Thyssen Forschung, Germany; (Dr. Uwer)
*Professor Y. Ueda, Osaka University, Japan.
*US Steel, U.S.A.; (Mr. S.J.Manganello)

(* indicates that some response was received. For some of the offshore organizations, the lack of response might have been due to incorrect addresses.)

APPENDIX B

SOURCE DOCUMENTS FOR DATA COMPILED IN THE DATA BASE (APPENDIX C)

197, 198x

APPENDIX B

Source Documents For Strength and Toughness Data Collection

B1 Kubo, T., et al; "A 100 mm Thick API 2W Gr. 60 Steel Plate Produced by TMCP and Its Application to Offshore Structures"; (Kawasaki Steel); OMAE Conference 1994; Vol III; p307. (Also, "Report for Prequalification Weldability Test of API2W Gr. 60 for Compliant Tower Development Project"; prepared by Kawasaki Steel for Shell Oil (witnessed by ABS); July 1993.

B2 Nakano, Y., et al; "Effect of Strength Mismatching on Fracture Behaviour of Notched, High Strength Steel Welded Joint", (Kawasaki Steel); OMAE Conference 1993; Vol III, p1.

B3 Yoshida, Y., et al; "Production of High Strength TMCP Steel Plate for Offshore Structures", (Nippon Steel), ibid, p207.

B4 Morabito, D., et al; "Toughness of Welded TMCP Steel Joints in Overmatching Conditions"; ibid; p507.

B5 Suzuki, S., et al; "Property Distribution Map to Understand HAZ CTOD Toughness"; (Sumitomo Steel); ibid; p753.

B6 Saitoh, N., et al; "Development of Offshore Use High Strength Steel Plates for Large Heat Input Welding"; (Nippon Steel); OMAE Conference 1992; Vol III, p65.

B7 Nakano, Y., et al; "Preheat and PWHT Free, 150mm Thick API 2W Grade 60 Steel Plate for Offshore Structures"; (Kawasaki Steel); OMAE Conference 1988; Vol III, 1988, p89.

B8 Kim, H.J., et al; "Application of TMCP Steels for Shipbuilding and Offshore Structures"; (Hyundai); Conf. Microalloyed HSLA Steels; ASM World Materials Congress; 1988; p205.

B9 Burget, W., et al; "Fracture Toughness of Sa-Multiwire Welded Joints on Modern TMCP Steels"; Conference Proceedings, Welding-1990; p177.

B10 Sandwell-Swan-Wooster Inc Report; "Preferential Corrosion and Mechanical Characteristics associated with the Welding of High Grade Materials for Arctic Service"; Report submitted to Canadian Coast Guard, August 1990.

B11 Nakano, Y., et al; "YS 500 MPa Steel Plate Products by TMCP for Offshore Structures"; (Kawasaki Steel) presented at the OMAE Conference in 1989, p269.

B12 Mottate, H., et al; "High Strength Steel Plates Manufactured by MACS for Offshore Structures"; data supplied by Kawasaki Steel, 1993. (Also, Kawasaki Steel/Mitsubishi Joint Report on YP 460 class, 30 mm thick MACS (TMCP) steel for icy water marine structure applications.

B13 "High Yield (Y.S. 460 Mpa) steel plate for Offshore Structures Produced by MACS (56mm thick); data (August 1986) supplied by Kawasaki Steel.

B14 "Mechanical Properties and Corrosion Test Result of YS 420 MPa Steel Plate and its Welded Joints"; data (September 1992) supplied by Kawasaki Steel.

B15 "Reference Data (YS 430 MPa) produced by MACS"; data (September 1987) supplied by Kawasaki Steel.

B16 Nakano, Y., et al; "Properties of 390 and 415 MPa Yield Strength Plates with Good Toughness in Large Heat Input Welded Joints"; Kawasaki Steel Technical Report No. 17; October 1987; p41.

B17 Nakano, N., et al; "High Strength Steel Plate for Ice-Breaking Vessels Produced by TMCP"; paper supplied by Sumitomo Steel (published in CIM 5).

B18 Someya, R., et al; "Development of High Strength Steel for Offshore Structures by the Accelerated Cooling Process"; The Sumitomo Search; No. 32; May 1986; p. 30.

B19 Data supplied by Rautarukki OY (Finland) on 420 and 500 MPa Steels; 1994.

B20 Yajima, H., et al; "Extensive Application of TMCP-manufactured High Tensile Steel and Offshore Structures"; Mitsubishi Heavy Ind. Technical Review; Vol 24, No. 1, Feb 1987 and Vol 25, No. 2, June 1988.

B21 Yajima, H., et al; "Toughness Required of Frigid Zone Offshore Structure Steel Plate 400 MPa in Yield Point and Newly Developed Heavy Thickness Plate"; Proc. 2nd International Offshore and Polar Engineering Conference; June 1992; p116. (Also, Kawasaki Steel/Mitsubishi Joint Report on YP390 class, 60 mm thick MACS (TMCP) steel for icy water marine structure applications.

B22 Lafrance, M., et al; "New TMCP 60 ksi (420 N/mm^2) Steel Plates produced by the Accelerated Cooling Process; Proc. of the 2nd Intl Offshore and Polar Eng Conf; San Francisco, June 1992.

B23 Harrison, P.L., and Hart, P.H.M.; "Influence of Steel Composition and Welding Procedure on the HAZ Toughness of Thick Section Structural Steels"; Intl Conf on the Metallurgy, Welding and Qualification of Microalloyed (HSLA) Steel Weldment; Houston; Nov 1990.

B24 Technical Data on DIMARINE Steels Received from Dillinger Hutte GTS (Subsidiary of Usinor); January 1995.

B25 Weld Procedure Qualification Tests carried out Hitatchi Zosen Corp in Support of Fabrication of a Submergible Barge Hull for CANMAR; 1985.

B26 Spurrier, J., et al; "Influence of Welding on Fracture Behaviour of New Low Carbon Structural Steels (Accelerated Cooled)"; Cranfield Inst of Technology Report; CIT 10 (826).

B27 NKK Technical Bulletin, "NK-LTC415 (NK-LTC42) High Strength Steel Plate with Minimum YS 415 N/mm^2 (42 kgf/mm^2) for Arctic Marine Structure Use, Produced by OLAC Process"; July 1990.

B28 NKK Technical Bulletin; "EH36-080 High Strength Steel Plate with Minimum YS 36 kfg/mm^2 and Good Toughness at -80°C for Arctic Marine Structure Use, Produced by OLAC Process"; Feb 1988.

B29 "Nippon Steel's High Strength Steel Plate Series for Ice Breaker and Frozen-Sea Structure'; Technical Literature Package prepared by Nippon Steel; Jan 1994.

B30 Shiwaku, T., et al; "YS 420 and 460 MPa Class High Strength Steel Plates for Arctic Offshore Structures Manufactured by TMCP"; 7th OMAE Conf; Houston; 1988; p95.

B31 Harneshang, I.S., et al; "HAZ Fracture Toughness in Low Carbon, Controlled Rolled and Accelerated Cooled Steel Used in North Sea Offshore Platform Structures', ibid, p181.

B32 Hackett, B.M., et al; "Metallurgical, Mechanical Property and Weldability Evaluation of Commercial Accelerated Cooled (AC)/Direct Quenched (DQ) Steels; Report DTRC/SME-89-56 published by David Taylor Research Center, Maryland; March 1990.

B33 Focht, E.M.; "Dynamic Tear and Axial Low-Cycle Fatigue Properties of Grade 65 and Grade 80 AC/DQ Steels"; Report CDNSWC/TM-61-94-02 published by Grderoch Division Naval Surface Warfare Center; Jan 1994.

B34 Dobi, D., et al; "Evaluation of Fracture Properties of Cold Deformed 450 YS TMCP Steel'; OMAE Conf., 1994; p315.

B35 Pontremoli, M., et al; "Properties of TMCP Heavy Plates for Offshore Applications with Reference to Their Fabrication Process"; OMAE Conf; 1990; p597.

B36 Krebs, H., et al; "Weld Metal and HAZ Properties of High Heat Input Weldments of TMCP Steels"; Welding-90; p201.

B37 de Lede, F., et al; "Fracture Behaviour of Weldments Containing Softened Zones"; Welding-90; p355.

B38 de Koning, A.C., et al; "Feeling Free Despite LBZ"; 7th OMAE Conf; 1988; p161.

B39 Watanabe, I., et al; "Evaluation of Coarse Grained HAZ Toughness by Wide Plate Testing"; 7th OMAE Conf; 1988; p387.

B40 Kurihara, M., et al; "Coarse Grain HAZ-Toughness Evaluation on Heavy Gauge TMCP Steel Plate by Wide Plate Tests"; 8th OMAE Conf; 1989; p649.

B41 Suzuki, S., et al; "Development of LBZ-Free Low Al-B-Treated Steel Plates"; 8th OMAE Conf; 1989; p657.

B42 Amano, K., et al; "Metallurgical and Welding Factors Controlling Local Brittle Zone in Weld HAZ"; 8th OMAE Conf; 1989; p83.

B43 Koda, M., et al; "Development of a 420 MPa Yield Strength Steel Plate for Arctic Offshore Structures"; 6th OMAE Conf; 1987; p45.

B44 Kozasu, I., et al; "Significance of Coarse Grain HAZ Toughness Against Brittle Fracture"; 6th OMAE Conf; 1987; p103.

B45 AMCA HAZ Report

B46 Gianetto, J. A., et al; "Heat affected zone toughness of a TMCP steel designed for low temperature application"; CANMET Report No ; Ottawa, 1995.

B47 Manigrasso, M., et al; "TMCP steel plates for offshore structures weldability evaluation"; OMAE Conf.; 1991; p 117.

B48 Pargeter, R.J., et al; "Welding and properties of welds in 450 - 550 N/mm^2 yield steels"; ibid; p 81.

B49 Technical Data on DI-MC Steels Received from Dillinger Hutte GTS (Subsidiary of Usinor); publication No 1/1993.

B50 Tagawa, H., et al; "Development of YS460MPa Grade steel plate for offshore structures with thermo-mechanically processed Cu bearing age hardenable steel"; Nioppon Kokan Technical Report; Overseas No. 50; 1987.

B51 Tanigawa, O., et al; "420 MPa and 500 MPa Yiels strength steel plates with high HAZ toughness produced by TMCP for offshore structures"; Kawasaki Technical Report No 29; November 1993.

B52 Spurrier, J., et al; "The influence of welding on materials performance offshore-Accelerated cooled steels"; Cranfield Institute of Technology; Final Reports for the period 1987-1989, and 1990-1991.

B53 NKK Technical Bulletin; "OLAC processed steel plate of Y.S. 355 MPa Grade for offshore structure use-Plate Thickness 120 mm"; published Aug. 1993.

B54 NKK Technical Bulletin; " The physical test results of OLAC processed steel conducted at NKK (in conjunction with Lloyd's and Oilfab Group Limited; July 1990.

B55 NKK Technical Bulletin; "EH36MOD steel plates produced by OLAC for arctic marine use structures"; published June 1990.

B56 NKK Technical Bulletin; "OLAC processed steel plate equivalent to BS4360-50E (Cu-Ni, 50 & 100 mm)"; published May 1990.

B57 "High strength steels in offshore engineering"; MTD Publication 95/100; published by The Marine Technology Directorate Limited, London, U.K..

B58 Suzuki, S., et al; "Metallurgical Design Basis, Qualification Testing, and Production History of 50 ksi and 60 ksi steel plate for the MARS TLP deck fabrication"; 1995 OMAE Conference; Vol. III; p 337.

(There is no B59 Source Document.)

B60 Consumable data suplied by Filarc Welding Industries B.V.; 1993.

B61 "Evaluation of Weld Metal Toughness-SMAW Process (Phase II)"; AMCA International Report 7-185-141-099 submitted to Supply and Services Canada (Govt. of Canada); December 1986.

B62 "Evaluation of Weld Metal Toughness-SAW Process (Phase II)"; Fleet Technology Limited Report E62522C submitted to Supply and Services Canada (Govt. of Canada); March 1989.

B63 "Evaluation of Weld Metal Toughness-FCAW Process (Phase II)"; Fleet Technology Limited Report E62522C submitted to Supply and Services Canada (Govt. of Canada); December 1989.

B64 "Toughness Evaluation of Commercial GMA welding Consumables"; Fleet Technology Report E62517C submitted to Supply and Services Canada (Govt. of Canada); July 1990.

B65 Thornton, C.E. and Webster, D.J.; "The development and application of C-Mn-Ni manual metal arc electrodes"; Presented at the International Conference Welding -90, Germany; 1990.

B66 Rodgers, K.J., et al; "Progress in the welding of higher strength steels for offshore applications"; presented at the 8th International OMAE Conf., The Hague; 1989; p309.

B67 Consumable data suplied by ESAB Welding & Cutting Products", data developed in 1993.

B68 Gianetto, J.A., et al; "Characeteristics of Weldments in High Strength Grade Arctic Steels: Report on Weld Metal Mechanical Properties"; MTL/CANMET Report MTL 93-17(CF); May 1993.

B69 Fleet Technology Contract Data (1994) released with the permission of Lincoln Electric Co., Toronto; (Bruce Clark).

B70 Fleet Technology Contract Data (1994) released with the permission of V. Vaidya of Canadian Liquid Air Co., Montreal.

APPENDIX C

THE ASSEMBLED DATA BASE

SHEET 1	STEEL DESCRIPTIONS
SHEET 2	BASE METAL TENSILE DATA
SHEET 3	BASE METAL TOUGHNESS DATA
SHEET 4	WELD DESCRIPTIONS
SHEET 5	CROSS-WELD STRENGTH DATA
SHEET 6	HAZ TOUGHNESS DATA
SHEET 7	WELD METAL TOUGHNESS DATA

SHEET 1 STEEL DESCRIPTIONS

STEEL DESCRIPTION

Record	Ref	Source	Year	Type	Application	Thickness	Spec Yield	Spec UTS	Chemical Composition												
									C	Si	Mn	P	S	Cu	Ni	Nb	ASA	Ti	TN	REM	V
1.0	1	Kawasaki	1994	API 2W60	Offshore	100	414	517	0.080	0.180	1.530	0.004	0.001	0.190	0.400	0.024	0.029		36.0		
2.0	2	Kawasaki	1993	Experiment	Experiment	50	500		0.100	0.160	1.550	0.003	0.002	0.240	0.500	0.030	0.034	0.005			
3.0	3	Nippon	1993	9000T		50	420	520	0.090		1.560	0.004	0.003				0.003				
4.0	3	Nippon	1993	T.O.	Development	50	420	520	0.080	0.200	1.500	0.004	0.002	0.200	0.200	0.010	0.003	0.010	20.0		
5.0	4	Italian Lab	1993	Nb	Offshore	50	355		0.060	0.230	1.610	0.019	0.004		0.350	0.024	0.022	0.029	98.0		
6.0	4	Italian Lab	1993	low Nb	Offshore	50	355		0.082	0.260	1.300	0.012	0.002		0.350	0.005	0.039	0.028	87.0		
7.0	5	Sumitomo	1993			30	460		0.070	0.230	1.510	0.007	0.001	0.300	0.480	0.010		0.015			
8.0	6	Nippon	1992	High HI	Offshore	50	460		0.060	0.150	1.290	0.006	0.003	0.870	0.670	0.008	0.033	0.008			
8.1	6	Nippon	1992	High HI	Offshore	32	460		0.060	0.150	1.290	0.006	0.003	0.870	0.670	0.008	0.033	0.008			
9.0	6	Nippon	1992	High HI	Offshore	50	420		0.060	0.170	1.560	0.005	0.003	0.360	0.330	0.010	0.032	0.008			
10.0	6	Nippon	1992	High HI	Offshore	50	355		0.060	0.140	1.480	0.003	0.003	0.290	0.330	0.009	0.033	0.006			
10.1	6	Nippon	1992	High HI	Offshore	32	355		0.060	0.140	1.480	0.003	0.003	0.290	0.330	0.009	0.033	0.006			
11.0	6	Nippon	1992	High HI	Offshore	50	500		0.080	0.130	1.590	0.004	0.003	0.550	0.770	0.008	0.033	0.011			
12.0	7	Kawasaki	1988	API 2W60	Offshore	150	414	517	0.080	0.390	1.540	0.007	0.003	0.190	0.310	0.019	0.023		27.0		
13.0	8	Hyundai	1988	TMCP	Ship																
14.0	9	Res. Lab	1990			50	420		0.050	0.270	1.520	0.014	0.001		0.470	0.016	0.020	0.007	50.0		0.1
15.0	10	CCG Study	1990	NKK	Ship	20	440	500	0.080	0.340	1.690	0.008	0.005	0.390	0.420	0.009	0.060	0.007	27.0		
16.0	10	CCG Study	1990	NKK	Ship	40	440	500	0.090	0.350	1.640	0.008	0.005	0.390	0.410	0.009	0.060	0.007	27.0		
17.0	10	CCG Study	1990	Nippon	Ship	20	440	500	0.080	0.190	1.680	0.012	0.005	0.330	0.410	0.013	0.044	0.009	39.0		
18.0	10	CCG Study	1990	Nippon	Ship	40	440	500	0.080	0.190	1.670	0.012	0.005	0.340	0.410	0.013	0.045	0.009	37.0		
19.0	10	CCG Study	1990	Kawasaki	Ship	20	440	500	0.110	0.180	1.700	0.010	0.005	0.180	0.820	0.027	0.040	0.006	27.0		
20.0	10	CCG Study	1990	Kawasaki	Ship	40	440	500	0.130	0.180	1.550	0.010	0.005	0.180	0.760	0.025	0.042	0.006	24.0		
21.0	10	CCG Study	1990	Sumitomo	Ship	20	440	500	0.090	0.260	1.590	0.008	0.005	0.270	0.380	0.013	0.039	0.011	27.0		
22.0	10	CCG Study	1990	Sumitomo	Ship	40	440	500	0.090	0.260	1.540	0.008	0.005	0.260	0.410	0.012	0.088	0.010	27.0		
23.0	11	Kawasaki	1989	DQ,T@550	Offshore	50	500	570	0.100	0.150	1.500	0.004	0.002	0.260	0.490	0.030	0.037	0.008	38.0	0.0	
24.0	12(55)	Kawasaki		DQ?	Offshore	30	490	588	0.095	0.290	1.340	0.007	0.002	0.260	0.270	0.018	0.027	yes	31.0	yes	
25.0	13	Kawasaki	1986	TMCP,MACS	Offshore	56	460		0.010	0.390	1.550	0.008	0.004	0.150	0.140	0.027	0.038	0.011	28.0		
26.0	14	Kawasaki	1992	TMCP,MACS	Offshore	32	420		0.070	0.180	1.330	0.005	0.001	0.240	0.680	0.016	0.030	0.009	26.0	0.0	
27.0	15	Kawasaki	1987	MCP,MACS (B	Offshore	40	430		0.080	0.240	1.360	0.009	0.002	0.140	0.150	0.019	0.029		32.0		
28.0	15	Kawasaki	1987	MCP,MACS (A	Offshore	40	430		0.110	0.340	1.420	0.010	0.003	0.010	0.020	0.017	0.024		33.0		
29.0	16	Kawasaki	1987	TMCP (A)	Ship	25	390	530	0.140	0.330	1.200	0.013	0.002	0.000		0.014	0.031	yes	31.0	yes	
30.0	16	Kawasaki	1987	TMCP (A)	Ship	30	390	530	0.140	0.330	1.200	0.013	0.002	0.000		0.014	0.031	yes	31.0	yes	
31.0	16	Kawasaki	1987	TMCP (E)	Ship	25	390	530	0.100	0.330	1.430	0.012	0.002			0.015	0.033	yes	36.0	yes	
32.0	16	Kawasaki	1987	TMCP	Caisson Rig	30	415	550	0.070	0.220	1.350	0.009	0.002	0.140	0.130	0.017	0.028	yes	27.0	yes	
33.0	17	Sumitomo		TMCP	Ice Breaker	75	353	490	0.060	0.110	1.380	0.009	0.001	0.300	0.860	0.010		0.020			
34.0	18	Sumitomo	1986	TMCP (C)		50	355	500	0.050	0.120	1.310	0.015	0.001	0.010	0.610	0.015	0.028	0.006			
35.0	18	Sumitomo	1986	TMCP (F)		50	355	500	0.070	0.150	1.340	0.016	0.003	0.020	0.290	0.022	0.030	0.010			
36.0	19	Rautarukki	1993	TMCP	Ship/Icebr.	20	400	500	0.100	0.240	1.330	0.015	0.001		0.030	0.020					
37.1	19	Rautarukki	1993	TMCP	Ship/Icebr.	40	400	500	0.060	0.220	1.480	0.011	0.002		0.040	0.030					
37.2	19	Rautarukki	1993	TMCP	Ship/Icebr.	50	400	500													
38.0	19	Rautarukki	1993	TMCP	Ship/Icebr.	60	390	450	0.070	0.260	1.520	0.012	0.004		0.210	0.040					
39.0	19	Rautarukki	1993	TMCP	Ship/Icebr.	40	480	570	0.070	0.140	1.480	0.011	0.003		0.760	0.030					
39.1	19	Rautarukki	1993	TMCP	Ship/Icebr.	20	480	570	0.070	0.140	1.480	0.011	0.003		0.760	0.030					
40.0	20	Mitsubishi			Ship	25 to 30	400	540	0.110	0.270	1.420	0.012	0.003			0.013		0.011			

41.0	1 (54)	Mitsubishi			Arctic Struct	60	400	530	0.070	0.110	1.450	0.010	0.001	0.260	0.730	0.012	0.035	yes	25.0	yes			
42.0	22	TS Indust. (Fr.)		TMCP API 2WGr60		40	414	517	0.084	0.290	1.510	0.007	0.001		0.390	0.015	0.028	0.011	40.0				
42.1	22	TS Indust. (Fr.)		TMCP API 2WGr60		20	414	517	0.084	0.290	1.510	0.007	0.001		0.390	0.015	0.028	0.011	40.0				
43.0	22	TS Indust. (Fr.)		TMCP API 2WGr60		60	414	517	0.084	0.290	1.510	0.007	0.001		0.390	0.015	0.028	0.011	40.0				
44.0	23	TWI	1987	Steel G		50	340	460	0.070	0.250	1.480	0.008	0.003	0.160	0.160	0.015	0.025	0.008	31.0				
45.0	23	TWI	1987	Steel F		50	340	460	0.080	0.230	1.450	0.010	0.003		0.020	0.010	0.031	0.006	37.0				
46.0	24	GTS	1995		Ship	25	355	490	0.100	0.280	1.490	0.014	0.002	0.010	0.020	0.030	0.023	0.010	60.0				
47.0	24	GTS	1995	TMR	Ship	25	355	490	0.100	0.280	1.510	0.012	0.002	0.010	0.020	0.030	0.023	0.010	50.0				
48.0	24	GTS	1995	TMR	Ship	25	355	490	0.100	0.290	1.510	0.015	0.002	0.010	0.020	0.030	0.024	0.010	60.0				
49.0	24	GTS	1995		Ship	25	355	490	0.100	0.290	1.520	0.013	0.002	0.070	0.020	0.030	0.023	0.010	50.0				
50.0	24	GTS	1995	TMCP	Ship	50	355	490	0.100	0.290	1.520	0.016	0.002	0.010	0.020	0.030	0.024	0.010	50.0				
51.0	24	GTS	1995	TMCP	Ship	50	355	490	0.100	0.290	1.520	0.015	0.002	0.010	0.020	0.030	0.024	0.010	50.0				
52.0	24	GTS	1995	TMCP	Ship	50	355	490	0.100	0.300	1.550	0.013	0.002	0.010	0.020	0.030	0.024	0.010	50.0				
53.0	24	GTS	1995	TMCP	Ship	50	355	490	0.100	0.300	1.560	0.012	0.001	0.010	0.020	0.030	0.026	0.010	60.0				
54.0	25	Hitachi	1985	Mod EH36	Barge	30	355	490	0.080	0.270	1.400	0.011	0.002	0.190	0.230	0.015	0.022						
55.0	25	Hitachi	1985	Mod EH36	Barge	70	355	490	0.070	0.350	1.470	0.007	0.002	0.150	0.140	0.020	0.023						
56.0	25	Hitachi	1985	Mod EH36		22	355	490	0.080	0.210	1.470	0.011	0.001				0.023						
57.0	25	Hitachi	1985	Mod EH36	Ship	45	355	490	0.070	0.220	1.350	0.009	0.002	0.140	0.130	0.017	0.028						
58.0	25	Hitachi	1985	Mod EH36		22	355	490	0.080	0.260	1.340	0.009	0.002			0.017	0.024						
59.0	26	Cranfield	1989	CLC 50E Nippon		50	340	460	0.070	0.140	1.300	0.004	0.001	0.120	0.180	0.060	0.026	0.010	30.0				
60.0	26	Cranfield	1989	OLAC 55f NKK		32	430	550	0.070	0.340	1.590	0.010	0.001	0.260	0.450	0.010							
61.0	26	Cranfield	1989	OLAC L361 mod		60	340	490	0.080	0.290	1.480	0.008	0.001	0.020			0.058	0.010	30.0				
62.0	27	NKK	1990	Steel B		50	415	550	0.082	0.320	1.580	0.008	0.001	0.260	0.450	0.008	0.004	0.004	30.0				
63.0	27	NKK	1990	Steel A		30	415	550	0.084	0.320	1.570	0.008	0.001	0.260	0.450	0.008	0.046	0.004	35.0				
64.0	28	NKK	1988		Arctic Marine	40	355	490	0.060	0.300	1.330	0.010	0.001	0.220	0.720		0.059	0.008	33.0				
64.1	28	NKK	1988		Arctic Marine	12	355	490	0.060	0.320	1.330	0.010	0.001	0.220	0.720		0.058	0.008	35.0				
65.0	29	Nippon	1994	Steel A		20	440	550	0.075	0.180	1.590	0.009	0.003	0.350	0.430	0.015	0.035	0.010					
66.0	29	Nippon	1994	Steel B		50	440	550	0.072	0.180	1.590	0.009	0.004	0.360	0.430	0.016	0.035	0.010					
67.0	29	Nippon	1994	Steel D		40	440	550	0.073	0.180	1.580	0.009	0.004	0.340	0.410	0.015	0.039	0.011					
68.0	29	Nippon	1994	Steel C		50	355	490	0.070	0.270	1.400	0.005	0.002	0.310	0.360		0.030	0.011					
69.0	29	Nippon	1994	Steel E		70	355	490	0.070	0.200	1.370	0.006	0.001	0.320	0.740		0.038	0.010					
69.1	29	Nippon	1994	Steel A		38	355	490	0.090	0.300	1.360	0.004	0.002				0.034	0.012					
69.2	29	Nippon	1994	Steel B		51	355	490	0.090	0.220	1.470	0.008	0.002			0.016	0.034	0.010					
69.3	29	Nippon	1994	Steel D		38	355	490	0.070	0.270	1.380	0.004	0.002	0.300	0.380		0.029	0.006					
69.4	29	Nippon	1994	Steel F		75	355	490	0.080	0.250	1.290	0.006	0.002	0.480	0.720		0.037	0.008					
70.0	30	Kobe	1988			30	460	570	0.030	0.240	1.450	0.007	0.002	0.520	0.470	0.041	0.027						
71.0	30	Kobe	1988			30	420	530	0.040	0.190	1.440	0.011	0.003	0.240	0.410	0.025	0.034	0.014					
72.0	31	Norske Hydro	1988	Nippon Steel		50	320	460	0.080	0.150	1.400	0.005	0.002	0.150	0.250	0.010	0.025	0.010	30.0				
73.0	31	Norske Hydro	1988	Nippon Steel		90	310	460	0.080	0.150	1.400	0.005	0.002	0.150	0.370	0.010	0.025	0.010	30.0				
74.0	31	Norske Hydro	1988	Nippon Steel		50	420		0.080	0.160	1.570	0.005	0.002	0.210	0.250	0.011	0.001	0.011	20.0				
75.0	32	DTRC				38			0.030	0.240	0.940			1.100	0.480	0.039		0.015	20.0				
76.0	34	GKSS	1994			20	450		0.090	0.340	1.340	0.013	0.001			0.031	0.044		40.0				
77.0	35	CSM, Italy		Steel B		50		510	0.059	0.230	1.610	0.010	0.004		0.350	0.024	0.022	0.029	98.0				
78.0	35	CSM, Italy		Steel A		50		510	0.069	0.330	1.560	0.016	0.004		0.360	0.002	0.008	0.013	92.0				
79.0	36	University, WG	1990			20	460		0.100	0.200	1.490	0.013	0.003			0.035	0.021	0.008		0.1			
80.0	36	University, WG	1990			35			0.100	0.200	1.490	0.013	0.003			0.035	0.021	0.008					
81.0	37	University, WG	1990			35			0.090	0.310	1.500	0.018	0.003			0.048	0.035	0.020	69.0	0.1			
82.0	38	Shell	1988		Offshore	50	340	460	0.110	0.300	1.540	0.007	0.002	0.240	0.225	0.020	0.028	0.010	20.0				

209

83.0	39	Nippon	1988			100	310	460	0.080	0.150	1.530	0.005	0.001	0.240	0.450	0.011	0.041	0.011			
84.0	40	NKK	1989	API2W Gr 50		89	345		0.080	0.300	1.540	0.004	0.001	0.300	0.460	0.012		0.007	40.0		
85.0	41	Sumitomo	1989	Steel A2		38			0.060	0.150	1.410	0.007	0.003	0.130	0.430		0.004	0.009	46.0		
86.0	41	Sumitomo	1989	Steel A3		38			0.080	0.140	1.500	0.009	0.002			0.007	0.004	0.009	44.0		
87.0	42	Kawasaki	1989			50			0.120	0.300	1.450	0.005	0.002	0.300	0.300	0.015	0.028				
88.0	43	Kawasaki			Arctic offshor	38	414	551	0.070	0.260	1.350	0.011	0.003	0.140	0.140	0.016	0.030	0.007	26.0	0.0	
89.0	44	Nippon	1987			83			0.080	0.290	1.540	0.003	0.001	0.330	0.460	0.010					
89.1	44	Nippon	1987			100			0.100	0.420	1.560	0.006	0.001	0.190	0.290	0.030					
90.0	45	Fleet Tech.	1986	Macs		50	355	490	0.070	0.260	1.320	0.006	0.002	0.010	0.020	0.017	0.034	0.020	31.0		
91.0	46	CCG	1995	MACS	Ship	40	440	500	0.110	0.180	1.550	0.010	0.004	0.180	0.680	0.027	0.040	0.006	25.0		
92.1	47	Italy	1991		Offshore	50			0.070	0.320	1.560	0.017	0.004		0.330	0.003	0.008	0.013	94.0		
92.2	47	Italy	1991		Offshore	16			0.070	0.320	1.560	0.017	0.004		0.330	0.003	0.008	0.013	94.0		
92.3	47	Italy	1991		Offshore	32			0.070	0.320	1.560	0.017	0.004		0.330	0.003	0.008	0.013	94.0		
92.4	47	Italy	1991		Offshore	80			0.070	0.320	1.560	0.017	0.004		0.330	0.003	0.008	0.013	94.0		
93.1	47	Italy	1991		Offshore	16			0.060	0.230	1.610	0.010	0.004		0.350	0.024	0.022	0.029	98.0		
93.2	47	Italy	1991		Offshore	32			0.060	0.230	1.610	0.010	0.004		0.350	0.024	0.022	0.029	98.0		
93.3	47	Italy	1991		Offshore	80			0.060	0.230	1.610	0.010	0.004		0.350	0.024	0.022	0.029	98.0		
93.4	47	Italy	1991		Offshore	50			0.060	0.230	1.610	0.010	0.004		0.350	0.024	0.022	0.029	98.0		
94.0	48	TWI	1991	TMCP		25	500		0.040	0.240	1.450	0.007	0.002	0.530	0.510	0.034	0.036	0.010	50.0		
95.0	48	TWI	1991	TMCP		50	500		0.100	0.160	1.500	0.004	0.002	0.250	0.500	0.032	0.038	0.005	30.0		
96.0	48	TWI	1991	DQT		20	500		0.070	0.290	1.470	0.017	0.002	0.010	0.030	0.028	0.034	<.002	50.0		0.0
97.0	49	GTS	1993			50	430	510	0.090	0.250	1.550	0.011	0.005		0.250	0.020					0.0
98.0	50	NKK	1987	Steel D		30	460	570	0.036	0.250	1.280	0.007	0.004	1.090	0.570	0.012	0.030	0.011	35.0		
99.0	50	NKK	1987	Steel E		75	460	570	0.030	0.240	1.480	0.004	0.004	1.050	0.590	0.010	0.020	0.009	24.0		
100.0	51	Kawasaki	1993	Steel A		102	414	517	0.080	0.180	1.530	0.004	0.001	0.190	0.400	0.024	0.029		36.0		
101.0	51	Kawasaki	1993	Steel B		60	400	530	0.070	0.110	1.450	0.010	0.001	0.260	0.730	0.012	0.035		25.0		
102.0	51	Kawasaki	1993	Steel C		50	500	570	0.100	0.150	1.500	0.004	0.002	0.260	0.490	0.030	0.037		38.0		
103.0	52	Cranfield	1991	Nippon		50			0.090	0.100	1.550	0.007	0.004	0.550	0.750	0.009	0.001	0.017	38.0		
104.0	52	Cranfield	1989	Kobe		30			0.040	0.220	1.520	0.005	0.003	0.600	0.490						
105.0	52	Cranfield	1989	NKK		50			0.070	0.340	1.590	0.010	0.001	0.260	0.450	0.010					
107.0	12	Mitsubishi		Max		30	470	600	0.096	0.290	1.330	0.007	0.002	0.250	0.260	0.017	0.027		31.0		
108.0	53	NKK	1993		offshore	120	315	460	0.080	0.300	1.540	0.004	0.002	0.290	0.430	0.009	0.029	0.006	35.0		
109.0	54	NKK/Lloyds	1986/87		offshore	50	340	460	0.070	0.290	1.550	0.005	0.001	0.190	0.230		0.048	0.006	30.0		
110.0	54	NKK/Lloyds	1986/87		offshore	100	325	460	0.080	0.150	1.550	0.005	0.001	0.250	0.440	0.011	0.041	0.011	40.0		
111.0	55	NKK	1990		offshore	25	355	490	0.070	0.290	1.430	0.015	0.001	0.180	0.390		0.055	0.012	31.0		
112.0	55	NKK	1990		offshore	32	355	490	0.070	0.300	1.450	0.018	0.002	0.190	0.360		0.059	0.010	25.0		
113.0	55	NKK	1990		offshore	32	355	490	0.080	0.290	1.420	0.015	0.001	0.190	0.340		0.057	0.004	17.0		
114.0	55	NKK	1990		offshore	34	355	490	0.070	0.280	1.480	0.021	0.001	0.200	0.350		0.053	0.010	17.0		
115.0	55	NKK	1990		offshore	40	355	490	0.080	0.300	1.480	0.016	0.001	0.200	0.350		0.059	0.010	24.0		
116.0	55	NKK	1990		offshore	50	355	490	0.070	0.300	1.490	0.022	0.001	0.210	0.350		0.054	0.011	15.0		
117.0	55	NKK	1990		offshore	75	340	490	0.080	0.310	1.480	0.013	0.001	0.220	0.320		0.065	0.007	26.0		
118.0	56	NKK	1990		offshore	50	340	460	0.080	0.270	1.450	0.011	0.001	0.180	0.330		0.057	0.007	38.0		
119.0	56	NKK	1990		offshore	100	325	490	0.090	0.290	1.480	0.009	0.001	0.200	0.350		0.051	0.006	32.0		
120.0	57	Cranfield	1994	TS TFK 460T	offshore	40	460		0.090	0.300	1.540	0.009	0.002	0.010	0.380	0.017	0.028	0.007			0.1
121.0	57	Cranfield	1994	460 TiO	offshore	50	460		0.090	0.100	1.550	0.007	0.004	0.550	0.750	0.009	0.001	0.017			0.0
122.0	58	Sumitomo	1995		offshore	102	345	448	0.060		1.440										
123.0	58	Sumitomo	1995		offshore	76	441	517	0.060		1.440										

SHEET 2 BASE METAL TENSILE DATA

BASE MATERIAL TENSILE DATA

Record	T,L	Location depth fraction	Yield	Tensile	Thickness	Target Yield	Target Tensile
1.0	L	0.25	439	535	100	414	517
1.0	L	0.50	428	530	100	414	517
1.0	T	0.25	451	556	100	414	517
1.0	T	0.50	420	528	100	414	517
1.0	T	0.00	467	584	100	414	517
2.0	L	0.25	504	606	50	500	--
2.0	T	0.25	503	607	50	500	--
3.0			487	580	50	420	520
5.0	T	full	435	537	50	355	--
5.0	L	full	428	534	50	355	--
6.0	T	full	380	490	50	355	--
6.0	L	ful	370	480	50	355	--
7.0		full	467	557	30	460	--
8.0	L	0.25	560	578	50	460	--
8.0	T	0.25	567	585	50	460	--
8.1	L	full	569	602	32	460	--
8.1	T	full	553	615	32	460	--
9.0	L	0.25	433	523	50	420	--
9.0	T	0.25	468	539	50	420	--
10.0	L	0.25	420	494	50	355	--
10.0	T	0.25	413	499	50	355	--
10.1	L	full	434	485	32	355	--
10.1	T	full	441	511	32	355	--
11.0	T	0.25	528	573	50	500	--
12.0	T	0.25	431	519	150	414	517
12.0	T	0.50	416	519	150	414	517
14.0			470	550	50	420	--
15.0	L		502	588	20	440	500
15.0	L		505	590	20	440	500
15.0	L		508	588	20	440	500
16.0	L		475	573	40	440	500
16.0	L		446	575	40	440	500
16.0	L		469	570	40	440	500
17.0	L		485	564	20	440	500
17.0	L		484	564	20	440	500
17.0	L		478	568	20	440	500
18.0	L		487	561	40	440	500
18.0	L		475	561	40	440	500
18.0	L		475	562	40	440	500
19.0	L		505	570	20	440	500
19.0	L		504	572	20	440	500
19.0	L		497	568	20	440	500
20.0	L		453	559	40	440	500
20.0	L		458	566	40	440	500
20.0	L		458	569	40	440	500
21.0	L		470	543	20	440	500

21.0	L		478	542	20	440	500
21.0	L		477	558	20	440	500
22.0	L		470	570	40	440	500
22.0	L		466	566	40	440	500
22.0	L		487	582	40	440	500
23.0	L	0.25	515	591	50	500	570
23.0	T	0.25	530	603	50	500	570
24.0	T	0.25	529	637	30	490	588
24.0	T	0.50	519	637	30	490	588
24.0	L	0.50	510	637	30	490	588
24.0	L	0.25	510	637	30	490	588
25.0	T	0.25	488	597	56	460	--
26.0			481	572	32	420	--
27.0	T	0.25	468	559	40	430	--
27.0	T	0.50	471	556	40	430	--
27.0	L	0.25	457	554	40	430	--
27.0	L	0.50	470	551	40	430	--
28.0	T	0.25	457	569	40	430	--
28.0	T	0.50	460	569	40	430	--
28.0	L	0.25	457	565	40	430	--
28.0	L	0.50	447	561	40	430	--
29.0	L	0.25	441	569	25	390	530
29.0	L	0.50	436	569	25	390	530
29.0	T	0.25	461	579	25	390	530
29.0	T	0.50	456	579	25	390	530
30.0	T	0.25	456	569	30	390	530
30.0	T	0.50	446	569	30	390	530
30.0	L	0.25	436	564	30	390	530
30.0	L	0.50	446	564	30	390	530
31.0	L	0.25	441	549	25	390	530
31.0	L	0.50	441	549	25	390	530
31.0	T	0.25	451	554	25	390	530
31.0	T	0.50	451	549	25	390	530
32.0	L	0.25	451	564	30	415	550
32.0	L	0.50	451	559	30	415	550
32.0	T	0.25	481	569	30	415	550
32.0	T	0.50	470	559	30	415	550
33.0	T	0.25	379	534	75	353	490
33.0	T	0.50	370	529	75	353	490
34.0	T	full	392	548	50	355	500
35.0	T	0.25	443	545	50	355	500
35.0	L		394	558	50	355	500
36.0			470	560	20	400	500
37.1			470	560	40	400	500
37.2			450	560	50	400	500
38.0			450	560	60	390	450
39.0			530	640	40	480	570
39.1			530	640	20	480	570
41.0	L	0.25	480	539	60	400	530
41.0	L	0.50	475	549	60	400	530
41.0	T	0.25	495	549	60	400	530

41.0	T	0.50	485	554	60	400	530
42.1			471	550	20	414	517
42.0			448	545	40	414	517
43.0			425	545	60	414	517
44.0			414	555	50	340	460
45.0			415	506	50	340	460
46.0	T	0.25	493	564	25	355	490
46.0	L	0.25	435	528	25	355	490
47.0	T	0.25	487	565	25	355	490
47.0	L	0.25	416	505	25	355	490
48.0	T	0.25	470	552	25	355	490
48.0	L	0.25	399	491	25	355	490
49.0	T	0.25	487	567	25	355	490
49.0	L	0.25	427	520	25	355	490
50.0	T	0.25	407	533	50	355	490
50.0	L	0.25	408	531	50	355	490
51.0	T	0.25	428	549	50	355	490
51.0	L	0.25	402	536	50	355	490
52.0	T	0.25	429	555	50	355	490
52.0	L	0.25	399	527	50	355	490
53.0	T	0.25	400	532	50	355	490
53.0	L	0.25	414	530	50	355	490
54.0	T		370	570	30	355	490
56.0	T		450	520	22	355	490
57.0			440	540	45	355	490
58.0			460	530	22	355	490
62.0	L	0.25	475	565	50	415	550
62.0	T	0.25	484	574	50	415	550
62.0	L	0.50	450	562	50	415	550
62.0	T	0.50	471	572	50	415	550
63.0	T	0.25	529	625	30	415	550
63.0	L	0.25	501	606	30	415	550
63.0	T	0.50	511	623	30	415	550
63.0	L	0.50	513	607	30	415	550
64.0	L		417	512	40	355	490
64.0	T		417	516	40	355	490
64.1	L		391	520	12	355	490
64.1	T		393	525	12	355	490
65.0	L	full	494	563	20	440	550
65.0	T	full	490	578	20	440	550
66.0	L	full	488	566	50	440	550
66.0	T	full	500	577	50	440	550
66.0	L	0.25	499	551	50	440	550
66.0	T	0.25	509	570	50	440	550
66.0	L	0.50	468	553	50	440	550
66.0	T	0.50	490	571	50	440	550
67.0	L	full	513	568	40	440	550
67.0	T	full	517	599	40	440	550
67.0	L	0.25	487	578	40	440	550
67.0	T	0.25	506	592	40	440	550
67.0	L	0.50	481	571	40	440	550

67.0	T	0.50	502	592	40	440	550
68.0	L	0.25	408	502	50	355	490
68.0	T	0.25	418	518	50	355	490
68.0	L	0.50	382	498	50	355	490
68.0	T	0.50	394	507	50	355	490
69.0	L	0.25	436	508	70	355	490
69.0	T	0.25	449	519	70	355	490
69.0	L	0.50	400	494	70	355	490
69.0	T	0.50	410	506	70	355	490
69.1	L	0.25	402	500	38	355	490
69.1	T	0.25	412	510	38	355	490
69.2	L	0.25	402	529	51	355	490
69.2	T	0.25	422	539	51	355	490
69.3	L	full	418	499	38	355	490
69.3	T	full	438	511	38	355	490
69.4	L	0.25	422	510	75	355	490
69.4	T	0.25	441	519	75	355	490
69.4	L	0.50	392	490	75	355	490
69.4	T	0.50	402	490	75	355	490
70.0	T	0.25	512	591	30	460	570
71.0	T	0.25	450	559	30	420	530
72.0			390		50	320	460
73.0			380		90	310	460
74.0			455	565	50	420	--
75.0	T		572	620	38	--	--
75.0	L		572	607	38	--	--
76.0	L		446	544	20	450	--
76.0	T		469	563	20	450	--
77.0	T		435	537	50	--	510
77.0	L		428	525	50	--	510
78.0	T		418	503	50	--	510
78.0	L		395	507	50	--	510
79.0			445	525	20	460	--
80.0			420	540	35	--	--
81.0	L		470	580	35	--	--
82.0	T	full	514	615	50	340	460
83.0	T	0.25	365	478	100	310	460
83.0	T	0.50	363	472	100	310	460
84.0	T	0.25	469	546	89	345	--
84.0	T	0.50	444	529	89	345	--
87.0	T		470	568	50	--	--
88.0	L	0.25	461	568	38	414	551
88.0	L	0.50	451	568	38	414	551
88.0	T	0.25	480	578	38	414	551
88.0	T	0.50	480	578	38	414	551
89.0	L	0.25	391	518	83	--	--
89.0	L	0.50	376	505	83	--	--
89.1	L	0.25	369	482	100	--	--
91.0			485	577	40	440	500
92.1	T	full	418	503	50	--	--
92.1	L	full	395	507	50	--	--

92.2	T	full	441	512	16	--	--
92.2	L	full	409	495	16	--	--
92.3	T	full	423	518	32	--	--
92.3	L	full	407	567	32	--	--
92.4	T	full	379	490	80	--	--
93.1	T	full	451	512	16	--	--
93.1	L	full	426	496	16	--	--
93.2	T	full	442	530	32	--	--
93.2	L	full	434	519	32	--	--
93.3	T	full	375	484	80	--	--
93.4	T	full	435	537	50	--	--
93.4	L	full	428	525	50	--	--
94.0			479	568	25	500	--
95.0			516	593	50	500	--
96.0			496	598	20	500	--
97.0			460	555	50	430	510
98.0	L	0.25	560	600	30	460	570
98.0	L	0.50	550	595	30	460	570
99.0	L	0.25	510	595	75	460	570
99.0	L	0.50	500	595	75	460	570
100.0	L	0.25	439	535	102	414	517
100.0	T	0.25	451	556	102	414	517
100.0	L	0.50	428	530	102	414	517
100.0	T	0.50	420	528	102	414	517
101.0	L	0.25	480	539	60	400	530
101.0	T	0.25	480	549	60	400	530
101.0	L	0.50	495	549	60	400	530
101.0	T	0.50	485	554	60	400	530
102.0	L	0.25	515	591	50	500	570
102.0	T	0.25	530	603	50	500	570
102.0	L	0.50	504	596	50	500	570
102.0	T	0.50	523	589	50	500	570
107.0	L	0.25	520	650	30	470	600
107.0	L	0.50	520	650	30	470	600
107.0	T	0.25	540	650	30	470	600
107.0	T	0.50	535	650	30	470	600
108.0	L	0.25	409	501	120	315	460
108.0	T	0.25	410	504	120	315	460
108.0	L	0.50	355	474	120	315	460
108.0	T	0.50	356	474	120	315	460
109.0	L	0.25	412	480	50	340	460
109.0	T	0.25	402	480	50	340	460
109.0	L	0.50	410	471	50	340	460
109.0	T	0.50	381	480	50	340	460
110.0	L	0.25	366	473	100	325	460
110.0	T	0.25	369	480	100	325	460
110.0	L	0.50	358	474	100	325	460
110.0	T	0.50	364	478	100	325	460
111.0	T	full	431	523	25	355	490
111.0	L	full	414	509	25	355	490
112.0	T	full	417	519	32	355	490

112.0	L	full	392	499	32	355	490
113.0	T	full	417	511	32	355	490
113.0	L	full	401	496	32	355	490
114.0	T	full	402	505	34	355	490
114.0	L	full	388	495	34	355	490
115.0	L	0.25	423	499	40	355	490
115.0	T	0.25	431	509	40	355	490
115.0	L	0.50	414	506	40	355	490
115.0	T	0.50	420	510	40	355	490
116.0	L	0.25	420	530	50	355	490
116.0	T	0.25	428	535	50	355	490
116.0	L	0.50	400	527	50	355	490
116.0	T	0.50	409	529	50	355	490
117.0	L	0.25	386	504	75	340	490
117.0	T	0.25	373	509	75	340	490
117.0	L	0.50	366	501	75	340	490
117.0	T	0.50	374	513	75	340	490
118.0	L	0.25	417	519	50	340	460
118.0	T	0.25	416	525	50	340	460
118.0	L	0.50	405	521	50	340	460
118.0	T	0.50	396	517	50	340	460
119.0	L	0.25	360	519	100	325	490
119.0	T	0.25	369	519	100	325	490
119.0	L	0.50	358	501	100	325	490
119.0	T	0.50	356	509	100	325	490
120.0			460			460	--
121.0			499	570		460	--
122.0	T		381	496	102	345	448
122.0	T		413	530	102	345	448
123.0	T		441	537	76	441	517
123.0	T		458	551	76	441	517

SHEET 3 BASE METAL TOUGHNESS DATA

Base Material Toughness

Record	T,L	Location depth fraction	Temp	CVN	FATT	NDTT	Kca test type	CTOD [mm]	Spec	Comments
1.0	L	0.25	-60	382	-73					
1.0	L	0.25	-80	130	-73					
1.0	L	0.50	-60	421	-86					
1.0	L	0.50	-80	397	-86					
1.0	T	0.25	-60	364	-92					
1.0	T	0.25	-80	277	-92					
1.0	T	0.50	-60	368	-84					
1.0	T	0.50	-80	292	-84					
1.0	T	0.00	-80	273	-99	-70				
1.0	T	0.00	-80	156	-92	-60				3% strain age
1.0	T	0.00	-80	305	-95	-45				5% strain age
1.0			-10					1.90		B x B spec.
3.0	L	0.25	-40	282						Avg. from prod.
3.0	T	0.25	-80	300	-95					
3.0	L	0.50	-40	196						Avg. from prod.
3.0	L	0.50	-80	200	-90					
3.0	T	0.50	-60	120	-60					
7.0			-50		-110			1.55		
8.0	L	0.25			-125					
8.0	T	0.25			-100					
8.1	L	0.25			-120					
8.1	T	0.25			-85					
9.0	L	0.25			-115					
9.0	T	0.25			-115					
10.0	L	0.25			-120					
10.0	T	0.25			-110					
10.1	L	0.25			-130					
10.1	T	0.25			-120					
11.0	T	0.25			-125					
12.0	T	0.25	-60	206	-100	-70				
12.0	T	0.50	-60	167	-70	-55				NDTT @ 0.5t
14.0			-72	47	-55					
15.0						-80				
16.0						-90				
17.0						-105				
18.0						-105				
19.0						-85				
20.0						-75				
21.0						-85				
22.0						-80				
23.0	L	0.25	-60	268	-105					
23.0	T	0.25	-60	214	-95					
24.0	L	0.25	-60	234	-125	-95				
24.0	L	0.25	-80	222						
24.0	L	0.50	-60	222	-97					
24.0	L	0.50	-80	165						
24.0	T	0.25	-60	154	-95					

24.0	T	0.25	-80	139					
24.0	T	0.50	-60	142	-75				
24.0	T	0.50	-80	93					
24.0	Z	0.50	-60	61	-41				
24.0	Z	0.50	-80	15					
24.0	T	0.25	-60	106	-69				5% strain age
24.0	T	0.25	-80	69					5% strain age
24.0			-40				1.20	B(=30)x2B	
24.0			-40				1.30	B(=30)x2B	
24.0			-60				0.40	B(=30)x2B	
24.0			-60				0.99	B(=30)x2B	
24.0			-80				0.16	B(=30)x2B	
24.0			-80				0.26	B(=30)x2B	
24.0	L		-41			374		500x500	Double tension
24.0	L		-56			295		500x500	Double tension
24.0	L		-67			171		500x500	Double tension
24.0	L		-99			72		500x500	Double tension
25.0	L	0.25	-60	165	-65				
25.0	L	0.25	-80	78					
25.0	L	0.50	-60	119	-75				
25.0	L	0.50	-80	121					
25.0	T	0.25	-60	145	-70				
25.0	T	0.25	-80	90					
25.0	T	0.50	-60	108	-60				
25.0	T	0.50	-80	64					
25.0	.		-10				1.33		
25.0			-10				1.35		
26.0		0.25	-60	380					
27.0	L	0.25	-60	279	-88				
27.0	L	0.25	-80	221					
27.0	L	0.50	-60	246	-80				
27.0	L	0.50	-80	130					
27.0	T	0.25	-60	208	-86				
27.0	T	0.25	-80	195					
27.0	T	0.50	-60	162	-75				
27.0	T	0.50	-80	85					
27.0	T	0.25	-60	178	-63				5% strain age
28.0	L	0.25	-60	210	-80				
28.0	L	0.25	-80	134					
28.0	L	0.50	-60	141	-71				
28.0	L	0.50	-80	99					
28.0	T	0.25	-60	112	-67				
28.0	T	0.25	-80	83					
28.0	T	0.50	-60	77	-47				
28.0	T	0.50	-80	56					
28.0	T	0.25	-60	54	-50				5% strain age
29.0	L	0.25	-60	219	-67				
29.0	L	0.25	-80	74					
29.0	L	0.50	-60	153	-64				
29.0	L	0.50	-80	72					
29.0	T	0.25	-60	171	-66				

29.0	T	0.25	-80	34						
29.0	T	0.50	-60	79	-46					
29.0	T	0.50	-80	33						
29.0	T	0.25	-60	58	-41					5% strain age
30.0			0				170	1.80		
30.0	L	0.25	-60	195	-73					
30.0	L	0.25	-80	129						
30.0	L	0.50	-60	113	-52					
30.0	L	0.50	-80	47						
30.0	T	0.25	-60	171	-76					
30.0	T	0.25	-80	123						
30.0	T	0.50	-60	103	-46					
30.0	T	0.50	-80	30						
30.0	T	0.25	-60	148	-68					5%strain age
31.0	L	0.25	-60	297	-113					
31.0	L	0.25	-80	302						
31.0	L	0.50	-60	306	-97					
31.0	L	0.50	-80	238						
31.0	T	0.25	-60	286	-103					
31.0	T	0.25	-80	227						
31.0	T	0.50	-60	233	-93					
31.0	T	0.50	-80	184						
31.0	T	0.25	-60	100	-72					5%strain age
31.0	T		-60					1.90		
31.0			-25				186			Double tension
31.0			-40				110			Double tension
32.0	L	0.25	-60	308	-114					
32.0	L	0.25	-80	293						
32.0	L	0.50	-60	298	-105					
32.0	L	0.50	-80	272						
32.0	T	0.25	-60	208	-100					
32.0	T	0.25	-80	171						
32.0	T	0.50	-60	200	-87					
32.0	T	0.50	-80	149						
32.0			-60				186	1.30		Double tension
32.0	T	0.25	-60	159	-71					5% strain age
33.0	T	0.25	-75	212	-103	-90				
33.0	T	0.50	-75	203	-88					
33.0	Z	0.50	-75	64	-48					
33.0		0.00				-95				
33.0			-50				180			Esso test
33.0			-40					3.62		quasi-static
33.0			-20					0.23		100 times faster
33.0			-20					0.50		100 times faster
34.0	T		-80	216	-100					
34.0	T		-60	245						
34.0	L		-80	331	-100					
34.0	L		-60	384						
34.0		0.50	-60					1.00	30x60mm	
34.0			-60				237			Double tension
35.0	T		-80	200	-98					

35.0	T		-60	250					
35.0	L		-80	253	-100				
35.0	L		-60	277					
35.0			-60				190		Double tension
35.0			-50				253		Double tension
36.0	L&T		-60	180					Prod. lot avg. (lo
37.1	L&T		-60	180					Prod lot CVN (m
37.2						-65			
38.0						-55			
39.0	L&T		-60	180		-50			Prod lot CVN (
39.1						-75			
40.0			-40				110		Double tension
41.0	L	0.25	-80	312	-114				
41.0	L	0.50	-80	305	-115				
41.0	T	0.25	-80	329	-114				
41.0	T	0.50	-80	249	-106				
41.0			-75					0.40	
41.0			-75					1.67	
41.0			-100					0.47	
41.0			-100					0.20	
42.0		0.00	-40	272					
42.0		0.50	-40	295					
42.1		0.50	-40	192					
43.0		0.00	-40	336					
43.0		0.50	-40	293					
43.0		0.00	-40	265					5% strain age
43.0		0.25	-40	240					5% strain age
44.0		0.00	-90	50					
44.0		0.50	-95	50					
45.0		0.00	-70	50					
45.0		0.50	-90	50					
46.0	T	0.00	-40	175		-85			
46.0	T	0.00	-60	124					
47.0	T	0.00	-40	128		-90			
47.0	T	0.00	-60	111					
48.0	T	0.00	-40	133		-85			
48.0	T	0.00	-60	107					
49.0	T	0.00	-40	177		-85			
49.0	T	0.00	-60	116					
50.0	T	0.25	-40	272		-75			
50.0	T	0.50	-40	266					
50.0	L	0.50	-40	282					
50.0	T	0.25	-80	232					
50.0	L	0.25	-80	245					
51.0	T	0.25	-40	256		-75			
51.0	T	0.50	-40	263					
51.0	L	0.50	-40	283					
51.0	T	0.25	-80	177					
51.0	L	0.25	-80	238					
52.0	T	0.25	-40	233		-75			
52.0	T	0.50	-40	266					

52.0	L	0.50	-40	276			
52.0	T	0.25	-80	216			
52.0	L	0.25	-80	189			
53.0	T	0.25	-40	267		-70	
53.0	T	0.50	-40	272			
53.0	L	0.50	-40	265			
53.0	T	0.25	-80	200			
53.0	L	0.25	-80	84			
54.0	T		-50	300			
55.0			-50	330			
56.0	T		-50	298			
57.0	T		-50	321			
58.0			-50	325			
59.0	T		-80	280			50% FATT, sim
59.0	L		-80	280			
60.0	T		-80	255			50% FATT, sim
60.0	T		-40	282			
61.0			-100	50			
61.0			-60	125			
61.0			-40	168			
62.0	L	0.25	-80	292	-122	-85	
62.0	T	0.25	-80	309	-121		
62.0	L	0.50	-80	311	-105		
62.0	T	0.50	-80	263	-100		
62.0	T	0.25	-60	270	-88		5% strain aged
63.0	L	0.25	-80	203	-153	-140	
63.0	T	0.25	-80	241	-155		
63.0	L	0.50	-80	252	-140		
63.0	T	0.50	-80	193	-126		
63.0	T	0.25	-60	214	-120		5% strain aged
64.0	L	0.25	-80	408	-122	-80	
64.0	T	0.25	-80	404	-115		
64.0	L	0.50	-80	402	-135		
64.0	T	0.50	-80	361	-110		
64.0	T	0.25	-80	367	-100		5% strain aged
64.1	L	0.50	-80	321	-124		
64.1	T	0.50	-80	272	-104		
65.0	L	0.25	-60	269	-129	-100	
65.0	T	0.25	-60	179	-100		
65.0	L	0.50	-60	252	-122		
65.0	T	0.50	-60	153	-101		
66.0	L	0.25	-60	307	-133	-95	
66.0	T	0.25	-60	230	-114		
66.0	L	0.50	-60	296	-113		
66.0	T	0.50	-60	158	-93		
66.0	L	0.25	-60	275	-110		strain aged
66.0	T	0.25	-60	190	-90		strain aged
67.0	L	0.25	-60	301	-127		
67.0	T	0.25	-60	185	-106		
67.0	L	0.50	-60	277	-112		
67.0	T	0.50	-60	163	-91		

68.0	L	0.25	-80	196	-104	-75			
68.0	T	0.25	-80	204	-90				
68.0	L	0.50	-80	189	-88				
68.0	T	0.50	-80	182	-84				
68.0			-40				196		
69.0	L	0.25	-80	364	-113	-90			
69.0	T	0.25	-80	335	-120				
69.0	L	0.50	-80	419	-115				
69.0	T	0.50	-80	375	-105				
70.0	T	0.25	-60	286	-102				
71.0	T	0.25	-60	274	-114				
70.0	T		-60					1.00	
71.0	T		-80					1.00	
72.0	T		-40	250					range 200 - 300
73.0	T		-40	250					range 200 - 300
74.0			-40	200					
75.0	T		-85	191					91J min
76.0	L		-60	210	-80				
76.0	T		-60	195	-68				
77.0	T	0.00	-40	355	-70				
77.0	T	0.50	-40	280	-60				
78.0	T	0.00	-40	318	-80				
78.0	T	0.50	-40	147	-40				
79.0			-125	27	-90				
80.0	T		-105	27	-80				
81.0			-74	50	-55				
82.0	T	0.00	-60	145		-60			70J min
82.0	T	0.50	-60	140					
82.0			-10					1.83	
82.0			-10					0.88	
82.0			-10					1.32	
83.0	T	0.00	-80	333		-65			
83.0	T	0.50	-80	205					
84.0	T	0.25	-40	277	-95	-90			
84.0	T	0.50	-40	244	-76	-60			
84.0			-50					>1	
88.0	L	0.25	-80	237	-130				
88.0	L	0.25	-60	247					
88.0	L	0.50	-60	230	-127				
88.0	L	0.50	-80	191					
88.0	T	0.25	-60	204	-100				
88.0	T	0.25	-80	172					
88.0	T	0.50	-60	129	-95				
88.0	T	0.50	-80	110					
89.0	L	0.25			-91				
89.0	L	0.50			-64				
92.1	T	0.00	-40	318	-80				
92.1	T	0.50	-40	147	-44				
92.2	T	0.00	-40	156					
92.2	L	0.00	-40	271					
92.3	T	0.00	-40	355					

92.3	T	0.50	-40	343		
92.4	T	0.50	-40	125		
92.4	T	0.00	-40	315		
92.4	L	0.50	-40	216		
92.4	L	0.00	-40	376		
93.4	T	0.00	-40	285	-70	
93.4	T	0.50	-40	250	-60	
93.1	T	0.00	-40	279		
93.1	L	0.00	-40	321		
93.2	T	0.00	-40	356		
93.2	T	0.50	-40	343		
93.3	T	0.50	-40	218		
93.3	T	0.00	-40	373		
93.3	L	0.50	-40	378		
93.3	L	0.00	-40	400		
94.0			-40	298		
95.0			-40	260		
96.0			-40	219		
97.0	T	0.25	-60	220		
98.0	L	0.25			-125	-70
98.0	L	0.50			-115	
98.0	T					-85
99.0	L	0.25			-96	
99.0	L	0.50			-80	
100.0	L	0.25	-80	130	-73	
100.0	L	0.25	-60	382		
100.0	T	0.25	-80	277	-92	
100.0	T	0.25	-60	364		
100.0	L	0.50	-80	397	-86	
100.0	L	0.50	-60	421		
100.0	T	0.50	-80	292	-84	
100.0	T	0.50	-60	368		
101.0	L	0.25	-80	312	-114	
101.0	L	0.25	-60	305		
101.0	T	0.25	-80	329	-114	
101.0	T	0.25	-60	315		
101.0	L	0.50	-80	213	-115	
101.0	L	0.50	-60	307		
101.0	T	0.50	-80	250	-106	
101.0	T	0.50	-60	295		
102.0	L	0.25	-80	213	-105	
102.0	L	0.25	-60	268		
102.0	T	0.25	-80	169	-95	
102.0	T	0.25	-60	214		
102.0	L	0.50	-80	101	-77	
102.0	L	0.50	-60	185		
102.0	T	0.50	-80	86	-68	
102.0	T	0.50	-60	143		
103.0	T	0.00	-80	140		
103.0	T	0.50	-50	145		
104.0	T		-60	205		

104.0	T		-80	195				
104.0	L		-60	285				
104.0	L		-80	208				
105.0	T		-60	120				
105.0	T		-80	112				
107.0			-40				1194	
108.0	L	0.25	-60	367	-87	-50		NDTT at T/4
108.0	T	0.25	-60	252	-86			
108.0	L	0.50	-60	378	-76			
108.0	T	0.50	-60	102	-51			
108.0	T	0.25	-60	133	-57			5% ,strain aged
109.0	L	0.25	-80	329	-87	-60		
109.0	T	0.25	-80	360	-86			
109.0	L	0.50	-80	323	-76	-80		NDTT at T/2
109.0	T	0.50	-80	292	-51			
110.0	L	0.25	-80	331	-87	-85		
110.0	T	0.25	-80	322	-86			
110.0	L	0.50	-80	263	-76	-55		NDTT at T/2
110.0	T	0.50	-80	181	-51			
111.0	T	0.25	-80	244	-111	-110		
111.0	L	0.25	-80	261	-130			
112.0	L	0.25	-80	328	-145	-105		
112.0	T	0.25	-80	315	-133			
112.0	L	0.50	-80	220	-130			
112.0	T	0.50	-80	190	-116			
113.0	L	0.25	-80	334	-144	-110		
113.0	T	0.25	-80	338	-139			
113.0	L	0.50	-80	334	-130			
113.0	T	0.50	-80	336	-112			
113.0	T	0.25			-112			5% strain age
114.0	L	0.25	-80	314	-130	-120		
114.0	T	0.25	-80	305	-128			
114.0	L	0.50	-80	196	-118			
114.0	T	0.50	-80	148	-111			
115.0	L	0.25	-80	346	-122	-70		
115.0	T	0.25	-80	361	-119			
115.0	L	0.50	-80	330	-128			
115.0	T	0.50	-80	263	-111			
115.0	T	0.25			-96			
116.0	L	0.25	-80	334	-125	-80		
116.0	T	0.25	-80	317	-115			
116.0	L	0.50	-80	295	-105			
116.0	T	0.50	-80	191	-90			
116.0	T	0.25			-104			
117.0	L	0.25	-80	304	-91			
117.0	T	0.25	-80	255	-88			
117.0	L	0.50	-80	124	-74			
117.0	T	0.50	-80	83	-69			
118.0	L	0.25	-60	317	-106	-80		
118.0	T	0.25	-60	310	-100			
118.0	L	0.50	-60	362	-95			

118.0	T	0.50	-60	263	-90		
118.0	T	0.25			-81		
119.0	L	0.25	-60	338	-78	-65	
119.0	T	0.25	-60	270	-72		
119.0	L	0.50	-60	287	-70		
119.0	T	0.50	-60	173	-65		
120.0	T	0.00	-40	260			
120.0	T	0.50	-40	110			
121.0	T	0.00	-40	180			
121.0	T	0.50	-40	130			
122.0		0.50			-89	-65	NDTT at surface
123.0		0.50			-97	-90	NDTT at Surfac

SHEET 4 WELD DESCRIPTIONS

WELD DESCRIPTION

Record	Thick	Shape
1.0	100	K
2.0	50	half K
3.0	50	K
4.0	50	K
5.0	50	K
6.0	50	K
7.0	30	K
8.0	50	K
8.1	32	X
9.0	50	K
10.0	50	K
10.1	32	X
11.0	50	K
12.0	150	K
13.0	25	single V
14.0	50	K
23.0	50	half K
24.0	30	half K
24.1	30	V
24.2	30	V
25.0	56	2/3 K
26.0	32	2/3 K
29.0	25	single V
30.0	30	single V
31.0	25	single V
32.0	30	single V
33.0	75	double V
34.0	50	K or half K
35.0	50	K
36.0	20	single V
37.1	40	double V
38.0	60	double V
39.0	40	double V
40.0	25	single V
41.0	60	K
42.0	40	half K
44.0	50	half K
45.0	50	half K
46.0	25	double V
47.0	25	square
52.0	50	double V
53.0	50	double V
54.0	30	single V
59.0	50	half K
60.0	32	half K
61.0	60	single V
62.0	50	half K
63.0	30	half K & X

64.0	40	K
64.1	12	double sided
65.0	20	X
66.0	50	K,X
67.0	40	K
68.0	50	K
70.0	30	single V
71.0	30	single V
72.0	50	K
73.0	90	K
74.0	38	
79.0	20	Y/HY
80.0	35	DY/DHY
82.0	50	K
83.0	100	half K
84.0	89	half K
85.0	38	K
86.0	38	K
87.0	50	half K
88.0	38	single V
89.0	83	K
89.1	100	Half K
90.0	50	K
91.0	40	square
92.0	50	K
93.0	50	K
94.0	25	Half K
95.0	50	Half K
96.0	20	Half K
98.0	30	half K
99.0	75	half K
100.0	102	K
101.0	60	K & X
102.0	50	half K
103.0	50	
104.0	30	half K
105.0	50	half K
107.0	30	half K & V
108.0	120	K
109.0	50	Half K
110.0	100	Half K
112.0	32	Half K
113.0	32	Half K, Double Vee
115.0	40	Half K, Double Vee
118.0	50	Narrow gap, K
120.0	40	half K
121.0	50	half K
122.0	102	K
123.0	76	K

SHEET 5 CROSS-WELD STRENGTH DATA

WELD STRENGTH DESCRIPTION

Record	HI	Yield	UTS	Specified UTS	Failure Location	Process	Comment
1.0	0.80		574		BM	SMAW	
1.0	3.00		575		BM	SAW	
1.0	4.50		566		BM	SAW	
2.0	4.50		690	638	BM	Tandem SAW	
9.0	4.00		592		HAZ	SAW	
10.0	4.00		551		HAZ	SAW	
10.1	20.50		516		HAZ		
12.0	4.70		518		BM	Tandem SAW	
24.0	5.00		624		BM	Tandem SAW	24.1
24.0	20.20		610			One side, 3 wire SAW	24.2
24.0	13.00		630			Two side, 3 wire SAW	
25.0	4.70	493	591		BM	SAW	
29.0	26.00		574			E6	
30.0	16.00		574			1 side SAW	
29.0	26.00		549			E6	6mm dia H
30.0	16.00		544			1 side SAW	6mm dia H
31.0	14.90		534			1 side SAW	
31.0	14.90		526			1 side SAW	6mm dia H
32.0	14.70		559			E6	
32.0	20.20		569			1 side SAW	
32.0	20.20		522			1 side SAW	6mm dia H
32.0	14.70		533			E6	6mm dia H
33.0	3.50		556			GMAW	
36.0	2.50	421	587		BM	SMAW	
36.0	2.00	465	595		BM	SAW	
37.1	2.50	481	577		BM	SMAW	
37.1	2.60	480	598		BM	SAW	
38.0	1.20	422	542		BM	SMAW	
38.0	1.20	407	533		BM	SMAW	
38.0	5.00	417	532		BM	SAW	
38.0	5.00	410	535		BM	SAW	
39.0	1.20	495	618		BM	SMAW	
39.0	1.20	477	617		BM	SMAW	
39.0	5.00	501	621		BM	SAW	
39.0	5.00	529	624		BM	SAW	
41.0	5.00		568		BM	SAW	30x60mm
41.0	19.00		588		BM	SAW	30x60mm
46.0	5.00		547		BM	Tandem SAW	
47.0	27.00		555		BM	EGW	failed outsi
52.0	1.20		552		BM	SMAW	failed outsi
53.0	3.00		522		BM	SAW	failed outsi
54.0	11.50		548		BM	EGW	
62.0	5.00		607		HAZ	SAW	
62.0	10.00		597		WM	SAW	
63.0	5.00		576		BM	SAW	
63.0	10.00		589		BM	SAW	
64.0	5.00		549		BM	SAW	
64.1	3.70		523		BM		

65.0	5.10	594	BM	
65.0	2.30	610	BM	
66.0	4.50	594	WM	SMAW
67.0	4.50	606	WM	
70.0	10.00	599		
71.0	5.00	566		
71.0	10.00	557		
71.0	20.00	549		
88.0	13.60	576	HAZ	2 pass SAW
88.0	14.00	564	HAZ	4 pass SAW
94.0	2.00	568	BM	
95.0	3.00	610	BM	
96.0	2.00	605	BM	
98.0	4.90	613	BM	
100.0	3.00	575	BM	SAW
100.0	4.50	566	BM	SAW
101.0	5.00	569	BM	SAW
101.0	19.30	588	BM	SAW
102.0	3.50	634	BM	SAW
102.0	4.50	623	BM	SAW
107.0	5.00	637	BM	SAW
107.0	20.00	610	BM	SAW
107.0	13.00	630	BM	SAW
108	4.50	532	BM	SAW
113	2.30	511	BM	SMAW
113	5.00	508	BM	SAW
115	2.30	502	BM	SMAW
115	5.00	500	BM	SAW
118	2.80	538	BM	
118	3.50	540	BM	
118	4.50	533	BM	

SHEET 6 HAZ TOUGHNESS DATA

WELD TOUGHNESS DESCRIPTION

Record	HI	Process	Notch Location w.r.t. FL	Temp	CVN Depth Fraction	Avg CVN	Min CVN	CTOD [mm]	CTOD Spec	Comments
1.0	0.80	SMAW	0	-50	0.25	342	193			
1.0	0.80	SMAW	0	-70	0.25	239	180			
1.0	0.80	SMAW	2	-50	0.25	227	192			
1.0	0.80	SMAW	2	-60	0.25	61	10			
1.0	0.80	SMAW	SC HAZ	-50	0.25	181	154			
1.0	0.80	SMAW	SC HAZ	-60	0.25	66	12			
1.0	0.80	SMAW	SC HAZ	-70	0.50	114	79			
1.0	0.80	SMAW	0	-70	0.50	207	158			
1.0	0.80	SMAW	0	-10				0.75	BxB	RP2Z, BS5762
1.0	0.80	SMAW	0	-10				1.10	BxB	RP2Z, BS5762
1.0	0.80	SMAW	0	-10				1.80	BxB	RP2Z, BS5762
1.0	0.80	SMAW	0	-10				1.60	BxB	RP2Z, BS5762
1.0	0.80	SMAW	0	-10				1.90	BxB	RP2Z, BS5762
1.0	0.80	SMAW	0	-10				1.90	BxB	RP2Z, BS5762
1.0	0.80	SMAW	0	-10				1.43	BxB	RP2Z, BS5762
1.0	0.80	SMAW	SC HAZ	-10				1.40	BxB	RP2Z, BS5762
1.0	0.80	SMAW	SC HAZ	-10				1.80	BxB	RP2Z, BS5762
1.0	3.00	SAW	0	-50	0.25	217	208			
1.0	3.00	SAW	2	-50	0.25	403	334			
1.0	3.00	SAW	SC HAZ	-50	0.25	214	170			
1.0	3.00	SAW	0	-60	0.25	300	299			
1.0	3.00	SAW	0	-70	0.25	62	6			
1.0	3.00	SAW	SC HAZ	-60	0.25	151	25			
1.0	3.00	SAW	2	-90	0.25	182	154			
1.0	3.00	SAW	0	-60	0.50	194	168			
1.0	3.00	SAW	0	-70	0.50	25	17			
1.0	3.00	SAW	SC HAZ	-60	0.50	80	59			
1.0	3.00	SAW	0	-10				0.61	BxB	67% GCHAZ
1.0	3.00	SAW	0	-10				1.78	BxB	> 16% GCHAZ
1.0	3.00	SAW	0	-10				1.90	BxB	> 16% GCHAZ
1.0	3.00	SAW	0	-10				1.80	BxB	> 16% GCHAZ
1.0	3.00	SAW	0	-10				1.90	BxB	> 16% GCHAZ
1.0	3.00	SAW	0	-10				1.80	BxB	> 16% GCHAZ
1.0	3.00	SAW	SC HAZ	-10				1.40	BxB	
1.0	3.00	SAW	SC HAZ	-10				1.65	BxB	
1.0	3.00	SAW	SC HAZ	-10				1.87	BxB	
1.0	3.00	SAW	WM	-10				1.45	BxB	
1.0	3.00	SAW	WM	-10				1.41	BxB	
1.0	4.50	SAW	0	-50	0.25	438	431			
1.0	4.50	SAW	2	-50	0.25	421	415			
1.0	4.50	SAW	SC HAZ	-50	0.25	422	413			
1.0	4.50	SAW	0	-60	0.25	321	315			
1.0	4.50	SAW	0	-80	0.25	204	87			
1.0	4.50	SAW	SC HAZ	-60	0.25	237	174			
1.0	4.50	SAW	SC HAZ	-80	0.25	142	92			
1.0	4.50	SAW	2	-80	0.25	254	210			
1.0	4.50	SAW	0	-60	0.50	310	307			
1.0	4.50	SAW	0	-70	0.50	34	21			
1.0	4.50	SAW	SC HAZ	-60	0.50	321	316			
1.0	4.50	SAW	SC HAZ	-70	0.50	124	106			
1.0	4.50	SAW	0	-10				1.43	BxB	> 16% GCHAZ
1.0	4.50	SAW	0	-10				1.64	BxB	> 16% GCHAZ

1.0	4.50	SAW	0	-10				1.89	BxB	> 16% GCHAZ
1.0	4.50	SAW	0	-10				1.86	BxB	> 16% GCHAZ
1.0	4.50	SAW	0	-10				1.81	BxB	> 16% GCHAZ
1.0	4.50	SAW	0	-10				1.79	BxB	> 16% GCHAZ
1.0	4.50	SAW	0	-10				1.66	BxB	> 16% GCHAZ
1.0	4.50	SAW	SC HAZ	-10				1.58	BxB	
1.0	4.50	SAW	SC HAZ	-10				1.92	BxB	
1.0	4.50	SAW	SC HAZ	-10				1.61	BxB	
1.0	0.80	SAW	WM	-50	0.25	120				
1.0	3.00	SAW	WM	-50	0.25	121				
1.0	4.50	SAW	WM	-50	0.25	60				33J min
1.0	0.80	SAW	WM	-60	0.25	25				
1.0	0.80	SAW	WM	-10				1.95		
1.0	0.80	SAW	WM	-10				1.87		
1.0	4.50	SAW	WM	-10				0.88		
1.0	4.50	SAW	WM	-10				0.93		
2.0	4.50	Tandem SAW	HAZ	-10				0.32		27%CGHAZ
2.0	4.50	Tandem SAW	HAZ	-10				0.44		27%CGHAZ
2.0	4.50	Tandem SAW	HAZ	-10				0.27		31%CGHAZ
2.0	4.50	Tandem SAW	HAZ	-10				0.46		21%CGHAZ
2.0	4.50	Tandem SAW	HAZ	-10				0.76		11%CGHAZ
2.0	4.50	Tandem SAW	HAZ	-10				0.27		25%CGHAZ
2.0	4.50	Tandem SAW	HAZ	-10				0.26		33%CGHAZ
2.0	4.50	Tandem SAW	HAZ	-10				0.32		25%CGHAZ
2.0	4.50	Tandem SAW	HAZ	-10				0.43		22%CGHAZ
3.0	1.50	SMAW	0	-40	0.04	200	170			
3.0	1.50	SMAW	2	-40	0.04	270	260			
3.0	1.50	SMAW	5	-40	0.04	280	275			
3.0	1.50	SMAW	0	-40	0.50	260	245			
3.0	1.50	SMAW	2	-40	0.50	200	160			
3.0	1.50	SMAW	5	-40	0.50	198	150			
3.0	4.50	SAW	0	-40	0.04	280	270			
3.0	4.50	SAW	2	-40	0.04	270	260			
3.0	4.50	SAW	5	-40	0.04	280	265			
3.0	4.50	SAW	0	-40	0.50	113	60			
3.0	4.50	SAW	2	-40	0.50	203	100			
3.0	4.50	SAW	5	-40	0.50	250	240			
3.0	1.50	SMAW	0	-10				0.30	Bx2B	
3.0	1.50	SMAW	0	-10				0.30	Bx2B	
3.0	1.50	SMAW	0	-10				0.80	Bx2B	
3.0	1.50	SMAW	0	-10				1.00	Bx2B	
3.0	1.50	SMAW	0	-10				1.00	Bx2B	
3.0	1.50	SMAW	0	-10				1.00	Bx2B	
3.0	1.50	SMAW	0	-10				1.00	Bx2B	
3.0	1.50	SMAW	0	-10				1.00	Bx2B	
3.0	1.50	SMAW	0	-10				1.00	Bx2B	
3.0	1.50	SMAW	0	-10				1.00	Bx2B	
3.0	1.50	SMAW	1	-10				0.35	Bx2B	
3.0	1.50	SMAW	1	-10				0.80	Bx2B	
3.0	1.50	SMAW	1	-10				1.00	Bx2B	
3.0	1.50	SMAW	1	-10				1.00	Bx2B	
3.0	1.50	SMAW	1	-10				1.00	Bx2B	
3.0	1.50	SMAW	1	-10				1.00	Bx2B	
3.0	1.50	SMAW	1	-10				1.00	Bx2B	
3.0	1.50	SMAW	1	-10				1.00	Bx2B	
3.0	1.50	SMAW	1	-10				1.00	Bx2B	

3.0	1.50	SMAW	1	-10			1.00	Bx2B	
3.0	4.50	SAW	0	-10			0.40	Bx2B	
3.0	4.50	SAW	0	-10			0.50	Bx2B	
3.0	4.50	SAW	0	-10			0.80	Bx2B	
3.0	4.50	SAW	0	-10			0.00	Bx2B	
3.0	4.50	SAW	0	-10			0.90	Bx2B	
3.0	4.50	SAW	0	-10			0.90	Bx2B	
3.0	4.50	SAW	0	-10			0.90	Bx2B	
3.0	4.50	SAW	0	-10			0.90	Bx2B	
3.0	4.50	SAW	0	-10			0.90	Bx2B	
3.0	4.50	SAW	0	-10			0.90	Bx2B	
3.0	4.50	SAW	0	-10			0.90	Bx2B	
3.0	4.50	SAW	0	-10			0.90	Bx2B	
3.0	4.50	SAW	1	-10			0.70	Bx2B	
3.0	4.50	SAW	1	-10			0.80	Bx2B	
3.0	4.50	SAW	1	-10			0.90	Bx2B	
3.0	4.50	SAW	1	-10			0.90	Bx2B	
3.0	4.50	SAW	1	-10			0.90	Bx2B	
3.0	4.50	SAW	1	-10			0.90	Bx2B	
3.0	4.50	SAW	1	-10			0.90	Bx2B	
3.0	4.50	SAW	1	-10			0.90	Bx2B	
3.0	4.50	SAW	1	-10			0.90	Bx2B	
3.0	4.50	SAW	1	-10			0.90	Bx2B	
3.0	4.50	SAW	1	-10			0.90	Bx2B	
3.0	4.50	SAW	1	-10			0.90	Bx2B	
3.0	1.50	SMAW	WM	-40	0.00	150			Min 115 J
3.0	1.50	SMAW	WM	-40	0.50	165			Min 150 J
3.0	4.50	SAW	WM	-40	0.00	90			Min 80 J
3.0	4.50	SAW	WM	-40	0.50	230			Min 200 J
4.0	4.50		0	-10			0.37	Bx2B,a/w=0.5	
4.0	4.50		0	-10			0.50	Bx2B,a/w=0.5	
4.0	4.50		0	-10			0.67	Bx2B,a/w=0.5	
4.0	4.50		0	-10			0.90	Bx2B,a/w=0.5	
4.0	4.50		0	-10			0.90	Bx2B,a/w=0.5	
4.0	4.50		0	-10			0.90	Bx2B,a/w=0.5	
4.0	4.50		0	-10			0.90	Bx2B,a/w=0.5	
4.0	4.50		0	-10			0.90	Bx2B,a/w=0.5	
4.0	4.50		1	-10			0.28	Bx2B,a/w=0.5	
4.0	4.50		1	-10			0.43	Bx2B,a/w=0.5	
4.0	4.50		1	-10			0.80	Bx2B,a/w=0.5	
4.0	4.50		1	-10			0.90	Bx2B,a/w=0.5	
4.0	4.50		1	-10			0.90	Bx2B,a/w=0.5	
4.0	4.50		1	-10			0.90	Bx2B,a/w=0.5	
4.0	4.50		1	-10			0.90	Bx2B,a/w=0.5	
4.0	4.50		1	-10			0.90	Bx2B,a/w=0.5	
4.0	7.00		0	-10			0.61	Bx2B,a/w=0.5	
4.0	7.00		0	-10			0.90	Bx2B,a/w=0.5	
4.0	7.00		0	-10			0.90	Bx2B,a/w=0.5	
4.0	7.00		0	-10			0.90	Bx2B,a/w=0.5	
4.0	7.00		0	-10			0.90	Bx2B,a/w=0.5	
4.0	7.00		0	-10			0.90	Bx2B,a/w=0.5	
4.0	7.00		0	-10			0.90	Bx2B,a/w=0.5	
5.0	4.00	SAW	0	-10			0.05	Bx2B	28-45% GCHAZ
5.0	4.00	SAW	0	-10			0.08	Bx2B	28-45% GCHAZ
5.0	4.00	SAW	0	-10			0.50	Bx2B	28-45% GCHAZ
5.0	4.00	SAW	0	-10			0.75	Bx2B	28-45% GCHAZ

5.0	4.00	SAW	0	-10				2.00	Bx2B	28-45% GCHAZ
5.0	5.00	SAW	0	-10				0.05	Bx2B	28-45% GCHAZ
5.0	5.00	SAW	0	-10				0.08	Bx2B	28-45% GCHAZ
5.0	5.00	SAW	0	-10				0.15	Bx2B	28-45% GCHAZ
6.0	4.00	SAW	0	-10				0.30	Bx2B	28-45% GCHAZ
6.0	4.00	SAW	0	-10				0.35	Bx2B	28-45% GCHAZ
6.0	4.00	SAW	0	-10				0.70	Bx2B	28-45% GCHAZ
6.0	4.00	SAW	0	-10				1.45	Bx2B	28-45% GCHAZ
6.0	4.00	SAW	0	-10				1.50	Bx2B	28-45% GCHAZ
6.0	4.00	SAW	0	-10				2.00	Bx2B	28-45% GCHAZ
6.0	5.00	SAW	0	-10				0.35	Bx2B	28-45% GCHAZ
6.0	5.00	SAW	0	-10				0.51	Bx2B	28-45% GCHAZ
6.0	5.00	SAW	0	-10				0.62	Bx2B	28-45% GCHAZ
6.0	5.00	SAW	0	-10				1.60	Bx2B	28-45% GCHAZ
7.0	5.00	SAW	0	-50				0.05	Bx2B	
7.0	5.00	SAW	0	-50				0.07	Bx2B	
7.0	5.00	SAW	0	-50				0.08	Bx2B	
7.0	5.00	SAW	0	-50				0.08	Bx2B	
7.0	5.00	SAW	0	-50				0.17	Bx2B	
7.0	5.00	SAW	0	-50				0.22	Bx2B	
7.0	5.00	SAW	0	-50				0.39	Bx2B	
7.0	5.00	SAW	0	-50				0.68	Bx2B	
7.0	5.00	SAW	0	-50				0.92	Bx2B	
8.0	4.00	SAW	0	-60	0.25	212	200			
8.0	4.00	SAW	1	-60	0.25	247	235			
8.0	4.00	SAW	3	-60	0.25	270	265			
8.0	4.00	SAW	0	-60	0.50	251	225			
8.0	4.00	SAW	1	-60	0.50	233	200			
8.0	4.00	SAW	3	-60	0.50	202	190			
8.0	4.00	SAW	5	-60	0.50	228	215			
8.0	4.00	SAW	0	-30				2.00		
8.0	4.00	SAW	0	-30				2.00		
8.0	4.00	SAW	0	-30				2.00		
8.0	4.00	SAW	SC HAZ	-30				0.35		
8.0	4.00	SAW	SC HAZ	-30				0.75		
8.0	4.00	SAW	SC HAZ	-30				0.90		
8.0	4.00	SAW	SC HAZ	-30				2.00		
8.0	4.00	SAW	SC HAZ	-30				2.00		
8.0	4.00	SAW	SC HAZ	-30				2.00		
8.0	4.00	SAW	WM	-60	0.25	210				
8.0	4.00	SAW	WM	-60	0.25	220				
8.0	4.00	SAW	WM	-60	0.25	265				
8.0	4.00	SAW	WM	-60	0.50	225				
8.0	4.00	SAW	WM	-60	0.50	270				
8.0	4.00	SAW	WM	-60	0.50	275				
8.1	20.50	SAW	0	-60	0.25	50	45			
8.1	20.50	SAW	1	-60	0.25	40	35			
8.1	20.50	SAW	3	-60	0.25	40	35			
8.1	20.50	SAW	5	-60	0.25	45	35			
8.1	20.50	SAW	0	-60	0.50	45	40			
8.1	20.50	SAW	1	-60	0.50	40	30			
8.1	20.50	SAW	3	-60	0.50	40	35			
8.1	20.50	SAW	5	-60	0.50	66	35			
9.0	4.00	SAW	0	-60	0.25	182	100			
9.0	4.00	SAW	1	-60	0.25	243	200			

9.0	4.00	SAW	3	-60	0.25	243	220		
9.0	4.00	SAW	5	-60	0.25	217	200		
9.0	4.00	SAW	0	-60	0.50	180	170		
9.0	4.00	SAW	1	-60	0.50	230	180		
9.0	4.00	SAW	3	-60	0.50	128	115		
9.0	4.00	SAW	5	-60	0.50	170	130		
9.0	4.00	SAW	0	-30				0.20	
9.0	4.00	SAW	0	-30				0.55	
9.0	4.00	SAW	0	-30				1.20	
9.0	4.00	SAW	SC HAZ	-30				0.22	
9.0	4.00	SAW	SC HAZ	-30				0.25	
9.0	4.00	SAW	SC HAZ	-30				1.10	
9.0	4.00	SAW	0	-10				0.65	
9.0	4.00	SAW	0	-10				0.75	
9.0	4.00	SAW	0	-10				0.85	
9.0	4.00	SAW	SC HAZ	-10				0.38	
9.0	4.00	SAW	SC HAZ	-10				0.55	
9.0	4.00	SAW	SC HAZ	-10				0.70	
9.0	4.00	SAW	WM	-60	0.25	180			
9.0	4.00	SAW	WM	-60	0.50	190			
10.0	4.00	SAW	0	-60	0.25	213	160		
10.0	4.00	SAW	1	-60	0.25	235	225		
10.0	4.00	SAW	3	-60	0.25	235	210		
10.0	4.00	SAW	SC HAZ	-60	0.25	245	220		
10.0	4.00	SAW	0	-60	0.50	132	100		
10.0	4.00	SAW	1	-60	0.50	213	180		
10.0	4.00	SAW	3	-60	0.50	127	75		
10.0	4.00	SAW	SC HAZ	-60	0.50	128	65		
10.0	4.00	SAW	0	-30				2.00	Bx2B
10.0	4.00	SAW	0	-30				2.00	Bx2B
10.0	4.00	SAW	0	-30				2.00	Bx2B
10.0	4.00	SAW	0	-30				2.00	Bx2B
10.0	4.00	SAW	0	-30				2.00	Bx2B
10.0	4.00	SAW	0	-30				2.00	Bx2B
10.0	4.00	SAW	WM	-60	0.25	130			
10.0	4.00	SAW	WM	-60	0.25	150			
10.0	4.00	SAW	WM	-60	0.50	120			
10.0	4.00	SAW	WM	-60	0.50	160			
10.0	4.00	SAW	WM	-60	0.50	185			
10.1	20.50	SAW	0	-60	0.25	76	55		
10.1	20.50	SAW	1	-60	0.25	97	40		
10.1	20.50	SAW	3	-60	0.25	190	185		
10.1	20.50	SAW	SCHAZ	-60	0.25	290	300		
10.1	20.50	SAW	0	-60	0.50	100	30		
10.1	20.50	SAW	1	-60	0.50	96	78		
10.1	20.50	SAW	3	-60	0.50	133	108		
10.1	20.50	SAW	SCHAZ	-60	0.50	238	200		
11.0	4.50	SAW	0	-40	0.00	165	155		
11.0	4.50	SAW	1	-40	0.00	255	250		
11.0	4.50	SAW	3	-40	0.00	250	245		
11.0	4.50	SAW	0	-40	0.50	149	57		
11.0	4.50	SAW	1	-40	0.50	215	200		
11.0	4.50	SAW	3	-40	0.50	180	170		
11.0	4.50	SAW	0	-10				0.30	
11.0	4.50	SAW	0	-10				0.42	
11.0	4.50	SAW	0	-10				0.90	

11.0	4.50	SAW	0	-10				1.10		
11.0	4.50	SAW	0	-10				1.10		
11.0	4.50	SAW	0	-10				1.10		
11.0	4.50	SAW	0	-10				1.10		
11.0	4.50	SAW	0	-10				1.10		
11.0	4.50	SAW	0	-10				1.10		
11.0	4.50	SAW	0	-10				1.10		
11.0	4.50	SAW	WM	-40	0.00	210				
11.0	4.50	SAW	WM	-40	0.00	240				
11.0	4.50	SAW	WM	-40	0.00	250				
11.0	4.50	SAW	WM	-40	0.50	235				
11.0	4.50	SAW	WM	-40	0.50	260				
11.0	4.50	SAW	WM	-40	0.50	270				
12.0	4.60	Tandem SAW	0	-60	0.50	222	215			
12.0	4.60	Tandem SAW	0	-80	0.50	178	135			
12.0	4.60	Tandem SAW	HAZ	-60	0.50	178	55			
12.0	4.60	Tandem SAW	HAZ	-80	0.50	97	80			
12.0	4.60	Tandem SAW	0	-30				0.90	B(=70)xB	>18% GCHAZ
12.0	4.60	Tandem SAW	0	-30				1.10	B(=70)xB	>18% GCHAZ
12.0	4.60	Tandem SAW	0	-50				1.40	B(=70)xB	>18% GCHAZ
12.0	4.60	Tandem SAW	0	-50				0.14	B(=70)xB	>18% GCHAZ
12.0	4.60	Tandem SAW	0	-10				0.80	B(=70)xB	>18% GCHAZ
12.0	4.60	Tandem SAW	0	-10				0.90	B(=70)xB	>18% GCHAZ
12.0	4.60	Tandem SAW	HAZ	-10				1.30	B(=70)xB	
12.0	4.60	Tandem SAW	WM	-60	0.50	180				
12.0	4.60	Tandem SAW	WM	-80	0.50	160				
12.0	4.60	Tandem SAW	WM	-30				1.30	B(=70)xB	
13.0	17.30	SAW	0	-20		83	70			
13.0	17.30	SAW	2	-20		150	150			CVN>150
13.0	17.30	SAW	5	-20		150	150			CVN>150
13.0	17.30	SAW	WM	-20		50				45J minimum
14.0	3.00	SAW	0	-10				0.08	Bx2B	>15% GCHAZ
14.0	3.00	SAW	0	-10				0.42	Bx2B	>15% GCHAZ
14.0	3.00	SAW	0	-10				0.60	Bx2B	>15% GCHAZ
14.0	5.00	SAW	0	-10				0.42	Bx2B	>15% GCHAZ
14.0	5.00	SAW	0	-10				0.55	Bx2B	>15% GCHAZ
14.0	5.00	SAW	0	-10				0.95	Bx2B	>15% GCHAZ
14.0	5.00	SAW	0	-10				0.19	Bx2B	>15% GCHAZ
14.0	5.00	SAW	0	-10				0.19	Bx2B	>15% GCHAZ
14.0	5.00	SAW	0	-10				0.75	Bx2B	>15% GCHAZ
23.0	3.50	SAW	0	-10				1.01	Bx2B	>23% GCHAZ
23.0	3.50	SAW	0	-10				1.19	Bx2B	
23.0	3.50	SAW	0	-10				0.42	Bx2B	
23.0	3.50	SAW	0	-10				0.92	Bx2B	
23.0	3.50	SAW	0	-10				0.58	Bx2B	>49% GCHAZ
23.0	4.50	SAW	0	-10				0.88	Bx2B	
23.0	4.50	SAW	0	-10				0.91	Bx2B	>23% GCHAZ
23.0	4.50	SAW	0	-10				1.05	Bx2B	
23.0	4.50	SAW	0	-10				0.95	Bx2B	
23.0	4.50	SAW	0	-10				0.47	Bx2B	
23.0	4.50	SAW	0	-10				0.77	Bx2B	
23.0	3.50	SAW	0	-60	0.04	128	79			
23.0	4.50	SAW	0	-60	0.04	152	104			
24.0	5.00	Tanddem SAW	0	-60	0.50	116	63			
24.0	5.00	Tanddem SAW	0	-60	0.03	133	81			
24.0	5.00	Tanddem SAW	0	-80	0.03	81	46			

24.0	5.00	Tanddem SAW	1	-60	0.03	195	178			
24.0	5.00	Tanddem SAW	1	-80	0.03	151	112			
24.0	5.00	Tanddem SAW	3	-60	0.03	154	133			
24.0	5.00	Tanddem SAW	3	-80	0.03	135	123			
24.0	5.00	Tanddem SAW	5	-60	0.03	202	194			
24.0	5.00	Tanddem SAW	5	-80	0.03	167	126			
24.0	5.00	Tanddem SAW	0	-10				1.68	Bx2B, a/W=0.5	
24.0	5.00	Tanddem SAW	0	-10				1.07	Bx2B, a/W=0.5	
24.0	5.00	Tanddem SAW	0	-30				0.28	Bx2B, a/W=0.5	
24.0	5.00	Tanddem SAW	0	-30				2.20	Bx2B, a/W=0.5	
24.0	5.00	Tanddem SAW	0	-50				0.19	Bx2B, a/W=0.5	
24.0	5.00	Tanddem SAW	WM	-60		52				avg. value, 47J min.
24.0	5.00	Tanddem SAW	WM	-80		17				
24.0	5.00	Tanddem SAW	WM	-80		19				
24.0	5.00	Tanddem SAW	WM	-80		23				
24.0	5.00	Tanddem SAW	WM	-10				1.10	Bx2B	
24.0	5.00	Tanddem SAW	WM	-10				1.30	Bx2B	
24.0	5.00	Tanddem SAW	WM	-30				0.28	Bx2B	
24.0	5.00	Tanddem SAW	WM	-30				0.14	Bx2B	
24.0	20.20	3 wire SAW	0	-40	0.00	49	40			
24.0	20.20	3 wire SAW	0	-20	0.00	92	61			
24.0	20.20	3 wire SAW	1	-40	0.00	57	44			
24.0	20.20	3 wire SAW	1	-20	0.00	74	63			
24.0	20.20	3 wire SAW	3	-40	0.00	50	45			
24.0	20.20	3 wire SAW	3	-20	0.00	68	59			
24.0	20.20	3 wire SAW	5	-40	0.00	84	41			
24.0	20.20	3 wire SAW	5	-20	0.00	101	47			
24.0	20.20	3 wire SAW	0	-20	0.50	73	70			
24.0	20.20	3 wire SAW	0	-40	0.50	36	34			
24.0	13.00	3 wire SAW	0	-40	0.00	116	74			
24.0	13.00	3 wire SAW	0	-20	0.00	178	173			
24.0	13.00	3 wire SAW	1	-40	0.00	88	87			
24.0	13.00	3 wire SAW	1	-20	0.00	177	156			
24.0	13.00	3 wire SAW	3	-40	0.00	181	176			
24.0	13.00	3 wire SAW	3	-20	0.00	242	198			
24.0	13.00	3 wire SAW	5	-40	0.00	242	199			
24.0	13.00	3 wire SAW	5	-20	0.00	248	219			
24.0	13.00	3 wire SAW	0	-20	0.50	100	41			
24.0	13.00	3 wire SAW	0	-40	0.50	133	127			
25.0	4.70	SAW	0	-40	0.04	219	205			
25.0	4.70	SAW	1	-40	0.04	189	182			
25.0	4.70	SAW	SC HAZ	-40	0.04	185	166			
25.0	4.70	SAW	0	-40	0.25	108	70			
25.0	4.70	SAW	1	-40	0.25	205	187			
25.0	4.70	SAW	SC HAZ	-40	0.25	139	126			
25.0	4.70	SAW	0	-40	0.50	164	149			
25.0	4.70	SAW	1	-40	0.50	146	100			
25.0	4.70	SAW	SC HAZ	-40	0.50	133	101			
25.0	4.70	SAW	0	-10				1.23	Bx2B	Fracture mode V
25.0	4.70	SAW	0	-10				1.20	Bx2B	Fracture mode V
25.0	4.70	SAW	WM	-40	0.04	93				
25.0	4.70	SAW	WM	-40	0.04	70				
25.0	4.70	SAW	WM	-40	0.04	115				
25.0	4.70	SAW	WM	-40	0.25	163				
25.0	4.70	SAW	WM	-40	0.25	146				
25.0	4.70	SAW	WM	-40	0.25	175				

32.0	20.20	1 side SAW	3	-60	0.03	155				
32.0	20.20	1 side SAW	5	-60	0.03	175				
32.0	20.20	1 side SAW	0	-20				0.25	Bx2B	CTOD ≠ f(temp)
32.0	20.20	1 side SAW	0	-40				0.22	Bx2B	CTOD ≠ f(temp)
32.0	20.20	1 side SAW	0	-60				0.25	Bx2B	CTOD ≠ f(temp)
32.0	20.20	1 side SAW	0	-60				0.21	Bx2B	CTOD ≠ f(temp)
33.0	3.50	GMAW	0	-60	0.50	170				avg. value
33.0	3.50	GMAW	1	-60	0.50	250				avg. value
33.0	3.50	GMAW	3	-60	0.50	220				avg. value
33.0	3.50	GMAW	5	-60	0.50	210				avg. value
33.0	3.50	GMAW	5	-80	0.50	65				avg. value
33.0	3.50	GMAW	0	-40				0.30		groove shape not me
33.0	3.50	GMAW	0	-40				0.81		groove shape not me
33.0	3.50	GMAW	0	-40				0.53		groove shape not me
34.0	5.00	SAW	0	-40				0.70	30x60mm	
34.0	5.00	SAW	0	-60		80				avg value
35.0	5.00	SAW	0	-40				0.80	30x60mm	
35.0	5.00	SAW	0	-60				0.35	30x60mm	
35.0	5.00	SAW	0	-60				0.70	30x60mm	
35.0	5.00	SAW	0	-60		80				avg. value
36.0	2.50	SMAW	0	-40		152	134			
36.0	2.50	SMAW	1	-40		129	97			
36.0	2.50	SMAW	5	-40		230	229			
36.0	2.00	SAW	0	-40		74	58			
36.0	2.00	SAW	1	-40		227	194			
37.1	2.50	SMAW	0	-40		136	50			
37.1	2.50	SMAW	1	-40		224	191			
37.1	2.50	SMAW	5	-40		292	284			
37.1	2.60	SAW	0	-40		73	56			
37.1	2.60	SAW	1	-40		78	55			
38.0	1.20	SMAW	0	-40		216	157			
38.0	1.20	SMAW	1	-40		234	194			
38.0	1.20	SMAW	3	-40		237	196			
38.0	1.20	SMAW	5	-40		264	232			
38.0	5.00	SAW	0	-40		95	90			
38.0	5.00	SAW	1	-40		182	160			
38.0	5.00	SAW	3	-40		195	179			
38.0	5.00	SAW	5	-40		229	212			
38.0	1.20	SAW	WM	-40		119				
38.0	5.00	SAW	WM	-40		91				
39.0	1.20	SMAW	0	-40		58	39			
39.0	1.20	SMAW	1	-40		178	106			
39.0	1.20	SMAW	3	-40		178	158			
39.0	1.20	SMAW	5	-40		208	194			
39.0	5.00	SAW	0	-40		36	27			
39.0	5.00	SAW	1	-40		83	45			
39.0	5.00	SAW	3	-40		201	190			
39.0	5.00	SAW	5	-40		217	195			
39.0	1.20	SAW	WM	-40		152				
39.0	5.00	SAW	WM	-40		74				
40.0	15.00	FAB SEG Arc	0	-40		60				60J min value
40.0	15.00	FAB SEG Arc	0	0				0.30		
40.0	15.00	FAB SEG Arc	0	-20				0.15		
41.0	5.00	SAW	0	-60	0.00	261	254			
41.0	5.00	SAW	1	-60	0.00	267	242			
41.0	5.00	SAW	0	-60	0.25	236	212			

41.0	5.00	SAW	1	-60	0.25	281	256			
41.0	5.00	SAW	3	-60	0.25	349	337			
41.0	5.00	SAW	5	-60	0.25	352	348			
41.0	5.00	SAW	0	-60	0.50	276	229			
41.0	5.00	SAW	1	-60	0.50	284	249			
41.0	5.00	SAW	0	-50				0.54		
41.0	5.00	SAW	0	-50				0.94		
41.0	5.00	SAW	WM	-50				0.43		
41.0	5.00	SAW	WM	-50				0.47		
41.0	5.00	SAW	WM	-60		180				avg. value, min 140J
41.0	19.30	SAW	0	-60	0.00	75	38			
41.0	19.30	SAW	1	-60	0.00	70	63			
41.0	19.30	SAW	0	-60	0.25	58	15			
41.0	19.30	SAW	0	-50	0.25	93	71			
41.0	19.30	SAW	1	-60	0.25	105	40			
41.0	19.30	SAW	3	-60	0.25	161	41			
41.0	19.30	SAW	5	-60	0.25	295	250			
41.0	19.30	SAW	0	-60	0.50	36	29			
41.0	19.30	SAW	0	-40	0.50	40	24			
41.0	19.30	SAW	1	-60	0.50	125	64			
41.0	19.30	SAW	0	-50				0.64		
41.0	19.30	SAW	0	-50				0.14		
41.0	19.30	SAW	0	-50				0.62		
41.0	14.20	SAW	0	-60	0.00	74	54			
41.0	14.20	SAW	1	-60	0.00	123	69			
41.0	14.20	SAW	0	-60	0.25	43	19			
41.0	14.20	SAW	0	-50	0.25	30	30			
41.0	14.20	SAW	0	-40	0.25	113	26			
41.0	14.20	SAW	1	-60	0.25	41	32			
41.0	14.20	SAW	1	-50	0.25	50	37			
41.0	14.20	SAW	3	-60	0.25	77	54			
41.0	14.20	SAW	5	-60	0.25	301	281			
41.0	14.20	SAW	0	-60	0.50	52	22			
41.0	14.20	SAW	0	-40	0.50	165	102			
41.0	14.20	SAW	1	-60	0.50	194	183			
41.0	14.20	SAW	0	-50				0.22		
41.0	14.20	SAW	0	-50				0.35		
41.0	14.20	SAW	0	-50				0.47		
41.0	14.20	SAW	WM	-20				0.10		
41.0	14.20	SAW	WM	-20				0.12		
41.0	14.20	SAW	WM	-60	0.25	31				
41.0	14.20	SAW	WM	-40	0.25	48				
42.0	3.25	SAW	0	-40	0.01	147	109			
42.0	3.25	SAW	2	-40	0.01	175	147			
42.0	3.25	SAW	5	-40	0.01	206	189			
42.0	3.25	SAW	0	-40	0.50	224	194			
42.0	3.25	SAW	2	-40	0.50	199	153			
42.0	3.25	SAW	5	-40	0.50	154	92			
42.0	3.25	SAW	0.5	-10				1.25		
42.0	3.25	SAW	0.5	-10				1.51		
42.0	3.25	SAW	0.5	-10				1.64		
44.0	3.00	SAW	0	-10				0.26	Bx2B	Cleavage in ICGCHA
44.0	3.00	SAW	0	-10				1.76	Bx2B	
44.0	3.00	SAW	0	-10				1.70	Bx2B	
44.0	3.00	SAW	0	-10				1.75	Bx2B	
44.0	5.00	SAW	0	-10				0.32	Bx2B	

44.0	5.00	SAW	0	-10				0.11	Bx2B	Cleavage in ICGCHA
44.0	5.00	SAW	0	-10				0.61	Bx2B	
44.0	5.00	SAW	0	-10				0.55	Bx2B	
44.0	5.00	SAW	0	-10				0.13	Bx2B	
44.0	5.00	SAW	0	-10				0.36	Bx2B	
44.0	3.00	SAW	0	-62	0.50	35				
44.0	3.00	SAW	0	-57	0.50	50				
44.0	3.00	SAW	SC HAZ	-88	0.50	35				
44.0	3.00	SAW	SC HAZ	-86	0.50	50				
44.0	5.00	SAW	0	-64	0.50	35				
44.0	5.00	SAW	0	-60	0.50	50				
44.0	5.00	SAW	SC HAZ	-112	0.50	35				
44.0	5.00	SAW	SC HAZ	-108	0.50	50				
45.0	3.00	SAW	0	-30				0.64	Bx2B	>15% GCHAZ
45.0	3.00	SAW	0	-30				1.95	Bx2B	>15% GCHAZ
45.0	3.00	SAW	0	-30				1.12	Bx2B	<15% GCHAZ
45.0	3.00	SAW	0	-30				1.96	Bx2B	<15% GCHAZ
45.0	3.00	SAW	0	-30				1.98	Bx2B	<15% GCHAZ
45.0	5.00	SAW	0	-10				0.37	Bx2B	
45.0	5.00	SAW	0	-10				1.54	Bx2B	
45.0	5.00	SAW	0	-10				0.12	Bx2B	Cleavage from inclusi
45.0	5.00	SAW	0	-10				2.24	Bx2B	
45.0	5.00	SAW	0	-10				2.21	Bx2B	
45.0	5.00	SAW	0	-10				0.28	Bx2B	
45.0	1.00	FCAW	0	-10				1.71	Bx2B	>15% GCHAZ
45.0	1.00	FCAW	0	-10				0.16	Bx2B	>15% GCHAZ, cleava
45.0	3.00	SAW	0	-50	0.50	35				
45.0	3.00	SAW	0	-47	0.50	50				
45.0	3.00	SAW	SC HAZ	-83	0.50	35				
45.0	3.00	SAW	SC HAZ	-78	0.50	50				
45.0	5.00	SAW	0	-52	0.50	35				
45.0	5.00	SAW	0	-49	0.50	50				
45.0	5.00	SAW	SC HAZ	-124	0.50	35				
45.0	5.00	SAW	SC HAZ	-122	0.50	50				
45.0	1.00	FCAW	0	-73	0.50	35				
45.0	1.00	FCAW	0	-72	0.50	50				
46.0	5.00	Tandem SAW	WM	-40		50	44			
46.0	5.00	Tandem SAW	0	-40		88	60			
46.0	5.00	Tandem SAW	1	-40		59	48			
46.0	5.00	Tandem SAW	3	-40		200	196			
46.0	5.00	Tandem SAW	5	-40		276	268			
47.0	27.00	EGW	WM	0		64	56			
47.0	27.00	EGW	0	0		53	40			40J min; FL avg 23J
47.0	27.00	EGW	1	0		65	48			
47.0	27.00	EGW	3	0		117	72			
47.0	27.00	EGW	5	0		116	94			
47.0	27.00	EGW	7	0		221	184			
52.0	1.20	SMAW	0	-40		252	206			
52.0	1.20	SMAW	1	-40		275	244			
52.0	1.20	SMAW	3	-40		263	164			
52.0	1.20	SMAW	5	-40		229	184			
52.0	1.20	SMAW	WM	-40		258	228			
53.0	3.00	SAW	0	-40		160	158			
53.0	3.00	SAW	1	-40		186	174			
53.0	3.00	SAW	3	-40		206	180			
53.0	3.00	SAW	5	-40		246	234			

53.0	3.00	SAW	WM	-40		132	122			
54.0	11.50	EG	0	-50		158	127			
54.0	11.50	EG	1	-50		205	180			min 18J
54.0	11.50	EG	3	-50		299	298			
54.0	11.50	EG	5	-50		299	298			
54.0	11.50	EG	WM	-50		119	74			
59.0	6.00	SAW	0.5	-40		264				
59.0	6.00	SAW	0.5	-60		266				
59.0	6.00	SAW	0.5	-80		225				
60.0	6.00	SAW	0.5	-40		90				
60.0	6.00	SAW	0.5	-60		67				
61.0	4.10	SAW	0.5	-40		125				
61.0	4.10	SAW	0.5	-40		140				
61.0	4.10	SAW	0.5	-60		70				
61.0	4.10	SAW	0.5	-60		140				
62.0	5.00	SAW	0	-10				0.64	Bx2B	
62.0	5.00	SAW	0	-10				1.34	Bx2B	
62.0	5.00	SAW	0	-10				1.04	Bx2B	
62.0	5.00	SAW	WM	-10				1.95	Bx2B	
62.0	5.00	SAW	0	-60		84	27			
62.0	5.00	SAW	2	-60		286	260			
62.0	5.00	SAW	5	-60		281	270			
62.0	10.00	SAW	0	-60		49	39			
62.0	10.00	SAW	2	-60		53	43			
62.0	10.00	SAW	5	-60		189	110			
62.0	5.00	SAW	WM	-60		128				
62.0	10.00	SAW	WM	-60		95				
63.0	5.00	SAW	0	-10				1.80	Bx2B	avg 1.65
63.0	5.00	SAW	0	-10				1.89	Bx2B	
63.0	5.00	SAW	0	-10				1.27	Bx2B	
63.0	5.00	SAW	WM	-10				2.03	Bx2B	
63.0	5.00	SAW	WM	-10				1.74	Bx2B	
63.0	5.00	SAW	WM	-60		100				
63.0	10.00	SAW	WM	-10				1.63	Bx2B	
63.0	10.00	SAW	WM	-10				1.74	Bx2B	
63.0	10.00	SAW	WM	-60		162				
63.0	5.00	SAW	0	-60		103	35			
63.0	5.00	SAW	2	-60		288	263			
63.0	5.00	SAW	5	-60		303	302			
63.0	10.00	SAW	0	-60		136	67			
63.0	10.00	SAW	2	-60		95	72			
63.0	10.00	SAW	5	-60		279	264			
64.0	5.00	SAW	0	-80		225	210			
64.0	5.00	SAW	2	-80		150	100			
64.0	5.00	SAW	5	-80		200	150			
64.0	5.00	SAW	0	-50				1.59	Bx2B	
64.0	5.00	SAW	0	-50				0.49	Bx2B	
64.0	5.00	SAW	0	-50				2.80	Bx2B	
64.0	5.00	SAW	WM	-50				2.80	Bx2B	
64.0	5.00	SAW	WM	-80		176				
64.1	3.70	SAW	0	-80		77	72			
64.1	3.70	SAW	2	-80		63	61			
64.1	3.70	SAW	5	-80		117	45			
66.0	4.50	SAW	0	-60	0.25	185	150			
66.0	4.50	SAW	1	-60	0.25	170	168			
66.0	4.50	SAW	3	-60	0.25	195	188			

66.0	4.50	SAW	5	-60	0.25	230	225
66.0	4.50	SAW	WM	-60	0.25	185	
66.0	4.50	SAW	0	-60	0.50	155	145
66.0	4.50	SAW	1	-60	0.50	92	50
66.0	4.50	SAW	3	-60	0.50	145	130
66.0	4.50	SAW	5	-60	0.50	140	122
66.0	4.50	SAW	WM	-60	0.50	210	
67.0	2.30	SAW	0	-60	0.25	114	33
67.0	2.30	SAW	1	-60	0.25	175	160
67.0	2.30	SAW	3	-60	0.25	180	170
67.0	2.30	SAW	5	-60	0.25	215	210
67.0	2.30	SAW	WM	-60	0.25	85	
67.0	2.30	SAW	0	-60	0.50	100	90
67.0	2.30	SAW	1	-60	0.50	135	85
67.0	2.30	SAW	3	-60	0.50	165	120
67.0	2.30	SAW	5	-60	0.50	175	169
67.0	2.30	SAW	WM	-60	0.50	92	47
67.0	4.50	SAW	0	-60	0.25	175	160
67.0	4.50	SAW	1	-60	0.25	175	170
67.0	4.50	SAW	3	-60	0.25	200	189
67.0	4.50	SAW	5	-60	0.25	225	213
67.0	4.50	SAW	0	-60	0.50	100	72
67.0	4.50	SAW	1	-60	0.50	245	168
67.0	4.50	SAW	3	-60	0.50	147	127
67.0	4.50	SAW	5	-60	0.50	150	119
68.0	4.00	SMAW	0	-60	0.04	137	112
68.0	4.00	SMAW	1	-60	0.04	240	190
68.0	4.00	SMAW	3	-60	0.04	220	200
68.0	4.00	SMAW	5	-60	0.04	240	220
68.0	4.00	SMAW	WM	-60	0.04	120	57
68.0	4.00	SMAW	0	-60	0.25	156	67
68.0	4.00	SMAW	1	-60	0.25	235	212
68.0	4.00	SMAW	3	-60	0.25	240	211
68.0	4.00	SMAW	5	-60	0.25	250	223
68.0	4.00	SMAW	WM	-60	0.25	91	50
68.0	4.00	SMAW	0	-60	0.50	215	195
68.0	4.00	SMAW	1	-60	0.50	175	118
68.0	4.00	SMAW	3	-60	0.50	200	190
68.0	4.00	SMAW	5	-60	0.50	215	210
68.0	4.00	SMAW	WM	-60	0.50	107	64
68.0	7.00	SAW	0	-60	0.04	175	169
68.0	7.00	SAW	1	-60	0.04	225	150
68.0	7.00	SAW	3	-60	0.04	245	221
68.0	7.00	SAW	5	-60	0.04	328	270
68.0	7.00	SAW	WM	-60	0.04	175	
68.0	7.00	SAW	0	-60	0.25	265	250
68.0	7.00	SAW	1	-60	0.25	350	282
68.0	7.00	SAW	3	-60	0.25	300	275
68.0	7.00	SAW	5	-60	0.25	335	274
68.0	7.00	SAW	WM	-60	0.25	200	
68.0	7.00	SAW	0	-60	0.50	250	220
68.0	7.00	SAW	1	-60	0.50	280	
68.0	7.00	SAW	3	-60	0.50	325	300
68.0	7.00	SAW	5	-60	0.50	265	260
68.0	7.00	SAW	WM	-60	0.50	220	
70.0	4.50		0	-60		170	162

70.0	4.50		1	-60		250	235	
70.0	4.50		0	-30				1.30 groove shape not me
70.0	4.50		0	-30				2.00 groove shape not me
70.0	10.00		0	-60		110	52	
70.0	10.00		1	-60		65	50	
70.0	10.00		0	-30				0.35 groove shape not me
70.0	10.00		0	-30				1.20 groove shape not me
71.0	5.00		0	-60		280	270	
71.0	5.00		1	-60		320	315	
71.0	5.00		0	-60				2.00 groove shape not me
71.0	10.00		0	-60		62	52	
71.0	10.00		1	-60		110	67	
71.0	10.00		0	-60				0.30 groove shape not me
71.0	10.00		0	-60				0.40 groove shape not me
71.0	10.00		0	-30				0.80 groove shape not me
71.0	10.00		0	-30				0.90 groove shape not me
72.0	3.00		0	-10				2.08
72.0	3.00		0	-10				2.13
72.0	3.00		0	-10				2.00
72.0	5.00		0	-10				0.76
72.0	5.00		0	-10				1.92
72.0	5.00		0	-10				2.01
72.0	3.00		0	-40		>150		5% < 50J
73.0	3.00		0	-10				1.20 2% <0.2mm
73.0	3.00		0	-10				0.81
73.0	3.00		0	-10				0.86
73.0	5.00		0	-10				1.46
73.0	5.00		0	-10				1.09
73.0	5.00		0	-10				1.42
73.0	5.00		0	-10				0.79
74.0	11.50		HAZ	-40		250		avg., 95J min
78.0	5.00		HAZ	-10				0.35
78.0	5.00		HAZ	-10				1.65
78.0	5.00		HAZ	-10				0.63
78.0	5.00		HAZ	-10				0.54
78.0	5.00		HAZ	-10				0.67
78.0	5.00		HAZ	-10				0.67
78.0	5.00		HAZ	-10				1.62
78.0	5.00		HAZ	-10				0.37
79.0	3.00	SAW	0	-60		27		50% FATT -40°C
79.0	3.00	SAW & powder	0	-60		27		50% FATT -18°C
79.0	8.00	SAW	0	-40		27		50% FATT -18°C
80.0	3.00	SAW	0	-80		27		50% FATT -40°C
80.0	3.00	SAW & powder	0	-85		27		50% FATT -50°C
80.0	8.00	SAW	0	-70		27		50% FATT -25°C
81.0	2.60		0	-13		50		Cleavage @ 5C
81.0	2.60		0	-27		27		
81.0	2.60		SC HAZ	-65		50		Cleavage @ -36C
81.0	2.60		SC HAZ	-72		27		
81.0	4.50		0	-11		50		Cleavage @ -7C
81.0	4.50		0	-23		27		
81.0	4.50		SC HAZ	-40		50		Cleavage @ -36C
81.0	4.50		SC HAZ	-79		27		
82.0	4.50	SAW	0	-40	0.00	109	39	
82.0	4.50	SAW	0	-40	0.25	250	211	
82.0	4.50	SAW	0	-10				0.36 > 20% GCHAZ

12/6/95

82.0	4.50	SAW	0	-10				0.12		> 20% GCHAZ
82.0	4.50	SAW	0	-10				0.24		> 20% GCHAZ
84.0	4.50	SAW	0	-60	0.25	238	215			
84.0	4.50	SAW	0	-60	0.50	180	145			130J min
84.0	4.50	SAW	0	-20				0.75	Bx2B	
84.0	4.50	SAW	0	-20				1.40	Bx2B	
84.0	4.50	SAW	0	-20				1.40	Bx2B	
84.0	4.50	SAW	0	-40				0.31	Bx2B	
84.0	4.50	SAW	0	-40				0.74	Bx2B	
84.0	4.50	SAW	0	-40				1.20	Bx2B	
85.0	1.40	SMAW	0	-60		219	216			
85.0	1.40	SMAW	HAZ	-60		205	170			
85.0	1.40	SMAW	0	-60				0.35	Bx2B	
85.0	1.40	SMAW	0	-60				0.35	Bx2B	
85.0	1.40	SMAW	0	-40				0.37	Bx2B	
85.0	1.40	SMAW	0	-40				0.69	Bx2B	
85.0	5.00	SAW	0	-60		290	285			
85.0	5.00	SAW	HAZ	-60		279	273			
85.0	5.00	SAW	0	-60				1.10	Bx2B	
85.0	5.00	SAW	0	-60				1.35	Bx2B	
85.0	5.00	SAW	0	-40				1.10	Bx2B	
85.0	5.00	SAW	0	-40				1.15	Bx2B	
85.0	20.10	EGW	0	-60		202	189			
85.0	20.10	EGW	HAZ	-60		232	194			
86.0	1.00	GMAW	0	-60		153	76			
86.0	1.00	GMAW	HAZ	-60		170	163			
86.0	1.00	GMAW	0	-60				0.30	Bx2B	
86.0	1.00	GMAW	0	-60				0.57	Bx2B	
86.0	1.00	GMAW	0	-20				0.78	Bx2B	
86.0	1.00	GMAW	0	-20				0.95	Bx2B	
86.0	5.00	SAW	0	-60		262	233			
86.0	5.00	SAW	HAZ	-60		154	83			83J min
86.0	5.00	SAW	0	-60				1.05	Bx2B	
86.0	5.00	SAW	0	-60				1.30	Bx2B	
86.0	5.00	SAW	0	-20				1.30	Bx2B	
86.0	5.00	SAW	0	-20				1.30	Bx2B	
86.0	21.00	EGW	0	-60		174	132			
86.0	21.00	EGW	HAZ	-60		199	136			
87.0	3.50	SAW	HAZ	-10				0.20		
87.0	3.50	SAW	HAZ	-10				0.25		
87.0	3.50	SAW	HAZ	-10				0.38		
87.0	5.00	SAW	HAZ	-10				0.10		
87.0	5.00	SAW	HAZ	-10				0.12		
87.0	5.00	SAW	HAZ	-10				0.15		
87.0	5.00	SAW	HAZ	-10				0.16		
87.0	5.00	SAW	HAZ	-10				0.30		
87.0	5.00	SAW	HAZ	-10				0.20		
88.0	13.60		0	-60		94	40			
88.0	13.60		2	-60		100	40			
88.0	13.60		0	-60				0.20		
88.0	13.60		0	-60				0.30		
88.0	13.60		0	-60				0.60		
88.0	14.00		0	-60		175	155			
88.0	14.00		2	-60		180	125			
88.0	14.00		0	-60				0.18		
88.0	14.00		0	-60				0.21		

88.0	14.00		0	-60				0.45		
89.0	5.10		0	-10				0.45	BxB, a/w=0.5	invalid, API RP 2Z
89.0	5.10		0	-10				0.70	BxB, a/w=0.5	valid, API RP 2Z
89.0	5.10		0	-10				0.91	BxB, a/w=0.5	valid, API RP 2Z
89.0	5.10		0	-10				0.93	BxB, a/w=0.5	invalid, API RP 2Z
89.0	5.10		0	-10				1.12	BxB, a/w=0.5	invalid, API RP 2Z
89.0	5.10		0	-10				1.17	BxB, a/w=0.5	invalid, API RP 2Z
89.0	5.10		0	-10				1.31	BxB, a/w=0.5	invalid, API RP 2Z
89.0	5.10		0	-10				1.33	BxB, a/w=0.5	invalid, API RP 2Z
89.1	4.20		0	-10				0.06	Bx2B, a/w=0.5	valid, API RP 2Z
89.1	4.20		0	-10				0.26	Bx2B, a/w=0.5	valid, API RP 2Z
89.1	4.20		0	-10				0.19	Bx2B, a/w=0.5	valid, API RP 2Z
89.1	4.20		0	-10				0.62	Bx2B, a/w=0.5	valid, API RP 2Z
89.1	4.20		0	-10				0.10	Bx2B, a/w=0.5	valid, API RP 2Z
89.1	4.20		0	-10				0.10	Bx2B, a/w=0.5	valid, API RP 2Z
90.0	5.40	SAW	0	-40	0.00	149	145			
90.0	5.40	SAW	0	-60	0.00	151	149			
90.0	5.40	SAW	0	-40	0.50	147	145			
90.0	5.40	SAW	0	-50	0.50	45	14			
90.0	5.40	SAW	0	-60	0.50	10	7			
90.0	5.40	SAW	0	-30				0.85	Bx2B	>20% GCHAZ
90.0	5.40	SAW	0	-30				1.13	Bx2B	>20% GCHAZ
90.0	5.40	SAW	0	-30				1.05	Bx2B	>20% GCHAZ
90.0	5.40	SAW	0	-30				1.16	Bx2B	>20% GCHAZ
90.0	5.40	SAW	0	-30				0.61	Bx2B	>20% GCHAZ
90.0	5.40	SAW	0	-30				1.04	Bx2B	>20% GCHAZ
90.0	5.40	SAW	0	-50				0.13	Bx2B	>20% GCHAZ
90.0	5.40	SAW	0	-50				0.34	Bx2B	>20% GCHAZ
90.0	5.40	SAW	0	-50				0.18	Bx2B	>20% GCHAZ
90.0	5.40	SAW	0	-50				0.06	Bx2B	>20% GCHAZ
90.0	5.40	SAW	0	-50				0.29	Bx2B	>20% GCHAZ
91.0	1.50	SAW	0	-60	0.25	249	248			
91.0	1.50	SAW	2	-60	0.25	166	149			
91.0	1.50	SAW	0	-50				0.26	Bx2B	invalid
91.0	1.50	SAW	0	-50				0.17	Bx2B	30% GCHAZ
91.0	1.50	SAW	0	-50				0.73	Bx2B	invalid
91.0	1.50	SAW	0	-50				0.04	Bx2B	28% GCHAZ
91.0	1.50	SAW	0	-50				0.14	Bx2B	20% GCHAZ
91.0	3.00	SAW	0	-60		113	39			39J min, avg 31J if >5
91.0	3.00	SAW	2	-60		131	88			
91.0	3.00	SAW	0	-50				0.01	Bx2B	38% GCHAZ
91.0	3.00	SAW	0	-50				0.10	Bx2B	42% GCHAZ
91.0	3.00	SAW	0	-50				0.03	Bx2B	33% GCHAZ
91.0	3.00	SAW	0	-50				0.08	Bx2B	40 GCHAZ
91.0	3.00	SAW	0	-50				0.14	Bx2B	27% GCHAZ
92.0	4.00		0	-40		40	35			
92.0	4.00		0	-10				0.28	Bx2B	>15% GCHAZ
92.0	4.00		0	-10				0.35	Bx2B	>15% GCHAZ
92.0	4.00		0	-10				0.69	Bx2B	>15% GCHAZ
92.0	4.00		0	-10				1.01	Bx2B	>15% GCHAZ
92.0	4.00		0	-10				1.38	Bx2B	>15% GCHAZ
92.0	4.00		0	-10				1.96	Bx2B	>15% GCHAZ
92.0	5.00		0	-10				0.35	Bx2B	>15% GCHAZ
92.0	5.00		0	-10				0.54	Bx2B	>15% GCHAZ
92.0	5.00		0	-10				0.60	Bx2B	>15% GCHAZ
92.0	5.00		0	-10				0.64	Bx2B	>15% GCHAZ

92.0	5.00		0	-10				1.60	Bx2B	>15% GCHAZ
93.0	4.00		0	-40		38	22			
93.0	4.00		0	-10				0.07	Bx2B	>15% GCHAZ
93.0	4.00		0	-10				0.09	Bx2B	>15% GCHAZ
93.0	4.00		0	-10				0.10	Bx2B	>15% GCHAZ
93.0	4.00		0	-10				0.10	Bx2B	>15% GCHAZ
93.0	4.00		0	-10				0.13	Bx2B	>15% GCHAZ
93.0	4.00		0	-10				0.50	Bx2B	>15% GCHAZ
93.0	4.00		0	-10				0.77	Bx2B	>15% GCHAZ
94.0	2.00		0	-55		50				
94.0	2.00		0	-10				1.11		Valid
94.0	2.00		0	-10				1.02		Valid
94.0	2.00		0	-10				1.28		Valid
94.0	2.00		0	-10				1.14		Valid
94.0	2.00		0	-10				1.39		Valid
95.0	3.00		0	-40		50				
95.0	3.00		0	-10				0.20		Valid
95.0	3.00		0	-10				0.85		Valid
95.0	3.00		0	-10				0.94		Valid
95.0	3.00		0	-10				0.05		Valid
96.0	2.00		0	-55		50				
96.0	2.00		0	-10				0.76		Valid
96.0	2.00		0	-10				0.89		Valid
96.0	2.00		0	-10				1.05		Valid
96.0	2.00		0	-10				0.84		Valid
96.0	2.00		0	-10				0.78		Valid
98.0	4.90	SAW	0	-40	0.25	130	100			
98.0	4.90	SAW	1	-40	0.25	170	160			
98.0	4.90	SAW	3	-40	0.25	214	210			
98.0	4.90	SAW	0	-10				0.60		
98.0	4.90	SAW	0	-10				0.75		
98.0	4.90	SAW	WM	-40		90				
99.0	4.90	SAW	0	-40	0.25	300	290			
99.0	4.90	SAW	1	-40	0.25	310	300			
99.0	4.90	SAW	3	-40	0.25	330	325			
99.0	4.90	SAW	0	-10				0.40		
99.0	4.90	SAW	0	-10				0.70		
99.0	4.90	SAW	0	-10				0.70		
99.0	4.90	SAW	0	-10				0.90		
99.0	4.90	SAW	0	-10				0.90		
99.0	4.90	SAW	0	-10				1.10		
99.0	4.90	SAW	0	-10				1.10		
99.0	4.90	SAW	0	-10				1.10		
99.0	4.90	SAW	0	-10				1.10		
99.0	4.90	SAW	WM	-40		80				
99.0	4.90	SAW	WM	-40		150				
100.0	3.00	SAW	0	-40		234				
100.0	3.00	SAW	1	-40		317				
100.0	3.00	SAW	3	-40		453				
100.0	3.00	SAW	5	-40		441				
100.0	3.00	SAW	0	-10				0.61	Bx2B	RP2Z
100.0	3.00	SAW	0	-10				1.80	Bx2B	RP2Z
100.0	3.00	SAW	0	-10				1.80	Bx2B	RP2Z
100.0	3.00	SAW	0	-10				1.80	Bx2B	RP2Z
100.0	3.00	SAW	0	-10				1.90	Bx2B	RP2Z
100.0	3.00	SAW	WM	-40		162				

100.0	3.00	SAW	WM	-10			1.30	Bx2B	RP2Z
100.0	4.50	SAW	0	-40		217			
100.0	4.50	SAW	1	-40		295			
100.0	4.50	SAW	3	-40		442			
100.0	4.50	SAW	5	-40		434			
100.0	4.50	SAW	0	-10			1.40	Bx2B	RP2Z
100.0	4.50	SAW	0	-10			1.60	Bx2B	RP2Z
100.0	4.50	SAW	0	-10			1.60	Bx2B	RP2Z
100.0	4.50	SAW	0	-10			1.85	Bx2B	RP2Z
100.0	4.50	SAW	WM	-40		145			
100.0	4.50	SAW	WM	-10			0.85	Bx2B	
101.0	5.00	SAW	0	-60		231			
101.0	5.00	SAW	1	-60		276			
101.0	5.00	SAW	3	-60		342			
101.0	5.00	SAW	5	-60		345			
101.0	5.00	SAW	0	-50			0.52	Bx2B	RP2Z
101.0	5.00	SAW	0	-50			0.97	Bx2B	RP2Z
101.0	5.00	SAW	WM	-60		177			
101.0	5.00	SAW	WM	-50			0.42	Bx2B	
101.0	19.30	SAW	0	-60		57			
101.0	19.30	SAW	1	-60		103			
101.0	19.30	SAW	3	-60		158			
101.0	19.30	SAW	5	-60		289			
101.0	19.30	SAW	0	-50			0.14	Bx2B	RP2Z
101.0	19.30	SAW	0	-50			0.60	Bx2B	RP2Z
101.0	19.30	SAW	0	-50			0.58	Bx2B	RP2Z
101.0	19.30	SAW	WM	-60		88			
101.0	19.30	SAW	WM	-50			1.30	Bx2B	
102.0	3.50	SAW	0	-60		128			
102.0	3.50	SAW	1	-60		165			
102.0	3.50	SAW	3	-60		232			
102.0	3.50	SAW	5	-60		223			
102.0	3.50	SAW	0	-10			0.41	Bx2B	RP2Z
102.0	3.50	SAW	0	-10			0.60	Bx2B	RP2Z
102.0	3.50	SAW	0	-10			0.98	Bx2B	RP2Z
102.0	3.50	SAW	0	-10			1.10	Bx2B	RP2Z
102.0	3.50	SAW	WM	-60		107			
102.0	3.50	SAW	WM	-10			1.00	Bx2B	
102.0	4.50	SAW	0	-60		134			
102.0	4.50	SAW	1	-60		183			
102.0	4.50	SAW	3	-60		239			
102.0	4.50	SAW	5	-60		251			
102.0	4.50	SAW	0	-10			0.45	Bx2B	RP2Z
102.0	4.50	SAW	0	-10			0.80	Bx2B	RP2Z
102.0	4.50	SAW	0	-10			0.90	Bx2B	RP2Z
102.0	4.50	SAW	0	-10			0.95	Bx2B	RP2Z
102.0	4.50	SAW	0	-10			1.00	Bx2B	RP2Z
102.0	4.50	SAW	WM	-60		93			
102.0	4.50	SAW	WM	-10			0.70	Bx2B	
103.0	6.00	SAW	0	-80	0.00	145			TiO plate
103.0	6.00	SAW	0	-60	0.00	165			
103.0	6.00	SAW	0	-50	0.50	145			
104.0	0.80	SAW	0	-60		165			
104.0	4.00	SAW	0	-60		260			
104.0	4.00	SAW	0	-80		250			
105.0	6.00	SAW	0	-40		100	80		

107.0	20.00	SAW	0	-60	0.00	39	26	
107.0	20.00	SAW	1	-60	0.00	36	18	
107.0	20.00	SAW	0	-10				0.17
107.0	20.00	SAW	0	-10				0.13
107.0	20.00	SAW	0	-10				0.19
107.0	20.00	SAW	0	-10				0.29
107.0	20.00	SAW	0	-10				0.44
107.0	20.00	SAW	WM	-10				0.78
107.0	20.00	SAW	WM	-10				1.77
107.0	20.00	SAW	WM	-40				0.61
107.0	20.00	SAW	WM	-40				0.42
107.0	20.00	SAW	WM	-40				0.14
107.0	20.00	SAW	WM	-20				1.59
107.0	20.00	SAW	WM	-40		75		
107.0	20.00	SAW	WM	-60		44		
107.0	13.00	SAW	0	-60	0.00	84	59	
107.0	13.00	SAW	1	-60	0.00	50	32	
107.0	13.00	SAW	3	-60	0.00	143		
107.0	13.00	SAW	5	-60	0.00	241		
107.0	13.00	SAW	0	-60	0.50	68		
107.0	13.00	SAW	0	-10				0.30
107.0	13.00	SAW	0	-10				0.13
107.0	13.00	SAW	0	-30				0.15
107.0	13.00	SAW	0	-30				0.12
107.0	13.00	SAW	WM	-10				1.50
107.0	13.00	SAW	WM	-20				0.72
107.0	13.00	SAW	WM	-40				0.07
107.0	13.00	SAW	WM	-60		117		
108.0	4.50	SAW	0	-60	0.00	44		
108.0	4.50	SAW	0	-40	0.00	144		
108.0	4.50	SAW	0	-60	1.00	99		
108.0	4.50	SAW	2	-60	0.00	36		
108.0	4.50	SAW	2	-40	0.00	266		
108.0	4.50	SAW	2	-60	1.00	114		
108.0	4.50	SAW	5	-60	0.00	230		
108.0	4.50	SAW	5	-60	1.00	281		
108.0	4.50	SAW	0	-60	0.50	121		
108.0	4.50	SAW	2	-60	0.50	42		
108.0	4.50	SAW	5	-60	0.50	25		
108.0	4.50	SAW	2	-40	0.50	138		
108.0	4.50	SAW	5	-60	0.50	146		
109.0	4.50	SAW	0	-10				1.28
109.0	4.50	SAW	0	-10				1.23
109.0	4.50	SAW	0	-10				0.75
109.0	4.50	SAW	0	-10				1.77
109.0	4.50	SAW	0	-10				1.28
109.0	4.50	SAW	0	-10				1.81
109.0	4.50	SAW	0	-10				1.91
109.0	1.00	SMAW	0	-10				1.95
109.0	1.00	SMAW	0	-10				1.86
109.0	1.00	SMAW	0	-10				1.64
109.0	1.00	SMAW	0	-10				1.72
110.0	1.00	SMAW	0	-10				0.30
110.0	1.00	SMAW	0	-10				1.22
110.0	1.00	SAW	0	-10				1.48
110.0	1.00	SAW	0	-10				1.89

1	0.0	1.00	SAW	0	-10			0.73	
1	2.0	7.20	Tandem SAW	0	-60	0.25	132		
1	2.0	7.20	Tandem SAW	1	-60	0.25	285		
1	2.0	7.20	Tandem SAW	3	-60	0.25	343		
1	2.0	7.20	Tandem SAW	5	-60	0.25	330		
1	2.0	7.20	Tandem SAW	0	-60	0.50	104		
1	2.0	7.20	Tandem SAW	1	-60	0.50	99		
1	2.0	7.20	Tandem SAW	3	-60	0.50	122		
1	2.0	7.20	Tandem SAW	5	-60	0.50	187		
1	2.0	10.00	Tandem SAW	0	-60	0.25	116		
1	2.0	10.00	Tandem SAW	1	-60	0.25	101		
1	2.0	10.00	Tandem SAW	3	-60	0.25	301		
1	2.0	10.00	Tandem SAW	5	-60	0.25	326		
1	2.0	10.00	Tandem SAW	0	-60	0.50	85		
1	2.0	10.00	Tandem SAW	1	-60	0.50	85		
1	2.0	10.00	Tandem SAW	3	-60	0.50	123		
1	2.0	10.00	Tandem SAW	5	-60	0.50	220		
1	2.0	20.30	Tandem SAW	0	-60	0.25	64		
1	2.0	20.30	Tandem SAW	1	-60	0.25	40		
1	2.0	20.30	Tandem SAW	3	-60	0.25	50		
1	2.0	20.30	Tandem SAW	5	-60	0.25	191		
1	2.0	20.30	Tandem SAW	0	-40	0.25	140		
1	2.0	20.30	Tandem SAW	1	-40	0.25	121		
1	2.0	20.30	Tandem SAW	3	-40	0.25	191		
1	2.0	20.30	Tandem SAW	5	-40	0.25	303		
1	3.0	2.30	SMAW	0	-60	0.25	156		
1	3.0	2.30	SMAW	1	-60	0.25	275		
1	3.0	2.30	SMAW	0	-50			0.32	
1	3.0	5.00	SAW	0	-60	0.25	194		
1	3.0	5.00	SAW	2	-60	0.25	300		
1	5.0	2.30	SMAW	0	-60	0.20	259		
1	5.0	5.00	SAW	0	-60	0.25	118		
1	5.0	2.30	SMAW	0	-40			0.65	
1	5.0	10.00	SAW	0	-45	0.25	55		
1	8.0	2.80	GMAW	0	-60	0.00	144		
1	8.0	2.80	GMAW	2	-60	0.00	256		
1	8.0	2.80	GMAW	5	-60	0.00	279		
1	8.0	2.80	GMAW	0	-60	1.00	255		
1	8.0	2.80	GMAW	2	-60	1.00	209		
1	8.0	2.80	GMAW	5	-60	1.00	232		
1	8.0	3.50	SAW	0	-60	0.00	178		
1	8.0	3.50	SAW	2	-60	0.00	238		
1	8.0	3.50	SAW	5	-60	0.00	262		
1	8.0	3.50	SAW	0	-60	1.00	130		
1	8.0	3.50	SAW	2	-60	1.00	215		
1	8.0	3.50	SAW	5	-60	1.00	236		
1	8.0	4.50	SAW	0	-60	0.00	113		
1	8.0	4.50	SAW	2	-60	0.00	154		
1	8.0	4.50	SAW	5	-60	0.00	205		
1	8.0	4.50	SAW	0	-60	0.50	130		
1	8.0	4.50	SAW	2	-60	0.50	258		
1	8.0	4.50	SAW	5	-60	0.50	257		
1	2.0	0.70	FCAW	0	-40		385		
1	2.0	0.70	FCAW	1	-40		260		
1	2.0	0.70	FCAW	0	-10			0.49	B x 2B Valid
1	2.0	0.70	FCAW	0	-10			0.50	B x 2B Valid

1[illegible]2.0	0.70	FCAW	0	-10		0.60	B x 2B	Valid
1[illegible]2.0	3.00	SAW	0	-10		1.10	B x 2B	Valid
1[illegible]2.0	3.00	SAW	0	-10		2.00	B x 2B	Valid
1[illegible]2.0	3.00	SAW	0	-10		2.10	B x 2B	Valid
1[illegible]2.0	4.50	SAW	0	-10		2.30	B x 2B	Valid
1[illegible]2.0	4.50	SAW	0	-10		2.40	B x 2B	Valid
1[illegible]2.0	4.50	SAW	0	-10		2.50	B x 2B	Valid
1[illegible]2.0	3.00	SAW	0	-40	450			
1[illegible]2.0	3.00	SAW	2	-40	450			
1[illegible]2.0	4.50	SAW	0	-40	350			
1[illegible]2.0	4.50	SAW	3	-40	430			
1[illegible]3.0	0.70	FCAW	0	-40	230			
1[illegible]3.0	0.70	FCAW	1	-40	200			
1[illegible]3.0	0.70	FCAW	0	-10		0.50	B x 2B	Valid
1[illegible]3.0	0.70	FCAW	0	-10		1.05	B x 2B	Valid
1[illegible]3.0	0.70	FCAW	0	-10		2.05	B x 2B	Valid
1[illegible]3.0	3.00	SAW	0	-10		2.10	B x 2B	Valid
1[illegible]3.0	3.00	SAW	0	-10		2.20	B x 2B	Valid
1[illegible]3.0	3.00	SAW	0	-10		2.00	B x 2B	Valid
1[illegible]3.0	4.50	SAW	0	-10		2.10	B x 2B	Valid
1[illegible]3.0	4.50	SAW	0	-10		2.20	B x 2B	Valid
1[illegible]3.0	4.50	SAW	0	-10		2.20	B x 2B	Valid
1[illegible]3.0	3.00	SAW	0	-40	400			
1[illegible]3.0	4.50	SAW	0	-40	320			

SHEET 7 WELD METAL TOUGHNESS DATA

WELD METAL PROPERTY DATA

Record Ref.	Source	Manufacturer	Process	Consumable Wire	Size [mm]	Flux/Gas	Designation	Position	Heat Input [kJ/mm]	Thickness [mm]	Groove	Yield [MPa]	Ultimate [MPa]	CVN Location	Test Temperature [°C]	Avg. Abs. Energy [J]	Min. Abs. Energy [J]	Average CTOD [mm]	Minimum CTOD [mm]	Comments
60	Manufacturer	Filarc	FCAW	Filarc PZ6138	1.2	C25	E81T1-Ni1	2G	1	20	V		>544	0	-40	111	73			
60	Manufacturer	Filarc	FCAW	Filarc PZ6138	1.2	C25	E81T1-Ni1	2G	1	20	V		>544	Root	-40	115	114			
60	Manufacturer	Filarc	FCAW	Filarc PZ6138	1.2	C25	E81T1-Ni1	2G	1.2	25	T Butt			0	-40	85	81			
60	Manufacturer	Filarc	FCAW	Filarc PZ6138	1.2	C25	E81T1-Ni1	2G	1.2	25	T Butt			Root	-40	92	85			
60	Manufacturer	Filarc	FCAW	Filarc PZ6138	1.2	C25	E81T1-Ni1	2G	1.1	40	V		>536		-40	101	98			
60	Manufacturer	Filarc	FCAW	Filarc PZ6138	1.2	C25	E81T1-Ni1	2G	1.1	40	V		>536		-40	71	46			
60	Manufacturer	Filarc	FCAW	Filarc PZ6138	1.2	C25	E81T1-Ni1	2G	1	50	V		>526	0	-40	66	61			
60	Manufacturer	Filarc	FCAW	Filarc PZ6138	1.2	C25	E81T1-Ni1	2G	1	50	V		>526	Root	-40	89	72			
60	Manufacturer	Filarc	FCAW	Filarc PZ6138	1.2	C25	E81T1-Ni1	2G	1	50	V		>526		-10			0.56	0.54	
60	Manufacturer	Filarc	FCAW	Filarc PZ6138	1.2	C25	E81T1-Ni1	2G	1.1	70	V	628	654	0	-40	97	87			
60	Manufacturer	Filarc	FCAW	Filarc PZ6138	1.2	C25	E81T1-Ni1	2G	1.1	70	V	628	654	Root	-40	47	32			
60	Manufacturer	Filarc	FCAW	Filarc PZ6138	1.2	C25	E81T1-Ni1	2G	1.1	70	V	628	654	.	-10			0.63	0.6	
60	Manufacturer	Filarc	FCAW	Filarc PZ6138	1.2	C25	E81T1-Ni1	3G up	1.9	50	V			.	-10			0.93	0.91	
60	Manufacturer	Filarc	FCAW	Filarc PZ6138	1.2	C25	E81T1-Ni1	3G up	2.1	50	Double V			0	-50	86	76			
60	Manufacturer	Filarc	FCAW	Filarc PZ6138	1.2	C25	E81T1-Ni1	3G up	2.1	50	Double V			Root	-50	61	54			
60	Manufacturer	Filarc	FCAW	Filarc PZ6138	1.2	C25	E81T1-Ni1	3G up	2.1	50	Double V			.	-10			0.87	0.87	
60	Manufacturer	Filarc	FCAW	Filarc PZ6138	1.2	C25	E81T1-Ni1	3G up	1.4	50	Half K	646	674	0	-40	65	61			
60	Manufacturer	Filarc	FCAW	Filarc PZ6138	1.2	C25	E81T1-Ni1	3G up	1.4	50	Half K	648	674	Root	-40	77	44			
60	Manufacturer	Filarc	FCAW	Filarc PZ6138	1.2	C25	E81T1-Ni1	3G up	1.4	50	Half K	648	674	.	-10			0.36	0.21	
60	Manufacturer	Filarc	FCAW	Filarc PZ6138	1.2	C20	E81T1-Ni1	3G up	1.7	50	Double V	606	651	Root	-40	77	43			
60	Manufacturer	Filarc	FCAW	Filarc PZ6138	1.2	C20	E81T1-Ni1	3G up	1.7	50	Double V	606	651	Root	-50	62	47			
60	Manufacturer	Filarc	FCAW	Filarc PZ6138	1.2	C20	E81T1-Ni1	3G up	1.7	50	Double V	606	651	Root	-60	40	29			
60	Manufacturer	Filarc	FCAW	Filarc PZ6138	1.2	C20	E81T1-Ni1	3G up	1.7	50	Double V	606	651	0	-40	129	122			
60	Manufacturer	Filarc	FCAW	Filarc PZ6138	1.2	C20	E81T1-Ni1	3G up	1.7	50	Double V	606	651	0	-50	103	99			
60	Manufacturer	Filarc	FCAW	Filarc PZ6138	1.2	C20	E81T1-Ni1	3G up	1.7	50	Double V	606	651	0	-60	106	91			
60	Manufacturer	Filarc	FCAW	Filarc PZ6138	1.2	C20	E81T1-Ni1	3G up	1.7	50	Double V	606	651	.	-15			1.47	0.97	
60	Manufacturer	Filarc	FCAW	Filarc PZ6145	1.2	C20	E81T5-Ni1	3G up	2.3	25	Double V			Root	-40	134	120			
60	Manufacturer	Filarc	FCAW	Filarc PZ6145	1.2	C20	E81T5-Ni1	3G up	2.3	25	Double V			0	-40	96	88			
60	Manufacturer	Filarc	FCAW	Filarc PZ6145	1.2	C20	E81T5-Ni1	3G up	2.3	25	Double V			Root	-50	92	54			
60	Manufacturer	Filarc	FCAW	Filarc PZ6145	1.2	C20	E81T5-Ni1	3G up	2.3	25	Double V			0	-50	77	72			
60	Manufacturer	Filarc	FCAW	Filarc PZ6145	1.2	C20	E81T5-Ni1	3G up	2.3	25	Double V			Root	-60	55	51			
60	Manufacturer	Filarc	FCAW	Filarc PZ6145	1.2	C20	E81T5-Ni1	3G up	2.3	25	Double V			0	-60	80	70			
60	Manufacturer	Filarc	FCAW	Filarc PZ6145	1.2	C20	E81T5-Ni1	3G up	2.25	50	Double V	583	680	Root	-40	62	44			
60	Manufacturer	Filarc	FCAW	Filarc PZ6145	1.2	C20	E81T5-Ni1	3G up	2.25	50	Double V	583	680	Root	-50	49	44			
60	Manufacturer	Filarc	FCAW	Filarc PZ6145	1.2	C20	E81T5-Ni1	3G up	2.25	50	Double V	583	680	0	-40	100	82			
60	Manufacturer	Filarc	FCAW	Filarc PZ6145	1.2	C20	E81T5-Ni1	3G up	2.25	50	Double V	583	680	0	-50	61	48			
60	Manufacturer	Filarc	FCAW	Filarc PZ6145	1.2	C20	E81T5-Ni1	3G up	2.25	50	Double V	583	680		-10			1.04	0.71	
61	AMCA Report	CLA	SMAW	CLA LAS18 Plus	4		E7018-1	1G	2.3	50	Double V	483	574		-10			0.53	0.42	
61	AMCA Report	CLA	SMAW	CLA LAS18 Plus	4		E7018-1	1G	2.3	50	Double V	483	574		-30			0.25	0.09	
61	AMCA Report	CLA	SMAW	CLA LAS18 Plus	5		E7018-1	1G	3	50	Double V	483	574		-10			0.10	0.08	
61	AMCA Report	CLA	SMAW	CLA LAS18 Plus	5		E7018-1	1G	3	50	Double V	483	574		-30			0.045	0.03	
61	AMCA Report	CLA	SMAW	CLA Atomarc	3.2		E8018C1	1G	1.3	50	Double V	496	566		-30			0.98	0.09	
61	AMCA Report	CLA	SMAW	CLA Atomarc	3.2		E8018C1	1G	1.3	50	Double V	496	566		-40			0.26	0.235	
61	AMCA Report	CLA	SMAW	CLA Atomarc	4		E8018C1	1G	2.3	50	Double V	523	607		-30			1.88	0.39	
61	AMCA Report	CLA	SMAW	CLA Atomarc	4		E8018C1	1G	2.3	50	Double V	523	607		-40			0.15	0.10	
61	AMCA Report	CLA	SMAW	CLA Atomarc	5		E8018C1	1G	3	50	Double V	505	592		-30			0.18	0.06	
61	AMCA Report	CLA	SMAW	CLA Atomarc	5		E8018C1	1G	3	50	Double V	505	592		-30			0.16	0.10	
61	AMCA Report	CLA	SMAW	CLA Atomarc	5		E8018C1	1G	3	50	Single V	432	519		-10			0.41	0.32	High K
61	AMCA Report	CLA	SMAW	CLA Atomarc	5		E8018C1	1G	3	50	Single V	432	519		-30			0.13	0.06	
61	AMCA Report	CLA	SMAW	CLA Atomarc	5		E8018C1	1G	3	50	Single V	396	478		-10			0.37	0.26	Low K
61	AMCA Report	CLA	SMAW	CLA Atomarc	5		E8018C1	1G	3	50	Single V	396	478		-30			0.12	0.02	
61	AMCA Report	CLA	SMAW	CLA LAS18 Plus	4		E7018-1	1G	2.3	50	Double V			0	-50	56	48			
61	AMCA Report	CLA	SMAW	CLA LAS18 Plus	4		E7018-1	1G	2.3	50	Double V			0	-40	56	23			
61	AMCA Report	CLA	SMAW	CLA LAS18 Plus	4		E7018-1	1G	2.3	50	Double V			Root	-40	48	43			
61	AMCA Report	CLA	SMAW	CLA LAS18 Plus	4		E7018-1	1G	2.3	50	Double V			Root	-50	25	16			
61	AMCA Report	CLA	SMAW	CLA LAS18 Plus	5		E7018-1	1G	3	50	Double V			0	-40	136	136			
61	AMCA Report	CLA	SMAW	CLA LAS18 Plus	5		E7018-1	1G	3	50	Double V			0	-50	55	11			
61	AMCA Report	CLA	SMAW	CLA LAS18 Plus	5		E7018-1	1G	3	50	Double V			Root	-20	33	24			
61	AMCA Report	CLA	SMAW	CLA LAS18 Plus	5		E7018-1	1G	3	50	Double V			Root	-50	13	9			
61	AMCA Report	CLA	SMAW	CLA Atomarc	3.2		E8018-C1	1G	1.3	50	Double V			0	-70	104	104			
61	AMCA Report	CLA	SMAW	CLA Atomarc	3.2		E8018-C1	1G	1.3	50	Double V			0	-50	132	132			
61	AMCA Report	CLA	SMAW	CLA Atomarc	3.2		E8018-C1	1G	1.3	50	Double V			Root	-50	115	111			
61	AMCA Report	CLA	SMAW	CLA Atomarc	3.2		E8018-C1	1G	1.3	50	Double V			Root	-70	58	27			
61	AMCA Report	CLA	SMAW	CLA Atomarc	4		E8018-C1	1G	2.3	50	Double V			0	-70	79	68			
61	AMCA Report	CLA	SMAW	CLA Atomarc	4		E8018-C1	1G	2.3	50	Double V			0	-50	119	117			

61	AMCA Report	CLA	SMAW	CLA Atomarc	4		E8018-C1	1G	2.3	50	Double V			Root	-50	43	37			
61	AMCA Report	CLA	SMAW	CLA Atomarc	4		E8018-C1	1G	2.3	50	Double V			Root	-40	72	61			
61	AMCA Report	CLA	SMAW	CLA Atomarc	5		E8018-C1	1G	3	50	Double V			0	-70	105	91			
61	AMCA Report	CLA	SMAW	CLA Atomarc	5		E8018-C1	1G	3	50	Double V			0	-50	132	132			
61	AMCA Report	CLA	SMAW	CLA Atomarc	5		E8018-C1	1G	3	50	Double V			Root	-30	39	20			
61	AMCA Report	CLA	SMAW	CLA Atomarc	5		E8018-C1	1G	3	50	Double V			Root	-20	77	75			
61	AMCA Report	CLA	SMAW	CLA Atomarc	5		E8018-C1	1G	3	50	Single V			0	-70	88	84			High K
61	AMCA Report	CLA	SMAW	CLA Atomarc	5		E8018-C1	1G	3	50	Single V			0	-50	126	126			High K
61	AMCA Report	CLA	SMAW	CLA Atomarc	5		E8018-C1	1G	3	50	Single V			Root	-70	58	48			High K
61	AMCA Report	CLA	SMAW	CLA Atomarc	5		E8018-C1	1G	3	50	Single V			Root	-60	60	58			High K
61	AMCA Report	CLA	SMAW	CLA Atomarc	5		E8018-C1	1G	3	50	Single V			0	-70	79	62			Low K
61	AMCA Report	CLA	SMAW	CLA Atomarc	5		E8018-C1	1G	3	50	Single V			0	-60	113	108			Low K
61	AMCA Report	CLA	SMAW	CLA Atomarc	5		E8018-C1	1G	3	50	Single V			Root	-50	58	49			Low K
61	AMCA Report	CLA	SMAW	CLA Atomarc	5		E8018-C1	1G	3	50	Single V			Root	-40	58	37			Low K
62	FTL Report	Kobe	SAW	US36	4	PFH-55LT	F7A8-EH14	1G	5	50	Double V	440	545	0	-60	105	95			Interpass 150
62	FTL Report	Kobe	SAW	US36	4	PFH-55LT	F7A8-EH14	1G	5	50	Double V	440	545	0	-70	67	61			Interpass 150
62	FTL Report	Kobe	SAW	US36	4	PFH-55LT	F7A8-EH14	1G	5	50	Double V	440	545	Root	-60	136	118			Interpass 150
62	FTL Report	Kobe	SAW	US36	4	PFH-55LT	F7A8-EH14	1G	5	50	Double V	440	545	Root	-70	92	75			Interpass 150
62	FTL Report	Kobe	SAW	US36	4	PFH-55LT	F7A8-EH14	1G	5	50	Double V	440	545		-30			2.75	2.73	Interpass 150
62	FTL Report	Kobe	SAW	US36	4	PFH-55LT	F7A8-EH14	1G	5	50	Double V	440	545		-50			0.38	0.21	Interpass 150
62	FTL Report	Kobe	SAW	US36	4	PFH-55LT	F7A8-EH14	1G	3.5	50	Double V	456	543	0	-60	137	129			Interpass 150
62	FTL Report	Kobe	SAW	US36	4	PFH-55LT	F7A8-EH14	1G	3.5	50	Double V	456	543	0	-70	101	96			Interpass 150
62	FTL Report	Kobe	SAW	US36	4	PFH-55LT	F7A8-EH14	1G	3.5	50	Double V	456	543	Root	-60	112	109			Interpass 150
62	FTL Report	Kobe	SAW	US36	4	PFH-55LT	F7A8-EH14	1G	3.5	50	Double V	456	543	Root	-70	113	107			Interpass 150
62	FTL Report	Kobe	SAW	US36	4	PFH-55LT	F7A8-EH14	1G	3.5	50	Double V	456	543		-30			2.46	2.23	Interpass 150
62	FTL Report	Kobe	SAW	US36	4	PFH-55LT	F7A8-EH14	1G	3.5	50	Double V	456	543		-50			1.92	0.70	Interpass 150
62	FTL Report	Kobe	SAW	US36	4	PFH-55LT	F7A8-EH14	1G	3.5	50	Double V			0	-60	147	143			Interpass 232
62	FTL Report	Kobe	SAW	US36	4	PFH-55LT	F7A8-EH14	1G	3.5	50	Double V			0	-70	50	43			Interpass 232
62	FTL Report	Kobe	SAW	US36	4	PFH-55LT	F7A8-EH14	1G	3.5	50	Double V			Root	-60	94	92			Interpass 232
62	FTL Report	Kobe	SAW	US36	4	PFH-55LT	F7A8-EH14	1G	3.5	50	Double V			Root	-70	41	16			Interpass 232
62	FTL Report	Kobe	SAW	US36	4	PFH-55LT	F7A8-EH14	1G	3.5	50	Double V				-30			2.58	2.40	Interpass 232
62	FTL Report	Kobe	SAW	US36	4	PFH-55LT	F7A8-EH14	1G	3.5	50	Double V				-50			1.84	1.16	Interpass 232
62	FTL Report	Kobe	SAW	US36	4	PFH-55LT	F7A8-EH14	1G	3.5	50	Double V			0	-60	147	143			High/High K
62	FTL Report	Kobe	SAW	US36	4	PFH-55LT	F7A8-EH14	1G	3.5	50	Double V			0	-70	50	43			High/High K
62	FTL Report	Kobe	SAW	US36	4	PFH-55LT	F7A8-EH14	1G	3.5	50	Double V			Root	-60	94	92			High/High K
62	FTL Report	Kobe	SAW	US36	4	PFH-55LT	F7A8-EH14	1G	3.5	50	Double V			Root	-70	41	16			High/High K
62	FTL Report	Kobe	SAW	US36	4	PFH-55LT	F7A8-EH14	1G	3.5	50	Double V				-30			2.48	2.26	High/High K
62	FTL Report	Kobe	SAW	US36	4	PFH-55LT	F7A8-EH14	1G	3.5	50	Double V				-50			2.42	2.33	High/High K
62	FTL Report	Kobe	SAW	US36	4	PFH-55LT	F7A8-EH14	1G	3.5	50	Double V			0	-60	108	87			High/Low K
62	FTL Report	Kobe	SAW	US36	4	PFH-55LT	F7A8-EH14	1G	3.5	50	Double V			0	-70	81	81			High/Low K
62	FTL Report	Kobe	SAW	US36	4	PFH-55LT	F7A8-EH14	1G	3.5	50	Double V			Root	-60	118	98			High/Low K
62	FTL Report	Kobe	SAW	US36	4	PFH-55LT	F7A8-EH14	1G	3.5	50	Double V			Root	-70	87	64			High/Low K
62	FTL Report	Kobe	SAW	US36	4	PFH-55LT	F7A8-EH14	1G	3.5	50	Double V				-30			2.76	2.61	High/Low K
62	FTL Report	Kobe	SAW	US36	4	PFH-55LT	F7A8-EH14	1G	3.5	50	Double V				-50			0.78	0.58	High/Low K
62	FTL Report	Kobe	SAW	US36	4	PFH-55LT	F7A8-EH14	1G	3.5	50	Double V			0	-60	103	92			Low/Low K
62	FTL Report	Kobe	SAW	US36	4	PFH-55LT	F7A8-EH14	1G	3.5	50	Double V			0	-70	30	30			Low/Low K
62	FTL Report	Kobe	SAW	US36	4	PFH-55LT	F7A8-EH14	1G	3.5	50	Double V			Root	-60	115	104			Low/Low K
62	FTL Report	Kobe	SAW	US36	4	PFH-55LT	F7A8-EH14	1G	3.5	50	Double V			Root	-70	17	15			Low/Low K
62	FTL Report	Kobe	SAW	US36	4	PFH-55LT	F7A8-EH14	1G	3.5	50	Double V				-30			2.44	2.17	Low/Low K
62	FTL Report	ESAB	SAW	OK Autrod 12.34	4	OK 10.62	F9A10-EA4	1G	3.5	50	Double V				-50			2.17	0.88	Low/Low K
62	FTL Report	ESAB	SAW	OK Autrod 12.34	4	OK 10.62	F9A10-EA4	1G	3.5	50	Double V	586	698	0	-40	62	60			
62	FTL Report	ESAB	SAW	OK Autrod 12.34	4	OK 10.62	F9A10-EA4	1G	3.5	50	Double V	586	698	0	-50	34	32			
62	FTL Report	ESAB	SAW	OK Autrod 12.34	4	OK 10.62	F9A10-EA4	1G	3.5	50	Double V	586	698	Root	-40	72	72			
62	FTL Report	ESAB	SAW	OK Autrod 12.34	4	OK 10.62	F9A10-EA4	1G	3.5	50	Double V	586	698	Root	-50	47	37			
62	FTL Report	ESAB	SAW	OK Autrod 12.34	4	OK 10.62	F9A10-EA4	1G	3.5	50	Double V	586	698		-10			0.3	0.21	
62	FTL Report	ESAB	SAW	OK Autrod 12.34	4	OK 10.62	F9A10-EA4	1G	3.5	50	Double V	586	698		-30			0.14	0.09	
62	FTL Report	ESAB	SAW	OK Autrod 12.34	4	OK 10.62	F9A10-EA4	1G	5	50	Double V	573	693	0	-40	45	41			
62	FTL Report	ESAB	SAW	OK Autrod 12.34	4	OK 10.62	F9A10-EA4	1G	5	50	Double V	573	693	0	-50	40	31			
62	FTL Report	ESAB	SAW	OK Autrod 12.34	4	OK 10.62	F9A10-EA4	1G	5	50	Double V	573	693	Root	-40	76	76			
62	FTL Report	ESAB	SAW	OK Autrod 12.34	4	OK 10.62	F9A10-EA4	1G	5	50	Double V	573	693	Root	-50	52	42			
62	FTL Report	ESAB	SAW	OK Autrod 12.34	4	OK 10.62	F9A10-EA4	1G	5	50	Double V	573	693		-10			0.11	0.07	
62	FTL Report	ESAB	SAW	OK Autrod 12.34	4	OK 10.62	F9A10-EA4	1G	5	50	Double V	573	693		-30			0.11	0.07	
63	FTL Report	Kobe	FCAW	DW-55L	1.2	C25	E80T1-K2	1G	2	50	Double V	626	669	0	-40	45	37			
63	FTL Report	Kobe	FCAW	DW-55L	1.2	C25	E80T1-K2	1G	2	50	Double V	626	669	0	-50	41	37			
63	FTL Report	Kobe	FCAW	DW-55L	1.2	C25	E80T1-K2	1G	2	50	Double V	626	669	Root	-40	40	37			
63	FTL Report	Kobe	FCAW	DW-55L	1.2	C25	E80T1-K2	1G	2	50	Double V	626	669	Root	-30	56	56			
63	FTL Report	Kobe	FCAW	DW-55L	1.2	C25	E80T1-K2	1G	2	50	Double V	626	669		-30			0.18	0.06	
63	FTL Report	Kobe	FCAW	DW-55L	1.2	C25	E80T1-K2	1G	2	50	Double V	626	669		-50			0.06	0.04	
63	FTL Report	Kobe	FCAW	DW-55L	1.2	C25	E80T1-K2	1G	3	50	Double V	532	579	0	-40	52	39			

63	FTL Report	Kobe	FCAW	DW-55L	1.2	C25	E80T1-K2	1G	3	50	Double V	532	579	0	-50	42	38				
63	FTL Report	Kobe	FCAW	DW-55L	1.2	C25	E80T1-K2	1G	3	50	Double V	532	579	Root	-40	65	38				
63	FTL Report	Kobe	FCAW	DW-55L	1.2	C25	E80T1-K2	1G	3	50	Double V	532	579	Root	-50	61	53				
63	FTL Report	Kobe	FCAW	DW-55L	1.2	C25	E80T1-K2	1G	3	50	Double V	532	579		-10			0.16	0.03		
63	FTL Report	Kobe	FCAW	DW-55L	1.2	C25	E80T1-K2	1G	3	50	Double V	532	579		-30			0.08	0.07		
63	FTL Report	Kobe	FCAW	DW-55L	1.2	C25	E80T1-K2	1G	2	50	SingleV	588	645	0	-50	87	46				Low K
63	FTL Report	Kobe	FCAW	DW-55L	1.2	C25	E80T1-K2	1G	2	50	SingleV	588	645	0	-60	74	46				Low K
63	FTL Report	Kobe	FCAW	DW-55L	1.2	C25	E80T1-K2	1G	2	50	SingleV	588	645	Root	-50	65	20				Low K
63	FTL Report	Kobe	FCAW	DW-55L	1.2	C25	E80T1-K2	1G	2	50	SingleV	588	645	Root	-60	38	26				Low K
63	FTL Report	Kobe	FCAW	DW-55L	1.2	C25	E80T1-K2	1G	2	50	SingleV	588	645		-30			0.38	0.13		Low K
63	FTL Report	Kobe	FCAW	DW-55L	1.2	C25	E80T1-K2	1G	2	50	SingleV	588	645		-50			0.11	0.09		Low K
63	FTL Report	Kobe	FCAW	DW-55L	1.2	C25	E80T1-K2	1G	2	50	SingleV	594	636	0	-60	98	83				High K
63	FTL Report	Kobe	FCAW	DW-55L	1.2	C25	E80T1-K2	1G	2	50	SingleV	594	636	0	-70	59	12				High K
63	FTL Report	Kobe	FCAW	DW-55L	1.2	C25	E80T1-K2	1G	2	50	SingleV	594	636	Root	-60	77	58				High K
63	FTL Report	Kobe	FCAW	DW-55L	1.2	C25	E80T1-K2	1G	2	50	SingleV	594	636	Root	-60	56	30				High K
63	FTL Report	Kobe	FCAW	DW-55L	1.2	C25	E80T1-K2	1G	2	50	SingleV	594	636		-30			0.33	0.09		High K
63	FTL Report	Kobe	FCAW	DW-55L	1.2	C25	E80T1-K2	1G	2	50	SingleV	594	636		-50			0.06	0.04		High K
63	FTL Report	ESAB	FCAW	OK Tubrod 15.17	1.2	C25	E81T1-Ni1	1G	3	50	Double V			0	-30	82	69				
63	FTL Report	ESAB	FCAW	OK Tubrod 15.17	1.2	C25	E81T1-Ni1	1G	3	50	Double V			0	-40	31	31				
63	FTL Report	ESAB	FCAW	OK Tubrod 15.17	1.2	C25	E81T1-Ni1	1G	3	50	Double V			Root	-40	64	56				
63	FTL Report	ESAB	FCAW	OK Tubrod 15.17	1.2	C25	E81T1-Ni1	1G	3	50	Double V			Root	-20	102	93				
63	FTL Report	ESAB	FCAW	OK Tubrod 15.17	1.2	C25	E81T1-Ni1	1G	3	50	Double V				-10			0.14	0.03		
63	FTL Report	ESAB	FCAW	OK Tubrod 15.17	1.2	C25	E81T1-Ni1	1G	3	50	Double V				-30			0.05	0.03		
63	FTL Report	ESAB	FCAW	OK Tubrod 15.17	1.2	C25	E81T1-Ni1	1G	2	50	Double V			0	-40	86	80				
63	FTL Report	ESAB	FCAW	OK Tubrod 15.17	1.2	C25	E81T1-Ni1	1G	2	50	Double V			0	-60	62	58				
63	FTL Report	ESAB	FCAW	OK Tubrod 15.17	1.2	C25	E81T1-Ni1	1G	2	50	Double V			Root	-40	117	111				
63	FTL Report	ESAB	FCAW	OK Tubrod 15.17	1.2	C25	E81T1-Ni1	1G	2	50	Double V			Root	-50	71	43				
63	FTL Report	ESAB	FCAW	OK Tubrod 15.17	1.2	C25	E81T1-Ni1	1G	2	50	Double V				-30			0.32	0.11		
63	FTL Report	ESAB	FCAW	OK Tubrod 15.17	1.2	C25	E81T1-Ni1	1G	2	50	Double V				-50			0.05	0.04		
63	FTL Report	ESAB	FCAW	OK Tubrod 15.17	1.2	C25	E81T1-Ni1	3G	2	50	Double V			0	-40	87	84				
63	FTL Report	ESAB	FCAW	OK Tubrod 15.17	1.2	C25	E81T1-Ni1	3G	2	50	Double V			0	-60	50	43				
63	FTL Report	ESAB	FCAW	OK Tubrod 15.17	1.2	C25	E81T1-Ni1	3G	2	50	Double V			Root	-40	89	86				
63	FTL Report	ESAB	FCAW	OK Tubrod 15.17	1.2	C25	E81T1-Ni1	3G	2	50	Double V			Root	-60	52	43				
63	FTL Report	ESAB	FCAW	OK Tubrod 15.17	1.2	C25	E81T1-Ni1	3G	2	50	Double V				-30			0.49	0.29		
63	FTL Report	ESAB	FCAW	OK Tubrod 15.17	1.2	C25	E81T1-Ni1	3G	2	50	Double V				-50			0.21	0.12		
64	FTL Report	Linde	GMAW	65	1.2	C5		1G	1.65	30	Cons Test			0.5	-40	38	15				
64	FTL Report	Linde	GMAW	65	1.2	C5		1G	1.65	30	Cons Test			0.5	-20	56	35				
64	FTL Report	Linde	GMAW	HI-84	1.2	C5		1G	1.65	30	Cons Test			0.5	-40	98	70				
64	FTL Report	Linde	GMAW	HI-84	1.2	C5		1G	1.65	30	Cons Test			0.5	-60	56	35				
64	FTL Report	Nippon	GMAW	YM-28E	1.2	C5		1G	1.65	30	Cons Test			0.5	-60	124	15				
64	FTL Report	Nippon	GMAW	YM-28E	1.2	C5		1G	1.65	30	Cons Test			0.5	-40	127	120				
64	FTL Report	Nippon	GMAW	YM-28E	1.2	C5		1G	1.65	30	Cons Test	478	575		-30			0.81	0.64		Tens. Props @ -30C
64	FTL Report	Nippon	GMAW	YM-28E	1.2	C5		1G	1.65	30	Cons Test				-50			0.56	0.18		
64	FTL Report	Nippon	GMAW	YM-28E	1.2	C5		1G	2.2	30	Cons Test	497	583	0.5	-60	67					
64	FTL Report	Nippon	GMAW	YM-28E	1.2	C5		1G	2.2	30	Cons Test	497	583	0.5	-40	126					
64	FTL Report	Nippon	GMAW	YM-28E	1.2	C5		1G	2.2	30	Cons Test	497	583		-30			0.38	0.19		
64	FTL Report	Nippon	GMAW	YM-28E	1.2	C5		1G	2.2	30	Cons Test	497	583		-50			0.25	0.21		
64	FTL Report	Nippon	GMAW	YM-28E	1.2	C5		3G	0.7	30	Cons Test	614	639	0.5	-60	148					
64	FTL Report	Nippon	GMAW	YM-28E	1.2	C5		3G	0.7	30	Cons Test	614	639	0.5	-40	152					
64	FTL Report	Nippon	GMAW	YM-28E	1.2	C5		3G	0.7	30	Cons Test	614	639		-30			0.81	0.64		
64	FTL Report	Nippon	GMAW	YM-28E	1.2	C5		3G	0.7	30	Cons Test	614	639		-50			0.56	0.18		
64	FTL Report	Nippon	GMAW	YM-36E	1.2	C5		1G	1.65	30	Cons Test			0.5	-60	131	127				
64	FTL Report	Nippon	GMAW	YM-36E	1.2	C5		1G	1.65	30	Cons Test			0.5	-80	128	123				
64	FTL Report	Nippon	GMAW	YM-36E	1.2	C5		1G	1.65	30	Cons Test	627	690		-30			0.65	0.12		Tens. Props @ -30C
64	FTL Report	Nippon	GMAW	YM-36E	1.2	C5		1G	1.65	30	Cons Test				-50			0.33	0.06		
64	FTL Report	Kobe	GMAW	MG50LT	1.2	C5		1G	1.65	30	Cons Test			0.5	-60	121	110				
64	FTL Report	Kobe	GMAW	MG50LT	1.2	C5		1G	1.65	30	Cons Test			0.5	-40	130	112				
64	FTL Report	Kobe	GMAW	MG50LT	1.2	C5		1G	1.65	30	Cons Test	687	748		-30			0.55	0.44		Tens. Props @ -30C
64	FTL Report	Kobe	GMAW	MG50LT	1.2	C5		1G	1.65	30	Cons Test				-50			0.17	0.14		
65	Oerlikon	Oerlikon	SMAW	1.2% Mn-1% Ni	4		E7018-G	3G	2	50	Single V	529	620	0	-40	89	80				
65	Oerlikon	Oerlikon	SMAW	1.2% Mn-1% Ni	4		E7018-G	3G	2	50	Single V	529	620	0.5	-40	88	82				
65	Oerlikon	Oerlikon	SMAW	1.2% Mn-1% Ni	4		E7018-G	3G	2	50	Single V	529	620	Root	-40	77	64				
65	Oerlikon	Oerlikon	SMAW	1.2% Mn-1% Ni	4		E7018-G	3G	2	50	Single V	529	620		-10			1.24	1.2		
66	Brown & Root	Oerlikon	SAW	SD3/PD3NiMoPowder				1G		63	Single V	529	612	0	-40	152	149				
66	Brown & Root	Oerlikon	SAW	SD3/PD3NiMoPowder				1G		63	Single V	529	612	0	-50	134	127				
66	Brown & Root	Oerlikon	SAW	SD3/PD3NiMoPowder				1G		63	Single V	529	612	0.5	-40	169	157				
66	Brown & Root	Oerlikon	SAW	SD3/PD3NiMoPowder				1G		63	Single V	529	612	0.5	-50	154	137				
66	Brown & Root	Oerlikon	SAW	SD3/PD3NiMoPowder		OP121TT		1G		63	Single V	529	612		-10			1.31	1.08		
66	Brown & Root	Oerlikon	Tandem SAW	SD3 Mo		OP121TT		1G				592	657	0	-40	104	99				

66	Brown & Root	Oerlikon	Tandem SAW	SD3 Mo		OP121TT		1G				592	657	0	-50	82	75			
66	Brown & Root	Oerlikon	Tandem SAW	SD3 Mo		OP121TT		1G				592	657		-10			0.3	0.25	
66	Brown & Root	Oerlikon	Tandem SAW	SD3 1Ni		OP121TT		1G				488	575	0	-30	122	116			
66	Brown & Root	Oerlikon	Tandem SAW	SD3 1Ni		OP121TT		1G				488	575	0	-40	76	74			
66	Brown & Root	Oerlikon	Tandem SAW	SD3 1Ni		OP121TT		1G				488	575	0	-50	63	56			
66	Brown & Root	Oerlikon	Tandem SAW	SD3 1Ni		OP121TT		1G				488	575		-10			1.18	0.72	
66	Brown & Root	Oerlikon	Tandem SAW	SD2 3Ni		OP121TT		1G				659	738	0	-30	92	88			
66	Brown & Root	Oerlikon	Tandem SAW	SD2 3Ni		OP121TT		1G				659	738	0	-40	82	81			
66	Brown & Root	Oerlikon	Tandem SAW	SD2 3Ni		OP121TT		1G				659	738	0	-50	62	62			
66	Brown & Root	Oerlikon	Tandem SAW	SD2 3Ni		OP121TT		1G				659	738		-10			0.13	0.11	
66	Brown & Root	Oerlikon	Tandem SAW	SD3 1Ni 0.5Mo		OP121TT		1G				607	659	0	-30	97	92			
66	Brown & Root	Oerlikon	Tandem SAW	SD3 1Ni 0.5Mo		OP121TT		1G				607	659	0	-40	75	69			
66	Brown & Root	Oerlikon	Tandem SAW	SD3 1Ni 0.5Mo		OP121TT		1G				607	659	0	-50	62	53			
66	Brown & Root	Oerlikon	Tandem SAW	SD3 1Ni 0.5Mo		OP121TT		1G				607	659		-10			0.13	0.04	
66	Brown & Root	Oerlikon	SAW	SD3 1Ni 0.25Mo		OP121TT		1G	2.4	50	Double V	579	645	0	-50	119	109			
66	Brown & Root	Oerlikon	SAW	SD3 1Ni 0.25Mo		OP121TT		1G	2.4	50	Double V	579	645	0	-60	85	44			
66	Brown & Root	Oerlikon	SAW	SD3 1Ni 0.25Mo		OP121TT		1G	2.4	50	Double V	579	645	0	-70	54	41			
66	Brown & Root	Oerlikon	SAW	SD3 1Ni 0.25Mo		OP121TT		1G	2.4	50	Double V	579	645	Root	-50	91	42			
66	Brown & Root	Oerlikon	SAW	SD3 1Ni 0.25Mo		OP121TT		1G	2.4	50	Double V	579	645	Root	-50	99	77			
66	Brown & Root	Oerlikon	SAW	SD3 1Ni 0.25Mo		OP121TT		1G	2.4	50	Double V	579	645	Root	-50	54	46			
66	Brown & Root	Oerlikon	SAW	SD3 1Ni 0.25Mo		OP121TT		1G	2.4	50	Double V	579	645		-10			1.05	0.83	
66	Brown & Root	Oerlikon	Tandem SAW	SD3 1Ni 0.25Mo		OP121TT		1G	3.5	50	Single V	607	659	0	-50	114	85			
66	Brown & Root	Oerlikon	Tandem SAW	SD3 1Ni 0.25Mo		OP121TT		1G	3.5	50	Single V	607	659	0	-60	113	100			
66	Brown & Root	Oerlikon	Tandem SAW	SD3 1Ni 0.25Mo		OP121TT		1G	3.5	50	Single V	607	659	0	-70	64	42			
66	Brown & Root	Oerlikon	Tandem SAW	SD3 1Ni 0.25Mo		OP121TT		1G	3.5	50	Single V	607	659	Root	-40	75	69			
66	Brown & Root	Oerlikon	Tandem SAW	SD3 1Ni 0.25Mo		OP121TT		1G	3.5	50	Single V	607	659	Root	-50	43	39			
66	Brown & Root	Oerlikon	Tandem SAW	SD3 1Ni 0.25Mo		OP121TT		1G	3.5	50	Single V	607	659	Root	-60	42	37			
66	Brown & Root	Oerlikon	Tandem SAW	SD3 1Ni 0.25Mo		OP121TT		1G	3.5	50	Single V	607	659		-10			1.28	0.79	
66	Brown & Root	Oerlikon	SAW	SD3 1Ni 0.25Mo		OP121TT		1G	3.5	50	Half K	544	622	0	-40	128	117			Steel A
66	Brown & Root	Oerlikon	SAW	SD3 1Ni 0.25Mo		OP121TT		1G	3.5	50	Half K	544	622	0	-50	69	66			Steel A
66	Brown & Root	Oerlikon	SAW	SD3 1Ni 0.25Mo		OP121TT		1G	3.5	50	Half K	544	622	Root	-40	89	84			Steel A
66	Brown & Root	Oerlikon	SAW	SD3 1Ni 0.25Mo		OP121TT		1G	3.5	50	Half K	544	622	Root	-50	81	69			Steel A
66	Brown & Root	Oerlikon	SAW	SD3 1Ni 0.25Mo		OP121TT		1G	3.5	50	Half K	544	622		-10			0.44	0.27	Steel A
66	Brown & Root	Oerlikon	SAW	SD3 1Ni 0.25Mo		OP121TT		1G	3.5	50	Half K	513	591	0	-40	126	99			Steel A
66	Brown & Root	Oerlikon	SAW	SD3 1Ni 0.25Mo		OP121TT		1G	3.5	50	Half K	513	591	0	-50	105	74			Steel A
66	Brown & Root	Oerlikon	SAW	SD3 1Ni 0.25Mo		OP121TT		1G	3.5	50	Half K	513	591	Root	-40	105	96			Steel A
66	Brown & Root	Oerlikon	SAW	SD3 1Ni 0.25Mo		OP121TT		1G	3.5	50	Half K	513	591	Root	-50	76	68			Steel A
66	Brown & Root	Oerlikon	SAW	SD3 1Ni 0.25Mo		OP121TT		1G	3.5	50	Half K	513	591		-10			1.06	0.91	Steel A
67	Manufacturer	ESAB	SAW	OK Autrod 13.27		OK 10.62	F8A10-ENi2	1G			Cons. Test	495	570		-60	90				Typical values for DC+
67	Manufacturer	ESAB	SAW	OK Autrod 13.27+Powder		OK 10.62	F8A10-ENi2	1G			Cons. Test	500	560		-60	70				Typical values for DC+
67	Manufacturer	ESAB	MCAW	OK Tubrod 14.04		C20	E71TG-Ni2				Cons. Test	480	540		-60	70				Typical Values
67	Manufacturer	ESAB	FCAW	OK Tubrod 15.25		C20	E71T5-Ni2				Cons. Test	460	550		-60	70				Typical Values
68	CANMET/MTL	Lincoln	SSFCAW	NR 450	2		E71T8-Ni2	1G	1.75	Single V		522	587	0	-40	139				440 MPa Yd, Nippon BM
68	CANMET/MTL	Lincoln	SSFCAW	NR 450	2		E71T8-Ni2	1G	1.75	Single V		522	587	0	-60	89				440 MPa Yd, Nippon BM
68	CANMET/MTL	Lincoln	SSFCAW	NR 450	2		E71T8-Ni2	1G	1.75	Single V		528	596	0	-40	139				440 MPa Yd, KawasakiBM
68	CANMET/MTL	Lincoln	SSFCAW	NR 450	2		E71T8-Ni2	1G	1.75	Single V		528	596	0	-60	111				440 MPa Yd, KawasakiBM
68	CANMET/MTL	Lincoln	FCAW		1.1	C20	E81K2-H	1G	1.8	Single V		668	718	0	-40	25				440 MPa Yd, Nippon BM
68	CANMET/MTL	Lincoln	FCAW		1.1	C20	E81K2-H	1G	1.8	Single V		662	718	0	-60	23				440 MPa Yd, Nippon BM
68	CANMET/MTL	Lincoln	FCAW		1.1	C20	E81K2-H	1G	1.8	Single V		659	712	0	-40	31				440 MPa Yd, KawasakiBM
68	CANMET/MTL	Lincoln	FCAW		1.1	C20	E81K2-H	1G	1.8	Single V		659	712	0	-60	15				440 MPa Yd, KawasakiBM
68	CANMET/MTL	CLA	SMAW	Atomarc	5		E8018-C1	1G	2	Single V		517	587	0	-40	134				440 MPa Yd, Nippon BM
68	CANMET/MTL	CLA	SMAW	Atomarc	5		E8018-C1	1G	2	Single V		517	587	0	-60	66				440 MPa Yd, Nippon BM
68	CANMET/MTL	CLA	SMAW	Atomarc	5		E8018-C1	1G	2	Single V		556	622	0	-40	77				440 MPa Yd, KawasakiBM
68	CANMET/MTL	CLA	SMAW	Atomarc	5		E8018-C1	1G	2	Single V		556	622	0	-60	21				440 MPa Yd, KawasakiBM
68	CANMET/MTL	Oerlikon	SMAW	Tenacito 38R	4		E7018-G	1G	2	Single V		520	584	0	-40	136				440 MPa Yd, Nippon BM
68	CANMET/MTL	Oerlikon	SMAW	Tenacito 38R	4		E7018-G	1G	2	Single V		520	584	0	-60	42				440 MPa Yd, Nippon BM
68	CANMET/MTL	Oerlikon	SMAW	Tenacito 38R	4		E7018-G	1G	2	Single V		538	605	0	-40	104				440 MPa Yd, KawasakiBM
68	CANMET/MTL	Oerlikon	SMAW	Tenacito 38R	4		E7018-G	1G	2	Single V		538	605	0	-60	90				440 MPa Yd, KawasakiBM
69	Fleet Technology	Lincoln	FCAW	Outershield-81K2H	1.1		E81K2H					537			-15			0.65	0.58	
69	Fleet Technology	Lincoln	FCAW	Outershield-81K2H	1.1		E81K2H					612			-15			0.55	0.43	
69	Fleet Technology	Lincoln	FCAW	Outershield-81K2H	1.1		E81K2H					612			-50	66	66			
69	Fleet Technology	Lincoln	FCAW	Outershield-81K2H	1.1		E81K2H					524			-15			0.41	0.37	
69	Fleet Technology	Lincoln	FCAW	Outershield-81K2H	1.1		E81K2H					524			-50	87	81			
69	Fleet Technology	Lincoln	FCAW	Outershield-81K2H	1.1		E81K2H					539			-15			1.15	1.01	
70	Fleet Technology	CLA	SMAW	519-1V			E8018-C1			50					-15			0.5	0.34	
70	Fleet Technology	CLA	FCAW	520-1V			E81T-Ni1			50					-15			0.59	0.22	
70	Fleet Technology	CLA	FCAW	534-1V			E81T-Ni1			50					-15			0.55	0.48	
70	Fleet Technology	CLA		145-V						30					-15			0.43	0.12	
70	Fleet Technology	CLA		133-V						50					-15			0.83	0.48	

70	Fleet Technology	CLA		92-411						20		620			-15			0.24	0.18	
70	Fleet Technology	CLA	SMAW	498-V			E8018-C1	3G				574	698		-15			0.42	0.2	
70	Fleet Technology	CLA	SMAW	503-V			E8018-C1	1G				555	655		-15			0.37	0.25	
70	Fleet Technology	CLA	SMAW	506-V			E8018-C1	3G				582	665		-15			0.5	0.16	
1 (53)	Manufacturer	Kawasaki	SAW	KW30T	1.2	KB100	EG-F7A8	1G	0.8	100	K	583	635	0.25	-50	120	68			
1 (53)	Manufacturer	Kawasaki	SAW	KW30T	1.2	KB100	EG-F7A8	1G	0.8	100	K	583	635	0.25	-60	25	19			
1 (53)	Manufacturer	Kawasaki	SAW	KW30T	1.2	KB100	EG-F7A8	1G	0.8	100	K	583	635		-10			1.92	1.87	
1 (53)	Manufacturer	Kawasaki	SAW	KW101B	4	KB100	EG-F7A8	1G	3	100	K	592	637	0.25	-50	121	47			
1 (53)	Manufacturer	Kawasaki	SAW	KW101B	4	KB100	EG-F7A8	1G	3	100	K	592	637	0.25	-70	37	34			
1 (53)	Manufacturer	Kawasaki	SAW	KW101B	4	KB100	EG-F7A8	1G	3	100	K	592	637		-10			1.43	1.41	
1 (53)	Manufacturer	Kawasaki	Tandem SAW	KW101B	4	KB100	EG-F7A8	1G	4.5	100	K	509	598	0.25	-50	60	34			
1 (53)	Manufacturer	Kawasaki	Tandem SAW	KW101B	4	KB100	EG-F7A8	1G	4.5	100	K	509	598	0.25	-40	127	70			
1 (53)	Manufacturer	Kawasaki	Tandem SAW	KW101B	4	KB100	EG-F7A8	1G	4.5	100	K	509	598	0.25	-60	88	22			
1 (53)	Manufacturer	Kawasaki	Tandem SAW	KW101B	4	KB100	EG-F7A8	1G	4.5	100	K	509	598		-10			0.91	0.88	
3	Manufacturer	Nippon	SMAW	L-55SN	4			1G	1.5	50	K			0	-40	150	115			
3	Manufacturer	Nippon	SMAW	L-55SN	4			1G	1.5	50	K			0.5	-40	165	150			
3	Manufacturer	Nippon	SAW	YD	4.8	NB55L		1G	4.5	50	K			0	-40	90	80			
3	Manufacturer	Nippon	SAW	YD	4.8	NB55L		1G	4.5	50	K			0.5	-40	230	200			
6	Manufacturer	Nippon	SAW	YD		NB55		1G	4.5	50	K			0	-40	238	210			BM YP 500
6	Manufacturer	Nippon	SAW	YD		NB55		1G	4.5	50	K			0.5	-40	258	245			BM YP 500
6	Manufacturer	Nippon	SAW	YD		NB55		1G	4	50	K			0.25	-60	233	210			BM YP 460
6	Manufacturer	Nippon	SAW	YD		NB55		1G	4	50	K			0.5	-60	256	230			BM YP 460
6	Manufacturer	Nippon	SAW	YD		NB55		1G	4	50	K			0.25	-60	175	170			BM YP 420
6	Manufacturer	Nippon	SAW	YD		NB55		1G	4	50	K			0.5	-60	190	180			BM YP 420
6	Manufacturer	Nippon	SAW	YD		NB55		1G	4	50	K			0.25	-60	142	135			BM YP 355
6	Manufacturer	Nippon	SAW	YD		NB55		1G	4	50	K			0.5	-60	160	125			BM YP 355
6	Manufacturer	Nippon	SAW	Y-3NT		NB55L		1G	20.5	32	Single V			0.25	-60	52	35			BM YP 355
6	Manufacturer	Nippon	SAW	Y-3NT		NB55L		1G	20.5	32	Single V			0.5	-60	71	50			BM YP 355
6	Manufacturer	Nippon	SAW	Y-3NT		NB55L		1G	20.5	32	Single V			0.25	-60	39	28			BM YP 460
6	Manufacturer	Nippon	SAW	Y-3NT		NB55L		1G	20.5	32	Single V			0.5	-60	50	32			BM YP 460
7	Manufacturer	Kawasaki	Tandem SAW	KW3T		KB100		1G	4.4	150	K	519	631	0.5	-60	166	160			
7	Manufacturer	Kawasaki	Tandem SAW	KW3T		KB100		1G	4.4	150	K	519	631		-30			1.3		One spec. 70mm x 70mm
12	Manufacturer	Kawasaki	Tandem SAW	KW101B	4.8	KB110		1G	5	30	Half K	587	644	0	-40	147	96			
12	Manufacturer	Kawasaki	Tandem SAW	KW101B	4.8	KB110		1G	5	30	Half K	587	644	0	-60	52	47			
12	Manufacturer	Kawasaki	Tandem SAW	KW101B	4.8	KB110		1G	5	30	Half K	587	644	0	-80	20	17			
12	Manufacturer	Kawasaki	Tandem SAW	KW101B	4.8	KB110		1G	5	30	Half K	587	644		-10			1.2	1.1	
12	Manufacturer	Kawasaki	Tandem SAW	KW101B	4.8	KB110		1G	5	30	Half K	587	644		-30			0.21	0.14	
12	Manufacturer	Kawasaki	Tandem SAW	KW101B	4.8	KB110		1G	5	30	Half K	587	644		-50			0.19		
12 (55)	Kawasaki	Kobe	One side, 3 Wire SA	US-255		PFI - 50LT		1G	20.2	30	Single V	542	718	0	-40	55	52			
12 (55)	Kawasaki	Kobe	One side, 3 Wire SA	US-255		PFI - 50LT		1G	20.2	30	Single V	542	718	0	-60	44	39			
12 (55)	Kawasaki	Kobe	One side, 3 Wire SA	US-255		PFI - 50LT		1G	20.2	30	Single V	542	718	0	-40			0.39	0.135	
12 (55)	Kawasaki	Kobe	One side, 3 Wire SA	US-255		PFI - 50LT		1G	20.2	30	Single V	542	718	0	-60			0.13	0.099	
12 (55)	Kawasaki	Kobe	Two side, 3 Wire SA	US-255/US-49A		PFI - 50LT		1G	13	30	Single V	603	711	0	-40	139	131			
12 (55)	Kawasaki	Kobe	Two side, 3 Wire SA	US-255/US-49A		PFI - 50LT		1G	13	30	Single V	603	711	0	-60	117	84			
12 (55)	Kawasaki	Kobe	Two side, 3 Wire SA	US-255/US-49A		PFI - 50LT		1G	13	30	Single V	603	711	0	-20			0.722	0.722	
12 (55)	Kawasaki	Kobe	Two side, 3 Wire SA	US-255/US-49A		PFI - 50LT		1G	13	30	Single V	603	711	0	-40			0.074	0.074	
13	Manufacturer	Kawasaki	SAW	KW101B		KB110		1G	4.7	56	K	566	628	0	-40	92	70			
13	Manufacturer	Kawasaki	SAW	KW101B		KB110		1G	4.7	56	K	566	628	0.25	-40	161	146			
13	Manufacturer	Kawasaki	SAW	KW101B		KB110		1G	4.7	56	K	566	628	0.5	-40	139	117			
13	Manufacturer	Kawasaki	SAW	KW101B		KB110		1G	4.7	56	K	566	628		-10			2.1	0.8	
14	Manufacturer	Kawasaki	SAW	KW50C	4.8	KB100		1G	10	32	Double V			0.25	-40	211	198			
14	Manufacturer	Kawasaki	SAW	KW50C	4.8	KB100		1G	10	32	Double V			0.75	-40	127	119			
19	Rautarukki	ESAB	SMAW	OK73.68			E8018-C1	1G	1.2	40	Double V			0	-40	152	138			500 MPa steel
19	Rautarukki	Lincoln	SAW	Lincoln LNS 162		Lincoln P240	F7A10Eni2	1G	5	40	Double V			0	-40	74	63			500 MPa steel
19	Rautarukki	Lincoln	SAW	Lincoln LNS 162		Lincoln P240	F7A10Eni2	1G	5	60	Double V			0	-40	91	70			420 MPa steel
19	Rautarukki	Lincoln	SMAW	OK73.68			E8018-C1	1G	1.2	60	Double V			0	-40	119	95			420 MPa steel
19	Rautarukki	ESAB	SAW	OK Autrod 13.27(Powder)		OK 10.62		1G	2.6	40	Double V			0	-40	87	73			420 MPa steel
19	Rautarukki	ESAB	SAW	OK Autrod 13.27		OK 10.62		1G	2	20	Double V			0	-40	55	46			420 MPa steel
19	Rautarukki	ESAB	SMAW	OK 73.08			E8018-G	1G	2.5	40	Double V			0	-40	74	33			420 MPa steel
19	Rautarukki	ESAB	SMAW	OK 73.08			E8018-G	1G	2.5	20	Double V			0	-40	90	83			420 MPa steel
21 (54)	Manufacturer	Kawasaki	SAW	KW 30T		KB 100		1G	5	60	K			0.25	-60	180	141			
21 (54)	Manufacturer	Kawasaki	SAW	KW 30T		KB 100		1G	5	60	K				-50			0.45	0.43	
21 (54)	Manufacturer	Kobelco	SAW	US 255/US-49A		PFI50LT/PFH-50LT		1G	14.2	60	Double V			0.25	-40	48	46			
21 (54)	Manufacturer	Kobelco	SAW	US 255/US-49A		PFI50LT/PFH-50LT		1G	14.2	60	Double V				-20			0.11	0.1	
21 (54)	Manufacturer	Kawasaki	SAW	US 255		PF1-50LT		1G	19.3	60	Double V			0.25	-60	90	79			
21 (54)	Manufacturer	Kawasaki	SAW	US 255		PF1-50LT		1G	19.3	60	Double V				-50			1.57	1.36	
A24	GTS	SAF	SAW	AS40A	4	AS 462			5	25	Double V				-40	50	44			
A24	GTS	Lincoln	EGW	NR 431	2.4			3G	8.5	25	Square				-20	37	26			
A24	GTS	SAF	SMAW	SAFDRY 59A				1G	1.2	50	Double V				-40	258	228			

A24	GTS	Oerlikon	SAW	SD3	4	OP121TT	1G	3	50	Double V			-40	132	122						
A25	CANMAR/Hitachi	Nippon	EGW	EG-51S		CO2	3G	11.55	30	Single V/Gap			-50	119	74						
A25	CANMAR/Hitachi	Nippon	EGW	EG-51S		CO2	3G	11.55	30	Single V/Gap			-40	127	93						
A27	NKK	Kobelco	SAW	US36	4.8	PFH55LT	1G	5	30	Half K			-60	100							
A27	NKK	Kobelco	SAW	US36	4.8	PFH55LT	1G	5	30	Half K			-10			1.88	1.74				
A27	NKK	Kobelco	Tandem	US36	4.8	PFH55LT	1G	10.2	30	Double V			-60	162							
A27	NKK	Kobelco	Tandem	US36	4.8	PFH55LT	1G	10.2	30	Double V			-10			1.68	1.63				
A27	NKK	Kobelco	SAW	US36	4.8	PFH55LT	1G	5	50	K			-60	128							
A27	NKK	Kobelco	SAW	US36	4.8	PFH55LT	1G	5	50	K			-10			2.45	1.95				
A27	NKK	Kobelco	Tandem	US36	4.8	PFH55LT	1G	10.2	50	Double V			-60	95							
A27	NKK	Kobelco	Tandem	US36	4.8	PFH55LT	1G	10.2	50	Double V			-10			1.23	1.16				
A28	NKK	Kobelco	SAW	USIN	4	PFH60LT	1G	5	40	K			-60	224							
A28	NKK	Kobelco	SAW	USIN	4	PFH60LT	1G	5	40	K			-50			2.86	2.82				
A29	Nippon	Nippon	SMAW	N-110			1G	2	50	K			-40	180	165					For 0, 0.25 & 0.5 postn	
A29	Nippon	Nippon	SMAW	N-110			1G	2	50	K			-60	85	75					For 2mm subsfce postn	
A29	Nippon	Nippon	SMAW	N-110			3G	4	50	K			-40	135	120					0.25 postn	
A29	Nippon	Nippon	SMAW	N-110			3G	4	50	K			-60	91	50					0.25 postn	
A29	Nippon	Nippon	SAW	YE	4.8	NB55E	1G	7	50	K			-60	175	155					For 2mm subsfce postn.	
A29	Nippon	Nippon	SMAW	N-13				3.5	70	Double V			-60	160	145						
A29	Nippon	Nippon	GMAW	YM-3N				3.5	70	Double V			-60	83	60						
A29	Nippon	Nippon	SAW	YE		NB55E	1G	5	70	Double V			-60	173	165						
A29	Nippon	Nippon	SAW	YE		NB55E	1G	5	70	Double V			-70	106	75						
A29	Nippon	Nippon	SAW	YD	4.8	NB55E	1G	4.5	50	K			-60	185	180					0.25 CVN postn	
A29	Nippon	Nippon	SAW	YD	4.8	NB55E	1G	5.1	50	Double V			-60	175	170					0.25 CVN postn	
A29	Nippon	Nippon	SMAW	N-12	5		1G	2.3	50	Double V			-60	115	100					0.25 CVN postn	
A29	Nippon	Nippon	SMAW	N-12	5		1G	2.3	40	K			-60	94	47					0.5 CVN postn	
A29	Nippon	Nippon	SMAW	N-12	5		1G	2.3	40	Double V			-60	93	61					0.25 CVN postn	
A29	Nippon	Nippon	SAW	YD	4.8	NB55E	1G	5.1	20	Double V			-60	84	75					0.5 CVN postn	
A29	Nippon	Nippon	SMAW	N-12	5		1G	2.3	20	Double V			-60	63	40					0.25 CVN postn	
A36	Tech Uni, Aachen	ESAB	SAW	OK Autrod 7.32/Powder		OK 10.62	1G	3	20	Y/HY	560	680	-50	115						FeE 355 base metal	
A36	Tech Uni, Aachen	ESAB	Tandem SAW	OK Autrod 7.32		OK 10.62	1G	8.5	20	Y/HY	500	670	0	27						FeE 355 base metal	
A36	Tech Uni, Aachen	ESAB	SAW	OK Autrod 7.32/Powder		OK 10.62	1G	5	40	DY/DHY	625		-60	100						FeE 355 base metal	
A36	Tech Uni, Aachen	ESAB	Tandem SAW	OK Autrod 7.32		OK 10.62	1G	9.8	40	DY/DHY	505		20	27						FeE 355 base metal	
A36	Tech Uni, Aachen	Oerlikon	SAW	SD3		OP121TT	1G	3	20	Y/HY			-50	100						FeE 460 base metal	
A36	Tech Uni, Aachen	Oerlikon	SAW	SD3		OP121TT	1G	3	35	DH/DHY			-60	100						FeE 460 base metal	
A36	Tech Uni, Aachen	Oerlikon	SAW	SD3/Powder		OP121TT	1G	3	20	Y/HY			-45	100						FeE 460 base metal	
A36	Tech Uni, Aachen	Oerlikon	SAW	SD3/Powder		OP121TT	1G	3	35	DH/DHY			-35	100						FeE 460 base metal	
A36	Tech Uni, Aachen	Oerlikon	Tandem SAW	Fluxocord35.22.30/A105		OP122	1G	8.3	20	Y/HY			-35	27						FeE 460 base metal	
A36	Tech Uni, Aachen	Oerlikon	Tandem SAW	Fluxocord35.22.30/A105		OP122	1G	7.9	35	DH/DHY			-20	100						FeE 460 base metal	
A48	TWI	Oerlikon	SAW	SD3,1Ni,1/4Mo		OP121TT	1G	3	50	Half K/Root gap			-50	50						50mm, QT, 472 MPa Yd	
A48	TWI	Oerlikon	SAW	SD3,1Ni,1/4Mo		OP121TT	1G	2	25	Half K/Root gap			-50	67						25mm, TMCP, 479 MPa Yd	
A48	TWI	Oerlikon	SAW	SD3,1Ni,1/4Mo		OP121TT	1G	3	50	Half K/Root gap			-50	70						50mm, TMCP, 516 MPa Yd	
A48	TWI	Oerlikon	SAW	SD3,1Ni,1/4Mo		OP121TT	1G	2	15	Half K/Root gap			-50	90						15mm, QT, 482 MPa Yd	
A48	TWI	Oerlikon	SAW	SD3,1Ni,1/4Mo		OP121TT	1G	3	50	Half K/Root gap			-10			0.69	0.37			50mm, QT, 472 MPa Yd	
A48	TWI	Oerlikon	SAW	SD3,1Ni,1/4Mo		OP121TT	1G	2	25	Half K/Root gap			-10			1.24	1.04			25mm, TMCP, 479 MPa Yd	
A48	TWI	Oerlikon	SAW	SD3,1Ni,1/4Mo		OP121TT	1G	3	50	Half K/Root gap			-10			0.79	0.75			50mm, TMCP, 516 MPa Yd	
A48	TWI	Oerlikon	SAW	SD3,1Ni,1/4Mo		OP121TT	1G	2	15	Half K/Root gap			-10			0.4	0.36			15mm, QT, 482 MPa Yd	
A50	NKK	Kobelco	SAw	US255		PFH 80AK	1G	4.9	30	Half k		0.25	-40	115	95						
A50	NKK	Kobelco	SAw	US255		PFH 80AK	1G	4.9	30	Half k		0.25	-10			1.2					
A50	NKK	Kobelco	SAw	US255		PFH 80AK	1G	4.9	70	Half k		0.25	-40	115	80						
A51	Kawasaki	Kawasaki	SAW	KW101B		KB100	1G	3	101.6	K			-40	162							
A51	Kawasaki	Kawasaki	SAW	KW101B		KB100	1G	4.5	101.6	K			-40	145							
A51	Kawasaki	Kawasaki	SAW	KW101B		KB100	1G	3	101.6	K			-10			1.3	1.28				
A51	Kawasaki	Kawasaki	SAW	KW101B		KB100	1G	4.5	101.6	K			-10			0.85	0.82				
A51	Kawasaki	Kawasaki	SAW	KW30T		KB100	1G	5	60	K			-60	177							
A51	Kawasaki	Kawasaki	SAW	KW30T		KB100	1G	5	60	K			-50			0.45	0.45				
A51	Kawasaki	Kobelco	SAW	US255		PFI50LT	1G	19.3	60	Double V			-60	88							
A51	Kawasaki	Kobelco	SAW	US255		PFI50LT	1G	19.3	60	Double V			-50			1.5	1.2				
A51	Kawasaki	Kawasaki	SAW	KW50CM		KB100	1G	3.5	50	Half K			-60	107							
A51	Kawasaki	Kawasaki	SAW	KW50CM		KB100	1G	4.5	50	Half K			-60	83							
A51	Kawasaki	Kawasaki	SAW	KW50CM		KB100	1G	3.5	50	Half K			-10			1.13	1				
A51	Kawasaki	Kawasaki	SAW	KW50CM		KB100	1G	4.5	50	Half K			-10			0.85	0.7				
A53	NKK	Kobe	SAW	US36	4	PFH55LT	1G	4.5	120	Double Vee		0	-60	101							
A53	NKK	Kobe	SAW	US36	4	PFH55LT	1G	4.5	120	Double Vee		0.5	-60	206							
A53	NKK	Kobe	SAW	US36	4	PFH55LT	1G	4.5	120	Double Vee		1	-60	172							
A53	NKK	Kobe	SAW	US36	4	PFH55LT	1G	4.5	120	Double Vee			-10			1.18	1.16				
A55	NKK	Kobe	Tandem Saw	US 36	4	PFH55LT	1G	7.2	32	Half K		0.25	-60	88							
A55	NKK	Kobe	Tandem Saw	US 36	4	PFH55LT	1G	7.2	32	Half K		0.5	-60	77							
A55	NKK	Kobe	Tandem Saw	US 36	4	PFH55LT	1G	10	32	Half K		0.25	-60	68							

S98

A55	NKK	Kobe	Tandem Saw	US 36	4	PFH55LT		1G	10	32	Half K			0.5	-60	59				
A55	NKK	Kobe	3 Wire Saw	US 43	4,6.4	PFI 50		1G	20.3	32				0.25	-40	77				
A55	NKK	Kobe	3 Wire Saw	US 43	4,6.4	PFI 50		1G	20.3	32				0.5	-40	125				
A57	Sumitoomo/Shell	Kobe	FCAW	DW-55L		100% CO2	E80T1-K2		0.7	102	K				-10			0.25	0.11	
A57	Sumitoomo/Shell	Kobe	FCAW	DW-55L		100% CO2	E80T1-K2		0.7	76	K				-10			0.22		
A57	Sumitoomo/Shell	Kobe	SAW	W36		BV 55	F7P8-EH14	1G	3	102	K				-10			3		
A57	Sumitoomo/Shell	Kobe	SAW	W36		BV 55	F7P8-EH14	1G	3	76	K				-10			3		
A57	Sumitoomo/Shell	Kobe	SAW	W36		BV 55	F7P8-EH14	1G	4.5	102	K				-10			3		
A57	Sumitoomo/Shell	Kobe	SAW	W36		BV 55	F7P8-EH14	1G	4.5	76	K				-10			3		
A71		Lincoln NW	SMAW	KRYO 2	3.2		E9018G					612	687		-50	57				
A71		Lincoln NW	SMAW	KRYO 2	4		E9018G					544	626		-50	73				
A71		Lincoln NW	SMAW	KRYO 2	4		E9018G					544	626		-40	119				
A71		ESAB	SAW	OK Autrod 12.32	4	OK Flux 10.62							596		-50	80	78			
A71		Kobe	SMAW		4		E8018G		1.9	20					-60	125	110			
A71		Kobe	SMAW		4		E8018G		3.5	25					-60	150	148			
A71		Alloy Rods	FCAW	Dual Shield II81-K2	1.2	CO2	E80T1-K2					544	612		-50	81	79			
A71		Alloy Rods	FCAW	Dual Shield II81-K2	1.2	CO2	E80T1-K2		2						-60	55				
A71		Alloy Rods	FCAW	Dual Shield II81-K2	1.2	CO2	E80T1-K2		3.5						-60	45				
A71		Nippon Steel	SAW	Y-DX		NB-55L			2.5						-60	78	40			
A71		Nippon Steel	SAW	Y-DX		NB-55L			2.5						-50	123	90			
A71		Nippon Steel	SAW	Y-DX		NB-55L			4.5						-60	55	50			
A71		Lincoln	FCAW	Outershield 81 K2-H	1.2	C25	E81-K2	2G	0.73	20				0	-30	94	86			
A71		Lincoln	FCAW	Outershield 81 K2-H	1.2	C25	E81-K2	3G	1.3	20				0	-30	109	102			
A71		Lincoln	FCAW	Outershield 81 K2-H	1.2	C25	E81-K2	2G	1.2	40				0	-50	84	46			
A71		Lincoln	FCAW	Outershield 81 K2-H	1.2	C25	E81-K2	2G	1.3	40				0.5	-50	58	48			Root bead different WM
A71		Lincoln	FCAW	Outershield 81 K2-H	1.2	C25	E81-K2	2G	1	60				0	-50	69	63			
A71		Lincoln	FCAW	Outershield 81 K2-H	1.2	C25	E81-K2	2G	1.1	60				0.5	-50	66	60			Root bead different WM
A71		Lincoln	FCAW	Outershield 81 K2-H	1.2	C25	E81-K2	2G	1.65	40				0	-50	67	58			
A71		Lincoln	FCAW	Outershield 81 K2-H	1.2	C25	E81-K2	2G	1.3	40				0.5	-50	60	50			Root bead different WM
A71		Lincoln	FCAW	Outershield 81 K2-H	1.2	C25	E81-K2	3G	1.6	60				0	-50	48	38			
A71		Lincoln	FCAW	Outershield 81 K2-H	1.2	C25	E81-K2	3G	1.5	60				0.5	-50	65	56			
A71		Lincoln	FCAW	Outershield 81 K2-H	1.2	C25	E81-K2	2G	1.1	65				0	-50	71	66			
A71		Lincoln	FCAW	Outershield 81 K2-H	1.2	C25	E81-K2	2G	1.15	65				0.5	-50	50	48			
A71		Lincoln	FCAW	Outershield 81 K2-H	1.2	C25	E81-K2	3G	1.5	65				0	-50	88	75			
A71		Lincoln	FCAW	Outershield 81 K2-H	1.2	C25	E81-K2	3G	1.5	65				0.5	-50	76	46			
A71		Lincoln	FCAW	Outershield 81 K2-H	1.2	C25	E81-K2	2G	1.05	60				0	-50	62	53			
A71		Lincoln	FCAW	Outershield 81 K2-H	1.2	C25	E81-K2	2G	1.3	60				0.5	-50	64	54			
A71		Lincoln	FCAW	Outershield 81 K2-H	1.2	C25	E81-K2	3G	1.47	60				0	-50	65	54			
A71		Lincoln	FCAW	Outershield 81 K2-H	1.2	C25	E81-K2	3G	1.3	60				0.5	-50	49	36			
A71		Lincoln NW	SAW	LNS 162	3.2	P240	F710-ENi2	1G	1.5	40				0	-50	147	132			
A71		Lincoln NW	SAW	LNS 162	3.2	P240	F710-ENi2	1G	1.5	40				0.5	-50	114	95			SMAW Root
A71		CLA	SMAW	Atomarc 8018 C1	3.2		E8018 C1	6G	1.3	38				0	-50	94	80			
A71		CLA	SMAW	Atomarc 8018 C1	3.2		E8018 C1	6G	1.5	38				0.5	-50	38	32			Root bead KRYO 2
A71		Lincoln	FCAW	Outershield 81K2-H	1.2	C25	E80T1-K2	5G	1.6	38				0	-50	50	32			
A71		Lincoln	FCAW	Outershield 81K2-H	1.2	C25	E80T1-K2	5G	1.3	38				0.5	-50	50	33			Root bead KRYO 2
A71		CLA	SMAW	Atomarc 8018 C1	3.2		E8018 C1	3G	1.45	20				0	-30	131	130			
A71		CLA	SMAW	Atomarc 8018 C1	3.2		E8018 C1	3G	1.55	40				0	-50	100	88			
A71		CLA	SMAW	Atomarc 8018 C1	3.2		E8018 C1	3G	1.5	40				0.5	-50	70	40			Root bead KRYO 2
A71		CLA	SMAW	Atomarc 8018 C1	3.2-5		E8018 C1	2G	1.55	65				0	-50	61	35			
A71		CLA	SMAW	Atomarc 8018 C1	3.2-5		E8018 C1	2G	1.5	65				0.5	-50	46	41			
A71		Lincoln NW	SMAW	KRYO 2	3.2-5		E9018G	2G	1.25	30				0	-50	72	67			
A71		Lincoln NW	SMAW	KRYO 2	3.2-5		E9018G	2G	1.5	30				0.5	-50	72	50			
A71		Lincoln NW	SMAW	KRYO 2	3.2-4		E9018G	3G	1.6	30				0	-50	68	43			
A71		Lincoln NW	SMAW	KRYO 2	3.2-4		E9018G	3G	1.65	30				0.5	-50	58	42			
A71		Lincoln NW	SMAW	KRYO 2	3.2-5		E9018G	2G	1.6	50				0	-50	94	74			
A71		Lincoln NW	SMAW	KRYO 2	3.2-5		E9018G	2G	1.65	50				0.5	-50	58	46			
A71		Lincoln NW	SMAW	KRYO 2	3.2-4		E9018G	3G	1.6	50				0	-50	95	67			
A71		Lincoln NW	SMAW	KRYO 2	3.2-4		E9018G	3G	1.8	50				0.5	-50	58	36			
A71		Filarc	FCAW	PZ6138	1.2	C20	E81T1-Ni1	2G	1.16	30				0	-50	127	124			
A71		Filarc	FCAW	PZ6138	1.2	C20	E81T1-Ni1	2G	1.4	30				0.5	-50	110	106			
A71		Filarc	FCAW	PZ6138	1.2	C20	E81T1-Ni1	3G	1.6	30				0	-50	124	122			
A71		Filarc	FCAW	PZ6138	1.2	C20	E81T1-Ni1	3G	1.7	30				0.5	-50	144	142			
A71		Filarc	FCAW	PZ6138	1.2	C20	E81T1-Ni1	2G	1.3	50				0	-50	92	63			
A71		Filarc	FCAW	PZ6138	1.2	C20	E81T1-Ni1	2G	1.4	50				0.5	-50	90	73			
A71		Filarc	FCAW	PZ6138	1.2	C20	E81T1-Ni1	3G	1.7	50				0	-50	84	30			
A71		Filarc	FCAW	PZ6138	1.2	C20	E81T1-Ni1	3G	1.55	50				0.5	-50	124	116			
A71		Filarc	FCAW	PZ6138	1.2	C20	E81T1-Ni1	2G	1.2	30				0	-50	91	85			
A71		Filarc	FCAW	PZ6138	1.2	C20	E81T1-Ni1	2G	1.5	30				0.5	-50	108	101			
A71		ESAB	SAW	OK Autrod 12.32		OK 10.62		1G	1.6	16				0	-30	38	22			

A71	Kobe	SMAW	NB-1SJ	4		E8016-G	2G	1.7	50	0	-50	118	102	
A71	Kobe	SMAW	NB-1SJ	4		E8016-G	2G	1.75	50	0.5	-50	133	122	
A71	Kobe	SMAW	NB-1SJ	4		E8016-G	3G	2.2	50	0	-50	132	117	
A71	Kobe	SMAW	NB-1SJ	4		E8016-G	3G	2.45	50	0.5	-50	134	117	
A71	Kobe	SMAW	NB-1SJ	4		E8016-G	2G	1.45	30	0	-50	140	118	
A71	Kobe	SMAW	NB-1SJ	4		E8016-G	2G	1.7	30	0.5	-50	162	142	
A71	Kobe	SMAW	NB-1SJ	4		E8016-G	3G	1.85	30	0	-50	130	118	
A71	Kobe	SMAW	NB-1SJ	4		E8016-G	3G	2.3	30	0.5	-50	170	129	
A71	Kobe	SMAW	NB-1SJ	4		E8016-G	1G	2.1	25	0	-25	141	126	
A71	Nippon Steel	SAW	Y-D	4	NB-5L	F88-EG	1G	1.85	50	0	-50	125	104	
A71	Nippon Steel	SAW	Y-D	4	NB-5L	F88-EG	1G	1.85	50	0.5	-50	197	169	GMAW Root
A71	Nippon Steel	SAW	Y-D	4	NB-5L	F88-EG	1G	1.85	30	0	-50	179	166	
A71	Nippon Steel	SAW	Y-D	4	NB-5L	F88-EG	1G	1.75	30	0.5	-50	204	190	GMAW Root
A71	Nippon Steel	SAW	Y-D	4	NB-5L	F88-EG	1G	1.95	40	0	-45	212	189	
A71	Nippon Steel	SAW	Y-D	4	NB-5L	F88-EG	1G	1.95	40	0.5	-45	190	182	GMAW Root
A71	Kobe	SMAW	NB-1SJ	4		E8016-G	2G	1.7	40	0	-50	174	168	
A71	Kobe	SMAW	NB-1SJ	4		E8016-G	2G	1.95	40	0.5	-50	180	162	
A71	Kobe	SMAW	NB-1SJ	4		E8016-G	3G	2.55	40	0	-50	149	128	
A71	Kobe	SMAW	NB-1SJ	4		E8016-G	3G	2.5	40	0.5	-50	177	155	
A71	Alloy Rods	FCAW	Dual Shield II 81-K2	1.2	CO2	E80T1-K2	2G	1.1	50	0	-50	63	52	
A71	Alloy Rods	FCAW	Dual Shield II 81-K2	1.2	CO2	E80T1-K2	2G	1.7	50	0.5	-50	58	45	
A71	Alloy Rods	FCAW	Dual Shield II 81-K2	1.2	CO2	E80T1-K2	3G	1.7	50	0	-50	88	30	
A71	Alloy Rods	FCAW	Dual Shield II 81-K2	1.2	CO2	E80T1-K2	3G	1.7	50	0.5	-50	160	150	
A71	Alloy Rods	FCAW	Dual Shield II 81-K2	1.2	CO2	E80T1-K2	1G	2.25	25	0	-25	77	35	
A71	Alloy Rods	FCAW	Dual Shield II 81-K2	1.2	CO2	E80T1-K2	3G	2.2	13	0	-25	53	38	
A71	Alloy Rods	FCAW	Dual Shield II 81-K2	1.2	CO2	E80T1-K2	2G	1.05	40	0	-45	91	77	
A71	Alloy Rods	FCAW	Dual Shield II 81-K2	1.2	CO2	E80T1-K2	2G	2.25	40	0.5	-45	73	61	
A71	Alloy Rods	FCAW	Dual Shield II 81-K2	1.2	CO2	E80T1-K2	3G	1.55	40	0	-45	41	20	
A71	Alloy Rods	FCAW	Dual Shield II 81-K2	1.2	CO2	E80T1-K2	3G	1.9	40	0.5	-45	140	93	
A71	Alloy Rods	FCAW	Dual Shield II 81-K2	1.2	CO2	E80T1-K2	3G	1.55	40	0	-45	122	46	
A71	Alloy Rods	FCAW	Dual Shield II 81-K2	1.2	CO2	E80T1-K2	3G	1.55	40	0	-45	82	36	
A71	Alloy Rods	FCAW	Dual Shield II 81-K2	1.2	CO2	E80T1-K2	2G	1.6	20	0	-25	88	79	
A71	Alloy Rods	FCAW	Dual Shield II 81-K2	1.2	CO2	E80T1-K2	3G	1.95	20	0	-25	144	137	

APPENDIX D

APPROACH USED TO ARRIVE AT CURRENT SHIP STEEL CVN REQUIREMENTS IN CLASSIFICATION SOCIETY RULES (NKK APPROACH 1979)

The NKK Approach

This approach was formulated by the Japanese Classification Society NKK (Nippon Kaiji Kyokai) in 1979 and is based on wide plate test (centre-notched tension tests) results for ships steels [D.1].

The suitability of a steel for any particular location or structural member of the ship structure is judged in two stages. First, its minimum fracture toughness, K_c, is estimated from the CVN specimen (a certain minimum number of Joules at a specified temperature). Next, it is compared to the fracture toughness requirement for that location based on design conditions (service and residual stresses, service temperature and assumed allowable crack lengths). The steps involved in calculating the minimum anticipated fracture toughness can be summarized as follows:

Step 1: Estimate an absorbed energy transition temperature (T_E °C) corresponding to 50% fibrous fracture, from minimum specified CVN absorbed energy (E_τ in kg.m) at the test temperature T_τ using the equation:

$$E_T = \frac{1}{\sqrt{2\pi}} \int_{-\infty}^{T_t - T_E} \exp\left\{-\frac{1}{2}\left(\frac{T_t - T_E}{20}\right)^2\right\} dT_t$$

Step 2: Estimate the brittle fracture initiation temperature T_i (°C) as a function of the energy transition temperature (T_E), the steel thickness (t, mm) and yield strength (σ_y, kg mm^{-2}) as follows:

$$T_i = (0.00321\ \sigma_y + 0.391).T_E + 2.74\ \sqrt{t} - 278.59$$

This equation had been established based on wide plate tests (Figure D.1) with a centre machined notch 80 mm in length, and an applied stress of 0.5 σ_y.

Step 3: Estimate the fracture toughness (K_c - blunt notch, in kg mm$^{-3/2}$) of the steel using the expressions:

$$K_c = K_o \exp\{-k_o/(T + 273)\}$$

where $k_o = 562$°K (experimentally obtained material constant)

and $K_o = 5.6\ \sigma_y \exp\{562/(273 + T_i)\}$

The agreement between the estimated and actual values is shown in Figures D2(a) and D2(b).

Step 4: Estimate the fracture toughness (K_{cf} - fatigue sharpened notch) based on the experimentally established relationship:

$$K_{cf} = 0.68\ K_c$$

The procedures outlined above thus can be used to generate a table giving the minimum anticipated value for fracture toughness of steel plates for hull use as a function of its strength, thickness, CVN specification and temperature, and this is shown in Table D1 as reproduced from Reference D2.

For steel selection, these values need to be compared with the minimum fracture toughness needed based on the design parameters, and can be represented by the equation:

$$K_{c(required)} = (\alpha + \beta)\ \sigma_y \sqrt{\pi a}$$

where 2a, the maximum allowable through thickness crack length, is assumed to bee 250mm (for base material); α is the design stress as a fraction of the yield strength σ_y (also called the coefficient of utilization) and β is the magnitude of the residual (and reaction) stresses as a function of σ_y . For base metals, the flaw is assumed to be perpendicular to the weld, i.e., the high tensile weld longitudinal residual stresses are assumed to be perpendicular to the plane of the flaw; and for this situation, β is assumed to be 0.6.

Once the thickness and coefficient of utilization are established for a structural member, it is then straight forward to calculate $K_{c(required)}$ and then select a steel grade using the data in Table D1.

REFERENCES

D1. Nippon Kaiji Kyokai Document submitted to IACS, "Minimum Service Temperature of Hull Structural Steels", July 1979.

D2. Yajima, H., et al, "Materials Selection for Hull Steel Plates Based on Fracture Toughness", Technical Review, Nagasaki Technical Institute; Mitsubishi Heavy Industries Ltd., February 1981, p 52.

TABLE D1: Minimum K_c Values of Steel Plates for Hull Use, Specified in IACS Rules (Base Metal)

(unit : kg, $\overline{mm}/mm^2$)

Steel	Grade	Temp. (°C)	Thickness (mm)								
			10	15	20	25	30	35	40	45	50
Mild steel	A	0	548	534	507	482	471	459	448	438	428
		−10	507	493	469	446	435	425	415	405	396
		−20	466	453	431	410	400	390	381	372	364
		−30	425	414	393	374	365	356	348	340	332
		−40	385	375	356	339	330	323	315	308	301
		−50	345	336	320	304	297	290	283	276	270
	B	0	628	594	578	548	534	520	507	482	471
		−10	581	549	534	507	493	481	469	446	435
		−20	534	505	491	466	453	442	431	410	400
		−30	487	461	448	425	414	403	393	374	365
		−40	441	417	406	385	375	365	356	339	330
		−50	396	374	364	345	336	328	320	304	297
	D	0	727	635	646	628	611	578	563	548	534
		−10	672	633	597	581	565	534	520	507	493
		−20	618	582	549	534	519	491	478	466	453
		−30	564	531	501	487	473	448	436	425	414
		−40	511	481	454	441	429	406	395	385	375
		−50	458	432	407	396	385	364	355	345	336
	E	0	1 168	1 084	1 009	974	941	880	851	824	798
		−10	1 080	1 003	933	901	870	814	787	762	738
		−20	993	922	858	823	800	748	723	700	678
		−30	906	841	783	756	730	682	660	639	619
		−40	820	762	709	684	661	618	598	579	560
		−50	736	684	636	614	593	554	536	519	503
50kg mm² class high-tensile steel ($\sigma_Y \leqq 32$kg mm²)	AH	0	711	676	643	627	598	584	571	553	545
		−10	653	625	595	580	553	540	528	516	504
		−20	605	574	546	533	508	496	485	474	463
		−30	552	524	499	487	464	453	443	433	423
		−40	500	475	452	441	420	410	401	392	383
		−50	448	426	405	395	377	368	360	352	344
	DH	0	913	887	837	792	770	750	730	711	693
		−10	844	820	774	732	712	694	675	658	641
		−20	776	753	711	673	655	637	621	605	589
		−30	708	688	649	614	598	582	566	552	538
		−40	641	623	588	556	541	527	513	500	487
		−50	575	559	528	499	486	473	460	448	437
	EH	0	1 255	1 173	1 135	1 064	1 031	999	969	941	913
		−10	1 160	1 085	1 049	984	953	924	896	870	844
		−20	1 066	997	964	904	876	849	824	799	776
		−30	973	910	880	825	800	775	752	729	708
		−40	881	824	797	747	724	702	681	661	641
		−50	791	739	715	671	650	630	611	593	575

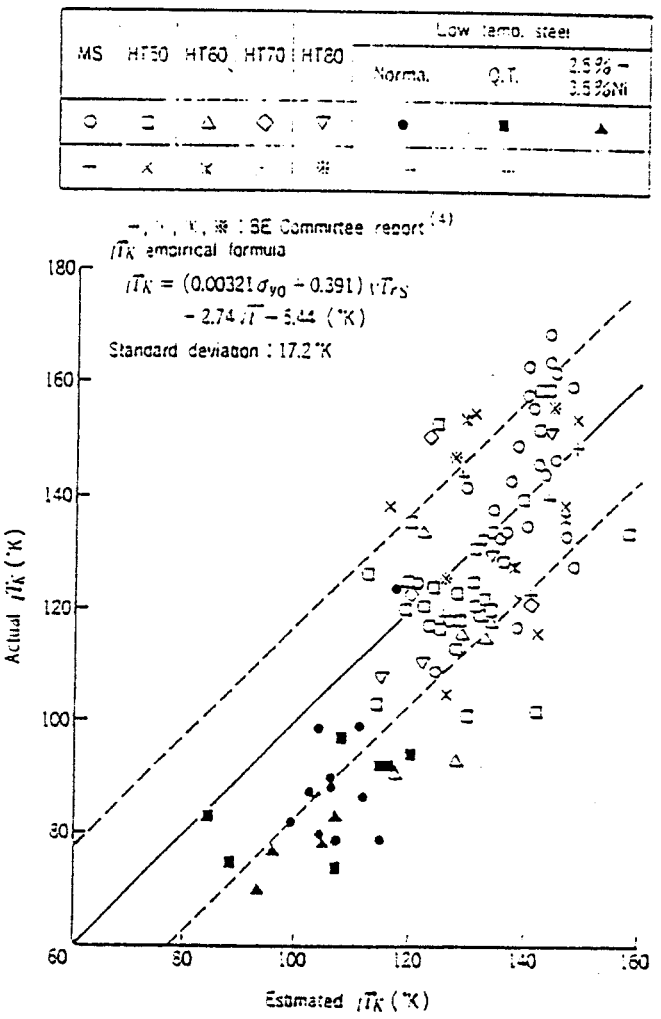

Figure D1: Measured and estimated values of critical temperature for brittle fracture initiation (base material) (Reproduced from Ref. D2)

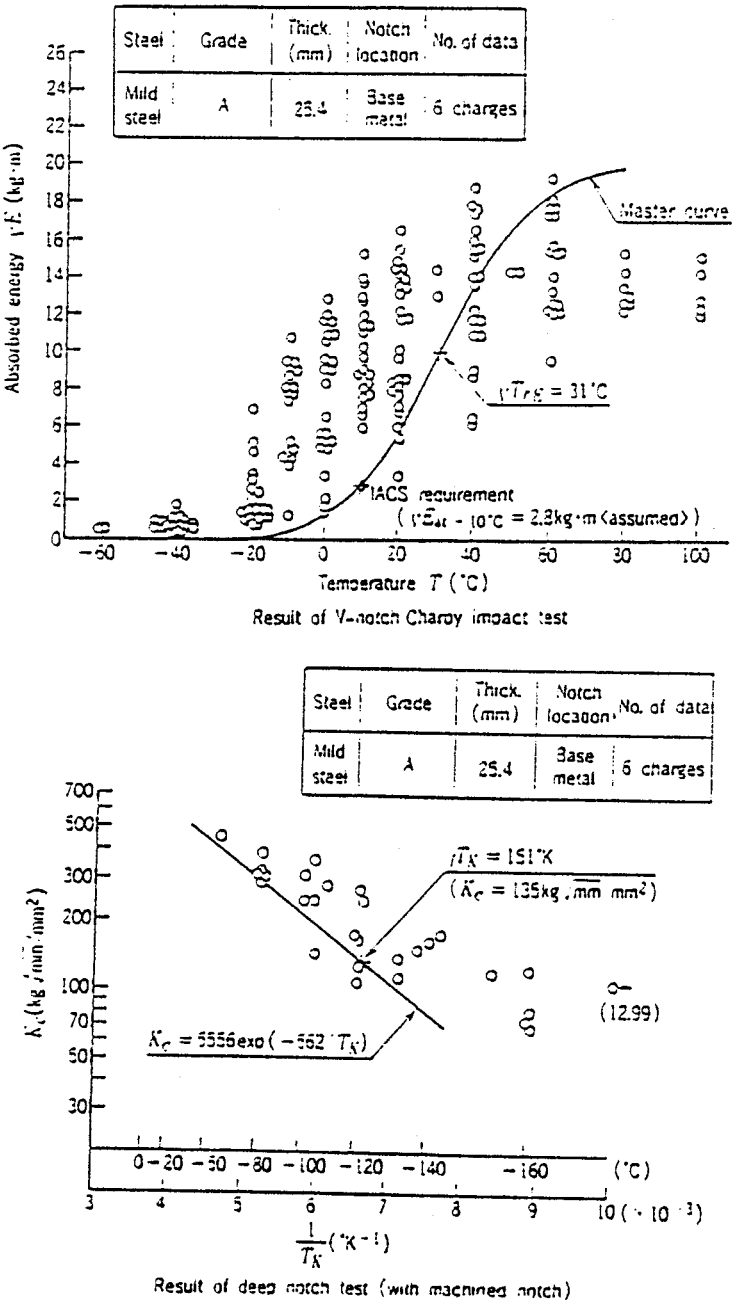

Figure D2(a): Measured and estimated values of fracture toughness of Grade A mild steel plate for hull use (25mm thick) (Reproduced from Ref. D2)

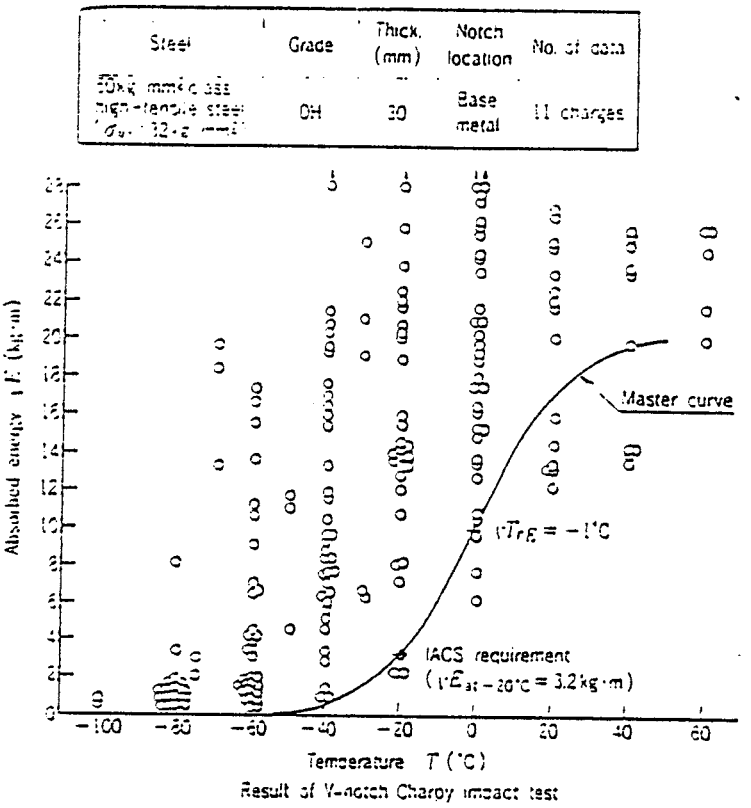

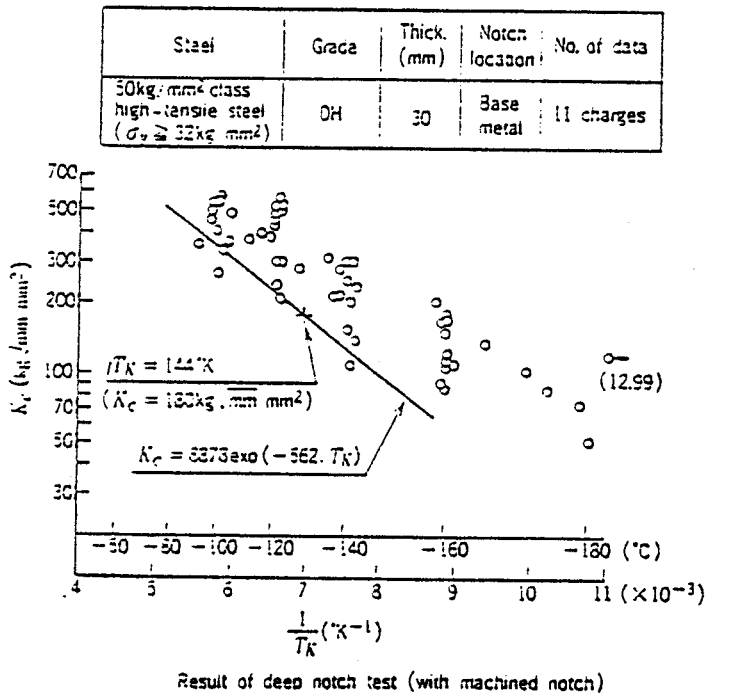

Figure D2(b): Measured and estimated values of fracture toughness of 50 kg/mm^2 class Grade DH high tensile steel plate for hull use (25.4mm thick) (Reproduced from Ref. D2)

PROJECT TECHNICAL COMMITTEE MEMBERS

The following persons were members of the committee that represented the Ship Structure Committee to the Contractor as resident subject matter experts. As such they performed technical review of the initial proposals to select the contractor, advised the contractor in cognizant matters pertaining to the contract of which the agencies were aware, performed technical review of the work in progress and edited the final report.

Chairman

Mr. William Hanzelek	-	American Bureau of Shipping

Technical Advisor

Mr. Harold Reemsnyder	-	Bethlehem Steel

Members

Mr. Alexander Wilson	-	American Iron & Steel Institute
Mr. Tom Buekema	-	United States Coast Guard
Mr. Ernest Czyryca	-	Naval Surface Warfare Center - Carderock Division
Mr. David Kihl	-	Naval Surface Warfare Center - Carderock Division
Mr. Ralph Sugden	-	Canadian Coast Guard
Mr. Calvin Hyatt	-	Defence Research Establishment Atlantic
Mr. Eric Focht	-	Naval Surface Warfare Center - Carderock Division

Contracting Officer's Technical Representative

Mr. William Siekierka	-	Naval Sea Systems Command

Marine Board Liaison

Dr. Robert Sielski	-	National Academy of Science

Executive Director, Ship Structure Committee

CDR Steve Sharpe	-	United States Coast Guard

277, 2784
all

COMMITTEE ON MARINE STRUCTURES

Commission on Engineering and Technical Systems

National Academy of Sciences - National Research Council

The **COMMITTEE ON MARINE STRUCTURES** has technical cognizance over the interagency Ship Structure Committee's research program.

Dr. John Landes, *Chairman*, University of Tennessee, Knoxville, TN

Mr. Howard M. Bunch, University of Michigan, Ann Arbor, MI

Dr. Dale G. Karr, University of Michigan, Ann Arbor, MI

Mr. Andrew Kendrick, NKF Services, Montreal, Quebec

Dr. John Niedzwecki, Texas A & M University, College Station, TX

Dr. Alan Pense, NAE, Lehigh University, Bethlehem, PA

Dr. Barbara A. Shaw, Pennsylvania State University, University Park, PA

Dr. Robert Sielski, National Research Council, Washington, DC

CDR Stephen E. Sharpe, Ship Structure Committee, Washington, DC

DESIGN WORK GROUP

Dr. John Niedzwecki, *Chairman*, Texas A&M University, College Station, TX

Dr. Bilal Ayyub, University of Maryland, College Park, MD

Mr. Ovide J. Davis, Pascagoula, MS

Mr. Andy Davidson, NASSCO, San Diego, CA

Dr. Maria Celia Ximenes, Chevron Shipping Co., San Francisco, CA

Mr. Jeffrey Geiger, Bath Iron Works, Bath, ME

Mr. Hugh Rynn, Sea-Land Services, Elizabeth, NJ

MATERIALS WORK GROUP

Dr. Barbara A. Shaw, *Chairman*, Pennsylvania State University, University Park, PA

Dr. David P. Edmonds, Edison Welding Institute, Columbus, OH

Dr. John F. McIntyre, Advanced Polymer Sciences, Avon, OH

Dr. Harold S. Reemsnyder, Bethlehem Steel Corp., Bethlehem, PA

Dr. Bruce R. Somers, Lehigh University, Bethlehem, PA

RECENT SHIP STRUCTURE COMMITTEE PUBLICATIONS

Ship Structure Committee Publications - A Special Bibliography This bibliography of SSC reports may be downloaded from the internet at: "http://www.dot.gov/dotinfo/uscg/hq/nmc/nmc/ssc1/index.htm".

SSC-395 Ship's Maintenance Project, Pt II & III B. Bea, T. Xu, K. Ma, R. Shulte-Strathaus 1997

SSC-394 Strength Assessment of Pitted Plate Panels J. Daidola, J. Parente, I. Orisamolu, K-t. Ma 1997

SSC-393 Evaluation of Ductile Fracture Models R. Dexter, M. Gentilcore 1997

SSC-392 Probability Based Ship Design: Implementation of Design Guidelines A. Mansour, P. Wirsching, G. White, B. Ayyub 1996

SSC-391 Evaluation of Marine Structures Education in North America R. Yagle 1996

SSC-390 Corrosion Control of Inter-hull Structures M. Kikuta, M. Shimko, D Ciscom 1996

SSC-389 Inspection of Marine Structures L. Demsetz, R. Cario, R. Schulte-Strathaus, B. Bea 1996

SSC-388 Ship Structural Integrity Information System-Phase II M. Dry, R. Schulte-Strathaus, B. Bea 1996

SSC-387 Guideline for Evaluation of Finite Elements and Results R. I. Basu, K. J. Kirkhope, J. Srinivasan 1996

SSC-386 Ship's Maintenance Project R. Bea, E. Cramer, R. Schulte-Strauthaus, R. Mayoss, K. Gallion, K. Ma, R. Holzman, L. Demsetz 1995

SSC-385 Hydrodynamic Impact on Displacement Ship Hulls - An Assessment of the State of the Art J. Daidola, V. Mishkevich 1995

SSC-384 Post-Yield Strength of Icebreaking Ship Structural Members C. DesRochers, J. Crocker, R. Kumar, D. Brennan, B. Dick, S. Lantos 1995

SSC-383 Optimum Weld-Metal Strength for High Strength Steel Structures R. Dexter and M. Ferrell 1995

SSC-382 Reexamination of Design Criteria for Stiffened Plate Panels by D. Ghose and N. Nappi 1995